DISCOVERY AND SYNTHESIS OF BIOACTIVE NATURAL PRODUCT PROBES FROM MARINE SYSTEMS

A Thesis
Presented to
The Academic Faculty

by

E. Paige Stout

In Partial Fulfillment
of the Requirements for the Degree
Doctor of Philosophy in the
School of Chemistry and Biochemistry

Georgia Institute of Technology
December 2010

DISCOVERY AND SYNTHESIS OF BIOACTIVE NATURAL PRODUCT PROBES FROM MARINE SYSTEMS

Approved by:

Dr. Julia Kubanek, Advisor
School of Chemistry and Biochemistry and
School of Biology
Georgia Institute of Technology

Dr. David M. Collard
School of Chemistry and Biochemistry
Georgia Institute of Technology

Dr. Stefan France
School of Chemistry and Biochemistry
Georgia Institute of Technology

Dr. Wendy L. Kelly
School of Chemistry and Biochemistry
Georgia Institute of Technology

Dr. Terry W. Snell
School of Biology
Georgia Institute of Technology

Date Approved: September 9, 2010

ACKNOWLEDGEMENTS

I would like to express my deepest appreciation to my thesis advisor, Julia Kubanek, for whom my admiration continually grows. She consistently expressed a sense of spirit and enthusiasm in research and teaching throughout my graduate studies, while also conveying the attitude and substance of a true genius. Her guidance has significantly expanded my research capabilities as she constantly challenged my scope of knowledge in the field of chemistry and biochemistry.

I would also like to thank my committee members, Professors David M. Collard, Stefan France, Wendy L. Kelly, and Terry W. Snell, for their support and encouragement have greatly enhanced the quality of this thesis.

In addition, I am greatly indebted to our collaborators Prof. Mark E. Hay (Georgia Tech); Prof. Karine Le Roch, Jacques Prudhomme, Serena Cervantes (University of California, Riverside); and Dr. James J. La Clair (Xenobe Research Institute) for enriching my research experience. I especially thank the Government of Fiji for permission to perform research in their territorial waters and for permission to export samples, as well as the U.S. National Institutes of Health's International Cooperative Biodiversity Groups program (grant No. U01 TW007401 to Profs. Hay and Kubanek) for research funding. Additional research funding was provided by the National Science Foundation (NSF grant BE/GenEn MCB-0412674 to Prof. Snell), the NSF Student Teaching and Enhancement Program Fellowship, and the Center for Drug Design, Development and Delivery Fellowship (GAANN).

My husband, Brooks Stout, has provided incessant support and patience throughout my graduate studies and thesis writing – and I am eternally grateful to him. My parents and family have also given continual encouragement, and without their love and support, I would not be here today.

TABLE OF CONTENTS

LIST OF TABLES

LIST OF FIGURES

LIST OF SCHEMES

NOMENCLATURE

^{1}H	proton
^{13}C	carbon-13
Ac	acetyl
BHT	butylated hydroxytoluene
CD	circular dichroism
COSY	correlation spectroscopy
DNMT-1	DNA methyltransferase
HMBC	heteronuclear multiple bond coherence
HSQC	heteronuclear single quantum correlation
IC_{50}	half maximal inhibitory concentration
MCPBA	*meta*-chloroperbenzoic acid
Me	methyl
µg/ml	micrograms per milliliter
µM	micromolar
NCI	National Cancer Institute
NMR	nuclear magnetic resonance
nM	nanomolar
NOE	nuclear Overhauser effect
NOESY	nuclear Overhauser effect spectroscopy
NRPS	non-ribosomal peptide synthetase
PP2A	protein phosphatase 2A
ROESY	rotating-frame Overhauser effect spectroscopy
spp.	species
TBTO	bis-(tributylin) oxide
TOCSY	totally correlated spectroscopy

SUMMARY

Flora and fauna from terrestrial and marine environments provide libraries of natural compounds for drug discovery. The last four decades have seen major advances in ocean exploration that have allowed chemists and biologists to explore previously inaccessible and rare marine organisms. To date, over 3,000 natural products have been reported from marine macroalgae, with properties of these compounds ranging from ecological roles to pharmacological activities. Chapter 2 contextualizes previous studies on marine macroalgal natural products, with particular attention to structurally-diverse natural products with ecological relevance and pharmaceutical potential, highlighting biosynthetic implications from complex secondary metabolites. Preference was given to recently discovered natural products, as well as to compounds that are particularly promising for future development as drugs in pharmacological studies.

The study of under-explored marine organisms can result in the discovery of structurally novel and unusual natural products with drug potential. Prior to 2005, no natural products had been reported from the Fijian red macroalgae *Callophycus serratus* or *Neurymenia fraxinifolia*. As a result of the work described in this thesis and others in the same research group, 33 novel bioactive natural products have now been isolated and elucidated from *C. serratus* – six of which are fully described in Chapter 3 – and two new secondary metabolites were discovered from *N. fraxinifolia* (Chapter 5), enriching the natural product library for drug development. The absolute stereochemistry of callophycolide A (Chapter 3), a unique non-brominated macrolide from *C. serratus*, was determined using a combination of Mosher's ester analysis, circular dichroism analysis with a dimolybdenum tetraacetate complex, and conformational analysis using NOEs. Several natural products isolated from *C. serratus* exhibited sub-micromolar inhibition against the human malaria parasite *Plasmodium falciparum*, including a drug-resistant

strain. The natural product neurymenolide A, isolated from *N. fraxinifolia*, and its hydrogenated semi-synthetic derivative inhibited the growth of the human pathogenic bacteria methicillin-resistant *Staphylococcus aureus* and was as potent as the antibiotic vancomycin. In addition, two known tocopherols, β-tocopherylhydroquinone and δ-tocopherylhydroquinone, were isolated from the coralline red macroalga *Amphiroa crassa,* presented in Chapter 3. By oxidizing δ-tocopherylhydroquinone to the corresponding δ-tocopherylquinone, antimalarial activity was increased by more than 20-fold.

Derivatization of the natural product bromophycolide A into fluorescent probes allowed the determination of a non-enzymatic mechanism of action against the human malaria parasite *P. falciparum* (Chapter 4). Through a combination of detailed SAR mapping, molecular fluorescent imaging of live cells, UV-VIS spectroscopic analyses, and protein affinity techniques, the mechanism of action of bromophycolide A against the human malaria parasite was determined to involve inhibition of heme crystallization. Heme crystallization inhibition prevents detoxification of heme to hemozoin in parasite food vacuoles and ultimately results in parasite death. The discovery and development of heme crystallization inhibitors is an excellent malaria drug target because heme crystallization is a physicochemical process rather than an enzymatic one that allows for facile evolution of resistance by the parasite. These studies identify a new class of natural products that target heme detoxification in both drug-sensitive and drug-resistant *P. falciparum* and suggest an avenue to circumvent drug resistance.

Natural products are not only excellent sources for drug discovery, but also as tools for the study of biological systems and chemical signaling. Steroids play fundamental roles regulating mammalian reproduction and development. While sex steroids and their receptors are well characterized in vertebrates and several arthropod

invertebrates, little is known about the hormones and receptors regulating reproduction in other invertebrate species. Evolutionary insights into ancient endocrine pathways can be gained by elucidating the hormones and receptors functioning in invertebrate reproduction. In collaboration with Professor Terry W. Snell and colleagues (Georgia Institute of Technology, School of Biology), a combination of genomic analyses, receptor imaging, ligand identification, target elucidation, and exploration of function through receptor knockdown, was used to illustrate that comparable progesterone chemoreception exists in the inv**e**rtebrate monogonont rotifer *Brachionus manjavacas* (Chapter 6), suggesting an ancient origin of the signal transduction systems commonly associated with the development and integration of sexual behavior in mammals.

CHAPTER 1

INTRODUCTION

Natural products have traditionally played an important role in drug discovery and were the basis of most medicines dating back to ancient civilizations.[1] Well-known natural product drugs include penicillin, morphine, and paclitaxel (Taxol™), which are used for the treatment of bacterial infections, excessive pain, and cancer, respectively. The aforementioned drugs originated from terrestrial sources, and while these sources continue to play an important role in natural product drug discovery, the oceans represent a relatively untapped resource for the discovery of novel chemistry.[2] Unique marine natural products possessing potent biological activities may have evolved as biochemical warfare between organisms in order to survive in an aggressive and demanding environment.[3] Selection pressures such as predation, herbivory, disease, and competition for space on highly populated coral reefs may apply adaptive pressure that favors individuals with chemical defenses. Marine organisms produce natural products with structures notably different from those produced by terrestrial organisms, possibly the result of distinctive environmental factors including high salinity and a relatively constant temperature.[2] For example, terpenoids from marine sponges often contain unusual functional groups, such as isocyanate, isonitrile, dichloroimines which are entirely unknown in terrestrial terpenoids. The hallmark of many marine natural products is high degree of halogenation, with about half of the known marine metabolites isolated to date containing bromine, chlorine and even iodine.[2] Many marine natural products exhibit remarkable biological activities, some of which have become molecular probes used in biomedical research.

New drugs are constantly in demand; for example, to combat drug resistance against anti-infectives and for better selectivity in cancer chemotherapy.[4] The first marine

anticancer drug, Yondelis®, an alkaloid from the sea squirt *Ecteinascidia turbinata*, was approved in 2007 for use against liposarcoma for which there were no prior superior treatments.[5] Other antitumor marine natural products in the pipeline of preclinical and clinical trials[6] include dolastatin-10,[7] discodermolide,[8] kahalalide F,[9] and bryostatin 1,[10] to name a few (Figure 1.1).

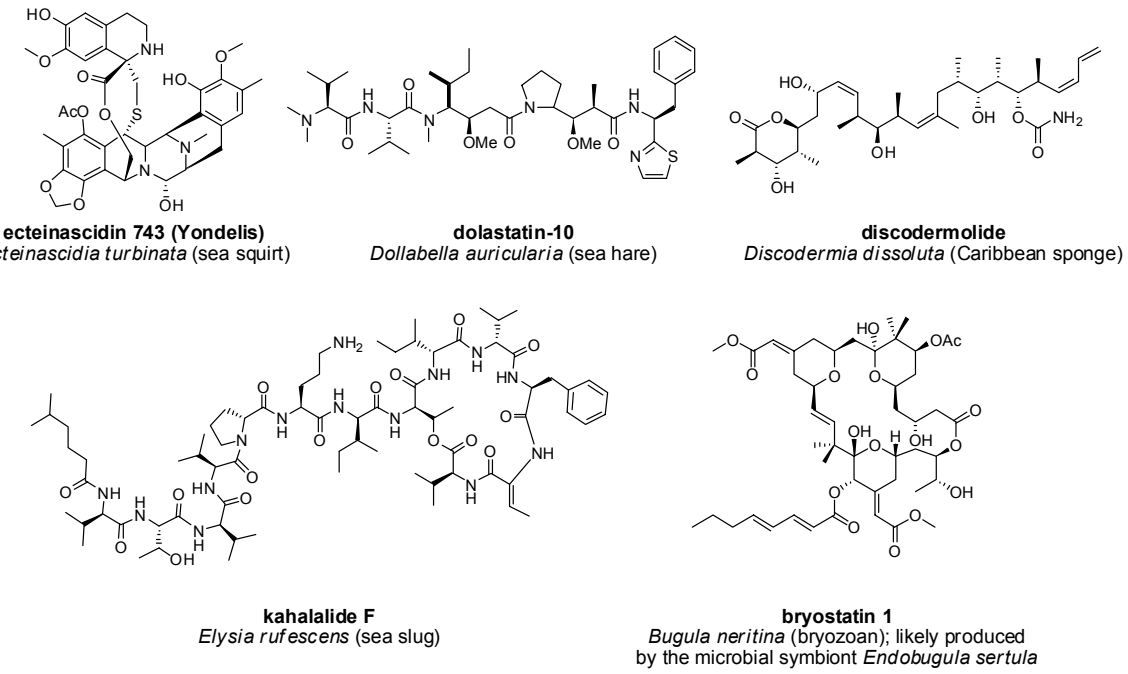

Figure 1.1. Anticancer natural products in preclinical or clinical trials isolated from marine organisms.

Marine natural products have also begun to play a significant role in the discovery of novel anti-infectives, such as antibiotics and antiparasitic drugs. Over two-thirds of current antibiotics are natural products or their derivatives, many of which were discovered from terrestrial soil bacteria such as the well studied actinomycetes.[11]Recent efforts to discover structurally novel antibiotics from soil microbes have led to the rediscovery of known scaffolds, and thus new sources are desperately needed to

overcome the constant evolving of drug resistance.[12] The study of marine actinomycetes has dramatically increased in recent years, and marine microbes have been shown to produce a wide variety of unique antibacterial compounds that show promise as new drug leads (Figure 1.2).[13] Furthermore, marine macroorganisms such as macroalgae (seaweeds) and sponges are exposed to a vast array of marine pathogenic microbes and show potential as excellent sources in the discovery of novel antibiotics.[14] For example, the alkaloid manzamine A, discovered from the marine sponge *Haliclona* sp., has demonstrated activity against tuberculosis, HIV, and malaria and is currently in preclinical trials.[15] The neurymenolides, isolated from the Fijian macroalga *Neurymenia fraxinifolia*, displayed low micromolar inhibition against both Gram-positive methicillin-resistant *Staphylococcus aureus* and Gram-negative *E. coli*, thus has the potential to be developed as a broad-spectrum antibiotic (Chapter 5).[14b]

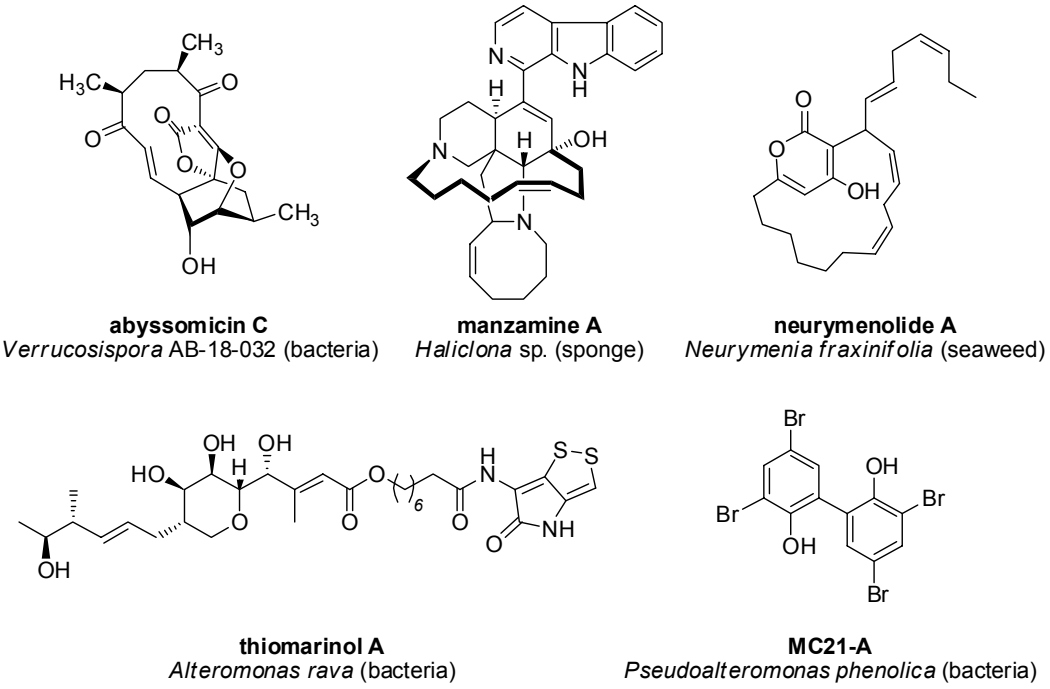

Figure 1.2. Antibacterial marine natural products.

Malaria represents another disease deserving immediate attention in drug discovery, as over 500 million cases of malaria are reported annually, causing one- to three-million deaths worldwide and drug resistance to current treatments is on the rise.[16] Prophylactic drugs remain expensive and inadequate, making the need for new treatments an immediate concern. Current antimalarial drugs of terrestrial origin include the artemisinins and quinines, products of terpene and alkaloid biosynthesis, respectively (Figure 1.3). In recent years, several marine organisms have shown promise in the discovery of new antimalarial treatments,[17] such as the manzamines as previously mentioned (Figure 1.2). Marine sources such as sponges, macroalgae, and microbes have potential as chemically-rich sources of compounds with antimalarial activity.[17] For example, several brominated meroditerpenes from the Fijian macroalga *Callophycus serratus* were shown to possess sub-micromolar activity against the malaria parasite as discussed in Chapter 3.[18]

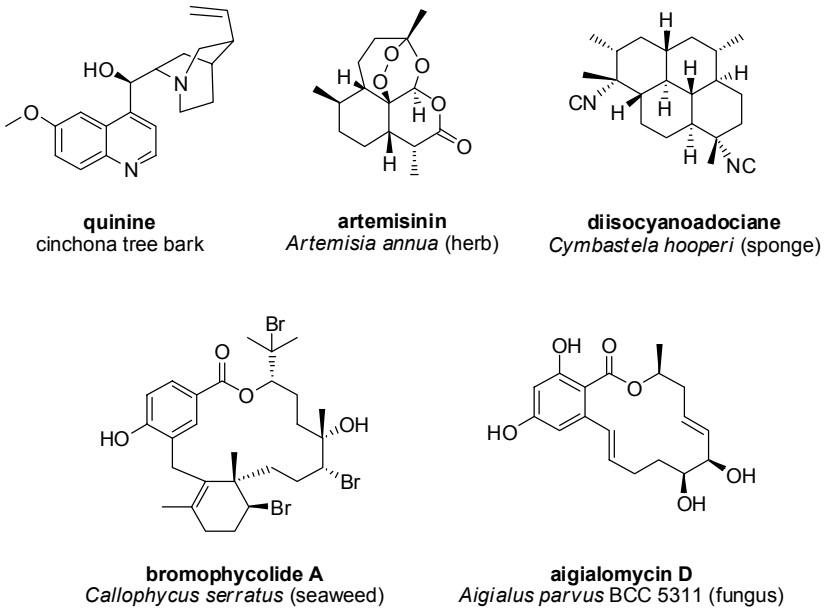

Figure 1.3. Antimalarial natural products: quinine and artemisinin originate from terrestrial sources, and diisocyanoadociane, bromophycolide A, and aigialomycin D were isolated from marine organisms.

A key aspect in advancing a bioactive natural product further along the drug discovery pipeline is to determine its mechanism of action towards its therapeutic target. Within therapeutic targets, thousands of biological macromolecules (especially proteins) represent potential targets for a bioactive compound. Two generalized approaches to identify a mechanism of action include 1) strategies in which specific molecular targets are screened and 2) "unbiased" methods such as proteomics, metabolomics, and affinity chromatography. The first approach includes target-based drug discovery, in which a natural product of interest or libraries of compounds are screened against a validated molecular target; for example, actin or tubulin binding in cancerous tumors. Natural products are well known for their ability to interact with both actin and tubulin, for example as tubulin polymerization inhibitors.[19] Therefore, natural products capable of binding actin or interacting with tubulin are highly desired and are screened for these specific interactions.

The second generalized approach searches for unknown molecular targets. For example, Boone *et al.* have developed a mutant yeast deletion library approach, in which mutant genes from the yeast *Saccharomyces cerevisiae* have are utilized to determine the molecular target of natural products.[20] This approach, however, requires that the natural product of interest possess moderate to potent activity against *S. cerevisiae*. Proteomic and metabolomic studies have seen major advances in recent years, and activity-based protein profiling (ABPP) has become a standard method.[21] A major advantage of ABPP, which is based on chemical probes reacting with mechanistically-related classes of enzymes, is the ability to examine the enzyme active site directly as opposed to being limited by protein abundance as with affinity-based methods. However, when applying ABPP to natural product mechanism of action studies, two major requirements exist; 1) the natural product must possess an intrinsic reactivity – or it should be plausible to synthetically introduce this reactivity – that allows for covalent

binding of the natural product to the protein target, and 2) the presence of a reporter group, such as a fluorescent tag.[21] Affinity chromatography-based methods are often employed; however, these methods also have constraints. As with ABPP, affinity methods require derivatization of the natural product with a tag, such as biotin or another antigen. This derivatization requires the presence of a synthetically accessible and reactive functional group, and functionalized natural products often suffer from decreased bioactivity which can cause difficulties in interpreting results.[22] Furthermore, affinity methods are dependent on natural product-protein affinity as well as protein abundance.

While affinity-based chromatographic methods have certain drawbacks, they can be employed successfully if the natural product of interest conforms to the required conditions. Biotin-avidin affinity is well established, and thus is commonly used in developing probes for protein affinity studies, although this system can result in problematic non-specific binding. As exploited in Chapters 4 and 6, a more specific affinity system utilizes a 7-dimethylamino-4-coumarin tag[23] for which a selective monoclonal antibody against the coumarin tag is available.[24] When fluorescent probes are developed from natural products, histological studies can also be performed to determine the intracellular localization of the probe, and thus natural product, to gain insight into potential mechanisms of action.

Natural products have evolved to encompass a broad range of chemical and functional diversity. This diversity enables small molecule natural products to target a sub-set of biomolecules in a highly selective fashion as a result of their structural and stereochemical complexity. These features make natural products not only excellent sources for drug discovery, but also tools for the study of biological systems and chemical signaling.[22] For example, Schreiber *et al*. used the fungal natural product trapoxin as a chemical probe to study histone deacetylation.[25] These studies revealed

the relationship between histone deacetylases, transcriptional regulation, and cell cycle progression, and thus led to the development of histone deacetylation inhibitors for cancer treatment.[26] As discussed in Chapter 6, natural products can also be used as probes in the understanding of chemical signaling and regulation of important biological processes such as reproduction in non-model organisms. Evolutionary insights into endocrine pathways were gained by elucidating the hormones and receptors functioning in reproduction, such as in the ancient marine micro-invertebrate *Brachionus manjavacas*.[27] These studies demonstrated that progesterone and its receptor exhibit a conservation of function over a broad expanse of animal phylogeny. Collectively, chemical probes are an essential component in the understanding of complex biological processes from a therapeutic and evolutionary perspective.

Reported herein is a collection of studies in which (1) underexplored tropical red macroalgae were investigated for unique bioactive natural products (Chapters 3 and 5); and (2) isolated bioactive natural products were derivatized to fluorescent probes for which (a) specific mechanisms of action in therapeutic targets were explored (Chapter 4) and (b) biological processes and chemical signaling were studied (Chapter 6). Efforts were focused on identifying natural products possessing antimalarial and antibacterial activities to address human diseases for which new drugs are urgently needed due to constantly evolving resistance to current medicines. A literature review on macroalgal natural products (Chapter 2) discusses the importance and impact of this field on both drug discovery and marine chemical ecology.

CHAPTER 2

MARINE MACROALGAL NATURAL PRODUCTS

Introduction

The ocean covers nearly 70% of the Earth and represents 90% of the biosphere, providing a home for over 30 phyla and 500,000 species of marine organisms.[28] These organisms have evolved over millions of years to produce a vast diversity of unique chemical compounds that fulfill varied functions. Among these are molecules with potent biological activities that may have evolved as biochemical warfare between organisms in order to persist in an aggressive environment. Marine organisms produce secondary metabolites that are structurally distinct from those produced by terrestrial organisms, possibly due to factors unique to marine environments such as high salinity and pressure and a relatively constant temperature.[2, 28] Unusual functional groups, such as isocyanate, isonitrile, dichloroimine, and halogenated functionalities occur predominantly in marine metabolites.[2]

Natural products from terrestrial plants and soil microbes have traditionally played an important role in drug discovery and were the basis of most early medicines.[1] The ocean, in contrast, was left virtually untapped of its vast resources until the early 1970s. Over the last several decades, scientists have discovered many distinctive types of biologically active secondary metabolites with unusual and exciting carbon skeletons from Chlorophyta (green algae), Phaeophyta (brown algae), and Rhodophyta (red algae). Scientific reports of new natural products from marine macroalgae have steadily increased since the 1980's (Figure 2.1). This chapter contextualizes studies on marine macroalgal natural products, with particular attention to structurally diverse natural products with ecological relevance and pharmaceutical potential, highlighting biosynthetic implications from structurally diverse metabolites. Preference is given to

recently discovered natural products, as well as to compounds that are particularly promising for future development as drugs in pharmacological studies.

A series of excellent reviews on marine natural product chemistry, organized phylogenetically, is published annually in *Natural Product Reports*.[29] In addition, many recent review articles have explored particular marine natural products based upon their specific biological activities, such as antitumor and cytotoxic compounds,[30] therapeutics for tuberculosis and malaria,[31] and antifoulants.[32] Furthermore, review articles are also available based on compound class, such as the review written by Gross & König on terpenoids from marine organisms with pharmacological activity.[2] Other reviews of interest are cited throughout the chapter.

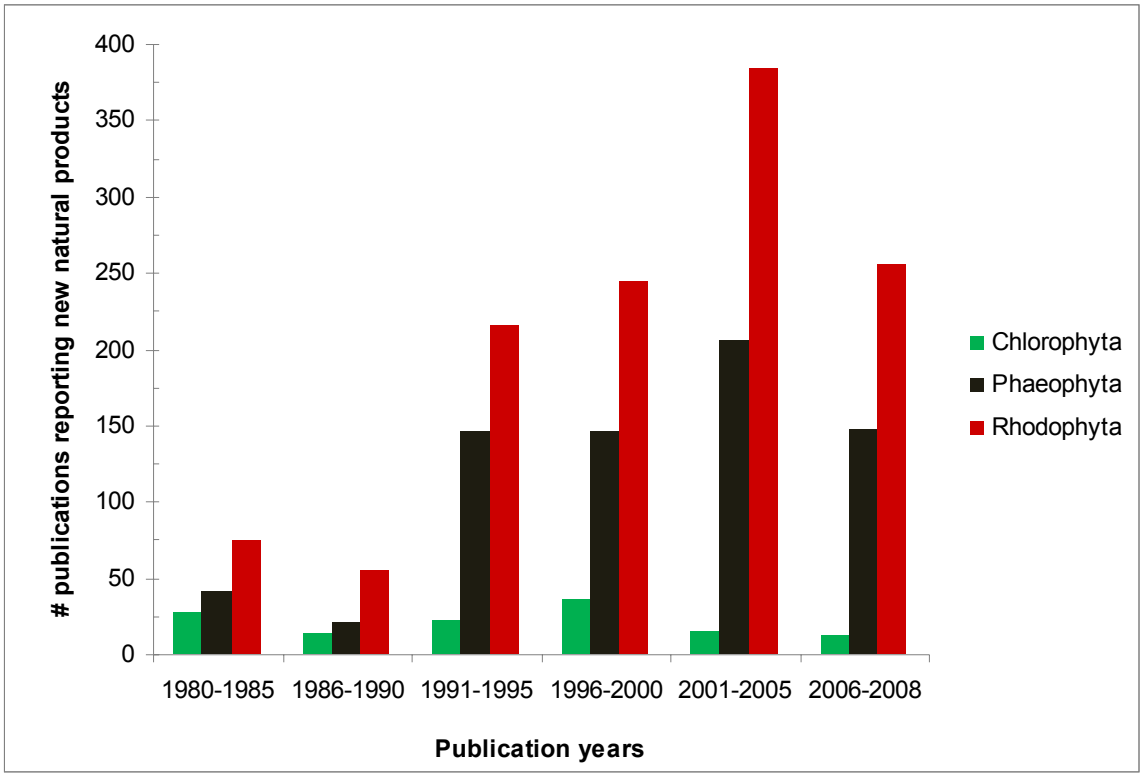

Figure 2.1. Reports of novel natural products from marine macroalgae since 1980. The search was conducted using Marinlit and ISI Web of Science, limiting output to chemistry journal research articles and notes, using a variety of keywords. Hits were verified to

ensure that natural products reported were new and discoveries were not double-counted. This figure may under-represent the actual discovery rate, if natural products were reported in non-chemistry journals and/or if keywords were different from those used for the literature search.

Isoprenoids

Marine macroalgae produce a wide variety of intriguing and diverse isoprenoid structures deriving from C_5 isoprene units,[33] and many reports have been published on the ecological roles of these metabolites.[34] Marine terpenoids are frequently found with halogenated functionalities and one or more rings, which can have important implications for their biological activities. Isoprenoid metabolites are derived via the classical mevalonate pathway or the more recently discovered deoxyxylulose phosphate pathway.[35] Isoprenoids are the dominant class of secondary metabolites known from macroalgae, representing 59% of the metabolites isolated to date from green algae, 46% from red algae, and 68% from brown algae.[3] Due to the substantial representation of isoprenoids among macroalgae, approximately half of this review will focus on novel isoprenoid carbon connectivities, ecological roles, and isoprenoids that have gained pharmaceutical interest.

Novel Connectivity and Cyclization Patterns

Due to the immense effort already applied to the discovery of isoprenoid natural products from macroalgae, uncovering novel carbon skeletons is now rare. However, several reports have recently been published on macroalgal isoprenoids that possess novel connectivities and cyclizations.

Labdanes

Labdane-based diterpenes (Figure 2.2) have been isolated from tissues of fungi, insects, marine organisms, and from essential oils, resins, and tissues of higher plants, and have been shown to possess a broad spectrum of biological activities.[36]

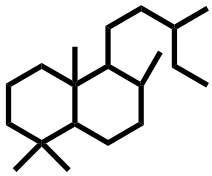

Figure 2.2. Labdane carbon skeleton

Two labdane-type brominated diterpenes (**1-2**) containing unprecedented seven- and eight- membered ether rings were isolated from the red alga *Laurencia obtusa,* collected in Mitikas Bay, Greece.[37]

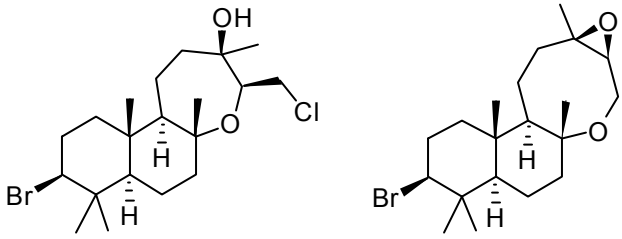

1 **2**

Metabolites **1** and **2** were proposed to share a common decalin precursor, formed from geranyllinalool (**3**) via cyclization and bromination, and the relative stereochemistry was assigned using ^{1}H-^{1}H scalar couplings and NOESY experiments.[37] Enzyme-catalyzed dehydration, followed by double-bond transposition, allylic chlorination, and epoxidation could give rise to the intermediate **4**. Nucleophilic attack of the C-8 hydroxyl group on either C-15 or C-14 could lead to metabolites **1** and **2** (Scheme 2.1).

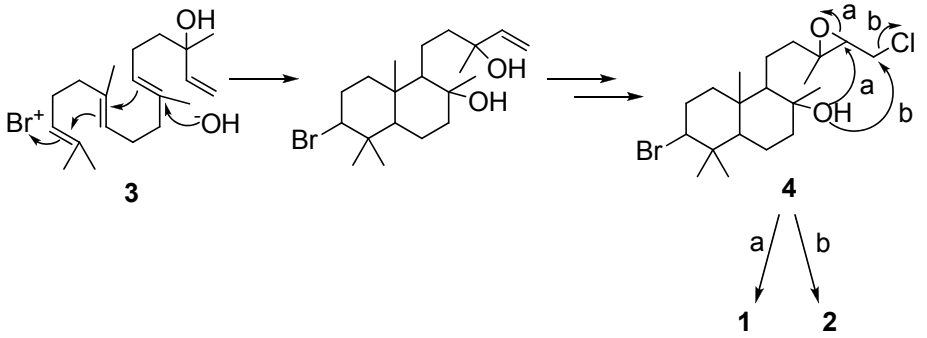

Scheme 2.1. Hypothesized biosynthetic pathway of **1**-**2**.[37]

Laurencia paniculata, collected from Qatari, Arabian Gulf, was found to produce (-)-paniculatol (**5**), an unusual labdane with a tetrahydropyran ring, and absolute stereochemistry was determined by X-ray crystallography.[38] More recently, two additional labdanes (**6-7**) with tetrahydropyran rings were indentified from an unknown Okinawan species of *Laurencia*, and absolute stereochemistry also established by a combination of 2D NMR spectral data and X-ray crystallographic data.[39] While labdanes originating from macroalgae have intriguing structures, no biological tests were reported for these metabolites.

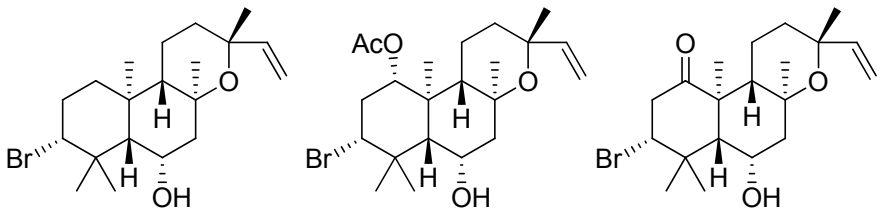

5 **6** **7**

Dactylomelane metabolites

Cyclization between C-6 and C-11 is an unusual skeletal characteristic for diterpenes (Figure 2.3), with only four marine species reported to utilize this pattern in secondary metabolism.

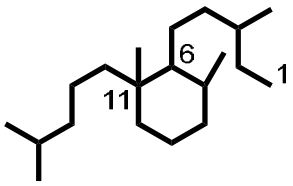

Figure 2.3. Dactylomelane cyclization

Two dactylomelane metabolites were isolated from sea hares *Aplysia dactylomela*[40] (dactylomelol, **8**) and *Aplysia punctata* (puctatene acetate, **10**),[41] and more recently, similar metabolites were found from two red algal species, *Sphaerococcus coronopifolius* (sphaerolabdadiene-3,14-diol, **9**)[42] and *Laurencia* sp.[43] *Laurencia* sp. (Tenerife, Canary Islands) produced a number of novel and relatively unstable hydroperoxide metabolites, such as dactylohydroperoxide C (**12**), in addition to **8** and puctatene (**11**).[43] Isolation of **8** and **11** from *Laurencia* suggests a macroalgal biogenesis for this class of diterpenes. The relative stereochemistries of **8-12** were established by analysis of NOE data. No biological activities were reported for these metabolites.

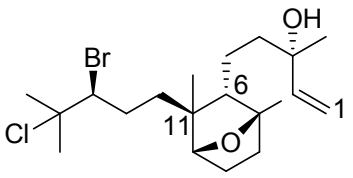

8

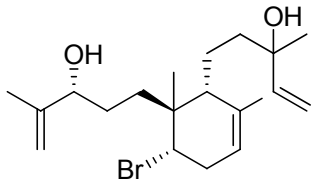

9

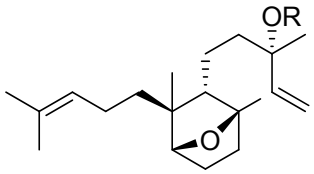

10 R = Ac
11 R = H

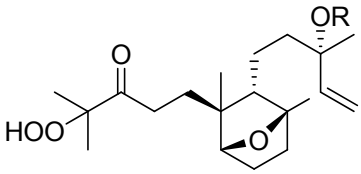

12

Meroditerpenes

Novel metabolites of mixed biogenesis are more likely to contain novel carbon skeletons than are the better-explored isoprenoid secondary metabolites. Therefore,

hybrid metabolites from macroalgae seem likely to become front-runners for exciting natural product discovery. Uncovering novel skeletons for new scaffolds remains an integral part of drug discovery.

Since 2005, 33 novel bioactive metabolites (e.g., bromophycolides A-B (**13-14**), callophycoic acid C (**15**), and callophycol A (**16**)) representing eight new carbon skeletons derived from mixed isoprenoid-shikimate biosynthesis, have been isolated from the red alga *Callophycus serratus* (Fiji Islands).[18, 44] The absolute configurations of **13-14** were determined by X-ray crystallography, and absolute stereochemistries of subsequent bromophycolides were established by analysis of NOE data and from inferring a common biogenesis as **13-14**. An X-ray crystal structure of callophycoic acid A (structure not shown) provided its configuration from which the absolute stereochemistries of other callophycolic acids were inferred, and relative stereochemistry of **16** was determined through analysis of NOESY data.[18a] Extracts yielding callophycoic acids and callophycols showed no signs of bromophycolides, which were found from collections at different sites, suggesting population-level variation in secondary metabolism leading to two chemotypes.[18a] The most cytotoxic secondary metabolite was **13**, with moderate *in vitro* cytotoxicity against a broad range of tumor types (mean IC_{50} = 6.7 μM). The G1 phase of the cell cycle was arrested when human ovarian cells were exposed to **13**, suggesting that apoptosis stemmed from cells arrested in G1.[44a] Interestingly, the callophycoic acids and callophycols were significantly less active in pharmacological assays than **13-14**, suggesting the importance of the macrocyclic lactone functionality.[18a] Nevertheless, compounds of both chemotypes suppressed growth of the algal pathogen *Lindra thalassiae* at and below natural concentrations, suggesting a potent antifungal chemical defense.[45]

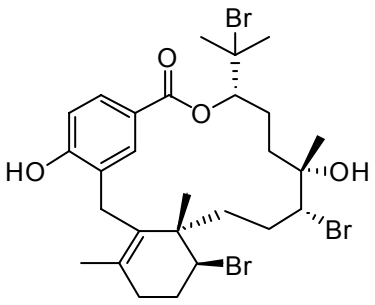

13

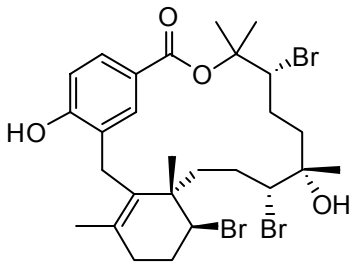

14

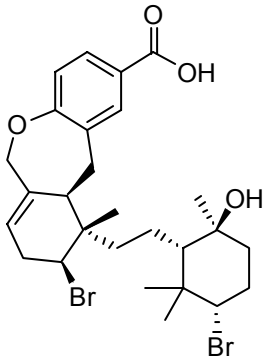

15

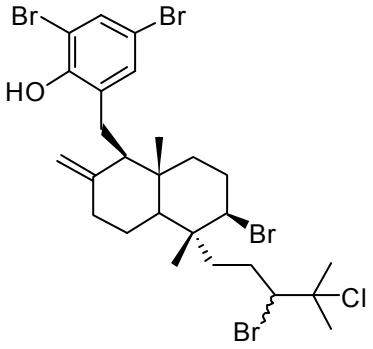

16

An extract of the brown alga *Cystoseira* sp. (Montaña Clara Island, Mediterranean Sea) exposed to acetylation reaction conditions yielded two novel meroditerpenes, cystoseirone diacetate (**17**), with an unusual C-6 to C-12 ether linkage, and amentol chromane diacetate (**18**), and whose relative stereochemistry was proposed from analysis of ROESY data.[46]

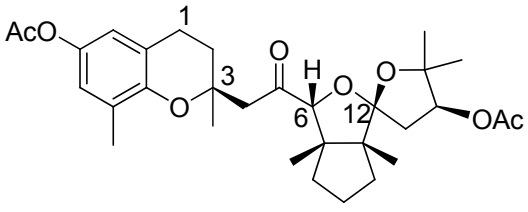

17

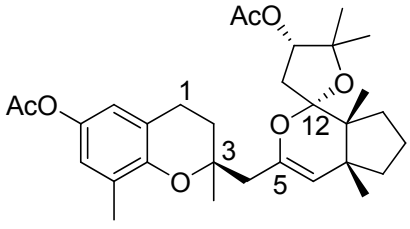

18

The biosynthesis of cystoseirone (the unacetylated, likely natural product) was hypothesized to arise from an oxidation of the enol-ether system found in **18**, with subsequent rearrangement.[46] This was tested by treating **18** with *m*-chloroperbenzoic

acid (MCPBA) in dichloromethane, which afforded two isomers, one of which was identical to **17** (Scheme 2.2).

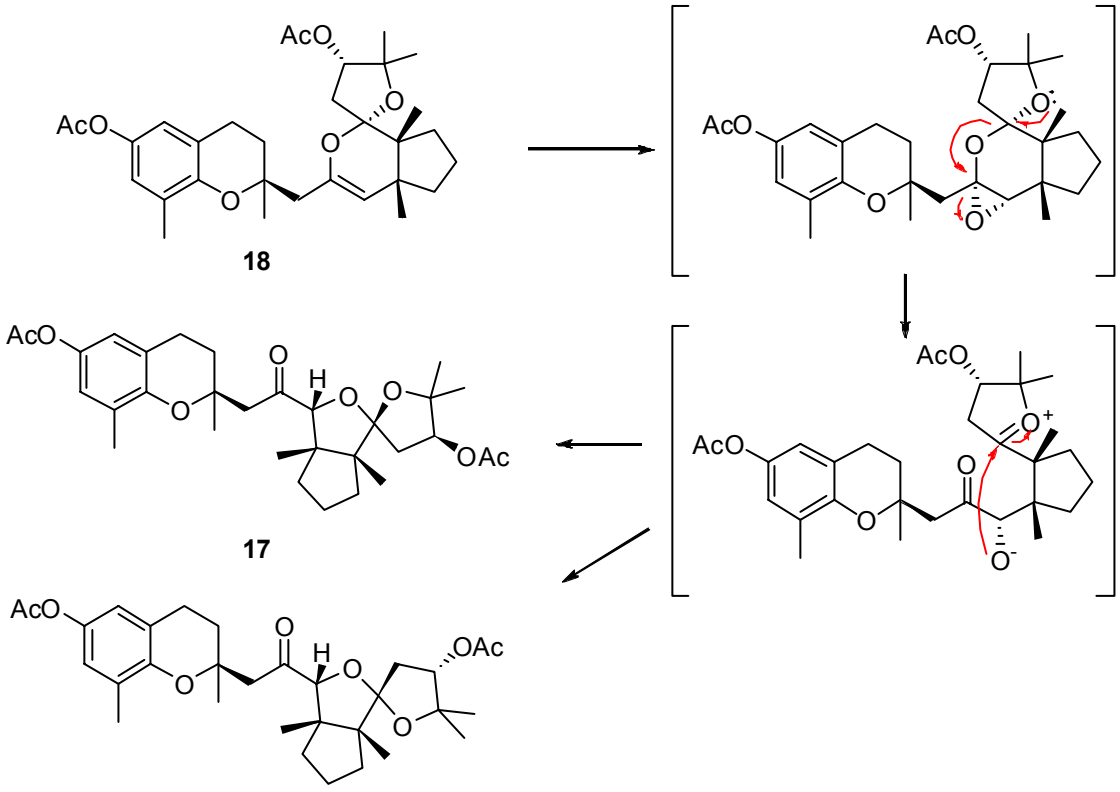

Scheme 2.2. Proposed mechanism for chemical transformation of **18** to **17** and its diastereomer.[46]

Chemical Ecology

Secondary metabolites have long been assumed to enhance the survival of macroalgae by providing defenses against consumers, competitors, or parasites.[3] Many field and laboratory studies have tested antifeedant and antifouling effects of macroalgal metabolites.[34a, 47] Fewer ecological studies have addressed antimicrobial or other antiparasitic defenses in macroalgae, despite the fact that marine organisms are frequently exposed to high concentrations of potentially harmful marine microbes.[14a]

Antiherbivore metabolites

Numerous reports and reviews focus on macroalgal-herbivore interactions and the mechanisms by which macroalgae tolerate or resist herbivory.[48] Many algal species deter herbivores by morphological, structural, or chemical defenses[49] or by associating with unpalatable algae or other benthic organisms.[50] Due to the extensive literature available on these interactions, the aim of this section is to highlight specific antiherbivore terpenes from macroalgae.

Three new diterpenoids, acutilol A (**19**), acutilol A acetate (**20**), and acutilol B (**21**) from the brown alga *Dictyota acutiloba,* were found to be potent feeding deterrents against both temperate and tropical herbivorous fishes and sea urchins, and whose relative stereochemistry was determined by NOESY experiments.[51] Common tropical and temperate herbivores were deterred by the acutilols at 20% of their natural concentrations, suggesting that these secondary metabolites provide an efficient chemical defense for *D. acutiloba*.[52] These compounds are structurally related to the common pachydictyane carbon skeleton, but the $\Delta^{1,10}$ double bond is an unusual feature for this compound class.[51] The pachydictyols and dictyols, first isolated in the 1970s, have also been shown to possess potent deterrent effects. Cruz-Rivera and Hay tested the antifeedant effects of dictyols against six mesograzers, and found that amphipods were deterred by dictyols, but the isopod *Paracerceis caudata* was not deterred.[53]

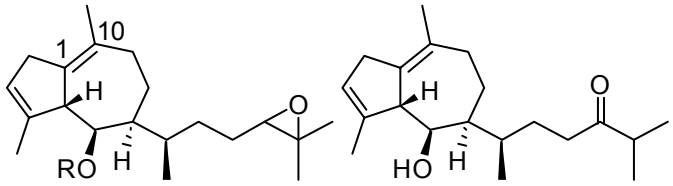

19 R = H
20 R = Ac

21

Halimeda spp. are well-studied green algae found in tropical areas characterized by high levels of herbivory.[54] Major metabolites from *Halimeda* include the diterpenes

halimedatetraacetate (**22**) and halimedatrial (**23**),[55] which act as feeding deterrents and allow the alga to persist in areas of intense herbivory.[56] Additional studies established that upon damage, levels of **22** decreased while the concentration of **23** increased, suggesting that upon wounding, the alga quickly converts **22** into the more deterrent **23** via a putative enzyme-mediated pathway.[57] One difficulty of working with activated defenses is that the use of extraction solvents may lead to spontaneous activation of reactive precursors, preventing assessment of the true "inactivated" state of defenses (Kubanek and Hay, unpublished). Nevertheless, activated defenses appear to be common among tropical macroalgae. Cetrulo and Hay found that upon wounding, 17% of species tested exhibited changes in palatability consistent with activated chemical defenses.[58]

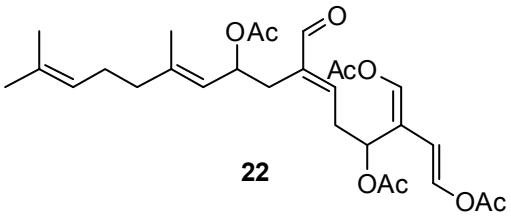

22

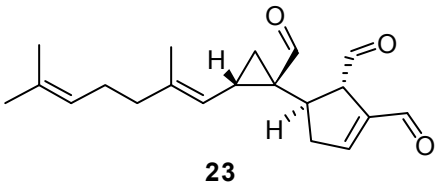

23

In a more recent example of activated macroalgal chemical defenses, caulerpenyne (**24**) from the invasive green alga *Caulerpa taxifolia,* was suggested to rapidly transform into oxytoxin 2 (**25**) upon wounding.[59] However, due to the labile nature of **25**, the authors were unable to test the hypothesis that **25** is more deterrent than **24**. Other studies testing the reactivity of 1,4-dialdehyde metabolites found in higher plants demonstrated that these compounds readily react with nucleophiles, making it difficult to use them in manipulative experiments.[60]

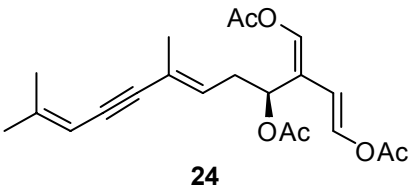

24

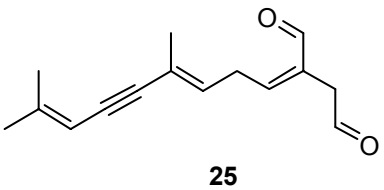

25

Antifouling metabolites

Solid surfaces exposed to seawater can undergo a series of changes leading to the accumulation of marine organisms, mainly consisting of microbial slimes, diatoms, barnacles, tunicates, bryozoans, and spores of marine algae.[61] Macroalgae, being a prolific source of bioactive natural products, may produce secondary metabolites to inhibit this process of fouling.[32] Since the 1970s, the antifouling effects of *Laurencia* spp. isoprenoids have been noted.[62] These metabolites, however, are generally toxic to many marine organisms and so their commercial development is not feasible.[63]

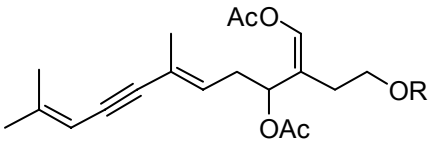

26

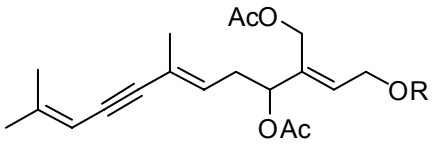

27

26a, 27d R = CH_3-$(CH_2)_4$-(CH=CH-$CH_2)_2$-$(CH_2)_6$CO-
26b, 27c R = CH_3-$(CH_2)_{14}$CO-
26c R = CH_3-CH_2-(CH=CH-$CH_2)_3$-$(CH_2)_6$CO-
26d R = CH_3-CH_2-(CH=CH-$CH_2)_5$-$(CH_2)_2$CO-
26e R = CH_3-$(CH_2)_{16}$CO-
26f R = CH_3-$(CH_2)_7$-CH=CH-$(CH_2)_9$CO-
26g R = CH_3-$(CH_2)_4$-(CH=CH-$CH_2)_4$-$(CH_2)_2$CO-
26h, 27e R = CH_3-CH_2-(CH=CH-$CH_2)_3$-$(CH_2)_4$CO-
26i R = CH_3-CH_2-(CH=CH-$CH_2)_4$-$(CH_2)_3$CO-
27a R = CH_3-$(CH_2)_{12}$CO-
27b R = CH_3-$(CH_2)_5$-CH=CH-$(CH_2)_7$CO-
27f R = CH_3-$(CH_2)_7$-CH=CH-$(CH_2)_7$CO-

Caulerpa prolifera, found in the shallow waters of Saronicos Gulf, Greece, is abundant and exhibits minimal fouling.[64] Fifteen acetylene sesquiterpenoid esters (**26a-i, 27a-f**) from this alga inhibited fouling in a manner similar to the biocide bis-(tributylin) oxide (TBTO).[64] Similar to *Laurencia* antifouling metabolites, **26-27** and TBTO are generally toxic, thus limiting the further development of these compounds.

To date, no macroalgal terpenes have been utilized commercially as antifoulants. Macroalgal furanones, however, are currently in development to prevent fouling. Macroalgae that are generally unfouled in the field are strong leads for the discovery of

novel antifoulants, especially if found in habitats where other organisms are highly fouled.

Antimicrobial metabolites

Despite a large body of literature describing the antimicrobial activities of macroalgal secondary metabolites, little evidence exists to date to support the hypothesis that algal secondary metabolites target marine pathogens at realistic natural concentrations.[65] Only a handful of studies demonstrate the ability of macroalgal secondary metabolites to effectively deter or suppress ecologically-relevant pathogens. Two novel triterpene sulfate esters, capisterones A and B (**28-29**) from the green alga *Penicillus capitatus,* suppressed growth of the marine fungal pathogen *Lindra thallasiae* when tested at and below whole-tissue natural concentrations.[66] Assignment of the relative stereochemistries of **28-29** relied on interpretation of 2D NMR spectral data. While work in this area of chemical ecology is progressing, the few studies reported thus far propose ecologically relevant assays as guides for future studies.[14a]

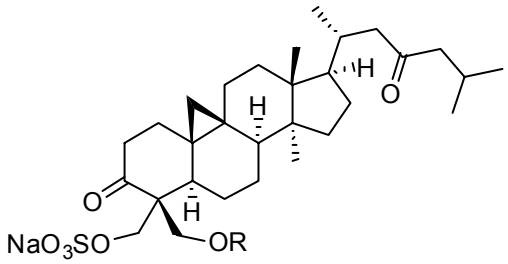

28 R = OAc
29 R = H

Metabolites with Pharmacological Potential

Halomon

Halogenated monoterpenes have been known from red algae since the mid-1970s, but it wasn't until the early 1990s that a metabolite with pharmaceutical potential moved to preclinical drug development. The pentahalogenated monoterpene halomon

(**30**) was isolated from extracts of the red alga *Portieria hornemannii* (Batan Island, Philippines) and its X-ray crystal structure, absolute stereochemistry, and complete ^{1}H and ^{13}C NMR assignments were reported.[67] Halomon (**30**) was associated with a novel cytotoxicity profile against diverse tumor types in the National Cancer Institute's (NCI) primary screening panel.[67] Several reports have been published on the total synthesis of **30** to aid its progress and development through preclinical trials.[68] Unfortunately, research and development of **30** as an anticancer agent has been limited to its failure to exhibit significant *in vivo* effects.[69]

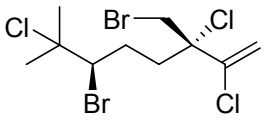

30

Polyether triterpenes

Squalene-derived polyether triterpenes (e.g., **31-34**) are a structurally-exciting group of marine algal natural products exhibiting a great diversity of ring sizes and intriguing biological activities. The first reported macroalgal polyether metabolite, thyrsiferol (**31**), from *Laurencia thyrsifera,* collected from New Zealand, was assigned the absolute structure **31** by X-ray crystallographic analyses based on thyrsiferol 18-acetate (**32**).[70] Following this discovery, several other structurally-related polyether metabolites were reported from *Laurencia* spp., including dehydrothyrsiferol (**33**)[71] and thyrsiferyl 23-acetate (**34**).[72] The latter exhibited superior activity against P-388 lymphoid neoplasm cells, with IC_{50} = 0.47 nM. Furthermore, **34** potently and selectively inhibited protein phosphatase 2A (PP2A), with no effect on protein phosphatases 1, 2B, 2C, or protein tyrosine phosphatase, making **34** a potential probe for identification of cellular processes dependent on PP2A.[73]

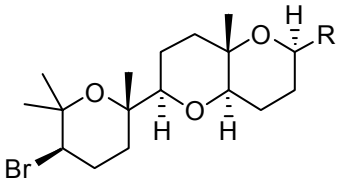

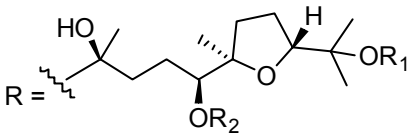

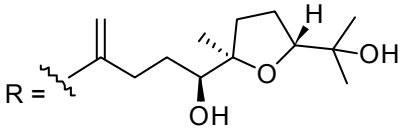

31 $R_1 = R_2 = H$
32 $R_1 = H$, $R_2 = Ac$
34 $R_1 = Ac$, $R_2 = H$

33

The potent and selective effects of **34** propelled further studies with this compound class. After discovering many new analogs from *Laurencia* spp., structure-activity relationships were established based on a combination of isolated natural products and synthetic analogs.[74] Fernandez *et al.* proposed that the spatial arrangement of the flexible chain affected metabolite bioactivity. From calculations of stable conformations of isolated polyethers using distance constraints established from NOE data, it was proposed that polyethers with C-15–C-19 chain turned downward were more potent than those with the side chain turned upward, as illustrated by comparing **33** (downward side chain, IC_{50} = 0.01 μg/ml) versus **35** (upward side chain, IC_{50} > 1 μg/ml) (Figure 2.4).[74a] The original structures and pharmacological activities drove synthetic efforts towards producing these compounds, and a thorough review of the total synthesis strategies is available.[75]

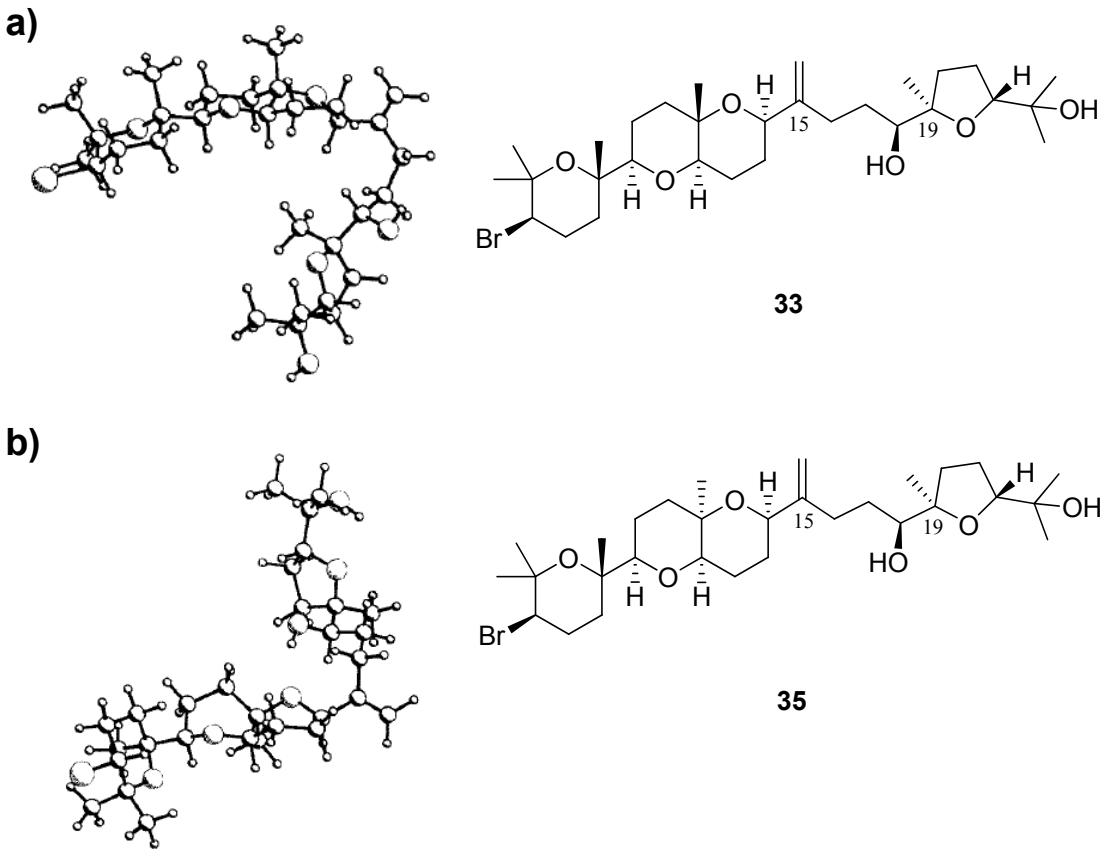

Figure 2.4. Stereoviews of proposed 3D structures of (a) **33** with downward side chain and (b) **35** with upward side chain, adapted from Fernandez *et al.* with permission.[74a]

Dolabellanes

Dolabellanes (Figure 2.5) are constituents of mollusks, coelenterates, and brown algae, and they are also found in terrestrial mold, liverwort, and higher plant species.[76] Several dolabellanes have shown potential for pharmaceutical application, exhibiting cytotoxic, antibacterial, antifungal, antiviral, and antimalarial activities.[76]

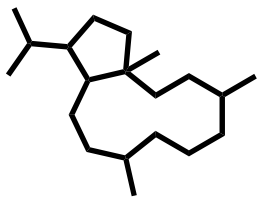

Figure 2.5. Dolabellane carbon skeleton

Dolabellanes **36-39** from the brown alga *Dictyota dichotoma* in Cortadura (Cádiz, Spain) exhibited mild activity *in vitro* cytotoxicity assays against P-388 mouse lymphoma, A549 human lung carcinoma, HT-29 human colon cancer carcinoma, and MEL-28 human melanoma tumor cell lines.[77] Dolabellane **37** exhibited IC_{50} = 1.2 μg/ml against P-388 and A549 tumor cell lines and IC_{50} =2.5 μg/ml against HT-29 and MEL-28 tumor cell lines.[77] Relative stereochemical assignments were made upon analysis of a series of NOE difference spectroscopy experiments.

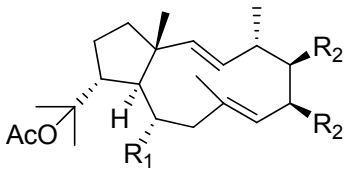

36 R_1 = OH; R_2 = H
37 R_1 = R_2 = H

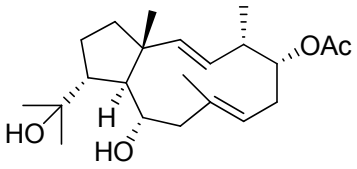

38

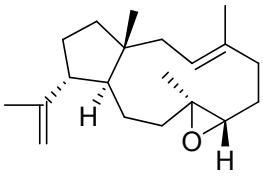

39

From *Dictyota dichotoma* collected near Sicily, Italy, four dolabellanes (**40-43**) were isolated, displaying activity against Gram-positive and Gram-negative bacteria.[78] Moreover, **40** exhibited significant *in vitro* activity against influenza and adenoviruses.[79] As with **36-39**, the relative stereochemistries of dolabellanes **40-43** were determined by NOE.

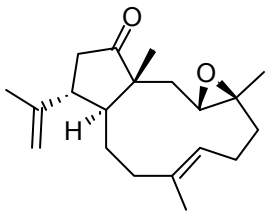

40

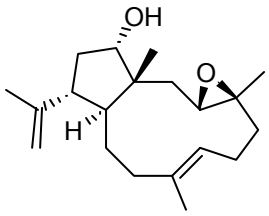

41

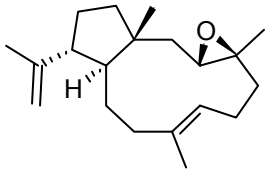

42

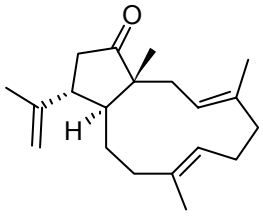

43

The diverse array of functionalities and stereocenters has made dolabellanes a challenge for synthetic chemists, who have helped to establish the absolute configurations of these natural products.[76] Several distinct strategies have been tackled, with macrocyclization as the key reaction.[76] Although macroalgal dolabellane diterpenes exhibit a range of pharmacologically relevant activities, no dolabellane metabolite has yet been pursued for further pharmaceutical development.

Fatty Acid and Polyketide Metabolites

The condensation of C_2 acetate units and their subsequent modification leads to a vast number of polyketide (acetogenin) and fatty acid-based metabolites. Complex structures are biosynthesized via reactions involving alkylation, phenolic oxidative coupling, oxidative cleavage of aromatic rings, cyclization, and the use of extension units other than acetate.[35] These secondary metabolites constitute the second most abundant class found in macroalgae, accounting for 19% of green algal metabolites and 38% of red algal metabolites.[3]

Polyketides

C_{15} Acetogenins

Although C_{15} acetogenins have been isolated from various algal species since the 1970s, novel derivatives are continually being reported, with mono-, di- and tri-, and tetra-cyclic structures possessing enyne and bromoallene functionalities. However, the discovery of acetogenins with new carbon skeletons is now rare. C_{15} acetogenin biological activities are generally weak to moderate.

The red alga *Laurencia obtusa* (Scanlon's Island, Ireland) was found to contain scanlonenyne (**44**), a novel acetogenin with a ketone at C-7.[80] No biological data were reported. A new brominated acetogenin, chinzallene (**45**), was isolated from an unknown species of *Laurencia* in Japanese waters (Chinzei, Saga, Prefecture) and is structurally-related to okamurallene (**46**), which is known from *Laurencia intricata*.[81] Relative stereochemistries of **44-46** were established by analysis of ^{1}H-^{1}H scalar couplings in combination with 2D NOE spectral data.

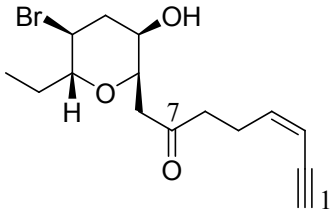

44

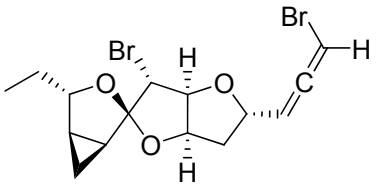

45

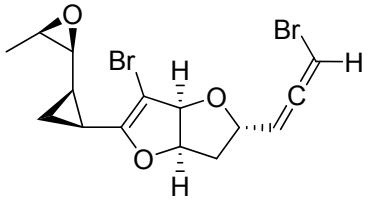

46

While acetogenins have frequently been isolated from *Laurencia* spp., it is unusual to see bromoallene and enyne metabolites co-occurring. Four novel acetogenins, laurendecumallenes A-B (**47-48**) and laurendecumenynes A-B (**49-50**), were discovered in *Laurencia decumbens* (Weizhou Island of Guangzi Province, P.R.

China), suggesting that these functional groups share a common biosynthetic pathway (Figure 2.6).[82] Stereochemical assignments are relative for **47-50**, as established through NOESY experiments.

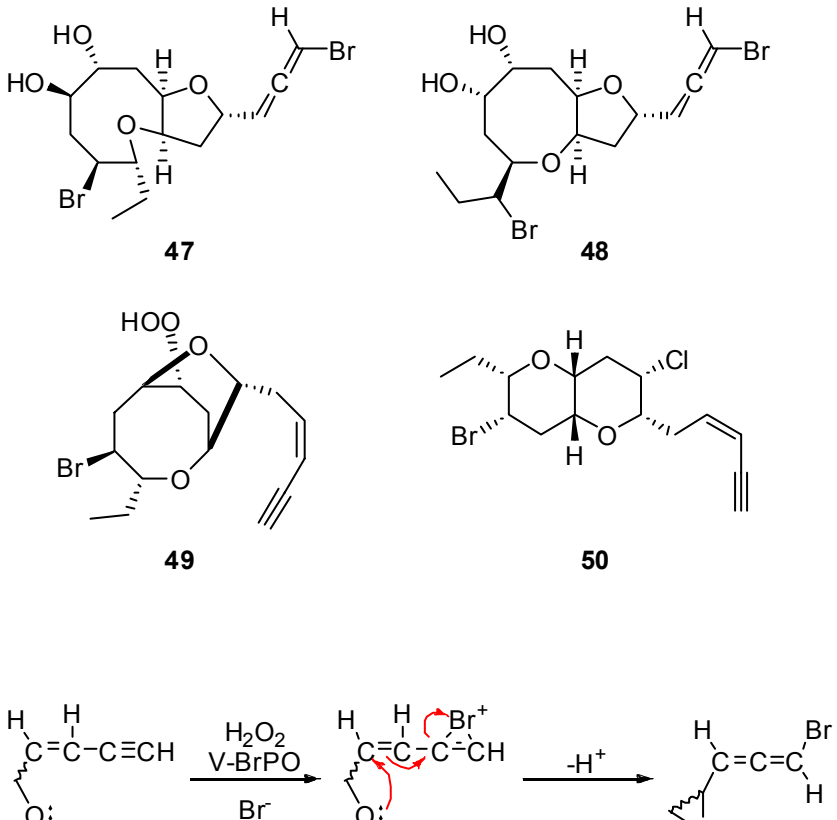

Figure 2.6. Proposed biogenesis of bromoallene from terminal enyne adapted from Ji *et al.* with permission.[82]

While structurally diverse, these known macroalgal acetogenins do not possess exciting pharmacological activities. Moreover, the ecological relevance of this compound class has not been well documented. However, due to the large database of acetogenins isolated from various species of *Laurencia,* many studies have used these metabolites for chemotaxonomic identification of species.[81b]

Lobophorolide

Strong antifungal activity against the marine pathogen *Lindra thalassiae* led to the isolation of lobophorolide (**51**), a polyketide from the brown alga *Lobophora variegata*.[83] Throughout the bioassay-guided fractionation, only **51** or fractions containing it inhibited fungal growth, suggesting that this compound accounts for all of the antifungal activity.[83] Significant antifungal effects were also observed against the human pathogen *Candida albicans* (IC_{50} = 1.3 μg/ml) and against human colon cancer cells (IC_{50} = 0.03 μg/ml). The structural similarity of **51** to tolytoxin[84] from cyanobacteria suggests that **51** is likely the product of a microbial symbiont; however, a putative symbiont has not been discovered to date. The relative and absolute stereochemistry of **51** was proposed to share that of tolytoxin, with the exception of C-6, for which Kubanek *et al.* argued an *R* configuration, as opposed to the *S* configuration proposed by Carmeli *et al.* in tolytoxin. A putative microbial origin was also supported by the patchy geographic distribution of **51** among collections of *L. variegata.*

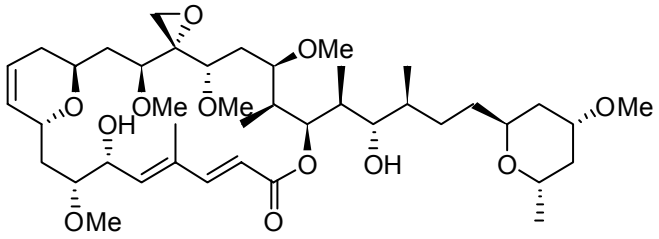

51

Manauealides

Several successive food poisonings reported from ingestion of the Hawaiian red alga *Gracilaria coronopifolia* (Waiehu, Maui) led to the identification of manauealides A-C (**52-54**), aplysiatoxin (**55**), and debromoaplysiatoxin (**56**), with the latter two implicated as causative agents.[85] To date, **51** and **52-56** are the only reports of macrocyclic polyketide metabolites isolated from macroalgae. The absolute configurations of **52-54** were established by comparison of CD spectra of these metabolites with that of **56**,

whose absolute configuration was previously established.[86] As with the case of **51**, Nagai *et al.* suggested that cyanobacteria could be the true producer of these toxins, since **55** and **56** were previously reported from cyanobacteria and a sea hare known to feed on cyanobacteria, and that cyanobacteria were sometimes found growing on *G. coronopifolia*.[87]

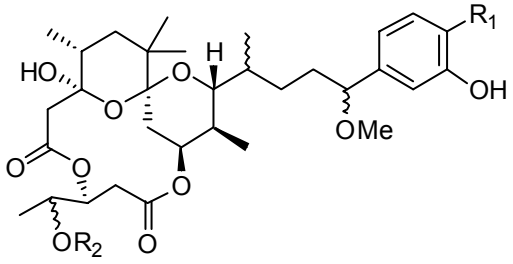

52 R_1 = Cl, R_2 = H
54 R_1 = H, R_2 = $COCH_3$

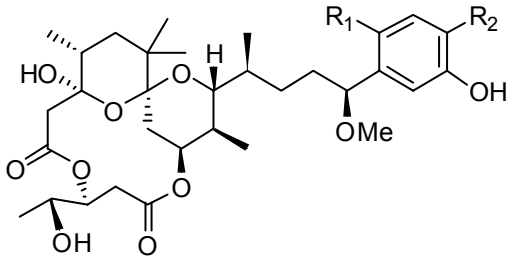

53 R_1 = H, R_2 = Br
55 R_1 = Br, R_2 = H
56 R_1 = H, R_2 = H

Fatty Acids

Acetylenic functionalities, as in peyssonenynes A and B (**57-58**) from the red alga *Peyssonnelia caulifera* (Yanuca Island, Fiji)[88] are rare for macroalgae, with only one previous report of lipid acetylenes, produced by the red alga *Liagora farinosa.*[89] Both **57** and **58** showed similar activity in a DNA methyltransferase (DNMT-1) enzyme inhibition assay, with an IC_{50} = 16 and 9 μM, respectively, but peyssopyrone (**59**), also from *P. caulifera,* was inactive.[88]

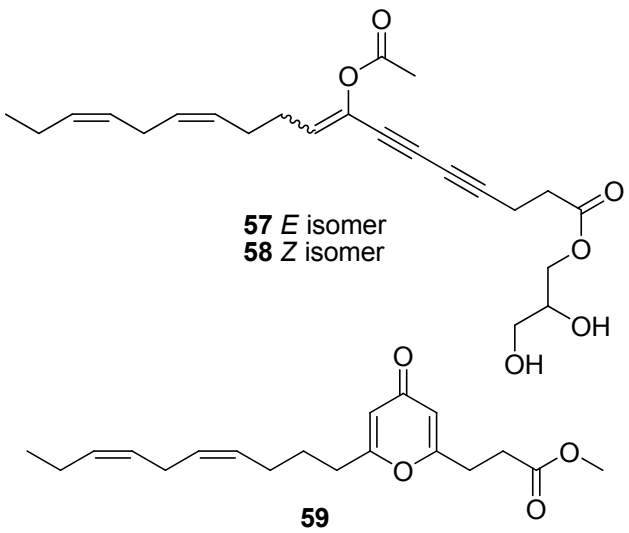

57 *E* isomer
58 *Z* isomer

59

Furanones

Many in-depth ecological studies have been performed using the red alga *Delisea pulchra,* which is known to produce a series of structurally-related brominated furanones (**60-63**).[90] These furanones inhibit fouling and bacterial attachment, acting as antagonists of bacterial communication normally mediated by acylated homoserine lactones, which regulate bacterial swarming and biofilm formation .[91] Dworjanyn *et al.* demonstrated chemically-mediated antifouling effects of furanones using surface extracts of *D. pulchra*, as well as pure furanones tested at natural surface concentrations.[92] These metabolites are also strongly deterrent to many herbivores at natural concentrations.[93] It seems reasonable to suggest that *D. pulchra* is able to compensate for the cost of producing these secondary metabolites by utilizing these furanones as a defense against multiple threats, such as biofouling, antimicrobial colonization, and herbivory.

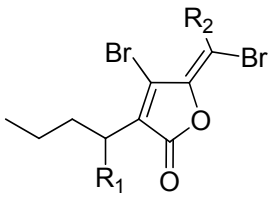

60 R_1 = H, R_2 = Br
61 R_1 = H, R_2 = H
62 R_1 = OAc, R_2 = H
63 R_1 = OH, R_2 = H

Shikimate Metabolites

Shikimic acid (**64**) is the biosynthetic precursor to an array of aromatic compounds, including benzoic and cinnamic acids.[35] This pathway is utilized by microorganisms and plants, but not by animals, who obtain essential shikimate building blocks like phenylalanine from their diets.[35] Red algae are known to be a prolific source of halogenated phenolic metabolites derived from shikimic acid, comprising approximately 5% of known algal metabolites.[3]

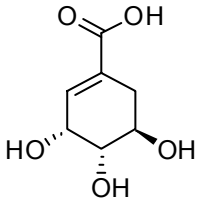

64

Halogenated Phenols

A number of bromophenols have been isolated from the genus *Rhodomela,* exhibiting various biological functions such as feeding deterrents.[94] Antibacterial assays led to the isolation of two new (**65-66**) and three known (**67-69**) bromophenols from the red alga *R. confervoides* (Qingdao, China).[95] Metabolite **69** exhibited moderate activity against *Staphylococcus epidermidis,* with a minimum inhibitory concentration of 35 μg/ml.[95]

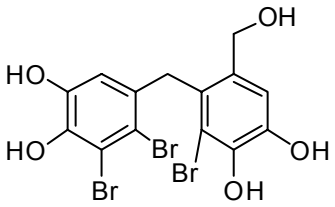

65

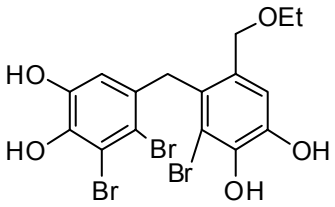

66

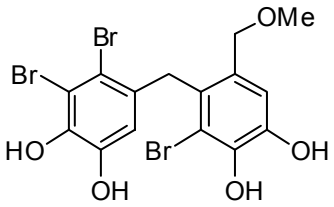

67

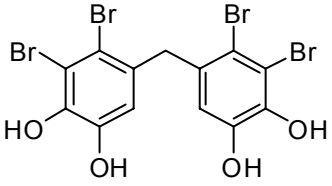

68

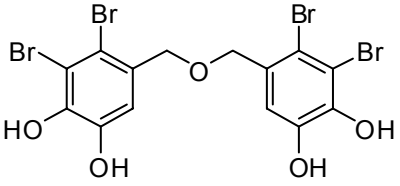

69

Three new (**70-72**) and three known (**73-75**) bromophenols from the red alga *Polysiphonia urceolata* (Qingdao, China), whose absolute configurations were determined by CD spectra, displayed significant radical scavenging activity when compared to known antioxidants, with IC_{50} values of 6-36 μM.[96] The radical scavenging activities of **70-72** were 10-fold to 13-fold more active than the known synthetic antioxidant butylated hydroxytoluene (BHT), making these metabolites potential leads as antioxidant drugs.

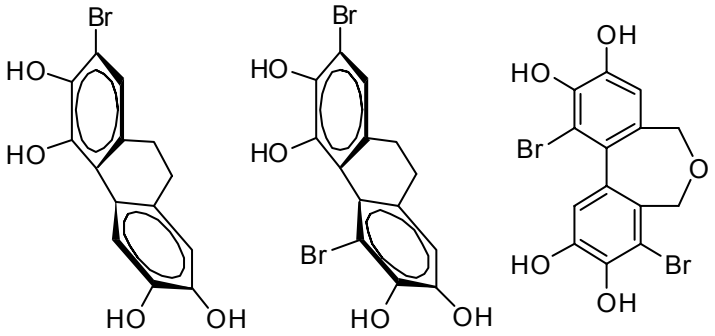

70 **71** **72**

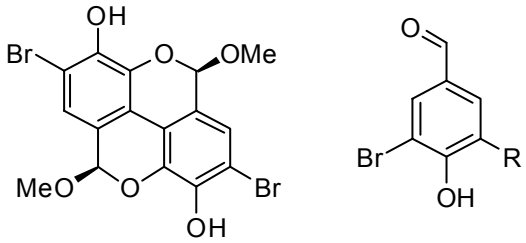

73

74 R = OH
75 R = Br

Nonribosomal Peptide Metabolites

Many natural peptides are synthesized by a sequence of enzyme-controlled processes carried out by a multifunctional enzyme of modular arrangement, similar to some polyketide synthases.[35] These nonribosomal peptide synthetases (NRPS) typically consist of an adenylation domain, a peptidyl carrier protein, and a condensation domain in order to carry out amide bond formation and some derivations of amino acid residues.[35]

Depsipeptides

Depsipeptides are a class of nonribosomal peptides cyclized via an ester bond and often contain nonproteinogenic amino acids. Several bioactive depsipeptides, ranging from a C_{31} tripeptide to a C_{75} tridecapeptide, were isolated from a sacoglossan mollusk, *Elysia rufescens,* and from its algal diet, *Bryopsis* sp. Collectively known as

kahalalides, these peptides display a range of biological activity. Kahalalide A (**76**) displayed moderate antimalarial activity and has been noted for its *in vitro* effects against *Mycobacterium tuberculosis*, while kahalalide E (**77**) selectively inhibits *Herpes simplex* II virus (HSV II).[97] Kahalalide F (**78**), whose absolute stereochemistry was determined by chemical degradation,[98] exhibits activity against select solid tumors and some AIDS-opportunistic infections, and is currently undergoing phase II clinical trials.[5c, 9a] Hill *et al.* reported strains of kahalalide-producing *Vibrio* sp. bacteria associated with *Bryopsis* sp. and *E. rufescens,* which suggests a microbial origin of these depsipeptides; however, natural product chemists await full description of this work in the peer-reviewed literature.[99]

Kahalalide G (**79**), the linear peptide form of **78**, has so far been found to be inactive in all bioassays.[97] To date, 17 kahalalides have been isolated and characterized from *Bryopsis* sp., but **78** remains the only kahalalide to advance to clinical trials for the possible treatment of lung cancer, other tumors, and AIDS.[100]

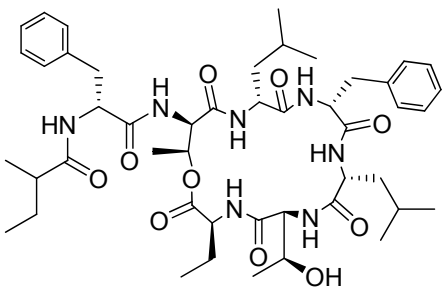

76

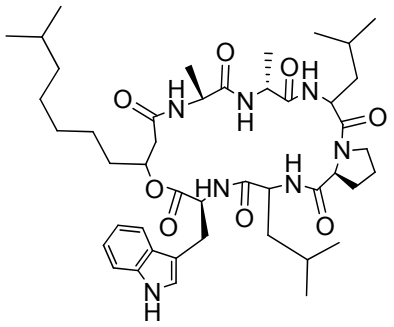

77

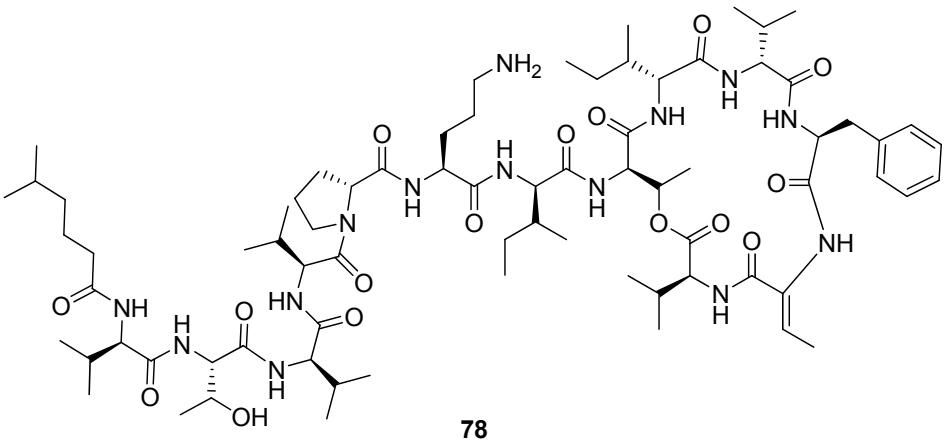

78

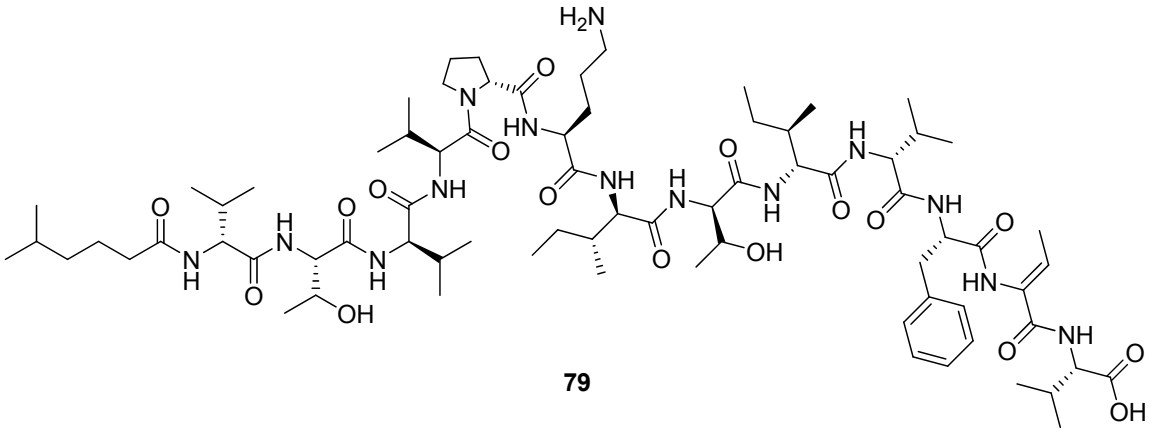

79

Alkaloid Metabolites

Algal compounds are rarely nitrogenous, possibly because macroalgae are often nitrogen-limited.[101] However, a handful of non-peptide, nitrogen-containing metabolites that possess interesting biological activity has been reported from macroalgae.

Indole Metabolites

Red algae of the genus *Chondria* are known for the production of cyclic polysulfides and terpenoids.[102] An unidentified species of *Chondria* (Buenos Aires, Argentina) was found to produce novel indolic metabolites, chondriamides A-B (**80-81**), with antiviral, antifungal and cytotoxic activities.[103] Chondriamide A (**80**) exhibited antiviral activity against HSV II with IC_{50} = 1 µg/ml, while **81** displayed antifungal activity against *Aspergillus oryzae* and *Trichonphyton mentagrophytes*.[103] Furthermore, **80-81** displayed moderate cytotoxicity against KB cell lines, with IC_{50} values of 0.5 µg/ml and <1 µg/ml, respectively.[104] Chondriamide C (**82**), from *Chondria atropurpurea*, exhibited *in vitro* anthelmintic activity against *Nippostrongylus brasiliensis* with EC_{80} of 90 µM.[105] Kuramochi *et al.* reported a total synthesis of **80** and **82** using a newly developed approach based on the Curtius rearrangement and acylation of alkenylcarbamate.[106]

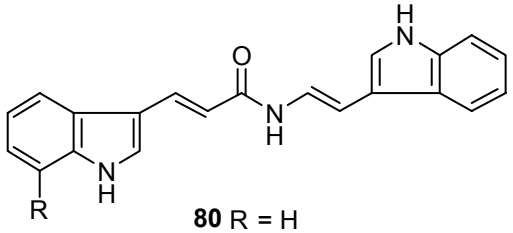

80 R = H
81 R = OH

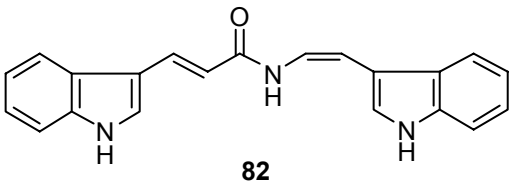

82

Almazoles A-B (**83-84**) were isolated from an unknown red algal species of *Haraldiophyllum* (Dakar, Senegal) containing a rare 2,5-disubstituted oxazole ring.[107] After recollection of *Haraldiophyllum* sp. some years later, **83-84** were not observed, perhaps because of geographic variation or compound instability, but another novel indole bearing an oxazolone ring, almazolone (**85**), was discovered.[108] Almazolone (**85**) was isolated as an 88:12 mixture of Z/E isomers, due to the photochemical and thermal instability of the compound. Guella *et al.* also synthesized **85** by condensation of indole-3-carboxaldehyde with 3-phenylpropionyl glycine.[108]

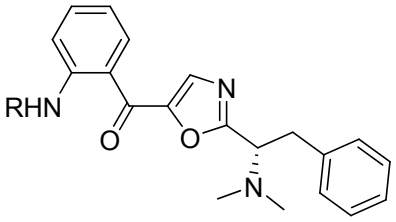

83 R = CHO
84 R = H

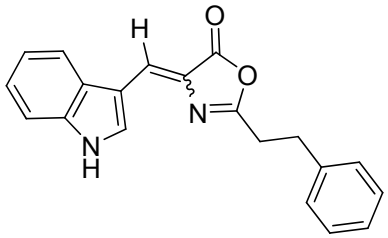

85

2,7-Naphthyridines

Gross *et al.* discovered two novel 2,7-naphthyridine metabolites, lophocladines A and B (**86-87**), from an unknown and understudied red alga species *Lophocladia* (Savusavu, Fiji Islands).[109] The only other naturally-occurring representative of this compound class comes from the terrestrial plant *Valeriana officinalis*.[110] Lophocladine B (**87**) exhibited moderate activity against lung and breast cancer cells, with IC_{50} values of 64.6 and 3.1 μg/ml, respectively, whereas **86** was found to be inactive in all assays.[109] NCI-H460 lung cancer cells showed morphologic changes when treated with **87**, depolymerizing 85% of the microtubules at 45 μM, but the potency of **87** is rather moderate when compared to other tubulin depolymerizing compounds.[109]

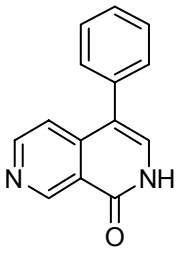

86

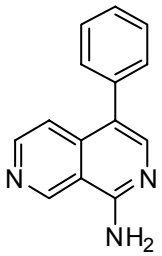

87

Glycolipids

Carbohydrates are one of the more common components of plants, animals, and microorganisms, with six-carbon sugars (hexoses) and five-carbon sugars (pentoses) being the most commonly encountered carbohydrate unit.[35] Medicinally-important natural products are frequented with various sugar units to form a class of compounds known as glycosides.[35] Macroalgae are known to produce a handful of biologically-active glycosides, representing another exciting class for pharmacological research.

The red alga *Gracilaria asiatica* (Indonesia) was found to produce gracilarioside (**88**) and gracilamides (**89-90**), possessing unusual cyclopropane-containing alkyl chains.[111] This was the first report of naturally-occurring marine ceramides with a cyclopropane ring. Fatty acid chain lengths and cyclopropane ring positions were determined using microscale chemical degradation. Furthermore, absolute configurations of **88-90** were established through a combination of chemical degradation and CD spectral analyses. These metabolites exhibited weak activity against melanoma cells, with 18.2% cell death at 20 µg/ml for **88** and 11.7% cell death at 30 µg/ml for **89-90**.[111]

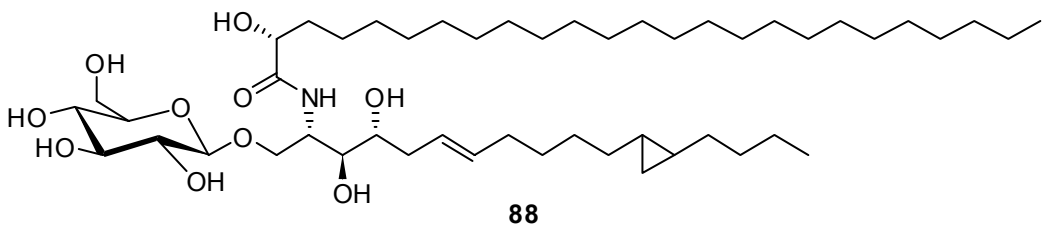

88

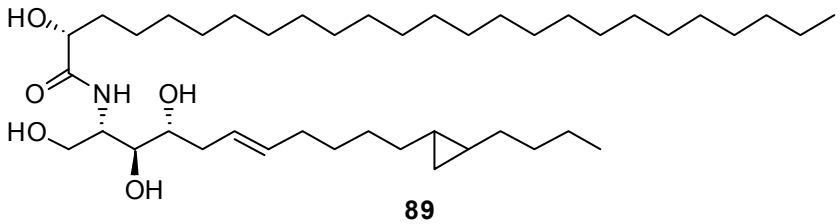

89

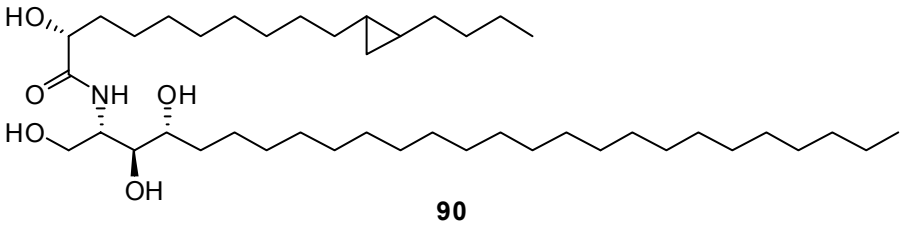

90

Human intoxication resulting after ingestion of the red alga *Polycavernosa tsudai* (Tanguisson Beach, Guam, previously called *Gracilaria edulis*) led to the isolation of toxic glycosidic macrolides, polycavernosides (**91-97**), with polycavernoside A (**91**) reported as the illness-causing agent.[112] The toxicity of **91** in mouse bioassays was established as 0.2-0.4 mg/kg, with human symptoms including diarrhea, vomiting, paresthesia, loss of consciousness, and in extreme cases, death.[112a, 113] Total synthesis of **91** was reported by Fujiwara and Murai and thus the absolute configuration of **91** was determined by CD analysis.[114] No reports have been published on the ecological role of these toxins in the producing organism.

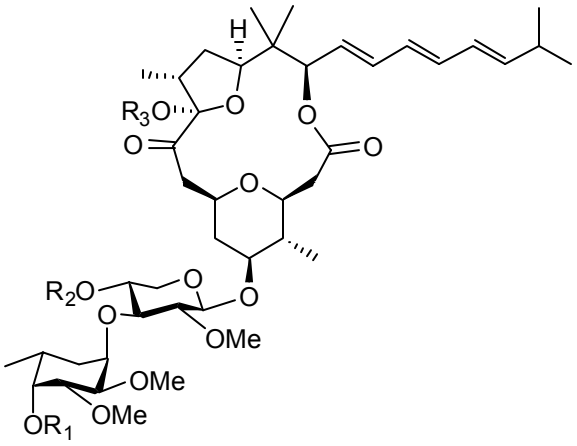

91 R_1 = H, R_2 = Me, R_3 = H
92 R_1 = H, R_2 = H, R_3 = H
93 R_1 = Me, R_2 = Me, R_3 = H
94 R_1 = Me, R_2 = Ac, R_3 = H
95 R_1 = Me, R_2 = H, R_3 = H
96 R_1 = Me, R_2 = Ac, R_3 = Me
97 R_1 = Me, R_2 = Me, R_3 = Me

A highly active antimitotic extract from the green alga *Avrainvillea nigricans* (Portsmouth, Dominica) yielded two novel glycolipids, nigricanosides A-B (**98-99**), representing a new class of ether-linked glycoglycerolipids.[115] Nigricanoside A dimethyl ester (**100**) was found to arrest human breast cancer MCF-7 cells in mitosis with IC_{50} = 3 nM, stimulating polymerization of tubulin.[115] Hydrogenation of the alkenes significantly reduced activity against the MCF-7 cells, establishing their importance. The ability of the potent nigricanosides to promote tubulin polymerization is without precedent among previously known glycoglycerolipids, making these metabolites an exciting anticancer drug lead.[115]

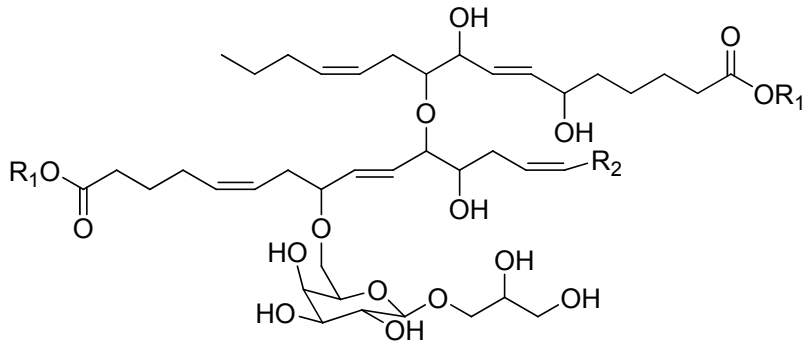

98 R_1 = H, R_2 = 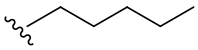

99 R_1 = H, R_2 = 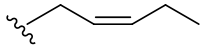

100 R_1 = Me, R_2 = 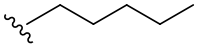

101 R_1 = Me, R_2 = 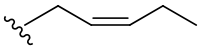

Conclusion

Structurally-diverse, bioactive metabolites are continually being reported from macroalgae. The rate of new natural product discovery increased substantially in the 1990's and has continued to increase through the 2000's, particularly from red macroalgae (Figure 2.1). However, it should be noted that most recent discoveries are featured in more specialized journals than in the early years and the discovery of new structural classes of secondary metabolites from macroalgae has become rare. Properties of macroalgal natural products range from pharmacological activities, such as antitumor, antimicrobial, and antiviral effects, to ecological roles such as herbivore deterrence and antimicrobial defenses. The large numbers of known isoprenoids and phenolic compounds lacking significant pharmacological activities make these structural classes less stimulating for future discoveries for pharmaceutical leads. However, rare and/or understudied macroalgal species could be promising for the discovery of new and exciting secondary metabolites, including compounds of mixed biogenesis. Some of the most structurally-complex and biologically-active molecules reported recently from macroalgae may in fact originate from marine microbes, which are a yet-underexplored

source of chemical innovation. Continued research on bioactive macroalgal natural products could stimulate the identification of structurally novel compounds as well as intriguing syntheses of compounds for biological and pharmacological research.

CHAPTER 3

UNUSUAL ANTIMALARIAL MERODITERPENES FROM FIJIAN RED MACROALGAE

Natural products have been the source of the most successful antimalarial drugs to date, including notably the quinines and artemisinins.[11, 17] The design and development of many synthetic antimalarial drugs has largely been inspired by these and other antimalarial natural products.[11] Thus, the discovery of novel chemistry from natural sources could provide new scaffolds for the development of much needed antimalarial treatments.

We previously discovered a structurally-novel class of brominated meroditerpene macrolides and non-macrocyclic metabolites, called bromophycolides and callophycoic acids, respectively, from the Fijian red macroalga *Callophycus serratus*.[18, 44] Our efforts to uncover antimalarial natural products from understudied tropical red macroalgae led us to continue exploring metabolites responsible for the potent antimalarial activity from two red algae in our library, *C. serratus* and the coralline alga *Amphiroa crassa*. Bioassay-guided fractionation led to the identification of an unusual non-brominated macrolide we named callophycolide A (**1**)[18c]; additional bromophycolides L (**2**), N (**3**) and O (**4**)[18b]; and callophycoic acids C (**5**) and D (**6**)[18a] from *C. serratus*. Two known tocopherols, β-tocopherylhydroquinone (**13**) and δ-tocopherylhydroquinone (**14**) were isolated from *A. crassa* (Figure 3.1).[18c]

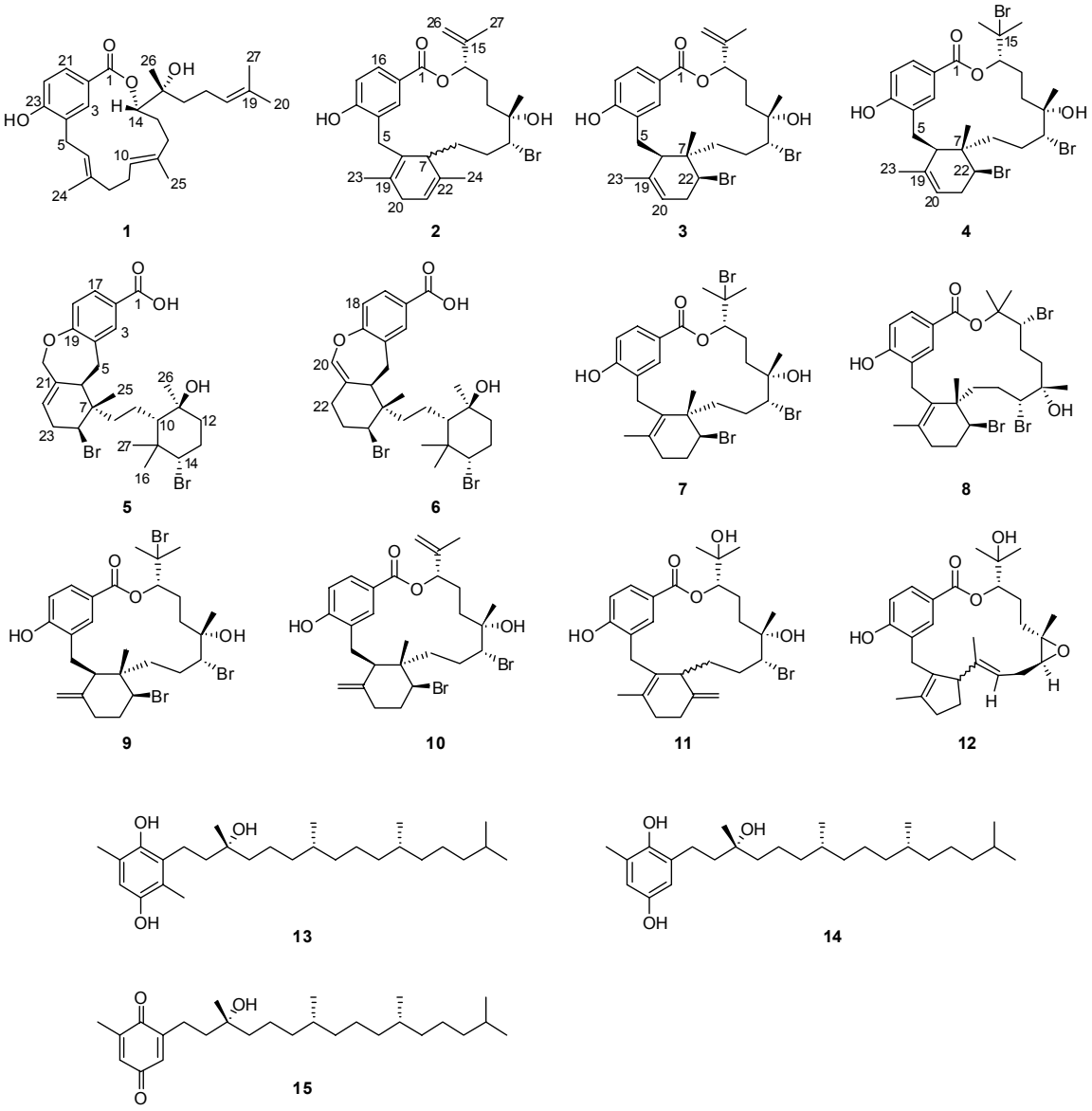

Figure 3.1. Meroditerpenes isolated from Fijian red macroalgae. Callophycolide A (**1**), bromophycolides L (**2**), N (**3**), and O (**4**), callophycoic acid C (**5**) and D (**6**), bromophycolides A (**7**), B (**8**), D (**9**), E (**10**), K (**11**) and debromophycolide A (**12**) were isolated from *Callophycus serratus*.[18, 44a, b] β-Tocopherylhydroquinone (**13**) and δ-tocopherylhydroquinone (**14**) were isolated from *Amphiroa crassa*. δ-tocopherylquinone (**15**) is an oxidation product of **14**.[18c]

Unlike previously isolated bromophycolides[44a, b], callophycolide A (**1**) did not display a characteristic brominated isotopic pattern with HRESIMS, but showed an $[M + H]^+$ *m/z* of 427.2825, appropriate for a formula of $C_{27}H_{38}O_4$. The *p*-hydroxybenzoate segment common to all reported *C. serratus* secondary metabolites[18a, b, 44] remained intact, apparent from the ^{13}C and ^{1}H NMR chemical shifts for positions 3 (δ_C 131.1; δ_H 7.85), 21 (δ_C 129.6; δ_H 7.73), 22 (δ_C 114.8; δ_H 6.78), and 23 (δ_C 158.0; OH δ_H 5.83). HMBC correlations from H_2-5 (δ 3.17, 3.49) to C-3, C-4 (δ 127.7), and C-23 connected the C-5 methylene to the *p*-hydroxybenzoate fragment, as in other bromophycolides, but surprisingly C-5 was not connected to a substituted cyclohexene. Instead, a linear isoprene unit was established through COSY correlations between both H_2-5 protons and H-6 (δ 5.45), as well as HMBC correlations from Me-24 (δ 1.60) to C-6 (δ 122.7), C-7 (δ 136.8), and C-8 (δ 39.3). COSY correlations failed to establish the vicinal relationship of H_2-8 (δ 2.17, 2.27) and H_2-9 (δ 2.15, 2.23) due to substantial chemical shift overlap; instead, HSQC-TOCSY correlations were used to connect well-resolved carbons at C-8 and C-9 (δ 23.8; Figure 3.2). COSY correlations between both H_2-9 protons and H-10 (δ 5.19) and HMBC correlations from Me-25 (δ 1.59) to C-10 (δ 123.5), C-11 (δ 135.2), and C-12 (δ 35.8) connected a second isoprene unit within **1**. HMBC correlations from H-14 (δ 4.75) to C-1 (δ 169.2), C-12 (δ 35.8), C-13 (δ 29.2), C-15 (δ 74.8), and Me-26 (δ_C 22.0) provided strong evidence in support of a macrocyclic lactone framework and accounted for a third isoprene fragment. Me-26 (δ_H 1.16) showed strong HMBC signals to C-14 (δ 82.1), C-15, and C-16 (δ 40.0), while vicinal COSY correlations established a C-16—C-17—C-18 connectivity. Allylic coupling was observed with weak COSY correlations between H-18 (δ 5.10) and both Me-20 (δ 1.66) and Me-27 (δ 1.60), establishing the diterpene head. This structural feature was further confirmed by HMBC

correlations from both Me-20 and Me-27 to C-18 (δ 124.3), C-19 (δ 131.8), and to each other, completing the planar connectivity of **1**.

ROESY data were used to assign the configurations of the olefins within the macrocyclic ring of **1**. NOEs observed between H-6 and both H_2-8 protons and between H_b-5 (δ 3.49) and Me-24 (δ 1.60) supported an *E* configuration for $\Delta^{6,7}$. Similarly, ROESY correlations between H-10 (δ 5.19) and H_a-12 (δ 1.87) as well as between H_b-9 (δ 2.23) and Me-25 (δ 1.59) suggested an *E* configuration for $\Delta^{10,11}$ (Figure 3.2).

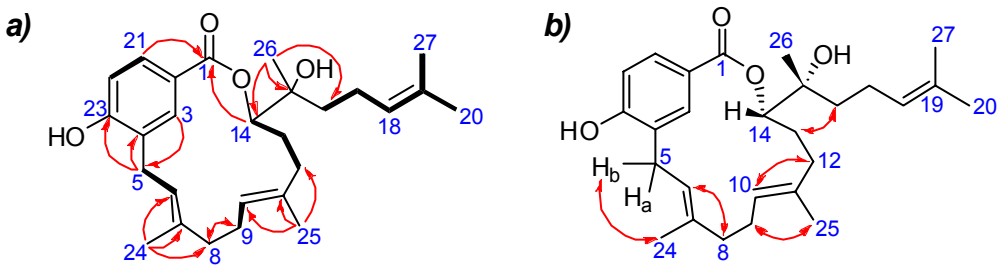

Figure 3.2. Key 2D NMR spectroscopic correlations establishing the connectivity of callophycolide A. (a) ^{1}H-^{1}H COSY (bold), HMBC (red single-headed arrows), and HSQC-TOCSY (blue double-headed arrow) correlations; (b) ROESY (red double-headed arrows) correlations establishing configurations for macrocyclic olefins in **1**.

Absolute configuration at C-14 was determined by analysis of Mosher ester data[116] derived from the methanolysis product **16** (Figure 3.3). Methanolysis product **16** was acylated with each of *R*-(−)- and *S*-(+)-α-methoxy-α-(trifluoromethyl)phenylacetyl chloride (MTPA-Cl) to produce the corresponding *S*- and *R*-MTPA esters **16a** and **16b**, respectively. Analysis of the ^{1}H NMR and HSQC-TOCSY spectra obtained for both esters permitted the assignment of the proton chemical shifts in proximity of the esterified carbon. Calculation of the $\Delta\delta_{S-R}$ values established the absolute configuration of C-14 as *S* based upon empirical rules proposed by Ohtani *et al.*[116] (Figure 3.3).

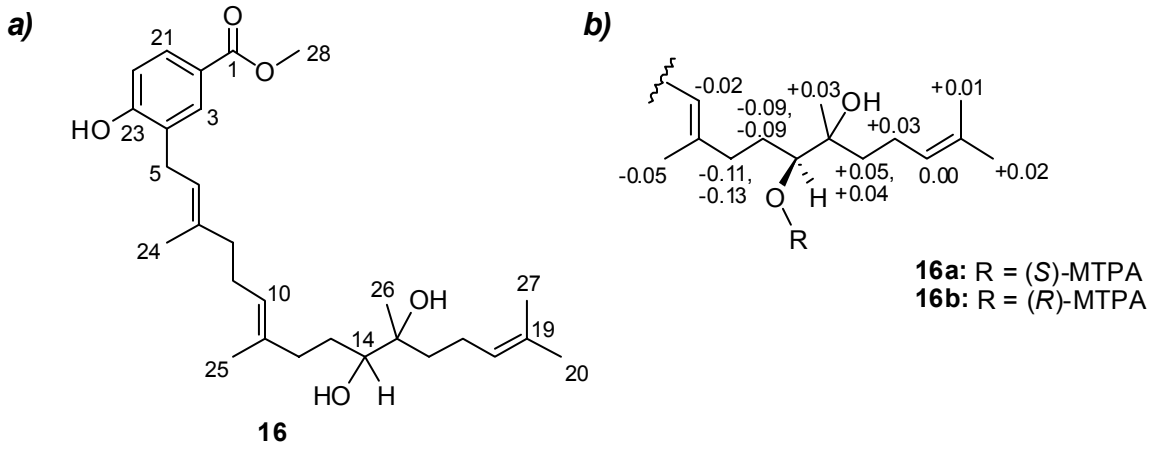

Figure 3.3. Mosher's ester analysis of callophycolide A (**1**). (a) methanolysis product **16**; (b) and $\Delta\delta_{S-R}$ values (ppm) for Mosher esters **16a** and **16b** from **16**.

Solution of the configuration at C-15 proved to be challenging relative to other stereocenters in **1**. Frelek *et al.* reported a circular dichroism (CD) spectroscopic method for determining the absolute configuration of restricted and flexible vicinal diols complexed with dimolybdenum tetraacetate.[117] After ligation to Mo_2, free-rotation about flexible diols is substantially reduced due to steric requirements of the transition metal complex. The energetically preferred conformation of a flexible diol ligated to Mo_2 in a bidentate fashion is an antiperiplanar orientation of the O—C—C—R groups, with the bulky R-groups pointing away from the Mo_2 complex and the vicinal diols in a *gauche* conformation.[117b] The CD spectrum of the *in situ* formed Mo_2 complex with **16** showed a negative Cotton effect at 310 nm, which corresponded to a negative O—C—C—O dihedral angle (Figure 3.4a) as predicted by the helicity rule proposed by Frelek *et al*.[117] Molecular modeling of a 14*S*, 15*S* configuration in accordance with the lowest energy conformation predicted a positive O—C—C—O dihedral angle, ruling out this diastereomer and suggesting a 14*S*, 15*R* configuration, whose preferred conformation of

the dimolybdenum complex could have yielded either a positive or negative torsional angle. A stable conformation of **1** should involve intramolecular hydrogen bonding between the C-15 hydroxy and C-1 carbonyl. This places the C-15 hydroxy *anti* to H-14 which is supported by NOEs observed between H-14 and both H_b-16 (δ 1.52) and Me-26; however this conformation is feasible for both 15*R* and 15*S*. An NOE correlation from H_b-16 to H_b-13 (δ 2.03) could differentiate between a 15*R* or 15*S* configuration (Figure 3.4b), and inspection of 1D NOE spectra (irradiating H_b-16, acquired at -10 ºC) showed the presence of this correlation. Lack of NOEs between H_2-13 protons and Me-26 implied an *anti* conformation of these groups and further supported a 15*R* stereochemical assignment (Figure 3.4b). Overall, the combination of Mosher's ester analysis, CD analysis with a dimolybdenum tetraacetate complex, and conformational analysis using NOEs argue strongly for an absolute stereochemistry of 14*S*, 15*R* for **1**.

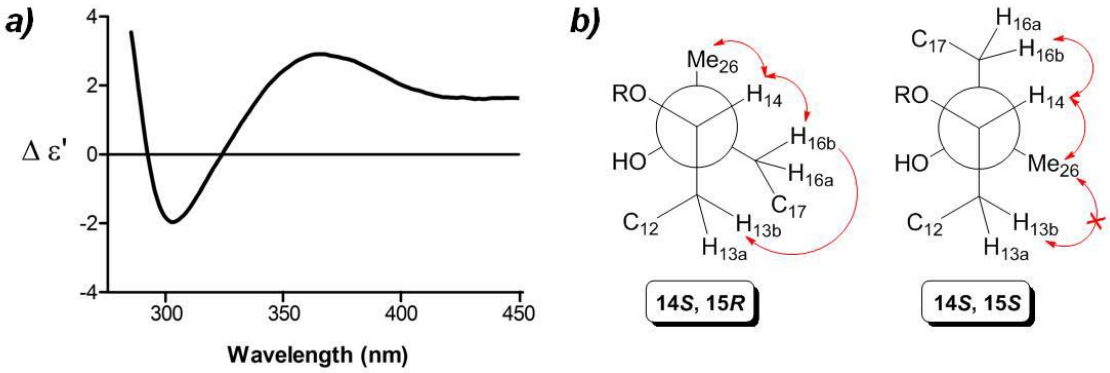

Figure 3.4. Analysis of C-15 stereochemistry in **1**. (a) CD spectrum of the *in situ* Mo_2-complex formed with methanolysis product **16**; (b) Observed NOE correlations (ROESY = double-headed arrow; 1D NOE = single-headed arrow) used to establish the relative stereochemistry at C-15 as *R* in **1**. NOEs that were not observed are indicated by an "x" through the arrow.

High resolution mass spectral data indicated that bromophycolide L (**2**) differed from the previously identified bromophycolide K (**11**)[18b] by a loss of one H_2O molecule, displaying an $[M - H]^-$ *m/z* of 501.1677, appropriate for a molecular formula of $C_{27}H_{35}O_4Br$. HMBC correlations from Me-27 (δ 1.79) to C-14 (δ 74.9), C-15 (δ 140.7), and C-26 (δ 111.5) suggested an isopropenyl diterpene head identical with that of bromophycolide E (**10**)[44b] (Appendix A). Likewise, HMBC correlations from both H-26 vinyl protons (δ 4.98, 5.07) to C-14, C-15, and C-27 (δ 19.5) confirmed this connectivity. Evaluation of ^1H, COSY, and HMBC NMR spectral data of **2** to that of **11** indicated an additional difference within the terpene carbocyclic system. HMBC correlations from Me-24 (δ 1.38) to C-7 (δ 49.0), C-21 (δ 122.5), and C-22 (δ 138.8) suggested that the rearranged terpene skeleton was present as in **11**; however, the unsaturation was determined to be endocyclic at $\Delta^{21,22}$ through COSY correlations of olefinic H-21 (δ 4.81) with H-20b (δ 2.42) and a weak long range COSY correlation between H-21 and Me-24 (Appendix A).

For **2**, similar NOEs were observed as for **10**, suggesting a 10*R,* 11*S,* 14*S* configuration.[44b] NOEs were present between H-7 (δ 3.41) and H-20b, located 1,4 relative to each other across their six-membered ring, thus suggesting a pseudo-boat conformation of this ring. The lack of stereocenters near C-7 prevented stereochemical assignment at this position, given that an *R* or *S* configuration would be expected to result in NOEs between the axial protons H-7 and H-20b.

The mass spectrum of bromophycolide N (**3**), with $[M - H]^-$ *m/z* of 581.0907, suggested yet another regioisomer of **10**, with a molecular formula of $C_{27}H_{36}O_4Br_2$. Comparison of ^1H, COSY, and HMBC NMR spectral data of **3** with that of **10** suggested a difference in the cyclohexenyl double bond. HMBC correlations observed from Me-23 (δ 1.50) to C-6 (δ 47.8), C-19 (δ 137.2), and C-20 (δ 120.3), along with COSY

correlations between both H-5 protons (δ 2.60, 2.83) and H-6 (δ 2.67), supported the $\Delta^{19,20}$ assignment. Because similar NOEs were observed for **3** as for **10**, 6*R*, 7*S*, 10*R*, 11*S*, 14*S*, 22*S* stereochemistry was proposed for **3** (Appendix A).

Bromophycolide O (**4**) exhibited an $[M - H]^-$ *m/z* of 661.0182 with a tribrominated isotopic pattern, appropriate for a molecular formula of $C_{27}H_{37}O_4Br_3$ as seen with bromophycolides A (**7**), B (**8**), and D (**9**). Inspection of 1D and 2D NMR spectral data of **4** suggested yet another 15-membered macrocyclic skeleton. As with **3**, regioisomerization of the cyclohexenyl double bond to $\Delta^{19,20}$ was supported by observation of HMBC correlations from Me-23 (δ 1.65) to C-6 (δ 43.7), C-19 (δ 135.8), and C-20 (δ 119.4), as well as COSY correlations between H-5a (δ 2.82) and H-6 (δ 2.84) and a long-range COSY correlation between Me-23 and H-20 (δ 5.33). Similar NOEs were observed for **4** as with **7** and **9**, thus a 6*R*, 7*S*, 10*R*, 11*S*, 14*S*, 22*S* stereochemistry was inferred for **4**.

Callophycoic acid C (**5**) gave a parent ion at *m/z* 581.0895, supporting a molecular formula of $C_{27}H_{36}O_4Br_2$. Callophycoic acids A[18a] and C (**5**) exhibited nearly identical ^1H and ^{13}C chemical shifts and 2D NMR correlations for C-1 through C-8 and C-17 through C-25 (Appendix A), indicating these molecules shared a common tricyclic structure. However, substantial differences in chemical shifts and 2D NMR correlations were found in the diterpenoid head. Assessment of sites of unsaturation indicated that this group included one more ring system than callophycoic acid A. COSY correlations were observed between H-8 (δ 1.78, δ 2.16) and H-9 (δ 1.41, δ 1.46), establishing connectivity between these methylenes. Likewise, COSY correlations between H-9 and H-10 (δ 1.29) established connectivity between these carbons, an assignment further supported by an HMBC correlation from H-10 to C-9 (δ 20.8). This proton also exhibited HMBC correlations to quaternary C-11 (δ 73.0) and C-15 (δ 41.6), and methyl C-16 (δ 30.8), establishing C-11—C-10—C-15—C-16 connectivity. In **5**, the singlets Me-16

(δ 1.16) and Me-27 (δ 0.87) shared identical HMBC correlations to C-10 (δ 57.6), C-14 (δ 68.9), and C-15, as well as to each other. These correlations were thus a starting point for establishing connectivity within spin systems of the cyclohexanol ring through COSY and additional HMBC correlations. Hydroxy and bromine groups were assigned at C-11 and C-14, respectively, on the basis of carbon and proton chemical shift arguments.

NOEs for the tricyclic moiety of **5** matched closely those of callophycoic acid A for which X-ray crystallography established absolute configuration, leading us to predict 6*R*, 7*S*, and 24*S* absolute configurations for **5**. Relative stereochemistry within the cyclohexanol ring was then established based on observed NOEs. First, H-10 and H-14 were assigned to diaxial positions on the same face of the ring, with NOEs observed between these protons. The diaxial orientation of these protons supported a chair conformation for the cyclohexanol ring, with the bulky alkyl substituent on C-10 and bromine on C-14 assigned equatorial positions. Me-16 was then assigned to an equatorial position on the same face as H-10 and H-14, based on NOEs between both of these protons and Me-16, an assignment further supported by the lack of NOEs between H-10 or H-14 and axial Me-27. Finally, Me-26 was assigned in an axial position on the opposite side of the ring to H-10 and H-14, based on an NOE between Me-26 and Me-27, and supported by the absence of an NOE between Me-26 and H-10 or H-14.

With the relative stereochemistry of the cyclohexanol moiety of **5** elucidated, the absolute stereochemistry of this ring was determined with a series of NOEs that established the orientation of this ring relative to the 6*R*, 7*S,* 24*S* tricycle. First, the conformation of the bond between C-9 and C-10 was determined by NOEs between H-9a and both Me-16 and Me-27, which supported H-9a pointing towards these two methyls. This assignment was further supported by the lack of an NOE between H-9a and Me-26. An NOE between H-9b and Me-26, but not between H-9b and Me-16 or Me-27, analogously prompted placement of H-9b pointing towards Me-26, thus establishing

the dominant conformation of the C-9—C-10 bond. Next, NOEs were observed between H-9a and H-24 and between H-9b and H-6, supporting a conformational preference of H-9a, Me-16, H-24, and Me-27 on one side of the molecule and H-9b, H-6, and Me-26 on the other side. Based on these correlations, a 10*S*, 11*S*, 14*S* stereochemistry was assigned for the cyclohexanol ring. The enantiomer (10*R*, 11*R*, 14*R*) should instead afford NOEs between H-9b and H-24 and between H-9a and H-6, but these correlations were not observed, thus confirming the cyclohexanol stereochemistry.

Callophycoic acid D (**6**) appeared structurally similar to **5**, with an identical molecular formula ($C_{27}H_{36}O_4Br_2$ from $[M-H]^-$ *m/z* 581.0889). The major difference between **5** and **6** occurred in the tricyclic moiety. ^1H and ^{13}C chemical shifts, and HMBC and COSY correlations for this group closely matched those observed for callophycoic acid B,[18a] prompting assignment of a tricycle with $\Delta^{20,21}$, as opposed to the $\Delta^{21,22}$ observed in **5**. The stereochemistry of **6** was established as 6*R*, 7*S,* 10*S*, 11*S*, 14*S*, 24*S* and the $\Delta^{20,21}$ olefin was assigned a *cis* conformation on the basis of NOE arguments analogous to those for **5**.

Previously reported bromophycolides and related non-macrocyclic callophycoic acids and callophycols[18a, 44a, b] exhibit antimalarial IC_{50} values ranging from 0.3 to >100 μM, providing a detailed structure-activity relationship (SAR) analysis for this class of compounds (bioactivity of select compounds listed in Table 3.1).[18b] The identification of **1** provides additional insight into the SAR for the 33 known *C. serratus* metabolites, in that **1** retains moderate antimalarial activity (IC_{50} = 5.2 μM, Table 3.1) despite the complete absence of bromine atoms, similar to debromophycolide A (**12**), whose antimalarial IC_{50} is > 100 μM. Furthermore, **1** has a carbon skeleton different than other bromophycolides, although its skeleton is not unprecedented and is shared with tocopherols.[118] The lactonization pattern through C-14 in **1** is unique, and the absence of a substituted

cyclohexene ring (compared to **7**, IC_{50} = 0.7 μM) suggests that this ring is not essential but can enhance antimalarial activity. Macrolides **3-4**, **7-10**, representing both 15- and 16-membered lactone frameworks, exhibited potent antimalarial activity with IC_{50} values of 0.3-4.8 μM, suggesting that neither mode of lactonization confers an inherent bioactivity advantage. Furthermore, a macrolide motif appears to be essential for antimalarial activity, considering that non-macrocyclic metabolites **5-6** were less active against *P. falciparum* (IC_{50} values of 59 and 76 μM, respectively).

While all tested *C. serratus* metabolites exhibited moderate anticancer activity against a panel of 12 human tumor cell lines, only **3** displayed some cell line selectivity, with an IC_{50} of 1.5 μM against the breast tumor cell line DU4475, the most sensitive cancer tested (Table 3.2). Callophycolide A (**1**) and all tested bromophycolides inhibited bacterial growth in the low micromolar range but most were ineffective at deterring growth of human pathogenic fungi and *Mycobacterium tuberculosis* (Table 3.1).

Table 3.1. Anti-infective activity of **1-15**.[18, 44a, b]

	antimalarial activity	antimicrobial MIC (μM)			
cmpd	IC_{50} (μM)	MRSA[a]	VREF[b]	*M. tuberculosis*	ARCA[c]
1	5.2	9.1	9.1	12	>250
2	9.8	8.2	26	49	46
3	1.4	13	13	>50	44
4	1.4	13	25	NT	>100
5	59	NT	NT	>100	NT
6	76	NT	NT	>100	NT
7	0.7	5.9	5.9	11	49
8	4.8	5.9	3.0	49	49
9	0.3	NT	NT	1.1	NT
10	0.8	NT	NT	95	NT
11	44	NT	NT	NT	NT
12	>100	NT	NT	>100	>500

Table 3.1 continued

13	190	>500	>500	NT	NT
14	220	>500	>500	>100	NT
15	10	>500	>500	NT	>500

[a]Methicillin-resistant *Staphylococcus aureus*; [b]Vancomycin-resistant *Enterococcus faecium*; [c]Amphotericin B-resistant *Candida albicans*; NT indicates not tested due to insufficient material

Table 3.2. Anticancer activity of **1-15**.[18, 44a, b]

cmpd	anticancer activity IC_{50} (μM)	
	mean[a]	cell line selectivity (IC_{50} max/IC_{50} min)
1	16	3.0
2	NT	-
3	8.6	15
4	9.7	3.5
5	21	1.7
6	23	1.5
7	6.7	4.8
8	28	3.8
9	9.0	2.3
10	12	6.4
11	31	3.6
12	>76	-
13	>25	-
14	>25	-
15	NT	-

[a]Mean of 12 cell lines;

Purified from extracts of *A. crassa*, tocopherylhydroquinones **13-14** were identified by a detailed analysis of their 1- and 2D NMR and MS spectral data and compared to related tocopherols previously reported.[119] While ^{1}H and ^{13}C NMR spectral data are available in the literature for vitamin E and related tocopherols, complete

spectral data for **13-14** were lacking. Therefore, we provide full NMR spectral data for **13-14** in the present study (Table 3.1 and Appendix A).

Tocopherols have been isolated and characterized from various brown algae including *Sargassum fallax*[120] and *Cystoseira stricta*,[119] but the identification of **13-14** represents the first isolation of tocopherols from red algae. This class of molecules has been shown to have a variety of functions in terrestrial vascular plants, including scavenging lipid peroxy radicals and preventing propagation of lipid peroxidation in membranes; protecting lipids and other membrane components by quenching and reacting with singlet oxygen and thus providing photo-protection for chloroplasts; and increasing membrane rigidity.[121] While a number of tocopherol derivatives have been isolated from brown macroalgae, their ecological functions are unclear. These compounds may function similarly as in vascular plants given the high exposure of many macroalgae to UV radiation, however this hypothesis has not been tested.

The biomedical potential of tocopherols and related compounds mainly relate to their antioxidant activities, as these compounds are well established in their radical scavenging activity.[122] Hydroquinones **13-14** showed weak activity against *P. falciparum* (IC_{50} values of 190 and 220 μM for **13** and **14**, respectfully (Table 3.2), but oxidation of **14** to quinone **15** increased the antimalarial activity by more than 20-fold to an IC_{50} of 10 μM, suggesting that the quinone functionality is essential for activity for tocopherol-related compounds. Unfortunately, following bioassays we did not have enough **12** to oxidize to the corresponding β-tocopherylquinone. This is the first report of tocopherols in red macroalge and of antimalarial activity for tocopherols **13-15**. Furthermore, **13-15** displayed no activity in cancer and microbial assays, although **15** was not tested against human cancer cells due to insufficient material. These macroalgal natural products are unusual scaffolds when compared to current natural antimalarial treatments, such as the

quinines and artemisinins. These meroditerpenes could inspire the development of novel templates for future antimalarial drugs.

Experimental Section

Biological material. *Callophycus serratus* (family Solieriaceae, order Gigartinales, class Rhodophyceae, phylum Rhodophyta) was collected at depths of 2-3 m from Yanuca in the Fiji Islands (18° 23' 57" S, 177° 57' 59" E) in 2008 and at depths from 9-15 m near Harold's Passage, Astrolobe Reef, Kadavu Province, Fiji (18° 46' 37" S, 178° 27' 74" E) in 2004. *Amphiroa crassa* (family Corallinaceae, order Corallinales, class Florideophyceae, phylum Rhodophyta) was collected at a depth of 20 m from the Coral Coast, Fiji (18° 12' 15" S, 177° 39' 35" W) in 2004. Samples were frozen at –80° C until extraction. Voucher specimens were identified by comparison with previously described morphological traits,[123] preserved in aqueous formalin, and deposited at the University of the South Pacific in Suva, Fiji and at Georgia Institute of Technology as ICBG-2004-23, ICBG-2004-43, ICBG-G-0004, ICBG-G-0005, ICBG-G-0021, and ICBG-G-0049 for *C. serratus* and ICBG-2004-103 for *A. crassa*.

Chemicals. Solvents used for extractions were reagent grade, and those used for HPLC and LC-MS were HPLC or Optima grade (Fisher Scientific). NMR solvents were purchased from Cambridge Isotope Laboratories. Commercially available reagents were purchased from Sigma-Aldrich (Milwaukee, WI) and used as received.

Isolation. Frozen *C. serratus* and *A. crassa* were each extracted with MeOH and MeOH/DCM (1:1, 1:2) and subjected to liquid partitioning between MeOH/H_2O (9:1) and petroleum ether. The MeOH/H_2O ratio of each species' aqueous fraction was then adjusted to 3:2 and partitioned against chloroform. The chloroform-soluble fraction for each species was then separated with multiple rounds of reversed-phase C_{18} HPLC

(Alltech Alltima C_{18}, 5 μm, 10 × 250 mm) with a gradient of MeCN (aq) to yield **1-6** from *C. serratus* and **9-10** from *A. crassa*.

Hydrolysis of callophycolide A (1). N_2-flushed vial was charged with **1** (4.0 mg, 9.4 μmol, 1.0 eq) in 45 μL Optima-grade MeOH, followed by 5 μL of 10M aqueous NaOH (3.0 mg, 75 μmol, 8.0 eq) at 20 ºC. The reaction was allowed to stir at 40 ºC for 18 h. After cooling to 22 ºC, 10 μL of 1 M HCl was added. The solution was separated via reversed-phase HPLC (Alltech Alltima C_{18}, 250 × 10 mm, 5 μm) without further work-up. Hydrolyzed callophycolide A eluted with 86% aqueous MeCN (2.0 mg, 58% yield, based on recovered starting material); methylated-hydrolyzed **7** eluted with 92% aqueous MeCN (1.3 mg, 38% yield, based on recovered starting material); and **1** was recollected, eluting with 98% aqueous MeCN (0.8 mg).

Preparation of MTPA Derivatives of 16. An N_2-flushed vial was charged with **16** (0.6 mg, 1.3 μmol, 1.0 eq) and dimethylaminopyridine (DMAP, 1.3 mg, 10.4 μmol, 8.0 eq) in 65 μL anhydrous pyridine and the solution was allowed to stir at 22 ºC for 25 min. *R*-(−)-α-methoxy-α-(trifluoromethyl)phenylacetyl chloride (10 μL, 10.4 μmol, 8.0 eq) was then added slowly via syringe. The reaction was allowed to stir at 22 ºC for 2 h under N_2. The solvent was removed under vacuum, and the resultant crude mixture was purified via reversed-phase HPLC (Alltech Alltima C_{18}, 250 × 10 mm, 5 μm). The *S*-MTPA ester (**16a**, 0.60 mg, 52% yield) eluted with 100% ACN. An identical procedure was carried out to obtain the *R*-MTPA ester (**16b**, 0.58 mg, 51% yield) with *S*-(+)-α-methoxy-α-(trifluoromethyl)phenylacetyl chloride.

Preparation of *in situ* Mo_2-complex formed with 16. Methanolysis product **16** (0.5 mg) was dissolved in 1.5 ml DMSO with dimolybdenum tetraacetate so that the molar ratio of the Mo_2-complex to **16** was 1:1. The solution was prepared 2 h before recording the CD spectrum.

Computational Method of Mo_2-complex formed with 16. Molecular modeling was performed on a personal computer using HyperChem for Windows (Student Version 7.5 from Hypercube, Inc.) using the molecular mechanics MM+ force field method as described in Górecki *et al*.[117b]

Oxidation of δ-tocopherylhydroquinone (14). An N_2-flushed vial was charged with **14** (0.35 mg, 0.8 μmol, 1.0 eq) in 0.15 ml MeCN and cooled to 0 ºC over an ice bath. 16 μL of a 0.5 M aqueous stock of ceric ammonium nitrate (4.5 mg, 8.3 μmol, 10 eq) was added via syringe to the vial and allowed to stir for 60 min at 0 ºC. Saturated $NaHCO_3$ (aq) was added (0.5 ml) to the reaction and extracted with EtOAc (3 × 0.5 ml). The combined organics were washed with brine, dried over $MgSO_4$, and concentrated *in vacuo*. Desired product **15** was purified with reversed-phase HPLC (Zorbax SB-C_8, 250 × 4.6 mm, 5 μm), eluting with 100% MeCN (0.32 mg, 92% yield). ^1H and ^{13}C NMR spectral data for **15** were identical to previously reported literature values.[124]

Analytical and spectroscopic methods. UV spectra were recorded in MeOH with a Spectronic 21D spectrophotometer using quartz cuvettes. Optical rotations were measured on a Jasco P-1010 spectropolarimeter with a 10 cm (8 ml) cell, with compounds dissolved in MeOH. Circular dichroism spectra were acquired on a Jasco J-810 spectropolarimeter and 1 mm pathlength cells were used. High-resolution mass spectra were generated using electrospray ionization with an Applied Biosystems QSTAR-XL hybrid Quadrupole-Time-of-Flight tandem mass spectrometer and Analyst QS software. LC-MS analyses were conducted using a Waters 2695 HPLC with Waters 2996 photodiode array UV detection and Micromass ZQ 2000 mass spectrometer with electrospray ionization. LC-MS chromatography was achieved with an Alltech Alltima C_{18} column (3 μm, 2.1 × 150 mm), using gradient mobile phases of MeCN (aq) with 0.1% acetic acid. NMR spectra were recorded on a Bruker DRX-500 instrument, using a 5 mm inverse detection probe for ^1H, COSY, ROESY, HSQC, and HMBC experiments, and a 5

mm broadband probe for ^{1}H, ^{13}C, and DEPT-135, and referenced to residual $CHCl_3$ (7.24 and 77.0 ppm, for ^{1}H and ^{13}C, respectively).

Pharmacological assays. All pharmacological assays were performed as previously described.[18b, 44a] Briefly, antimalarial activity was determined with a SYBR Green based parasite proliferation assay, adapted from Smilkstein[125] and Bennett.[126] *Plasmodium falciparum* parasites (3D7 strain MR4/ATCC, Manassas, VA) were cultured in human O+ erythrocytes as previously described.[127] Compounds were diluted in complete medium and 40 µl transferred to 96-well assay plates. To this 80 µl of complete media with 3D7 infected erythrocytes were dispensed in order to obtain a 2.5% hematocrit and 0.5% parasitemia in the assay. Uninfected erythrocytes were dispensed into the background wells at the same final hematocrit. Plates were incubated for 72 h in a low oxygen environment (96% N_2, 3% CO_2, 1% O_2) in a modular incubation chamber. The plates were sealed and placed in a -80 ^{o}C freezer overnight then thawed, and 120 µl of lysis buffer (20 mM Tris-HCl, pH 7.5, 5mM EDTA, 0.08% Triton X-100, 0.008% saponin with 0.2 µl/ml Sybr Green I) was dispensed into each well and incubated at 37 ^{o}C in the dark for 6 h. The plates were read with a Molecular Devices SpectraMAX Gemini EM at ex: 495 nm, em: 525 nm with 515 nm cut-off.

Antibacterial assays were performed using methicillin-resistant *Staphylococcus aureus* (MRSA, ATCC #33591) and vancoymcin-resistant *Enterococcus faecium* (VREF, ATCC #700221) as test pathogens. These bacterial strains were grown overnight at 37 ^{o}C in nutrient broth (BD Difco^{TM}) and brain heart infusion (BD Bacto^{TM}) media, respectively. Assay cultures were diluted to an optical density of 0.05, diluted 10-fold, and added to 96-well microtiter plates. Treatments and controls were suspended in DMSO, added to the top row of assay plates (final concentration 250 µg/ml), and serially diluted 1:1 down each column. Vancomycin and chloramphenicol were used as positive controls for MRSA and VREF, respectively, and DMSO was used as negative control. All

assay plates were sealed with parafilm and incubated overnight at 37 ^{o}C. The optical density was measured at 600 nm using a microplate reader, and the MIC of each compound was calculated using the analysis program SOFTmax PRO.

For the antifungal assay, amphotericin B-resistant *Candida albicans* (ATCC #90873) was grown overnight at 37 ^{o}C in YPM media (2 g yeast extract, 2 g peptone, 4 g D-Mannitol, 1 L DI water). A hemocytometer was used to determine cell density, and the assay culture was diluted to 1 × 10^4 cells/ml, before it was added to 96-well microliter plates. Treatments and controls were suspended in DMSO, added to the top row of the assay plate (final concentration 250 µg/ml), and serially diluted 1:1 down each column. A mixed nystatin/amphotericin B solution was used as a positive control, and DMSO was used as a negative control. All assay plates were incubated overnight at 37 ^{o}C. The optical density was then measured at 600 nm using a microplate reader and the optical density was measured at 600 nm using a microplate reader, and the MIC of each compound was calculated using the analysis program SOFTmax PRO.

Natural products were evaluated against a panel of 12 tumor cell lines including breast, colon, lung, prostate, and ovarian cancer cells. Specific cell lines were: BT-549, DU4475, MDA-MD-468, PC-3, SHP-77, LNCaP-FGC, HCT116, MDA-MB-231, A2780/DDP-S, Du145, CCRF-CEM, and A549. *In vitro* cytotoxicity was tested with the (3-(4,5-dimethylthiazol-2-yl)-5-(3-carboxylmethoxyphenyl)-2-(4-sulfophenyl)-2H-tetrazolium inner salt) MTS dye conversion assay as described previously.[128]

Antitubercular activity was assessed against *Mycobacterium tuberculosis* strain H_{37}Rv (ATCC 27294) using the alamar blue susceptibility test (MABA) as described previously.[129] Compounds were tested at a maximum concentration of 100 µM.

Callophycolide A (1): pale yellow oil (4.0 mg, 0.021% dry mass); $[\alpha]^{24}_{D}$ +200 (*c* 0.01 g/100 ml, MeOH); UV (MeOH) λ_{max} (log ε) 260 (4.06) nm; ^{1}H NMR ($CDCl_3$, 500 MHz)

and ^{13}C NMR ($CDCl_3$, 125 MHz) data, Table 3.1; NOE, COSY, and HMBC NMR data, see Appendix A; HRESIMS $[M + H]^+$ *m/z* 427.2825 (calcd for $C_{27}H_{39}O_4$, 427.2842) and [M + Na] *m/z* 449.2623 (calcd for $C_{27}H_{38}O_4Na$, 449.2668).

Bromophycolide L (2): white amorphous solid (0.3 mg, 0.007% dry mass); $[\alpha]^{24}_D$ +70 (*c* 0.033 g/100 ml, MeOH); UV (MeOH) λ_{max} (log ε) 262 (3.72) nm; ^1H NMR ($CDCl_3$, 500 MHz) and ^{13}C NMR ($CDCl_3$, 125 MHz) data, Table 3.1; NOE, COSY, and HMBC NMR data, see Appendix A; HRESIMS $[M - H]^-$ *m/z* 501.1677 (calcd for $C_{27}H_{34}O_4Br$, 501.1640).

Bromophycolide N (3): white amorphous solid (1.0 mg, 0.023% dry mass); $[\alpha]^{24}_D$ +101 (*c* 0.033 g/100 ml, MeOH); UV (MeOH) λ_{max} (log ε) 260 (3.42) nm; ^1H NMR ($CDCl_3$, 500 MHz) and ^{13}C NMR ($CDCl_3$, 125 MHz) data, Table 3.1; NOE, COSY, and HMBC NMR data, see Appendix A; HRESIMS $[M - H]^-$ *m/z* 581.0907 (calcd for $C_{27}H_{35}O_4Br_2$, 581.0902).

Bromophycolide O (4): white amorphous solid (0.5 mg, 0.012% dry mass); $[\alpha]^{24}_D$ +88 (*c* 0.011 g/100 ml, MeOH); UV (MeOH) λ_{max} (log ε) 260 (3.54) nm; ^1H NMR ($CDCl_3$, 500 MHz) and ^{13}C NMR ($CDCl_3$, 125 MHz) data, Table 3.1; NOE, COSY, and HMBC NMR data, see Appendix A; HRESIMS $[M - H]^-$ *m/z* 661.0182 (calcd for $C_{27}H_{36}O_4Br_3$, 661.0169).

Callophycoic acid C (5): white amorphous solid (2.5 mg, 0.009% dry mass); $[\alpha]^{24}_D$ -49 (*c* 0.031 g/100 ml, MeOH); UV (MeOH) λ_{max} (log ε) 258 (4.03) nm; ^1H NMR ($CDCl_3$, 500 MHz) and ^{13}C NMR ($CDCl_3$, 125 MHz) data, Table 3.1; NOE, COSY, and HMBC NMR data, see Appendix A; HR ESI-MS $[M - H]^-$ *m/z* 581.0895 (calcd for $C_{27}H_{35}O_4Br_2$, 581.0902).

Callophycoic acid D (6): white amorphous solid (1.6 mg, 0.006% dry mass); $[\alpha]^{24}_D$ +85 (*c* 0.018 g/100 ml, MeOH); UV (MeOH) λ_{max} (log ε) 258 (3.81) nm; ^1H NMR ($CDCl_3$,

500 MHz) and ^{13}C NMR ($CDCl_3$, 125 MHz) data, Table 3.1; NOE, COSY, and HMBC NMR data, see Appendix A; HR ESI-MS $[M - H]^-$ *m/z* 581.0889 (calcd for $C_{27}H_{35}O_4Br_2$, 581.0902).

β-Tocopherylhydroquinone (13): colorless oil (1.2 mg, 0.003% dry mass); $[\alpha]^{24}_D$ +2.2 (*c* 0.06 g/100 ml, MeOH); UV (MeOH) λ_{max} (log ε) 255 (3.93) nm; ^1H NMR ($CDCl_3$, 500 MHz) and ^{13}C NMR ($CDCl_3$, 125 MHz) data, Table 3.1; COSY and HMBC NMR data, see Appendix A; HRESIMS $[M-H-H_2O]^-$ *m/z* 415.3553 (calcd for $C_{28}H_{47}O_2$, 415.3576).

δ-Tocopherylhydroquinone (14): brown oil (2.8 mg, 0.006% dry mass); $[\alpha]^{24}_D$ +1.3 (*c* 0.14 g/100 ml, MeOH); UV (MeOH) λ_{max} (log ε) 255 (3.56) nm; ^1H NMR ($CDCl_3$, 500 MHz) and ^{13}C NMR ($CDCl_3$, 125 MHz) data, Table 3.1; COSY, and HMBC NMR data, see Appendix A; HRESIMS $[M-H-H_2O]^-$ *m/z* 401.3414 (calcd for $C_{27}H_{45}O_2$, 401.3419); $[2M-H-2H_2O]^-$ *m/z* 803.6876 (calcd for $C_{54}H_{91}O_4$, 803.6917).

CHAPTER 4

BROMOPHYCOLIDE A TARGETS HEME CRYSTALLIZATION IN THE HUMAN MALARIA PARASITE *PLASMODIUM FALCIPARUM*

Plasmodium falciparum, the most deadly human malaria parasite, poses a major threat to human health worldwide with over 500 million clinical cases and 1-2 million deaths annually.[16] Natural products and their synthetic derivatives have provided the greatest number of successful antimalarial treatments to date, representing approximately 65% of current drugs.[11] Quinine, discovered from cinchona tree bark, has been used to treat malaria since the 17th century and was the primary antimalarial drug until it was replaced by chloroquine, a synthetic derivative, in the 1940s.[130] Chloroquine became the mainstay antimalarial agent until resistant strains began to appear over a decade after its introduction. Artemisinin, isolated from the plant *Artemisia annua* used in traditional Chinese medicine, ushered in a new wave of antimalarials and became the most potent and rapid-acting drug available.[131] Several artemisinin synthetic derivatives have since been developed, and artemisinin-based combination therapies are currently being used throughout the world to treat this parasitic disease. However, artemisinin-resistant strains have recently been reported,[132] and new antiparasitic drugs are urgently needed.

Therapeutic development is complex due to the intricate host-guest interactions during the plasmodial life cycle. During its maturation, the malaria parasite is transferred to human hosts via mosquitoes, and after a transitory stage in the liver, the parasite resides in the hosts' red blood cells. While residing in red blood cells, the parasite catabolizes hemoglobin within its food vacuole for its nutritional benefit. This hemoglobin catabolism can be lethal as it releases free heme molecules which are toxic to the parasite.[133] However, the parasite overcomes heme toxicity through the crystallization of

free heme into non–toxic hemozoin, a non–enzymatic process which is crucial to parasite survival and thus an excellent antimalarial drug target.[134] Chloroquine has been shown to inhibit heme crystallization,[135] and structurally related antimalarial drugs such as quinine, amodiaquine and mefloquine have also been proposed to disrupt hemozoin formation. Resistance to chloroquine has been shown to occur through multiple mutations in a *P. falciparum* transmembrane protein that, when mutated, pumps chloroquine out of the food vacuole, significantly reducing the concentration of the drug.[136] The primary mechanism of action (MOA) for artemisinin remains in debate, although several hypotheses have been reported, including alkylation of heme by carbon-centered free radicals,[137] interference with proteins such as the sarcoplasmic/endoplasmic calcium ATPase (SERCA),[138] as well as damaging of normal mitochondrial functions.[139]

The identification of molecular targets for bioactive natural products is essential for understanding their MOAs, developing new drug leads, and anticipating evolution of resistance. We previously discovered a unique group of brominated macrocyclic meroditerpenes from the Fijian red macroalga *Callophycus serratus*[44a, b] and showed that this class of natural products is cytotoxic to *P. falciparum*.[18b, 44c] The most abundant natural product of this class with sub–micromolar inhibition of *P. falciparum* proliferation, bromophycolide A (**1**), induces a strong arrest of the parasite erythrocytic cycle,[140] and was therefore used to develop a fluorescent probe for both molecular imaging and affinity pull–down experiments to gain insights on the MOA of **1** against *P. falciparum*.

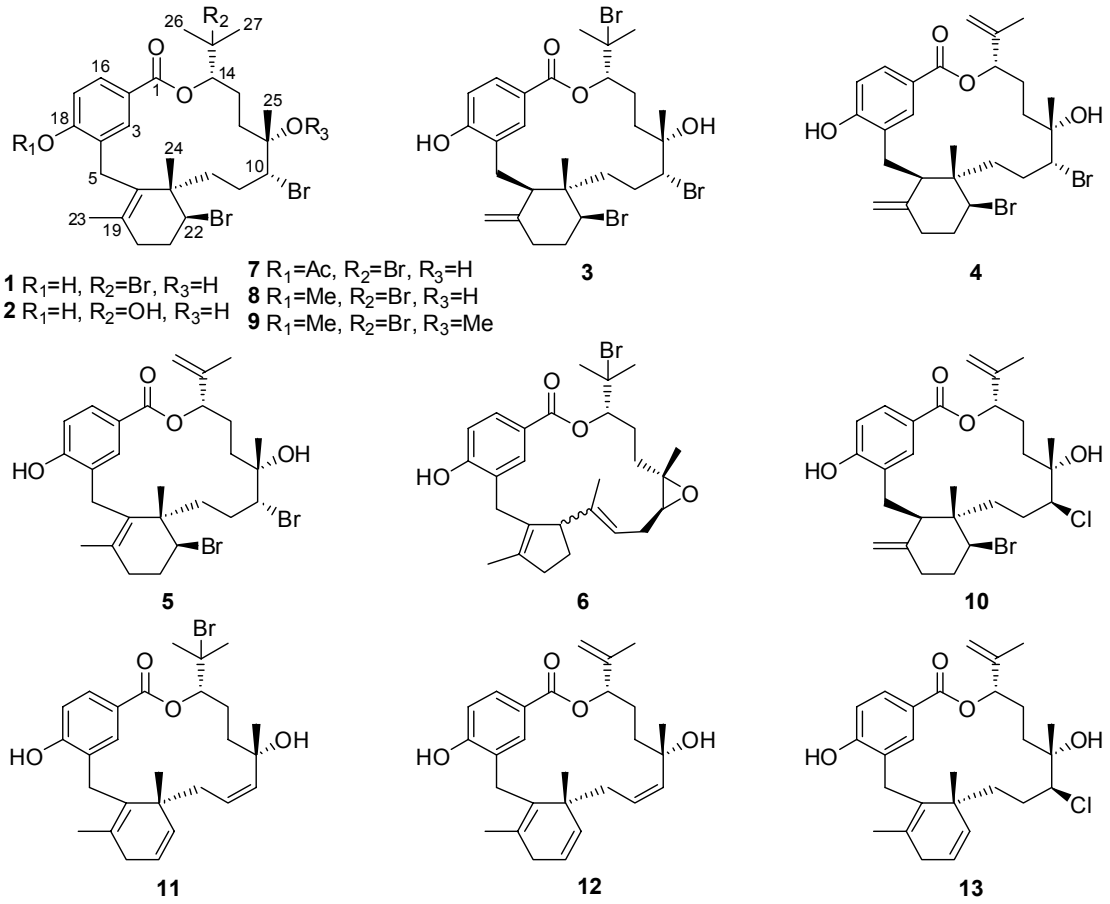

Figure 4.1. Bromophycolides A (**1**), C (**2**), D (**3**), E (**4**), M (**5**), and debromophycolide A (**6**) isolated from *Callophycus serratus*[18b, 44a, b] and semi-synthetic derivatives of bromophycolide A (**7-13**).

In order to maintain antimalarial activity while not compromising the integrity of potential receptor binding, attempts initially focused on connecting a linker through the tertiary alcohol at C11 since changes at this position resulted in only minor differences in activity, based on structure–activity relationship (SAR) trends gleaned from the known *C. serratus* natural products (see Figures 4.1 and 4.2). Unfortunately, all synthetic efforts failed at this position, likely due to both poor reactivity of tertiary alcohols and steric hindrance. From a synthetic perspective, the most chemically reactive and accessible

position in **1** is the phenolic hydroxyl at C18. Because the C18 phenol was conserved in all *C. serratus* metabolites and thus SAR data was lacking, we acetylated the phenol in **1** to test for changes in activity. Fortuitously, the acetylated derivative **7** resulted in an increase in activity (IC_{50} value of 241 nM, Table 4.1). Therefore, two fluorescent immunoaffinity fluorescent (IAF) tags[23] with varying chain lengths were each synthetically appended to **1** through an acetyl linkage (Scheme 4.1). The IC_{50} value of probe **15** was 271 nM, similar to that of **7**. Furthermore, both tag **14a** and **14b** were inactive against *P. falciparum*, exhibiting IC_{50} values >100 μM, suggesting that the activity observed in probe **15** was a result of the natural product.

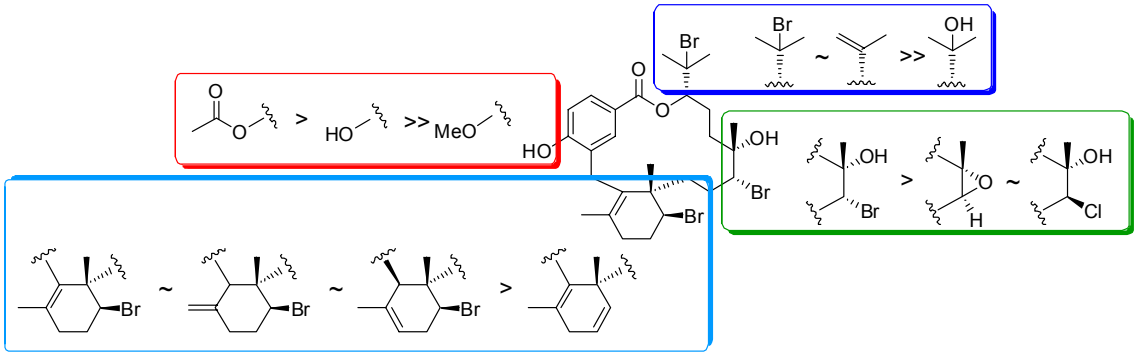

Figure 4.2. Structure-activity relationship summary of *C. serratus* natural products and bromophycolide A (**1**) semi-synthetic derivatives. Greater potency is indicated by “>”, lesser potency by “<”, similar potency by “~”.

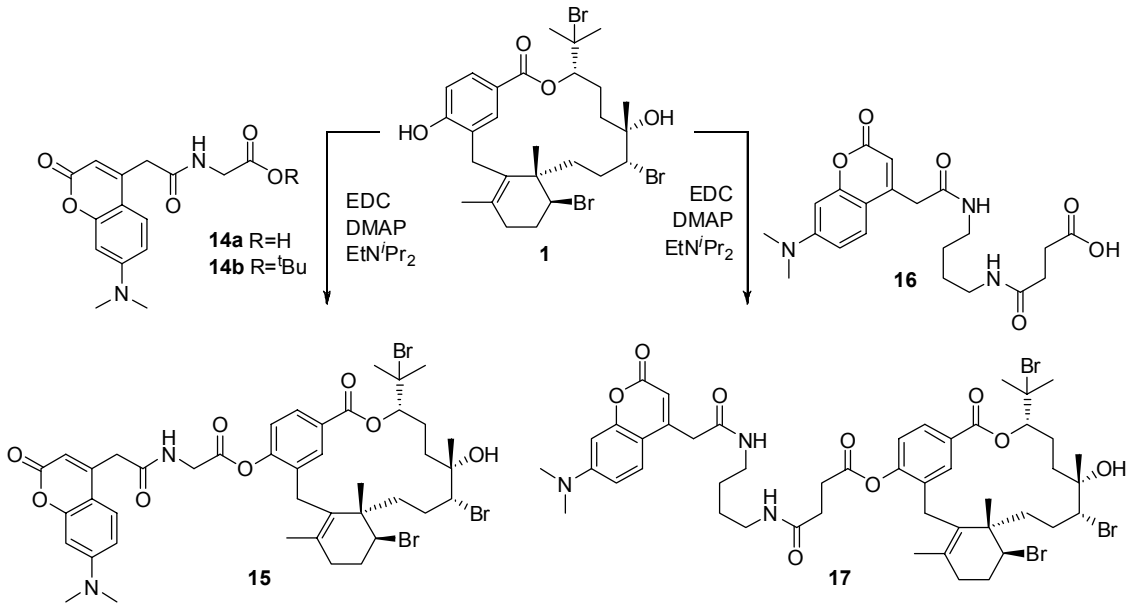

Scheme 4.1. Probes **15** and **17** were prepared by coupling acids **14** and **16**, respectively, with bromophycolide A (**1**). EDC = *N'*-(3-dimethylaminopropyl)-*N*-ethylcarbodiimide; DMAP = 4-dimethylaminopyridine; EtN^{i}Pr$_2$ = *N,N*-diisopropylethylamine; DMF = dimethylformamide.

With active probes in hand, we turned to confocal microscopy to study the intracellular distribution of probe **15** in *P. falciparum*–infected erythrocytes. Fluorescence was observed as small pockets in close proximity to the food vacuole (Figure 4.3), which was distinguished by the presence of hemozoin (dark crystals, Hz). No fluorescence was observed when *P. falciparum*–infected erythrocytes were incubated with either **14a** or **14b**, providing further evidence that **15** provided an effective mimic of the natural product (Figure 4.3). In order to determine its specific intracellular target, the histological localization of probe **15** was compared with that of fluorescent organelle and lipid probes by co–incubation and imaging using multichannel fluorescence confocal microscopy. Incubation of infected erythrocytes with both **15** and Nile Red, a neutral lipid stain,

repeatedly showed co–localization of the two stains, suggesting that **15** was associating with intracellular neutral lipids (Figure 4.4). Pisciotta *et al.* established that heme crystallization occurs inside neutral lipid nanospheres, which encompass hemozoin in *P. falciparum* food vacuoles.[141] Therefore, molecular imaging studies with **15** and infected erythrocytes suggested that heme crystallization was a putative target of **1**.

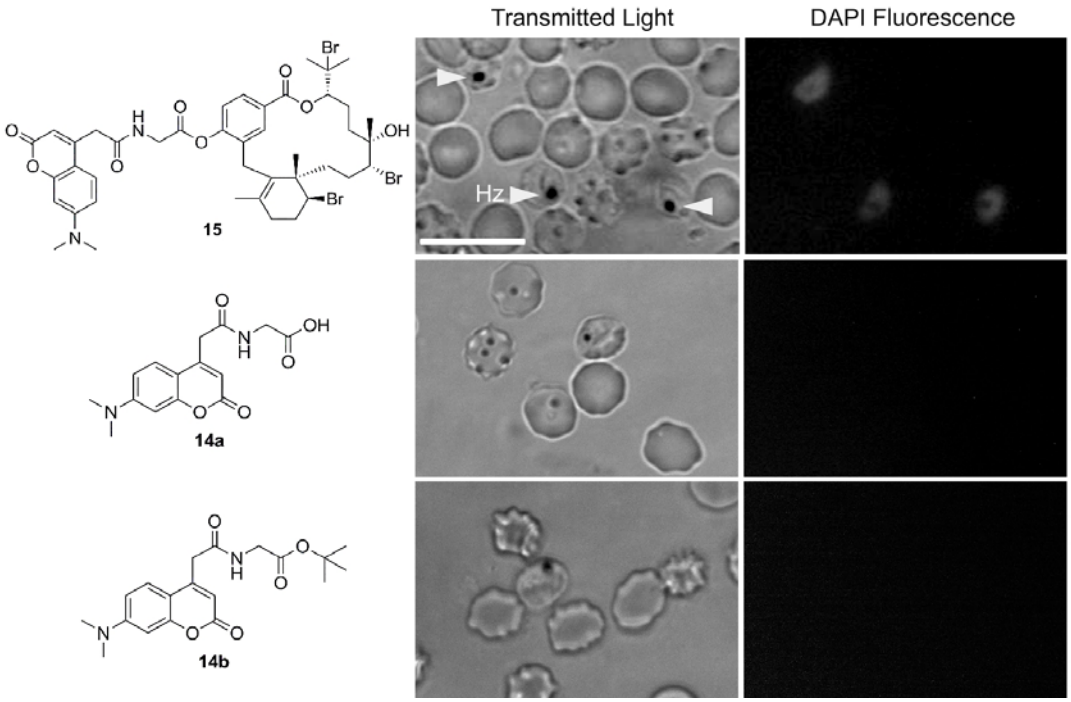

Figure 4.3. Intracellular localization images of probe **15** and controls in mixed-stage *P. falciparum*–infected erythrocytes. Confocal microscopy images of *live* parasites incubated with either 2 μM of bromophycolide A probe **15**, control tag **14a**, or **14b** in complete medium. Hemozoin (Hz) crystals were identified in the transmitted light image by dark crystals. Probe **15** localized around Hz, as seen in the fluorescent image. No fluorescence was observed when *P. falciparum*–infected erythrocytes were incubated with either **14a** or **14b**. Scale bar denotes 10 μm.

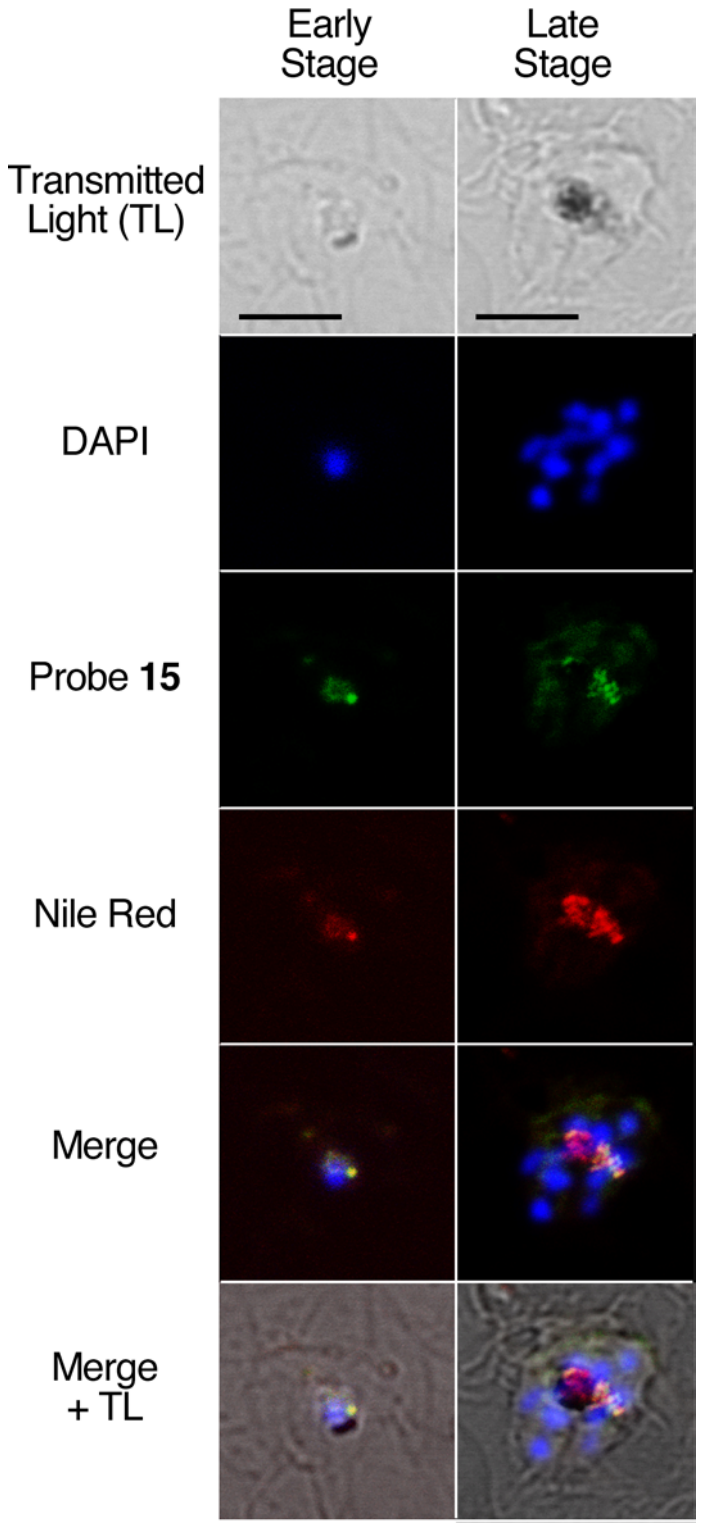

Figure 4.4. Confocal images of fixed parasites incubated with 2 μM probe **15** (green), 30 nM Nile Red (red), and 70 nM DAPI (blue). Co–localization of **15** and Nile Red (neutral

lipids) is indicated by the yellow merged image. Interesting, while probe **15** emission spectra showed a maximum at 450±10 nm (blue channel) in both complete medium and methanol, **15** fluoresced in the green channel (FITC) after parasite fixation with paraformaldehyde. The latter effect could result from solvatochromic effects while localized within the lipid environment. Bars denote 5 μm.

To further explore possible heme–bromophycolide interactions, the absorbance spectra of ferriprotoporphyrin IX (Fe(III)PPIX), commercially available heme, was recorded in 20 mM Hepes, pH 7.4 containing 40% DMSO, conditions that were previously demonstrated to evaluate monomeric Fe(III)PPIX.[142] Fe(III)PPIX gives characteristic absorption spectra with an intense Soret band at 402 nm and addition of **1** resulted in up to a 35% decrease in absorption at 402 nm, suggesting **1** forms a saturable complex with Fe(III)PPIX (Figure 4.5a). Absorption spectra with Fe(III)PPIX and **1** were collected over an 8 h period incubating at 37 ºC, and absorption at 402 nm continually decreased throughout the first 6 h and then reached a plateau (Figure 4.5b), implying that **1** is potentially a slower acting drug when compared to artemisinin.[143] Because heme crystallization is non-enzymatic, parasite-free colorimetric high-throughput screens for heme crystallization inhibitors have been developed[144] and refined.[145] Both **1** and **7** were tested for heme crystallization inhibition with the potent antimalarial drug amodiaquine acting as a positive control. Natural product **1** inhibited heme crystallization with an IC_{50} value of 2.5 molar equivalents of drug to heme, and **7** was slightly more effective than **1**, with an IC_{50} of 2.0 molar equivalents, consistent with growth inhibition assays (Table 4.2); IC_{50} values for amodiaquine were consistent with previously reported values.[144] Collectively, these data provided compelling evidence of heme crystallization inhibition as a molecular target of **1**.

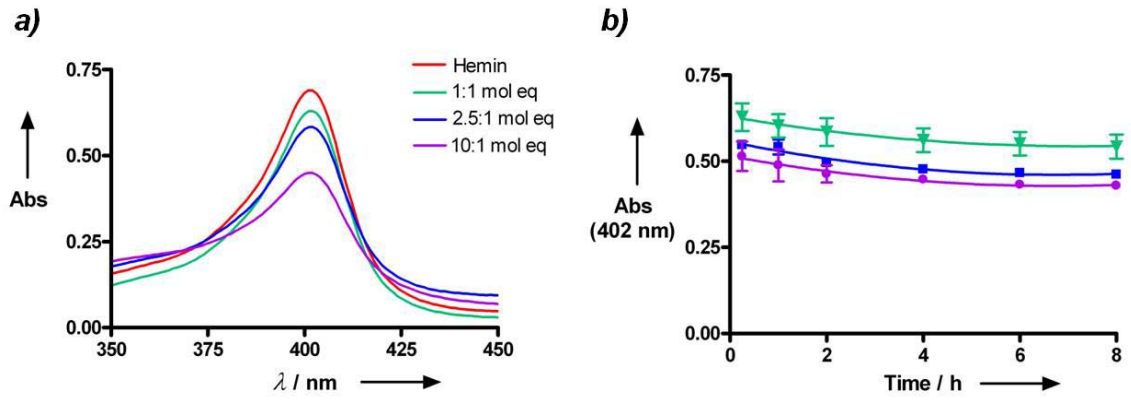

Figure 4.5. Spectroscopic changes observed when Fe(III)PPIX (hemin) is incubated with various concentrations of bromophycolide A (**1**). (a) Changes in the Soret band (402 nm) of hemin. The absorbance (Abs) at 402 nm decreases as concentration of **1** increases. Molar equivalent (mol eq) ratios are shown as natural product (**1**) to hemin. Spectra have been corrected for dilution by subtracting a reference cell at each concentration of **1**. (b) Incubation of hemin in the presence of **1** results in a continual decrease in absorbance at 402 nm over the course of several hours at 37 ºC, equilibrating around 6 h (n = 3); ▼ = 1:1 mol eq **1**: hemin; ■ = 2.5:1 mol eq **1**: hemin; ● = 10:1 mol eq **1**: hemin. Error bars indicate standard deviation. Conditions: 37 ºC (dark), 40% DMSO, 20 mM HEPES buffer, pH 7.4.

With a MOA established for **1**, potential protein targets were also explored. Taking advantage of the dual utility of probes **15** and **17**, *P. falciparum* lysates were screened for bromophycolide–binding protein targets. A selective monoclonal antibody (mAb) against the fluorescent tag[146] was available for co-immunoprecipitation (co-IP) with *P. falciparum* lysates and both probes **15** and **17**. Repeated IP experiments failed to result in isolation of any bromophycolide–binding proteins (see Appendix B). This anti–IAF–mAb affinity method has been successful with IP of protein targets in multiple systems in our labs, from cancerous cells[24, 146] to micro-invertebrates.[27] While a negative

IP experiment cannot prove the lack of a protein target, the lack of an isolated binding protein supports the observation that an MOA of **1** involves heme crystallization inhibition.

To date, we have isolated 33 unique *C. serratus* metabolites and IC_{50} values ranged from 0.3 to >100 μM, providing a small library to analyze SAR trends (representative natural products **1–6**, Figure 4.1).[18, 44] Several semi–synthetic derivatives of **1** were also prepared (**7–13**) to further enhance SAR studies and to provide insights for potential future designs of bromophycolide–inspired synthetic compounds. When examining the natural product SAR trends, the most striking observation related to the diterpene head. While replacing the bromine at C15 with an isoprene functionality caused little change in antimalarial activity, substitution of a hydroxyl group at C15 exhibited dramatic loss of activity (Table 4.1), suggesting that a hydrogen bond donating group is poorly suited in this position (Figure 4.2).

Table 4.1. Antimalarial activities of bromophycolides A (**1**), C (**2**), D (**3**), E (**4**), M (**5**), debromophycolide A (**6**), semi-synthetic derivatives of bromophycolide A (**7-13**), and probe **15**.

cmpd	*P. falciparum* (3D7) IC_{50} (μM)
1	0.66
2	56
3	0.35
4	0.82
5	0.55
6	>100
7	0.24
8	23
9	21
10	3.1
11	4.6
12	3.5
13	2.7
15	0.27

Moving to functional groups in the aliphatic macrocycle, synthetic modifications at C10 and C11 also did not significantly affect activity, and replacing the bromine at C10 with chlorine resulted in a slight decrease in activity, although it should be noted that the configuration at C10 was inverted (**4** vs. **10**). Regioisomerization of the double bond in the cyclohexene ring in both natural products and synthetic derivatives also demonstrated only minor alterations in activity (Figure 4.2). Interestingly, elimination of all bromines from **1** only moderately decreased the IC_{50} value from 0.65 to 3.5 μM (**1** vs. **12**) whereas the natural product **6** was completely inactive. The final portion of **1** to investigate was the *p*–hydroxybenzoate group. As previously discussed, acylation of the phenol in **1** to **7** resulted in a slight increase in activity. Surprisingly, methylation of the phenol in **1** to **8** led to a 30–fold decrease in activity. Collectively, these data suggest that positions C15 and C18 have the most striking effects on antimalarial activity.

The discovery and development of heme crystallization inhibitors remains an excellent malaria drug target because heme crystallization is a physicochemical process and thus less likely to provide the means for evolution of resistance.[147] Drug resistance most commonly involves mutations in a drug's target protein or proteins which regulate efflux in order to remove the drug ,[148] as the latter was shown for chloroquine resistance. Furthermore, both **1** and **7** effectively inhibited chloroquine-resistant parasites (Dd2) with IC_{50} values of 497 and 304 nM, respectively (Table 4.2), while exhibiting between 50- and 300-fold differences in activity between *P. falciparum* parasites and human Vero cells (Table 4.3).

Potential interactions of drug **1** with heme include $\pi-\pi$ complexation, hydrophobic interactions between heme and **1**, and hydroxyl group coordination to the iron center.[142] The increased potency of **1** (C18-OH) and **7** (C18-OAc) over **8** (C18-OMe) potentially suggests coordination of C18-OH with the iron center in heme, although $\pi-\pi$

complexation and hydrophobic interactions between heme and bromophycolides are also possible. The increased potency of **7** relative to **1** can be attributed to a higher affinity of an acetyl functionality for iron over a free hydroxyl group, while also explaining the significant decrease in activity when the phenolic hydroxyl was methylated as in **8**. Alternatively, Fe–OH coordination of bromophycolides with heme may require that the C18–OAc derivative **7** undergoes deacylation by esterases, making **7** a prodrug of the hydrophobic natural product **1**. This, however, is not supported by the cellular studies with probe **15** as shown in Figure 4.3 and 4.4.

Table 4.2. Efficacies of bromophycolide A (**1**), 18-OAc-bromophycolide A (**7**) and amodiaquine (AMQ) against three *Plasmodium falciparum* strains, in inhibition of heme crystallization, and cytotoxicity against healthy human cells.

cmpd	3D7 IC_{50} (nM)[a]	Dd2 IC_{50} (nM)[b]	HB3 IC_{50} (nM)[a]	IC_{50} for heme crystallization (equivalents)[c]
1	658	497	565	2.5 ± 0.13
7	241	304	431	2.0 ± 0.15
AMQ	7.8[d]	14[d]	8.5[d]	1.2 ± 0.19

[a]3D7 and HB3 = chloroquine-sensitive parasites
[b]Dd2 = chloroquine-resistant parasite
[c]IC_{50} values in Ncokazi & Egan[144] were reported as molar equivalents of drug to heme
[d]From Hawley *et al.*[149]

Table 4.3. Cytotoxicity of **1** and **7** against healthy human cells.

cmpd	Cytotoxicity (IC_{50} μM)		
	Vero	J774	HepG2
1	34.6	19.0	21.3
7	74.0	24.7	38.5

The molecular structures of the bromophycolides are notably different from quinine, chloroquine, and other known heme crystallization inhibitors, thus suggesting a new class of compounds that target heme crystallization. Moreover, red algae may represent an excellent source for the discovery of new antimalarials, as a recent study revealed a common evolutionary lineage for red algae and the malaria parasite.[150] Thus, red algae may produce secondary metabolites more likely to inhibit malaria parasite proliferation than many other organisms. As historically evident, natural products continue to provide a rich resource for the discovery of unique antimalarial drugs.

Experimental Section

General methods. Commercially available reagents were purchased from Sigma-Aldrich (Milwaukee, WI) or VWR Scientific (Brisbane, CA), and used as received. All reactions were performed under a nitrogen atmosphere unless otherwise noted. Reactions were monitored using thin-layer chromatography (TLC) using Silica Gel 60 F254 plates from EMD Chemicals (San Diego, CA), and visualized with a UV lamp at 254 nm. Solvents used for HPLC and LC-MS were HPLC or Optima grade (Fisher Scientific). NMR solvents were purchased from Cambridge Isotope Laboratories. 2,5-Dimethylfuran was used as an internal standard for quantitation by ^{1}H NMR spectroscopy.[151]

Structural analyses. NMR spectra were recorded on a Bruker DRX-500 instrument in $CDCl_3$ using a 5 mm inverse detection probe for ^{1}H, COSY, HSQC, and HMBC experiments, and a 5 mm broadband probe for ^{1}H and ^{13}C experiments, and referenced to residual $CHCl_3$ (7.24 and 77.0 ppm, for ^{1}H and ^{13}C, respectively). ^{13}C NMR spectra were not collected for compounds < 1.0 mg due to inadequate sensitivity. In these cases, structures were determined by analysis of ^{1}H NMR and high-resolution mass spectra and comparison to the 33 previously identified natural products for which

extensive 1- and 2D NMR spectral data were available, since synthetic modifications occurred at positions throughout the macrocycle for which well-resolved ^{1}H NMR chemical signals were apparent. High-resolution mass spectra were generated using electrospray ionization with an Applied Biosystems QSTAR-XL hybrid Quadrupole-Time-of-Flight tandem mass spectrometer and Analyst QS software in the mass spectral facilities at Georgia Institute of Technology. LC-MS analyses were conducted using a Waters 2695 HPLC with Waters 2996 photodiode array UV detection and Micromass ZQ 2000 mass spectrometer with electrospray ionization. LC-MS chromatography was achieved with an Alltech Alltima C_{18} (3 μm, 2.1 × 150 mm) column, using gradient mobile phases of aqueous acetonitrile with 0.1% acetic acid.

18-*O*-acetyl-bromophycolide A (7). Acetic anhydride (10 μl, 108 μmol) was added dropwise to a solution of bromophycolide A (**1**) (1.0 mg, 1.5 μmol) in anhydrous pyridine (50 μl) and allowed to stir at rt for 4 h. The reaction was concentrated *in vacuo* and the product was purified by reversed-phase HPLC using a gradient of aqueous MeCN (Alltech Alltima C_{18}, 10 × 250 mm, 5 μm) to yield **7** as a colorless oil (0.8 mg, 75%). ^{1}H NMR ($CDCl_3$, 500 MHz) δ: 8.08 (s, 1H); 7.93 (d, 1H, *J* = 10 Hz); 7.16 (d, 1H, *J* = 10 Hz); 4.67 (dd, 1H, *J* = 5, 15 Hz); 4.46 (t, 1H, *J* = 7.5 Hz); 3.48 (dd, 1H, *J* = 5, 15 Hz); 3.41 (d, 1H, *J* = 20 Hz); 3.17 (d, 1H, *J* = 20 Hz); 2.25-2.29 (m, 2H); 2.22 (s, 3H); 1.85-2.18 (m, 7H); 1.81 (s, 3H); 1.8 (s, 3H); 1.68-1.78 (m, 3H); 1.38 (s, 3H); 1.29 (s, 3H); 1.26 (s, 3H); 1.08 (m, 1H). HRESIMS: $[M + H]^+$ *m/z* 705.0467 (calcd for $C_{29}H_{40}Br_3O_5$, 705.0425); [M + Na] *m/z* 727.0170 (calcd for $C_{29}H_{39}Br_3O_5Na$, 727.0245).

18-methoxy-bromophycolide A (8). A solution of **1** (3.0 mg, 4.5 μmol) in THF (50 μl) was added dropwise to a suspension of sodium hydride (60% dispersion in mineral oil pre-washed with Et_2O, 0.54 mg, 14 μmol) in THF (150 μl) at 0 ºC. The mixture was stirred for 30 min at the same temperature. Methyl iodide (27 μl of a 0.5 M solution in THF) was added dropwise to the solution at 0 ºC and the resulting mixture was stirred for

7 h at rt. Saturated NH_4Cl (aq) was added to the solution at 0 ºC, followed by extraction with EtOAc (3 × 300 µl). The combined organic layers were washed with brine, dried over $MgSO_4$, and evaporated *in vacuo*. Purification of the product by reversed-phase HPLC using a gradient of aqueous MeOH (Zorbax C_{18}, 9.4 × 250 mm, 5 µm) yielded **8** as a colorless oil (2.5 mg, 81%). ^{1}H NMR ($CDCl_3$, 500 MHz) δ: 7.95 (s, 1H); 7.92 (d, 1H, *J* = 10 Hz); 6.89 (d, 1H, *J* = 10 Hz); 4.65 (dd, 1H, *J* = 5, 10 Hz); 4.48 (dd, 1H, *J* = 5, 12 Hz); 3.93 (s, 3H); 3.44 (m, 1H); 3.42 (d, 1H, *J* = 18 Hz); 3.21 (d, 1H, *J* = 18 Hz); 2.22-2.33 (m, 3H); 1.84-2.17 (m, 7H); 1.82 (s, 3H); 1.81 (s, 3H); 1.68-1.80 (m, 3H); 1.38 (s, 3H); 1.30 (s, 3H); 1.27 (s, 3H); 1.07 (m, 1H). ^{13}C NMR ($CDCl_3$, 125 MHz) δ: 165.9, 161.4, 133.1, 130.6, 130.4, 130.0, 127.5, 121.0, 109.7, 80.4, 73.9, 72.4, 67.3, 61.1, 55.6, 43.5, 37.6, 34.3, 33.7, 33.6, 31.6, 31.0, 30.5, 29.5, 28.6, 28.3, 26.1, 21.0. HRESIMS: $[M + H]^+$ *m/z* 677.0404 (calcd for $C_{28}H_{40}Br_3O_4$, 677.0477).

11, 18-dimethoxy-bromophycolide A (9). A solution of **8** (2.0 mg, 3.0 µmol) in THF (25 µl) was added dropwise to a suspension of sodium hydroxide (60% dispersion in mineral oil pre-washed with Et_2O, 0.48 mg, 12 µmol) in THF (50 µl) at 0 ºC. The mixture was stirred for 30 min and allowed to reach rt. Methyl iodide (25 µl of a 0.5 M solution in THF) was added dropwise to the solution at rt and the resulting mixture was stirred overnight. Saturated NH_4Cl (aq) was added to the solution, followed by extraction with EtOAc (3 × 200 µl). The combined organic layers were washed with brine, dried over $MgSO_4$, and evaporated *in vacuo*. Purification of the product by reversed-phase HPLC using a gradient of aqueous MeOH (Zorbax C_{18}, 9.4 × 250 mm, 5 µm) yielded **9** as a colorless oil (1.0 mg, 49%). ^{1}H NMR ($CDCl_3$, 500 MHz) δ: 7.94 (d, 1H, *J* = 10 Hz); 7.88 (s, 1H); 6.89 (d, 1H, *J* = 10 Hz); 4.96 (dd, 1H, *J* = 7, 12 Hz); 4.50 (m, 1H); 3.93 (s, 3H); 3.62 (s, 3H); 3.53 (d, 1H, *J* = 18 Hz); 3.34 (d, 1H, *J* = 18 Hz); 3.07 (dd, 1H, *J* = 5, 10 Hz); 2.47-2.55 (m, 1H); 2.29 (m, 2H); 2.12-2.19 (m, 1H); 1.83-1.94 (m, 5H); 1.74 (s, 3H); 1.72 (s, 3H); 1.51 (s, 3H); 1.32-1.42 (m, 3H); 1.16 (s, 3H); 0.89 (s, 3H). ^{13}C NMR ($CDCl_3$, 125 MHz) δ:

166.3, 161.6, 133.3, 131.8, 131.0, 130.1, 128.1, 120.6, 109.5, 78.6, 68.7, 65.2, 63.8, 59.9, 55.5, 43.1, 39.9, 31.8, 30.9, 30.4, 29.3, 29.0, 28.1, 24.6, 24.5, 23.9, 20.7, 19.5, 19.4. HRESIMS: $[M + H]^+$ *m/z* 691.0584 (calcd for $C_{29}H_{42}Br_3O_4$, 691.0633).

10-(*S*)-Cl-bromophycolide E (10). Lithium chloride (8 µl, 8.2 µmol, of a 1M solution in warmed DMF) was added dropwise to a solution of bromophycolide E (**4**) (1.6 mg, 2.7 µmol) in DMF (100 µl) at rt. The reaction was allowed to stir at 70 ºC for 6 h. The reaction was allowed to cool and deionized H_2O was added (0.5 ml) to the solution, followed by extraction with EtOAc (3 × 0.5 ml). The combined organic layers were washed with brine, dried over $MgSO_4$, and evaporated *in vacuo* and the product was purified by reversed-phase HPLC using a gradient of aqueous MeOH (Zorbax C_{18}, 9.4 × 250 mm, 5 µm) to yield **10** as a white powder (0.13 mg, 8.8%). ^{1}H NMR ($CDCl_3$, 500 MHz) δ: 7.83 (s, 1H); 7.68 (d, 1H, *J* = 10 Hz); 6.74 (d, 1H, *J* = 10 Hz); 5.38 (s, 1H); 5.26 (br s –OH); 5.14 (m, 1H); 4.95 (s, 1H); 4.92 (s, 1H); 4.85 (s, 1H); 4.34 (dd, 1H, *J* = 5, 12 Hz); 4.03 (d, 1H, *J* = 12 Hz); 3.12 (dd, 1H, *J* = 15, 20 Hz); 2.57 (d, 1H, *J* = 20 Hz); 2.47 (m, 1H); 2.29-2.38 (m, 3H); 1.99-2.10 (m, 5H); 1.91 (m, 2H); 1.79 (s, 3H); 1.66-1.75 (m, 3H); 1.37 (s, 3H); 0.96 (s, 3H). HRESIMS $[M – H]^-$ *m/z* 537.1283 (calcd for $C_{27}H_{35}BrClO_4$, 537.1407).

$\Delta^{9,10}$- $\Delta^{21,22}$-Bromophycolide A (11). Lithium chloride (3.8 mg, 90 µmol) was added to a solution of **1** (10 mg, 15 µmol) in DMF (1 ml) at rt. The reaction was allowed to stir at 70 ºC for 6 h. The reaction was allowed to cool and deionized H_2O was added (5 ml) to the solution, followed by extraction with EtOAc (3 × 5 ml). The combined organic layers were washed with brine, dried over $MgSO_4$, and evaporated *in vacuo* and the product was purified by reversed-phase HPLC using a gradient of aqueous MeOH (Zorbax C_{18}, 9.4 × 250 mm, 5 µm) to yield **11** as a white powder (0.1 mg, 1.3%). ^{1}H NMR ($CDCl_3$, 500 MHz) δ: 8.37 (s, 1H); 7.68 (d, 1H, *J* = 10 Hz); 6.74 (d, 1H, *J* = 10 Hz); 5.42 (m, 1H); 5.41 (m, 1H); 5.11 (br s, –OH); 4.63 (m, 2H); 3.81 (dd, 1H, *J* = 8, 17 Hz); 3.65 (d, 1H, *J* = 20 Hz);

3.21 (d, 1H, *J* = 20 Hz); 2.51 (m, 2H); 1.92-2.10 (m, 5H); 1.74-1.82 (m, 1H); 1.45 (s, 3H); 1.39 (s, 3H); 1.37 (s, 3H); 1.32 (s, 3H); 1.28 (s, 3H); 1.20 (m, 1H). HRESIMS $[M - H]^-$ *m/z* 501.1442 (calcd for $C_{27}H_{34}BrO_4$, 501.1640).

$\Delta^{9,10}$- $\Delta^{21,22}$-Bromophycolide M (12). Lithium chloride (3.8 mg, 90 µmol) was added to a solution of **1** (10 mg, 15 µmol) in DMF (1 ml) at rt. The reaction was allowed to stir at 70 ºC for 6 h. The reaction was allowed to cool and deionized H_2O (5 ml) was added to the solution, followed by extraction with EtOAc (3 × 5 ml). The combined organic layers were washed with brine, dried over $MgSO_4$, and evaporated *in vacuo* and the product was purified by reversed-phase HPLC using a gradient of aqueous MeOH (Zorbax C_{18}, 9.4 × 250 mm, 5 µm) to yield **12** as a white power (0.15 mg, 2.4%). ^{1}H NMR ($CDCl_3$, 500 MHz) δ:7.94 (s, 1H); 7.75 (d, 1H, *J* = 10 Hz); 6.75 (d, 1H, *J* = 10 Hz); 5.70 (br d, 1H, *J* = 10 Hz); 5.33 (br d, 1H, *J* = 12 Hz); 5.14 (br s,–OH); 5.10 (br d, 1H, *J* = 10 Hz); 5.00 (s, 1H); 4.89 (s, 1H); 4.61 (m, 1H); 3.62 (d, 1H, *J* = 18 Hz); 3.20 (d, 1H, *J* = 18 Hz); 2.64-2.78 (m, 2H); 2.59 (m, 1H); 1.78 (s, 3H); 1.63-1.72 (m, 4H); 1.54 (s, 3H); 1.45 (s, 3H); 1.30-1.37 (m, 2H); 1.24 (m, 1H); 1.13 (s, 3H). HRESIMS: $[M - H]^-$ *m/z* 421.2430 (calcd for $C_{27}H_{33}O_4$, 421.2378).

10-(*S*)-Cl-$\Delta^{21,22}$-bromophycolide M (13). Lithium chloride (3.8 mg, 90 µmol) was added to a solution of **1** (10 mg, 15 µmol) in DMF (1 ml) at rt. The reaction was allowed to stir at 70 ºC for 6 h. The reaction was allowed to cool and deionized H_2O was added (5 ml) to the solution, followed by extraction with EtOAc (3 × 5 ml). The combined organic layers were washed with brine, dried over $MgSO_4$, and evaporated *in vacuo* and the product was purified by reversed-phase HPLC using a gradient of aqueous MeOH (Zorbax C_{18}, 9.4 × 250 mm, 5 µm) to yield **13** as a white powder (2.0 mg, 29%). ^{1}H NMR ($CDCl_3$, 500 MHz) δ: 8.01 (s, 1H); 7.79 (d, 1H, *J* = 8 Hz); 6.79 (d, 1H, *J* = 8 Hz); 5.77 (m, 1H); 5.46 (d 1H, *J* = 10 Hz); 5.39 (br s, –OH); 5.30 (m, 1H); 5.00 (s, 1H); 4.88 (s, 1H); 3.85 (d, 1H, *J* = 10 Hz); 3.49 (d, 1H, *J* = 17 Hz); 3.35 (d, 1H, *J* = 17 Hz); 2.75 (d, 1H, *J* = 22 Hz); 2.64 (d,

1H, *J* = 22 Hz); 1.90-2.02 (m, 3H); 1.77 (s, 3H); 1.63-1.75 (m, 5H); 1.51 (s, 3H); 1.23 (s, 3H); 1.16 (s, 3H); 0.85 (m, 1H). ^{13}C NMR ($CDCl_3$, 125 MHz) δ: 165.5, 157.5, 143.1, 135.3, 131.9, 130.8, 129.8, 129.3, 125.4, 122.6, 122.4, 115.0, 111.1, 76.2, 74.6, 72.2, 40.7, 37.4, 33.7, 31.9, 30.2, 28.7, 28.3, 27.6, 26.6, 20.5, 18.9. HRESIMS $[M - H]^-$ *m/z* 457.1126 (calcd for $C_{27}H_{34}ClO_4$, 457.2145).

Bromophycolide A 'short-linker' probe (15). *N'*-(3-dimethylaminopropyl)-*N*-ethylcarbodiimide (EDC) (11 µl, 60 µmol) was added to a solution of 2,5-dioxopyrrolidin-1-yl 2-(2-(7-(dimethylamino)-2-oxo-2H-chromen-4-yl)acetamido)acetate (**14**) (9.1 mg, 30 µmol), 4-dimethylaminopyridine (DMAP) (6 µl, 6 µmol, of a 1M solution in DMF), and **1** (5 mg, 7.5 µmol) in 3:2 DMF/CH_2Cl_2 (0.3 ml), followed by slow addition of *N,N*-diisopropylethylamine (EtN^iPr_2, 20 µl). The reaction was allowed to stir at rt for 24 h and then was quenched with saturated $NaHCO_3$ solution (0.5 ml). The solution was extracted with EtOAc (3 × 0.75 ml). The combined organic layers were washed with brine, dried over $MgSO_4$, and evaporated *in vacuo* and the product was purified by reversed-phase HPLC using a gradient of aqueous MeCN and 0.2% TFA (Alltech Alltima C_{18}, 10 × 250 mm, 5 µm) to yield **15** (1.6 mg, 22%). ^{1}H and ^{13}C NMR data table provided in Appendix A. HRESIMS: $[M + H]^+$ *m/z* 949.1286 (calcd for $C_{42}H_{52}Br_3N_2O_8$, 949.1274).

IAF tag 16. A three-step process was used to prepare tag **16**. HATU (570 mg, 1.5 mmol) was added to a solution of 7-dimethylamino-4-coumarin acetic acid (247.2 mg, 1 mmol) and EtN^iPr_2 (0.42 ml, 3 mmol) in anhydrous DMF (3 mL). After 1 h at rt, *N*-Boc-1,4-diaminobutane (225.3 mg, 1.2 mmol) in anhydrous DMF (1 ml) was added and the mixture was stirred for 4 h at rt. The contents were dried via rotary evaporation. The crude product was suspended in DCM (10 ml) and applied to a Dry Column Vacuum Chromatography (DCVC) column containing 80 g of Silica Gel (15–40 µm Silica Gel 60 from EM Sciences) and eluted with 5% MeOH in EtOAc. Drying via rotary evaporation provided the Boc-protected amide (395.2 mg) along with approximately 10% of 7-

dimethylamino-4-methylcoumarin (a product of the decarboxylation of 7-dimethylamino-4-coumarin acetic acid). This mixture was then dissolved in dry CH_2Cl_2 (10 ml) using ultrasonification and treated with TFA (2 ml) at rt. TLC analysis showed clean removal of the Boc protecting group within 4 h. The resulting mixture was dried by the flow of Argon and the residue was rotary evaporated twice from EtOAc (20 ml) and toluene (10 ml) and then dissolved in anhydrous DMF (5 ml) containing EtN^iPr_2 (0.84 mL, 6 mmol). Solid succinic anhydride (250.1 mg, 2.5 mmol) was added and the mixture was stirred at rt. After 12 h, the mixture was dried via rotary evaporation and **16** was obtained by silica flash chromatography using a gradient consisting of 2:1 hexanes:EtOAc, 1:1 hexanes:EtOAc, EtOAc, 1:10 MeOH:EtOAc and 1:5 MeOH:EtOAc. Tag **16** (317.1 mg, 76%) was obtained as a light yellow powder after evaporation of selected fractions. ^{1}H NMR (DMSO-d_6, 400 MHz) δ: 12.05 (br s, –OH); 8.18 (t, –NH, J = 5.3); 7.81 (t, –NH, J = 5.5); 7.52 (d, 1H, J = 9.0); 6.72 (dd, 1H, J = 2.3, 9.0); 6.54 (d, 1H, J = 2.3); 5.98 (s, 1H); 3.57 (s, 2H); 3.05 (m, 4H); 3.00 (s, 6H); 2.40 (t, 2H, J = 7.1); 2.27 (t, 2H, J = 7.0); 1.37 (m, 4H). ^{13}C NMR (DMSO-d_6, 100 MHz) δ: 173.9, 170.7, 167.6, 160.7, 155.4, 152.8, 151.4, 126.0, 109.4, 109.0, 108.2, 97.5, 38.5, 38.2, 30.0, 29.2, 26.6, 26.4. ESIMS $[M + H - H_2O]^+$ *m/z* 400.43; $[M + H]^+$ *m/z* 418.43; [M + Na] *m/z* 440.41; $[M - H]^-$ *m/z* 416.50.

Bromophycolide A 'long-linker' probe (17). EDC (15 µl, 81 µmol) was added to a solution of 4-(4-(2-(7-(dimethylamino)-2-oxo-2H-chromen-4-yl)acetamido)butylamino)-4-oxobutanoic acid (**16**) (11 mg, 27 µmol), DMAP (10 µl, 10 µmol, of a 1M solution in DMF), and **1** (4.5 mg, 6.8 µmol) in 3:2 DMF/CH_2Cl_2 (0.3 ml), followed by slow addition of EtN^iPr_2 (20 µl). The reaction was allowed to stir at rt for 24 h and then was quenched with saturated $NaHCO_3$ solution (0.5 ml). The solution was extracted with EtOAc (3 × 0.75 ml). The combined organic layers were washed with brine, dried over $MgSO_4$, and evaporated *in vacuo* and the product was purified by reversed-phase HPLC using a

gradient of aqueous MeCN and 0.2% TFA (Alltech Alltima C_{18}, 10 × 250 mm, 5 μm) to yield **17** (2.1 mg, 29%). ^{1}H and ^{13}C NMR data table provided in Appendix A. HRESIMS: $[M + H]^+$ *m/z* 1062.2021 (calcd for $C_{48}H_{63}Br_3N_3O_9$, 1062.2114).

Parasite culture. 3D7, HB3 and Dd2 *P. falciparum* malaria parasites (MRA-102, 155, 156, MR4, ATCC® Manassas, Virginia) were cultured in human type O+ erythrocytes in complete medium (RPMI 1640, 0.043 mg/ml gentamicin (Gibco), 0.014 mg/ml Hypoxanthine (Acros), 38.5 mM HEPES (Sigma), 0.18% sodium bicarbonate (Gibco), 0.20% glucose (MP Biomedical), 2.57 mM NaOH (Sigma), 0.21% albumax (Gibco), and 4.3% human serum as previously described.[127] Cultures were maintained in 25 cm^2 cell culture treated flasks (Corning) at a volume of 10 ml and were gassed for 30 s with an environment of 3% CO_2, 1% O_2, and 96% N_2, then incubated at 37 °C. Synchronization of culture was achieved through sorbitol lysis of mature stage using 5% sorbitol (Fisher) and fine tuned by another lysis 8 h later.

Growth inhibition assay with *Plasmodium falciparum.* Antimalarial activity was determined with a SYBR Green based parasite proliferation assay, adapted from Smilkstein[125] and Bennett.[126] *P. falciparum* parasites were cultured in human O+ erythrocytes as described in the previous section. Compounds were diluted in complete medium and 40 μl transferred to 96-well assay plates. To this, 80 μl of complete media with malaria infected erythrocytes were dispensed in each well, with final assay percentages at 2.5% hematocrit and 0.5% parasitemia. Uninfected erythrocytes were added to the background wells at the same final hematocrit percentage. Plates were incubated for 72 h in a low oxygen environment (96% N_2, 3% CO_2, 1% O_2) in a modular incubation chamber. The plates were sealed and placed in a -80 ^{o}C freezer overnight then thawed, and 120 μl of lysis buffer (20 mM Tris-HCl, pH 7.5, 5 mM EDTA, 0.08% Triton X-100, 0.008% saponin with 0.2 μl/ml Sybr Green I (Invitrogen)) was dispensed into each well and incubated at 37 ^{o}C in the dark for 6 h. Fluorescence of each well was

read with a Molecular Devices SpectraMAX Gemini EM at excitation: 495 nm, emission: 525 nm with 515 nm cut-off.

Fluorescence microscopy

Live cell confocal imaging. Samples were prepared in optical bottom 96-well assay plates (Costar #3614, Corning, NY). Parasite cultures were diluted to 0.025% hematocrit and 6% parasitemia in complete medium and 240 μl was added to each well. Probe **15** was incubated with samples for 1 h at 37°C, in the dark at a final concentration of 2 μM. The BD Pathway HT (BD Biosciences Bioimaging, Rockville, MD) incubation chamber was set at 37 °C and 5% CO_2.

Confocal microscopy with fixed cells. Mixed-stage or synchronized *P. falciparum* cultures at 6-8% parasitemia were incubated with 2 μM probe **15** or control probes **14a** or **14b** for 1 h at 37 ºC**.** The following conditions were used for the sub-cellular labeling of parasites: 50 nM Lysosensor Green 189 for 1 min; 70 nM DAPI for 10 min; 1 μM ERTracker Green for 30 min, 500 nM MitoTracker Red 580 for 1 h, 500 nM BODIPY 505/515 for 30 min or 30 nM Nile Red for 10 min. All stains were diluted fresh into complete medium and incubated at 37ºC. Following incubation, infected red blood cells were washed in complete medium and 7 μl of the resulting thick pellet was added onto a glass slide and allowed to dry in the dark. After drying, samples were fixed using 4% paraformaldehyde for 20 minutes at room temperature before mounting. Images were obtained using a Leica TCS SP2 confocal microscope (Leica Microsystems Inc., Bannockburn, IL).

Heme-1 UV-VIS spectroscopic analyses

Spectroscopic analyses were performed similar to those reported in Egan & Ncokazi.[152] A stock solution of porcine hemin (Sigma) was made (0.0012 M) using molecular grade DMSO and stored in the dark. Working Fe(III)PPIX solutions (2.0×10^{-6} M) were

prepared fresh by mixing 16 µl of stock hemin solution with 4 ml DMSO and 1 ml of Hepes buffer (0.2 M, pH 7.4) and making the final volume up to 10 ml with Optima grade H_2O. These working solutions were adjusted to pH 7.4. Next, 150 µl of working solution (40% DMSO, 20 mM HEPES buffer, pH 7.4) was added to each well in a Corning Costar® black, clear bottom 96-well assay plate (Promega). Blank wells contained either 40% DMSO, 20 mM HEPES buffer, pH 7.4 without hemin or 40% DMSO, 20 mM HEPES buffer, pH 7.4 with bromophycolide A (**1**) and no hemin. Bromophycolide A (**1**) was added to wells containing hemin in 3 µl DMSO at various concentrations, ranging from 0.5-20 molar equivalents (mol eq) of **1** to 1 mol eq of hemin. UV-VIS spectroscopic analyses were performed with a BioTek Synergy 4 multi-mode microplate reader at 37 ºC in the dark. Absorbance spectra were collected from 350-700 nm with 1 nm steps at time = 15 min, 1 h, 2 h, 4 h, 6 h, and 8 h, with 3 replicates for each heme:drug (**1**) concentration. Spectra were corrected for dilution by subtracting a reference cell at each concentration of **1**.

Heme crystallization inhibition assay

Heme crystallization inhibition assays were performed as previously described.[144-145] Briefly, 30 µl of a 0.3 mM solution of hemin in 0.1 M NaOH was added to rows B-H in a round-bottom 96-well microtiter plate, and 50 µl of the 0.3 mM hemin solution was added to row A. Amodiaquine and DMSO were used as positive and negative controls, respectively. Controls, **1**, or **7** were added to wells in row A in 10 µl DMSO (starting concentration of either 6, 5, or 4 mol eq relative to hemin) and serial diluted by half down each column, discarding 30 µl from the final row. Next, 10 µl of a 9.8 M sodium acetate solution (pH 4.8) was added to each well, and the plate was incubated for 2 h at 60 ºC. After cooling for 15 min, 75 µl of a 14% (v/v) pyridine solution in 20 mM Hepes (pH 7.5) was added to each well and the plate was centrifuged at 2000 rpm for 1 min. Next, 50 µl of each supernatant was transferred into a flat-bottom 96-well plate and the absorbance

was measured at 405 nm using a microplate reader. The IC_{50} of each compound was calculated using the dose concentration at 50% inhibition on a sigmoidal dose response curve generated using GraphPad Prism version 4.00 for Windows.

Immunoprecipitation with *P. falciparum* cell lysates

A 0.15% saponin solution was used to lyse erythrocytes and isolate parasites, and samples were washed twice with PBS. Parasite pellet was incubated on ice for 5 minutes in cytoplasmic lysis buffer (20 mM HEPES pH 7.9, 10 mM KCl, 1 mM EDTA, 1 mM EGTA, 1 mM DTT, 0.5 mM PMSF, 0.65% Igepal, 1x Roche cocktail inhibitor tablet). Samples were centrifuged at 1500 g for 10 min at 4 ºC, supernatant was collected, and the resulting pellet was re-suspended with nucleus lysis buffer (20 mM HEPES pH7.9, 0.1 M NaCl, 0.1 mM EDTA, 0.1 mM EGTA, 1.5 mM $MgCl_2$, 1 mM DTT, 25% glycerol, 1 mM PMSF, 1x Roche cocktail inhibitor tablet) and incubated for 20 min at 4 ºC. After centrifugation at 6000 g for 10 min at 4 ºC, the supernatant was collected and combined with cytoplasmic proteins. The remaining pellet was sonicated in cytoplasmic lysis buffer, centrifuged, and then all supernatants were combined. The total protein concentration was determined to be 5 mg/ml total protein by Bradford analysis. Probe **15** or **17** (2 µM or 20 µM) was added to lysates for 1 or 4 h and incubated at 4 ºC with constant rotation. Next, 50 µl of Affigel 10 resin containing 3.5 mg/ml of the XRI-TF35 mAb was added to the probe/lysate mixture for an additional 2 h or 14 h with agitation at 4 ºC. As negative controls, tag **14a** (2 µM), **14b** (2 µM), or 0.7% DMSO was added to lysates. Samples were then washed with wash buffer (0.5% Tritonx-100, 25 mM Tris-HCl pH 7.5, 150 mM NaCl, 2 mM EDTA, 2 mM PMSF, 1x Roche cocktail inhibitor tablet) three times. Proteins were either eluted from the resin by incubation with 35 µl of 1 mg/ml of **14a** in RIPA buffer for 1 h at rt, or laemmli buffer was added directly to samples and boiled for 5 min at 100 ºC to elute proteins. Proteins were resolved by 16% SDS-PAGE and detected with Coomassie stain or Silver stain. All SDS-PAGE images of varying

immunoprecipitation conditions with either probe **15**, **17**, or negative controls were identical.

CHAPTER 5

ANTIBACTERIAL NEURYMENOLIDES FROM THE FIJIAN RED ALGA *NEURYMENIA FRAXINIFOLIA*

α-Pyrone-containing natural products have been found in bacteria, fungi, plants, and animals, and exhibit a wide range of biological activities, such as antimicrobial, antineoplastic, and anti-HIV effects.[153] Despite the abundance of α-pyrone analogs in nature, only one species, the red alga *Phacelocarpus labillardieri,* has previously been reported to produce macrocyclic α-pyrones.[154] Herein we report the discovery of two novel macrocyclic α-pyrones, neurymenolides A (**1**) and B (**2**), the first report of natural products from the red alga *Neurymenia fraxinifolia* (Figure 5.1).

Extracts of *N. fraxinifolia* collected from Taveuni, Fiji were first separated by reversed-phase column chromatography guided by growth-inhibitory effects against methicillin-resistant *Staphylococcus aureus* (MRSA). Following reversed-phase, normal-phase, and chiral high performance liquid chromatography (HPLC), **1** and **2** were isolated.

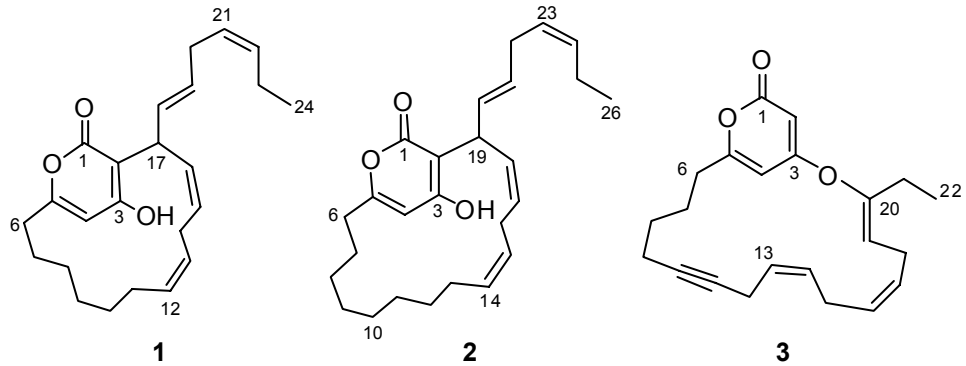

1 **2** **3**

Figure 5.1. Novel natural products from *N. fraxinifolia*, neurymenolides A and B (**1** and **2**), and natural product (**3**) from *P. labillardieri*.[154b]

Neurymenolide A (**1**) displayed an $[M+H]^+$ *m/z* of 369.2428 by HRESIMS, suggesting a molecular formula of $C_{24}H_{33}O_3$. Analysis of ^1H, ^{13}C, DEPT NMR, and IR spectra indicated six carbon-carbon double bonds, one carbonyl, and based upon the index of hydrogen deficiency, two rings (Table 5.1). Three quaternary carbons displayed ^{13}C NMR chemical shifts at 164.7-165.1 ppm, supporting the presence of one ester group (IR 1680 cm^{-1}) and two aromatic carbinol carbons, accounting for all three oxygen atoms. These data and UV spectrophotometric properties of **1** (λ_{max} = 295 nm) were consistent with the literature on hydroxyl-substituted α-pyrones.[154b, 155] HMBC correlations from the aromatic hydroxyl proton (δ 6.48) to C-3 (δ 164.7) and C-4 (δ 101.4), as well as correlations from H-4 (δ 5.81) to C-2 (δ 103.9), C-6 (δ 33.5), and C-1 (δ 165.1) and/or C-5 (δ 165.1), confirmed the hydroxy-substituted α-pyrone ring (Figure 5.2; Appendix A). Additional 2D NMR spectral data led to the identification of a macrocyclic ring connected via the pyrone system by C-5–C-6 and C-2–C-17 bonds, with H-17 (δ 4.55) coupled to C-2 and H-6 coupled to C-5 in the HMBC spectrum (Figure 5.2). Double bonds within the macrocycle were assigned at $\Delta^{12,13}$ (δ 131.0, 126.6) and $\Delta^{15,16}$ (δ 135.2, 127.0) based upon COSY correlations between olefinic protons and adjacent methylenes (Figure 5.2). Finally, the unsaturated 7-carbon aliphatic chain at C-17 was established through COSY and HMBC correlations, terminating with Me-24 (δ 14.2).

Table 5.1. ^{13}C and ^{1}H NMR spectral data for **1** and **2** (500 MHz; in $CDCl_3$).

	1		**2**	
	δ ^{13}C	**δ ^{1}H ($J_{H,H}$)**	**δ ^{13}C**	**δ ^{1}H ($J_{H,H}$)**
1	165.1	-	165.0	-
2	103.9	-	103.8	-
3	164.7	-	164.3	-
4	101.4	5.81 s	101.2	5.77 s
5	165.1	-	165.0	-
6	33.5	2.30 ddd (14, 11, 3.3), 2.61 ddd (14, 10, 3.1)	33.3	2.26 ddd (15, 11, 3.2), 2.63 ddd (15, 11 3.4)
7	25.6	1.57 m, 1.86 m	24.6	1.49 m, 1.82 m
8	26.9	1.24 m, 1.34 m	25.2	1.15 m, 1.22 m
9	27.7	1.18 m, 1.35 m	27.1	1.08 m, 1.25 m
10	27.1	1.07 m, 1.15 m	29.7	1.24 m, 1.30 m
11	26.6	1.76 m, 1.83 m	28.7	1.18 m, 1.23 m
12	131.0	5.23 m	26.7	1.20 m, 1.27 m
13	126.6	5.21 m	27.6	1.88 m, 2.01 m
14	27.0	2.52 br d (17), 2.85 m	131.3	5.34 m
15	135.2	5.65 m	126.4	5.32 m
16	127.0	5.64 m	26.8	2.63 m, 2.94 m
17	36.5	4.55 br s	134.9	5.60 m
18	129.4	5.61 m	127.0	5.67 m
19	129.9	5.61 m	36.2	4.61 br s
20	30.0	2.77 m	129.9	5.62 m
21	125.9	5.30 dt (11, 7.2)	130.4	5.62 m
22	132.9	5.42 dt (11, 7.2)	35.3	2.71 m
23	20.5	2.00 p (15, 7.4)	126.8	5.33 m
24	14.2	0.93 t (7.4)	133.5	5.43 m
25	-	-	25.5	1.99 m
26	-	-	13.8	0.94 t (7.5)
OH	-	6.48 br s	-	6.40 br s

br=broad; s=singlet; d=doublet; dd=doublet of doublets; t=triplet; m=multiplet

Due to substantial chemical shift overlap in the olefinic region of the ^{1}H NMR spectrum of **1**, *E/Z* stereochemistry could not be assigned using *J* couplings. Instead,

ROESY NMR spectral data for well resolved allylic protons were used (Figure 5.2). NOEs were observed between H-11b (δ 1.83) and both H-14s (δ 2.52, 2.85), suggesting a *Z* configuration at $\Delta^{12,13}$. Similarly, correlations between both H-14s and H-17 implied a *Z* configuration at $\Delta^{15,16}$. No NOEs were observed between H-17 and H_2-20 (δ 2.77), suggesting an *E* configuration at $\Delta^{18,19}$. Finally, NOEs between H_2-20 and H_2-23 (δ 2.00) were evident, supporting a *Z* configuration at $\Delta^{21,22}$. We were unable to assign the stereochemistry of chiral C-17; thus at present, the absolute stereochemistry of **1** is unknown.

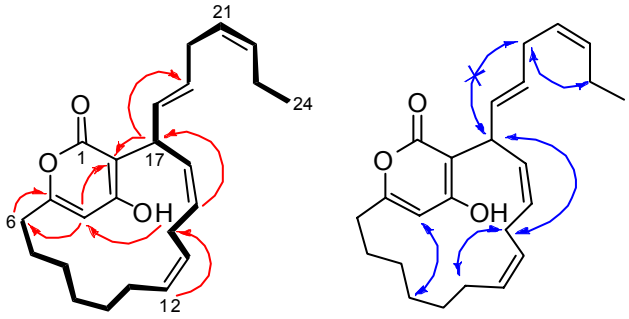

Figure 5.2. Key COSY (bold) and HMBC (red single-headed arrow) correlations established the macrocyclic α-pyrone system of neurymenolide A (**1**). NOE correlations (blue double-headed arrows) established the configurations of the double bonds in **1**.

High-resolution mass spectral data indicated that neurymenolide B (**2**) possessed two additional methylene units relative to **1**, displaying an $[M+H]^+$ *m/z* 397.2765, consistent with a molecular formula of $C_{26}H_{37}O_3$. Comparison of ^1H and ^{13}C NMR spectral data of **2** with that of **1** suggested that the α-pyrone and linear aliphatic systems were identical. The two extra methylenes were assigned in the macrocyclic ring, based on a combination of COSY and HMBC correlations (Appendix A). Equivalent NOEs were observed for **1** and **2**, suggesting that the *E/Z* stereochemistry is identical for both natural products of *N. fraxinifolia*.

HPLC purification of **1** using several different stationary phases consistently resulted in two peaks, each of which split again into the same two peaks when re-analyzed using the same HPLC column. NMR spectral and optical rotation data were identical for material collected from each of these peaks, which led to the hypothesis that **1** consists of quickly interchanging rotational isomers (atropisomers). Synthetic reports of related compounds suggest planar chirality due to the restricted rotation about the α-pyrone ring.[156] Because **1** contains a stereogenic carbon (C-17), these two atropisomers would be expected to behave as diastereomers. To further explore this hypothesis, **1** was acetylated to yield 3-*O*-acetylneurymenolide A, separated by HPLC, and then analyzed by ^{1}H NMR spectroscopy. The added bulk of the acyl group slowed the rotation about the α-pyrone enough to yield two distinguishable sets of ^{1}H chemical shifts and two HPLC peaks that equilibrated over the course of several hours, rather than the minute time-scale conversion observed for atropisomers of **1**. Rotational isomerization was not observed with **2**, which is reasonable given the larger macrocyclic ring size of **2** relative to **1.**

The two unique macrolides described in this study each represent new carbon skeletons and only the second example of macrocyclic α-pyrones occurring in nature. Macrocyclic pyrones isolated from *Phacelocarpus labillardieri* (e.g., **3**; Figure 5.1) are connected through an ether bond at C-3, unlike the neurymenolides. However, all of these macrocyclic pyrones would be expected to share a common biogenesis. Given the similar chemistry of *N. fraxinifolia* and *P. labillardieri*, it is interesting to note that the two red algal species are only distantly related, sharing the class Florideophyceae. This is the first report of chemistry from the red alga *N. fraxinifolia,* although its family, Rhodomelaceae, is well studied.[29]

The biosynthesis of the neurymenolides is expected to occur by successive condensations of malonyl-CoA, beginning at the aliphatic chain terminus and ending at the α-pyrone carbonyl. These natural products may be formed by a mixed polyketide/fatty acid biosynthetic pathway,[35] with previous such examples reported involving both prokaryotes and eukaryotes.[157] One could envision the neurymenolides arising from diketide extention of eicosapentaenoic acid or docosahexaenoic acid, with macrocyclization promoted by an enolate attack with loss of water (Scheme 5.1); however, it is unclear whether the macrocyclization or the α-pyrone formation occurs first. The *E* configuration at $\Delta^{18,19}$ could potentially occur through a free radical process common to eicosanoids.[35]

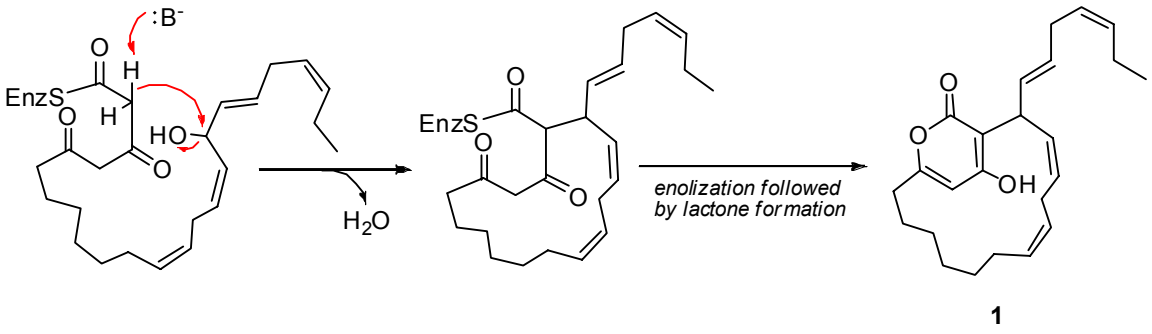

1

Scheme 5.1. Proposed biosynthesis of neurymenolide A (**1**) from a putative polyketide-extended eicosapentaenoic acid-derived precursor.

Neurymenolide A (**1**) exhibited moderately potent activity against methicillin-resistant *Staphylococcus aureus* (MRSA) and vancomycin-resistant *Enterococcus faecium* (VREF) (IC_{50} of 2.1 μM and 4.5 μM, respectively, Table 5.2). Moderate *in vitro* cytotoxicity against DU4475 breast tumor cells was also observed for **1** (IC_{50} of 3.9 μM), as well as moderate to weak activity against 11 other tumor cell lines (IC_{50} values

ranging from 5.4 to 28 μM, Table 5.3). Neurymenolide B (**2**) was slightly less active against MRSA and considerably less active in all other pharmacological assays (Table 5.2 and 5.3), suggesting that the size or conformational restriction of the macrocyclic ring is important for biological activity. 3-*O*-acetylneurymenolide A (mixed atropisomers) was also less active against MRSA (IC_{50} of 11 μM), signifying the importance of the aromatic hydroxyl group for antibacterial activity.

Table 5.2. Antibacterial activities of **1-2**.

	antibacterial IC_{50} (μM)		
cmpd	MRSA	VREF	*M. tuberculosis*
1	2.1	4.5	>100
2	7.8	31	>100

Table 5.3. Additional pharmacological activities of **1-2**.

	anticancer IC_{50} (μM)			
cmpd	mean[a]	DU4475[b]	antimalarial IC_{50} (μM)	antifungal IC_{50} (μM)
1	8.8	3.9	68	>680
2	39	19	>100	>680

[a] Mean of 12 cell lines; [b] breast tumor cell line

The current study describes structurally novel macrocyclic α-pyrones, establishing the first report of chemistry from the red alga *Neurymenia fraxinifolia*. Determining **1** to be present as interchanging atropisomers presented an exciting chemical challenge, and the putative polyketide/fatty acid biogenesis of the neurymenolides represents another example of the diversity of the acetogenic pathway. Neurymenolide A (**1**) shows promise as a novel template for the design and development of new antibiotics.

Experimental Section

Biological material. *Neurymenia fraxinifolia* (family Rhodomelaceae, order Ceramiales, class Florideophyceae, phylum Rhodophyta) was collected at depths of 20-25 m from Taveuni, Fiji, offshore from Waitabu Marine Protected Area near Lavena Village (16^{o} 48' 97" S, 179^{o} 50' 84" W) in July 2006. *N. fraxinifolia* was stored at -60 ^{o}C until extraction 15 months later. One sample was placed directly in methanol and stored until further analysis. One voucher specimen (G-0086) was deposited at the University of the South Pacific, Fiji, and the second was stored at Georgia Institute of Technology.

Chemicals. Solvents used for extractions were reagent grade, and those used for HPLC and LC-MS were HPLC or Optima grade (Fisher Scientific). NMR solvents were purchased from Cambridge Isotope Laboratories. Commercially available reagents were purchased from Sigma-Aldrich (Milwaukee, WI) and used as received.

Isolation. *N. fraxinifolia* was exhaustively extracted with methanol and methanol/dichloromethane (1:1, 1:2). The extracts were combined, filtered, and reduced *in vacuo.* The crude extract was separated with HP20ss resin into four fractions, eluting with (1) 1:1 methanol: water, (2) 4:1 methanol: water, (3) 100% methanol, and (4) 100% acetone. The antibacterial HP20ss fractions 3 and 4 were separated by C_{18} reversed-phase HPLC (Alltech Alltima C_{18}, 5 μm, 10 × 250 mm) using a gradient of methanol and water, followed by normal phase silica gel HPLC (Agilent Zorbax RX-SIL, 5 μm, 9.4 × 250 mm) with 85:15 hexanes: ethyl acetate to yield neurymenolides A and B (**1-2**). Because **1** appeared to isomerize on normal phase silica gel, separation by chiral HPLC (Astec Chirobiotic T, 5 μm, 4.6 × 250 mm) was attempted with 78:12 hexanes: ethyl acetate; again, **1** eluted as two peaks. When the material from each peak was reinjected onto the chiral column, the same two peaks consistently reappeared. The two HPLC

peaks from **1** were stored separately under N_2 at -80 ^oC, along with **2**, until characterization and pharmacological testing was conducted.

Acetylation of neurymenolide A (1). To a solution of **1** (10 mg, 0.027 mmol) in pyridine (0.5 ml) was added acetic anhydride (20 µl, 0.21 mmol) under a nitrogen atmosphere. The reaction was stirred at room temperature for 12 h and then diluted with cold water (10 ml) and extracted with ethyl acetate (10 ml). The organic layer was dried over $MgSO_4$ and evaporated. The residue was separated via reversed-phase HPLC (Alltech Alltima C_{18}, 5 µm, 10 × 250 mm), eluting with 100% acetonitrile, yielding 9.8 mg (88% yield) of 3-*O*-acetylneurymenolide A, acetylated atropisomers of **1**. The two atropisomers were present in a 3:2 ratio, based on HPLC-UV peak integration and ^1H NMR spectral integration. Only ^1H chemical shifts differing from that of **1** (Table 5.1) are listed. ^1H-NMR ($CDCl_3$, 500 MHz) for major atropisomer δ: 5.98 (H-4, s); 4.49 (H-17, br s); 2.80 (H-14b, m); 2.72 (H_2-20, m); 2.43 (H-14a, br d, J = 17); 2.21 (H_3-26, s) ppm. ^{13}C-NMR ($CDCl_3$, 250 MHz) for major atropisomer δ: 166.6; 164.2; 163.7; 158.5; 132.5; 130.2; 130.0; 129.8; 129.4; 129.3; 127.2; 126.3; 117.3; 103.7; 37.1; 33.7; 30.0; 27.2; 27.1; 26.9; 26.4; 26.2; 25.5; 21.2; 20.5; 14.2 ppm. ^1H-NMR ($CDCl_3$, 500 MHz) for minor atropisomer δ: 6.0 (H-4, s); 4.14 (H-17, m); 2.80 (H-14b, m); 2.72 (H_2-20, m); 2.43 (H-14a, br d, J = 17); 2.34 (H_3-26, s) ppm. ^{13}C-NMR ($CDCl_3$, 250 MHz) for minor atropisomer δ: 167.1; 165.0; 162.1; 157.2; 132.6; 130.1; 129.8; 129.7; 129.4; 129.4; 127.5; 126.3; 116.9; 102.5; 37.5; 33.8; 30.0; 27.6; 27.4; 27.1; 26.9; 25.8; 25.5; 20.9; 20.5; 14.2 ppm. ESI-MS for both atropisomers $[M + H]^+$ *m/z* 411.3, 100%, $[M + H - COCH_3]^+$ *m/z* 369.3, 15%.

Analytical and spectroscopic methods. UV spectra were recorded in MeOH with a Spectronic 21D spectrophotometer using quartz cuvettes. Optical rotations were measured on a Jasco P-1010 spectropolarimeter with a 10 cm (8 ml) cell, with compounds dissolved in MeOH. Circular dichroism spectra were acquired on a Jasco J-

810 spectropolarimeter and 1 mm pathlength cells were used. High-resolution mass spectra were generated using electrospray ionization with an Applied Biosystems QSTAR-XL hybrid Quadrupole-Time-of-Flight tandem mass spectrometer and Analyst QS software. LC-MS analyses were conducted using a Waters 2695 HPLC with Waters 2996 photodiode array UV detection and Micromass ZQ 2000 mass spectrometer with electrospray ionization. LC-MS chromatography was achieved with an Alltech Alltima C_{18} column (3 μm, 2.1 × 150 mm), using gradient mobile phases of MeCN (aq) with 0.1% acetic acid. NMR spectra were recorded on a Bruker DRX-500 instrument, using a 5 mm inverse detection probe for ^{1}H, COSY, ROESY, HSQC, and HMBC experiments, and a 5 mm broadband probe for ^{1}H, ^{13}C, and DEPT-135, and referenced to residual $CHCl_3$ (7.24 and 77.0 ppm, for ^{1}H and ^{13}C, respectively).

Pharmacological assays. All pharmacological assays were performed as outlined in the Experimental Section of Chapter 3.

Neurymenolide A (1): colorless oil (2.9 mg, 0.098% plant dry mass); $[\alpha]^{24}_{D}$ -150 (*c* 0.02 g/100 ml, MeOH); UV (ACN) λ_{max} 295 nm (log ε = 3.39); IR (NaCl) ν_{max} 3350 (br), 3010, 2860, 2660, 1680, 1570, 1440, 1280, 1160, 970 cm^{-1}; ^{1}H and ^{13}C NMR ($CDCl_3$, 500 MHz) data see Table 1; COSY, HMBC, and NOE data, see Appendix A; HR ESI-MS $[M + H]^+$ *m/z* 369.2428 (calcd for $C_{24}H_{33}O_3$, 369.2429).

Neurymenolide B (2): colorless oil (1.0 mg, 0.013% plant dry mass); $[\alpha]^{24}_{D}$ -240 (*c* 0.02 g/100 ml, MeOH); UV (ACN) λ_{max} 295 nm (log ε = 3.41); ^{1}H and ^{13}C NMR ($CDCl_3$, 500 MHz) data see Table 1; COSY, HMBC, and NOE data, see Appendix A; HR ESI-MS $[M + H]^+$ *m/z* 397.2756 (calcd for $C_{26}H_{37}O_3$, 397.2743).

CHAPTER 6

CONSERVATION OF PROGESTERONE HORMONE FUNCTION IN INVERTEBRATE REPRODUCTION

Introduction

Sex steroids and their receptors have been well studied in vertebrate animals, but much less is known about the mechanisms by which they regulate physiology and behavior in invertebrates.[158] Recent gene sequencing, bioinformatics, and protein synthesis approaches suggested that modern nuclear steroid receptors evolved from an ancient receptor which arose 0.6 to 1.2 billion years ago, before a common bilateral ancestor diverged into the deuterostomes and protostomes.[159] This ancient receptor is postulated to have been activated by estrogen, the terminal product in steroid biosynthesis, with intermediates progesterone and testosterone acquiring uses as hormones later in evolutionary history.[160] The discovery of estrogen receptor homologs in mollusks[161] and annelids[162] indicated that Lophotrochozoan lineages have not lost this type of hormone chemoreception, despite the use of non-androgen steroid hormones in Ecdyzoans (e.g., ecdysteroids in insects; dafachronic acids in *C. elegans*). Recently an estrogen-like receptor was identified in *C.elegans*,[163] supporting the hypothesis that steroid receptors are ancient and widespread. In addition, progesterone activates non-nuclear, membrane-associated receptors in vertebrates and invertebrates with impacts on behavior and reproduction.[164] However, substantial gaps still remain in the phylogenetic distribution of sex steroid receptors in many invertebrates and their functions in sexual differentiation, development, reproduction, and behavior are unclear.

The invertebrate monogonont rotifer *Brachionus manjavacas* belongs to the Lophotrochozoa, one of the three major animal clades whose origin pre-dates the Cambrian period 543 million years ago.[165] An essential attribute of monogonont rotifers

is their ability to reproduce both asexually and sexually. Although this flexible reproductive strategy is central to their evolutionary success, little is known about how reproduction is regulated in rotifers or the molecules involved in reproductive signaling in most non-arthropod invertebrates.[166]

The switch from asexual to sexual reproduction in *B. manjavacas* is triggered in a quorum sensing process by a secreted pheromone called the mixis-inducing protein.[167] *N*-terminal sequencing of 17 amino acids from the mixis-inducing protein established that this fragment was identical to a putative steroidogenesis-inducing protein reported from humans.[168] This observation led to the hypothesis that steroid hormones may be involved in regulating sexual reproduction in *B. manjavacas*. We were also encouraged by the fact that the sex steroid receptor family is ancient, arising early in metazoan evolution.[159] Genome-mining of a rotifer cDNA library led to the identification of a 799 nucleotide sequence (GenBank accession FJ829246) with 60-80% homology to multiple membrane-associated progesterone receptors, including that of the sea urchin *Strongylocentrotus purpuratus* and several *Drosophila* species. The presence of a progesterone receptor in *B. manjavacas* led us to explore its role in endocrine signaling and reproductive physiology.

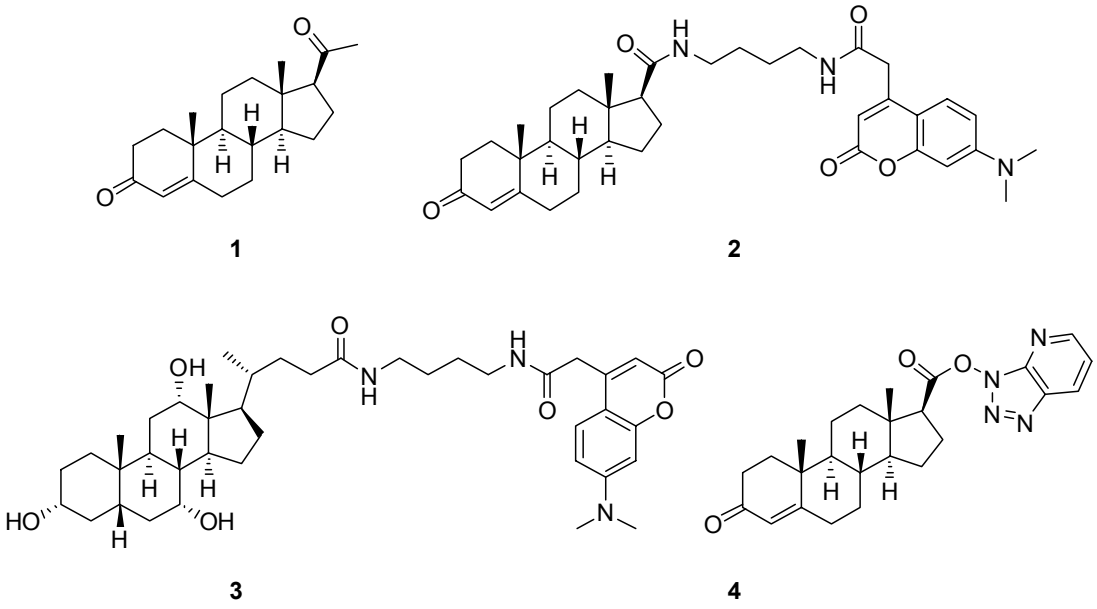

Figure 6.1. Progesterone (**1**), and a panel of probes including the IAF-labeled progesterone probe **2**, an IAF-labeled control steroid probe **3**, and a reactive steroid probe **4**.

We designed and synthesized a molecular probe suitable for both histological analyses in live rotifers and subsequent protein isolation studies by immunoaffinity methods. By installing a 7-dimethylamino-4-coumarin tag,[23] also called an immunoaffinity fluorescent (IAF) tag,[146] onto progesterone (**1**), the resulting probe (**2**, Figure 6.1) could be used for both receptor imaging and *in vitro* isolation of a progesterone-binding receptor in *B. manjavacas* because of the availability of a selective monoclonal antibody (mAb) against the IAF tag. Incubation of live and dead rotifers with **2** consistently resulted in its localization in reproductive organs, including the ovaries, vitellarium (yolk gland), oviduct, and egg in females, and the seminal vesicle, rudimentary gut, and sperm duct in males (Figure 6.2a). Eggs attached to females fluoresced only when punctured, suggesting that the eggshell prevented probe uptake.

Using the natural auto-fluorescence of the algal food *Tetraselmis suecica* (excitation at 488 nm) to compare with localization of **2** (excitation at 375 nm), we confirmed that **2** was not localizing in the digestive system as a result of ingestion (Figure 6.2b). Furthermore, male rotifers do not feed and lack stomachs, providing evidence that the staining of male reproductive organs is due to the membrane permeability of **2** rather than digestive absorption.

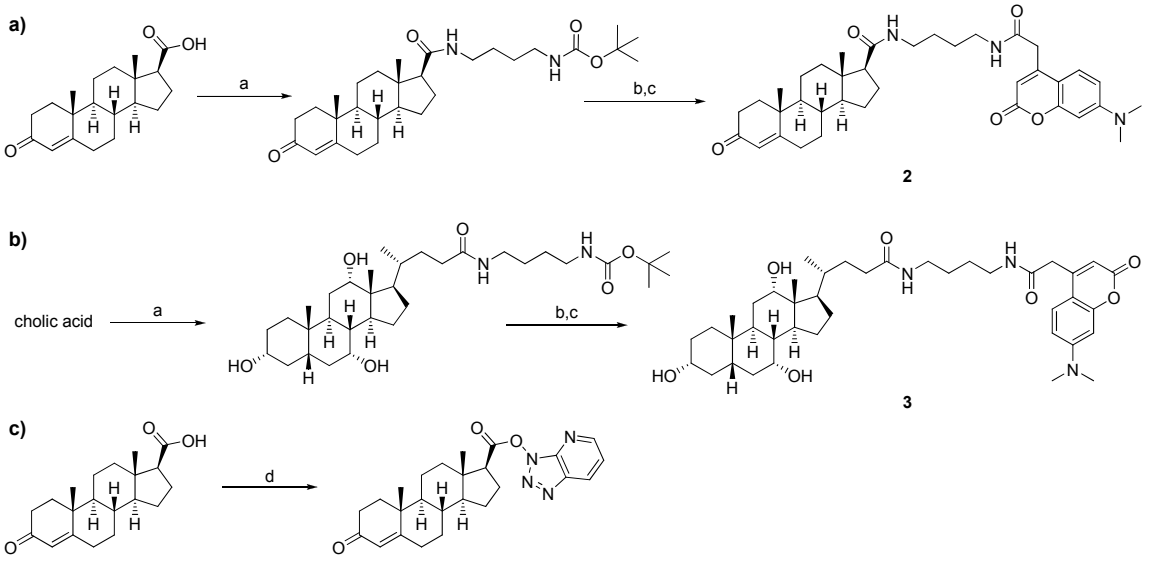

Scheme 6.1. Synthesis of steroid probes. (a) Synthesis of IAF labeled progesterone probe **2**. Reagents and conditions: **a)** *N*-boc-1,4,-butyldiamine, HATU, DMF, 89%; **b)** TFA, CH_2Cl_2, rt; **c)** 7-dimethylamino-4-coumarinacetic acid, Et*i*Pr_2, HATU, DMF, 67% over two steps. (b) Synthesis of IAF labeled control probe **3**. Reagents and conditions: **a)** *N*-boc-1,4-butanediamine, Et_3N, HATU, DMF, 80%; **b)** TFA, CH_2Cl_2, rt; **c)** 7-dimethylamino-4-coumarinacetic acid, Et_3N, HATU, DMF, 52% over two steps. (c) Synthesis of reactive ester **4**. Reagents and conditions: **a)** HATU, DMF, 94%.

The specificity of the rotifer progesterone receptor for progestin-like molecules was investigated. An IAF-labeled control steroid probe (**3**, Figure 1) was synthesized in a similar method as **2** (Scheme 6.1a), but using cholic acid as a starting material (Scheme 6.1b). Imaging experiments with live rotifers resulted in a lack of localization of **3** or a dye control in the reproductive organs of either *B. manjavacas* females or males (Figure 6.2a). These results suggest that the rotifer progesterone receptor exhibits strong specificity for its ligand.

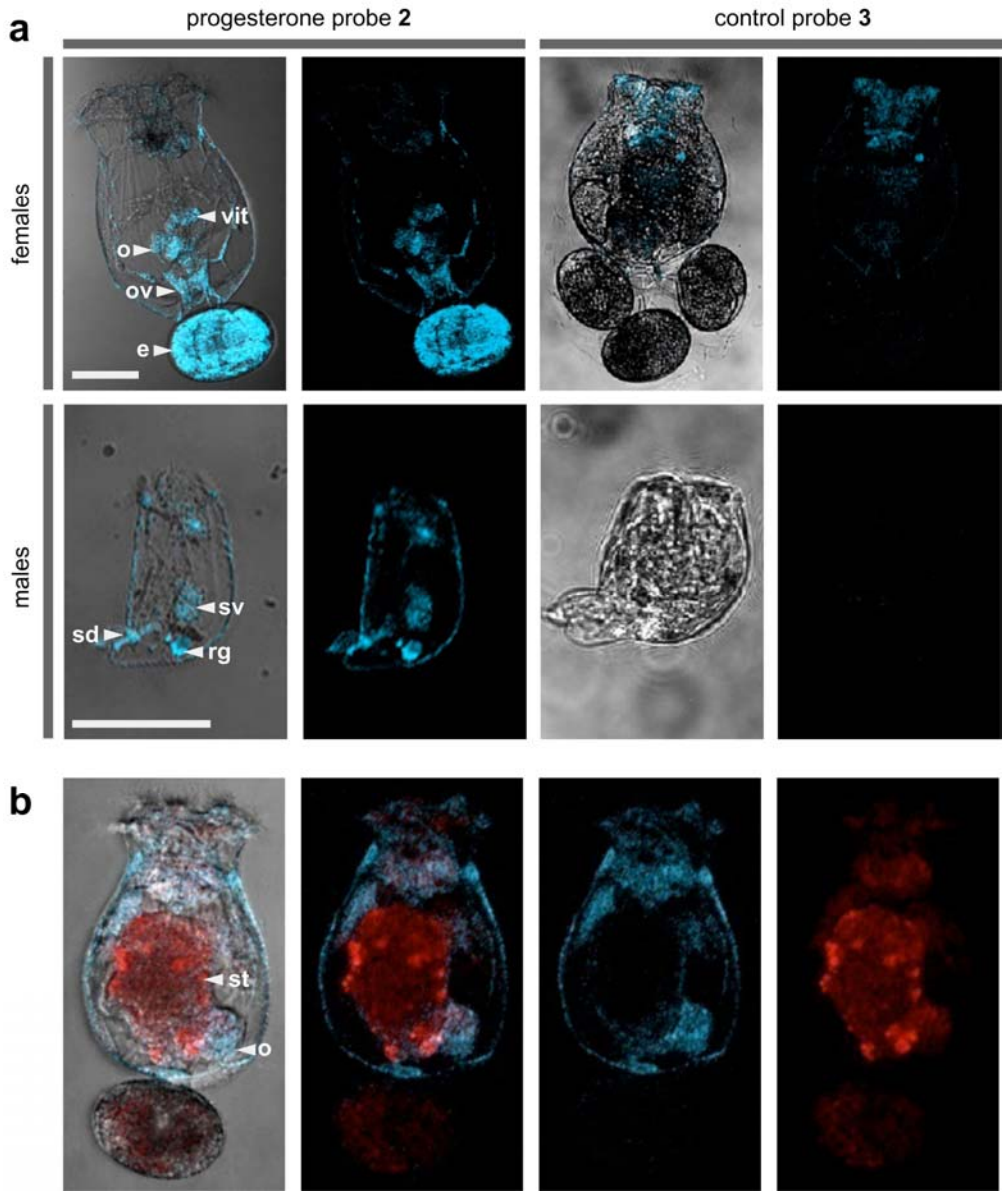

Figure 6.2. Imaging studies with the rotifer *Brachionus manjavacas*. (a) Confocal fluorescence microscopic images depicting rotifers treated with **2** or **3**. (b) Two-color confocal images showing a female rotifer fed *Tetraselmis suecica* then treated with **2**; *T. suecica* autofluoresces in the red channel, and **2** fluoresces in the blue channel. Scale bars denote 100 μm. Blue and red fluorescence were collected with excitation at 375±10 nm and emission at 458±10 nm and excitation at 488±10 nm and emission at 518±10 nm, respectively. Organelles are noted by: vit = vitellarium (yolk gland); o = ovaries; ov =

oviduct; e = egg; sv = seminal vesicle; rg = rudimentary gut; st = stomach, and sd = sperm duct.

These observations led us to screen for the presence of steroid hormones in rotifers. *B. manjavacas* biomass was extracted and lipophilic (i.e., steroid-containing) fractions were subjected to normal-phase high performance liquid chromatography (HPLC). Three sterols were isolated in sufficient quantities for characterization, identified as campesterol (**5**) at 18 mg/g dry biomass, campesta-5,7-dien-3-β-ol (**6**) at 12 mg/g, and 5-α-campest-7-en-3-β-ol (**7**) at 4.1 mg/g (Figure 6.3). Campesterol (**5**) is a known plant sterol found in the green alga *T. suecica,* the food of *B. manjavacas*;[169] thus, it was concluded that sterols **5**-**7** were of dietary origin. When rotifer extracts were screened using a progesterone enzyme immunoassay (EIA), we found that **1** was present at a concentration of 3.1 ng/g dry biomass. To further support these data, we analyzed partially purified rotifer extracts using LC-tandem mass spectrometry (LC-MS/MS) in multiple reaction monitoring mode and unequivocally showed that **1** was present at a concentration of 4.4 ng/g dry rotifer biomass, comparable to the progesterone EIA result.

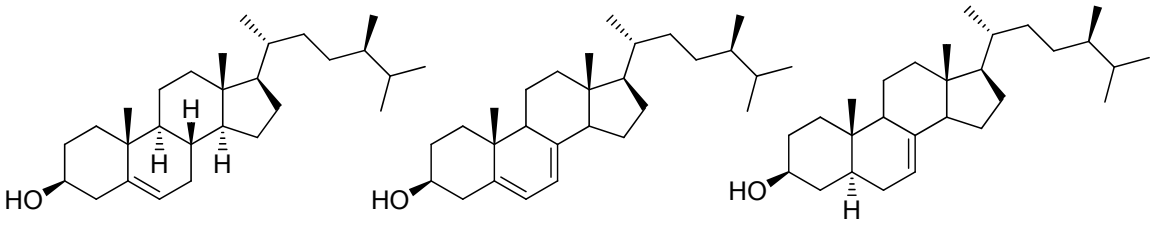

5 **6** **7**

Figure 6.3. Steroids isolated from *Brachionus manjavacas* including campesterol (24*R*-ergost-5-en-3β-ol, **5**), campesta-5,7-dien-3-β-ol (**6**), and 5-α-campest-7-en-3-β-ol (**7**). Authentic standards of **5** and **7** were purchased from Sigma-Aldrich for verification of

structures. Campesterol was purchased as a 65:35 mixture of crystalline 24*R*-ergost-5-en-3β-ol and 24*S*-ergost-5-en-3β-ol, distinguishable via ^{13}C NMR spectroscopy. Carbon-13 NMR spectral data was acquired for both the authentic standard and the isolated rotifer steroid. ^{13}C NMR spectral data for the isolated rotifer steroid **5** were identical to 24*R*-ergost-5-en-3β-ol ^{13}C NMR chemical shifts, consistent with the hypothesis that **5-7** were of dietary (algal) origin. Sterol **6** was identified by comparing spectrometric data to reported literature values.

We then applied an immunoprecipitation (IP) technique[146] to screen for progesterone-binding proteins in crude lysates of *B. manjavacas*. Lysates were incubated with **2** and immunoprecipitated with an Affigel-Hz resin containing a mouse mAb engineered with affinity against the IAF tag. Two bands at approximately 70 and 82 kDa were observed by SDS-PAGE over several repeated experiments (L2 and L3, Figure 6.4a). These bands were confirmed to arise from selective binding to **2** since the addition of **1** to the lysate prior to IP reduced the isolation of the two proteins (L4, Figure 6.4a).

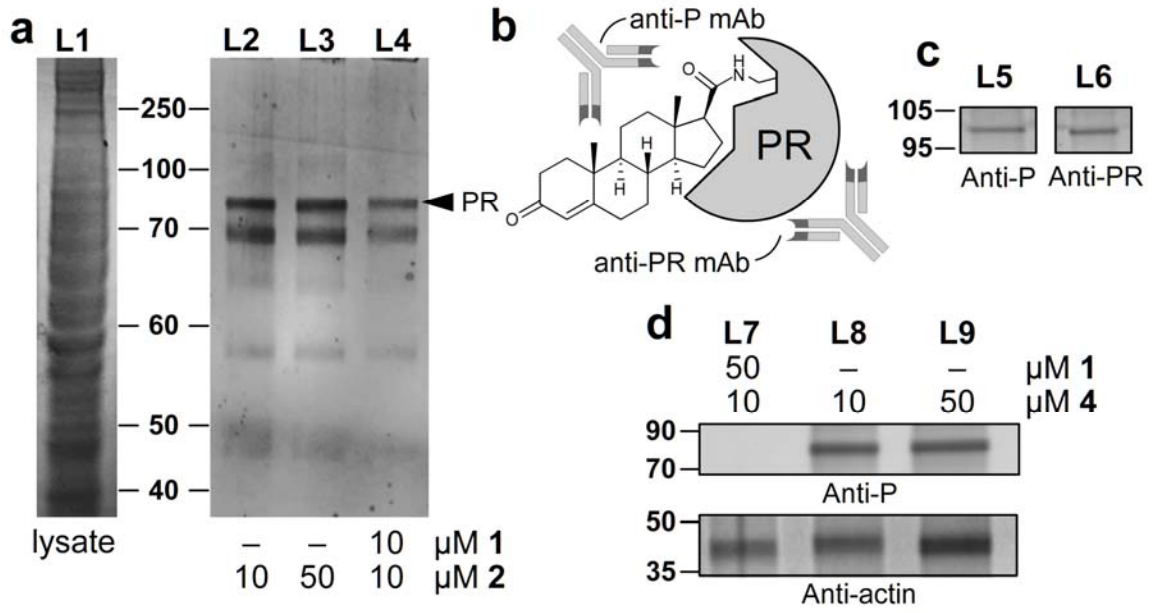

Figure 6.4. Immunoprecipitation (IP) of a rotifer progesterone receptor (PR). (a) SDS-PAGE analysis depicting the IP of B. manjavacas lysate (L1) in the presence of **2** (L2-L3). IP of lysates treated with **1** showed a reduction in the isolated proteins (L4). (b) Reactive probe **4** was designed to form a covalent adduct with a PR by formation of an amide with the side chain amine of a lysine residue. The resulting covalent adducts can be selectively identified using an anti-progesterone mAb (anti-P) and can be validated using an anti-progesterone receptor mAb (anti-PR). (c) Demonstration of **4** using mammalian MCF-7 cell lysates. Western blot analyses depicting the presence of a 100 kDa protein in MCF-7 cell lysates incubated with **4**. Comparable bands corresponding to the MCF-7 PR were identified after incubation with an anti-P mAb in L5 or an established anti-PR mAb in L6. (d) Western blot analysis of *B. manjavacas* lysate treated with **4** showed a single major band at 82 kDa after treatment with **4** (L8-L9). This band could be ablated by the co-treatment with **1** (L7). Loading control was conducted with actin (A).

Tryptic-digest LC-MS/MS analyses were conducted on crude IP mixtures incubated with **2** and compared to crude lysates obtained without **2**. Over three

repetitions, we identified two key tryptic fragments with *m/z* of 1239.57 and 1589.74 appearing only in IP lysates treated with **2**. Subsequent in-gel digestion gave comparable fragments *m/z* of 1239.12 and 1589.48 from the band at 82 kDa (PR, Figure 6.4a). Analyses of the digested peptides indicated that these masses arose from the respective peptides EWEMQFLEK and DFYGPGGPYSVFAGR, as predicted by the nucleotide sequence of FJ829246, and were up to 92% identical to peptide sequences observed in related progesterone receptors. These data provided strong evidence for the presence of a progesterone receptor within *B. manjavacas*.

To further support this conclusion, we designed and synthesized a probe containing a reactive 7-aza-benzotriazole ester (**4**, Figure 6.1 and Scheme 6.1c), with the goal of covalently labeling the active site of a progesterone receptor through formation of an amide bond by displacement of the 7-aza-benzotriazole ester in **4** via nucleophilic side-chain residues proximal to the steroidal binding pocket of the receptor. This approach was validated by Western blot analysis of a human cell lysate (MCF-7), which delivered a band at 100 kDa when treated with **4** and developed with an anti-progesterone mAb (anti-P mAb). A comparable band corresponding to the MCF-7 progesterone receptor was identified after staining with an established anti-progesterone receptor mAb (L5 and L6, Figure 6.4c), thereby confirming the assignment. Reactive probe **4** was presented to protein lysates prepared from whole *B. manjavacas,* which were then immunoprecipitated using the anti-P mAb to isolate proteins that bound to or were modified by **4** (Figure 6.4d). Over multiple repetitions, Western blot analyses identified a band at 82 kDa (L8 and L9, Figure 6.4d) corresponding to the rotifer progesterone receptor, which could be blocked by pre-treating the lysates with **1** (L7, Figure 6.4d).

The function of the rotifer progesterone receptor was explored using RNA interference (RNAi) by transfection of female rotifers with dsRNA representing a 507 bp

fragment of the progesterone receptor gene (FJ829246). Quantitative real-time PCR demonstrated a 62% decrease (n = 12) in expression of this gene relative to phosphate buffered saline (PBS)-control treated animals. Using confocal fluorescence microscopy we observed an 85% reduction in binding of **2** (n = 6, two sample, one-tailed paired t-test, P = <0.0001, Figure 6.5a) when compared to rotifers treated with dsRNA from the rotifer elongation factor gene (control). The decrease in binding of **2**, and therefore progesterone, in RNAi experiments confirms that the rotifer gene FJ829246 functions as a progesterone receptor.

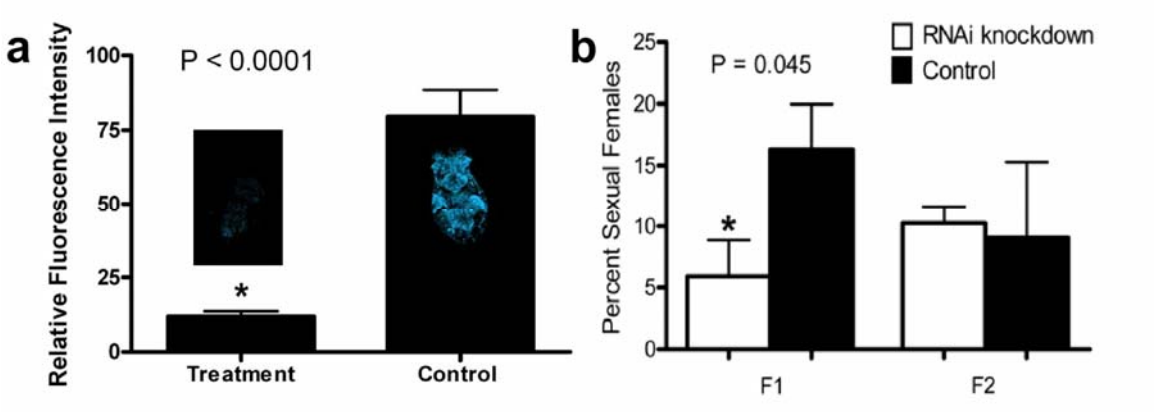

Figure 6.5. RNAi experiments with female rotifers transfected with dsRNA from the rotifer progesterone receptor gene (treatment), dsRNA from the rotifer enlongation factor gene (control for **a**), or with PBS (control for **b**). (a) Relative fluorescence intensity of female rotifers incubated with **2** (n = 6, two sample, one-tailed paired t-Test, P < 0.0001; error bars denote standard error). (b) Percent sexual females in first generation rotifer daughters, F1, and second generation rotifer daughters, F2 (n = 4, two sample, one-tailed paired t-Test, P = 0.045 for F1; n = 4, two sample, one-tailed paired t-Test, P = 0.434 for F2; error bars denote standard error).

RNAi experiments were also used to gain mechanistic insights of the rotifer progesterone receptor and effects on rotifer reproduction. Females transfected with the

dsRNA progesterone receptor gene fragment or with PBS buffer were incubated for 72 hours, followed by counting of sexual and asexual females. Rotifers exposed to the dsRNA rotifer progesterone receptor gene fragment experienced a 64% decrease in induction of sexuality in first generation daughters (F1) when compared to controls (n = 4, two sample, one-tailed paired t-test, P = 0.045), but no significant effect on induction of sexuality was observed in second generation females (F2) after an additional 96 hour incubation (n = 4, two sample, one-tailed paired t-test, P = 0.434, Figure 6.5b). Mating behavior of males towards sexual females was also explored by counting the number of males circling females, and no significant difference was observed between RNAi treatments and controls (36% circling for RNAi treatments, 39% circling for buffer-only controls; n = 3, two sample, one-tailed paired t-test, P = 0.374). Almost twice as many asexual maternal females failed to produce clonal daughters when transfected with the dsRNA rotifer progesterone receptor gene fragment compared to controls (n = 9, two sample, one-tailed t-test, P = 0.022).

Discussion

These studies identify a rotifer progesterone receptor and provide evidence that supports progesterone chemoreception as a key regulatory step involved in rotifer reproduction. Using a dual fluorescent and affinity probe (**2**), we demonstrated localization of a progesterone-specific chemoreceptor to sex organs within female and male rotifers, while also establishing ligand-selective binding using a control steroid probe (Figure 6.2). These data are consistent with specific recognition of 3-keto steroids by their receptor, as illustrated by progesterone binding interactions to the human progesterone receptor.[170] Because of the structural similarity of progesterone (**1**) and testosterone, **2** may have been expected to detect testosterone receptors in our imaging experiments. However, testosterone receptors were not detected in the transcriptomes

of either female or male *B. manjavacas*, although these transcriptomes are not yet fully sequenced.

Two complementary methods, progesterone EIA and LC-MS/MS, established the presence of **1** in rotifer tissues at 3-4 ng/g dry biomass, consistent with its role as a natural ligand for the progesterone receptor. Progesterone (**1**) is present in mammals at very low levels, generally <2 ng/ml in human blood with the exception of pregnant females,[171] comparable to the low concentration of progesterone observed in rotifers. Although we conclude that rotifers use progesterone, the involvement of additional very closely related invertebrate steroids, such as 6β-hydroxyprogesterone found in hemolymph of the crayfish *Astacus leptodactylus*,[172] cannot be ruled out.

In vitro target elucidation studies with fluorescent probe **2** and reactive probe **4** suggested the presence of an 82 kDa rotifer progesterone receptor through the use of two affinity methods[173] and were supported by the peptides EWEMQFLEK and DFYGPGGPYSVFAGR found via MS/MS analyses (Figure 6.4 and Appendix B). While the 82 kDa band is consistent with the size of many membrane progesterone receptors belonging to the progestin and adiponectin receptor family (PAQR),[174] it did not match the predicted ~20 kDa size of our rotifer nucleotide sequence (FJ829246). The rotifer progesterone receptor gene is most closely related to progesterone receptor membrane components (PGRMC); previously identified PGRMCs range in size from 18-22 kDa but form complexes with larger proteins such as cytochrome b5, thus resulting in complexes of much higher molecular weights.[175] The observed 82 kDa band may represent a protein complex containing the rotifer PGRMC or a larger rotifer membrane progesterone receptor related to the PAQR family. Complete identification of the gene sequences for additional steroid receptors in *B. manjavacas* will be available upon the full sequencing of its genome.

RNAi knockdown of the gene FJ829246 further confirmed the identification of the rotifer progesterone receptor, with a 62% decrease in gene expression measured by qPCR and an 85% decrease in progesterone binding to the receptor in intact rotifers (Figure 6.5a), establishing the function of our gene. The 64% decrease in induction of sexuality for daughters of female rotifers exposed to RNAi (Figure 6.5b), while other biological functions such as mating behavior were unaffected, indicated that the progesterone signaling is necessary for hormonal regulation in these animals. Furthermore, RNAi treated maternal females showed a doubling of the rate of reproductive failure among asexual females. Together, these data suggest that the rotifer progesterone receptor plays a central role in rotifer sexual reproduction, including the transition from asexual to sexual reproduction. These findings build on the growing evidence of evolutionary conservation of progesterone receptor function and mechanism over a wide span of eukaryotes.[176]

Collectively, our data demonstrate that progesterone (**1**), a well-studied hormone with known importance in mammalian reproduction, plays a central role in reproduction of the ancestral microinvertebrate *B. manjavacas* (Rotifera), and thus progesterone and its receptor exhibits a conservation of function over a broad expanse of animal phylogeny. This study provides further evidence to support the ancient origin of steroid hormonal regulation and suggests that endocrine regulation of mammalian reproduction may be derived from primitive regulatory pathways.

Experimental Section

General methods. Commercially available reagents were purchased from Sigma-Aldrich (Milwaukee, WI), AK Scientific (Mountain View, CA), or VWR Scientific (Brisbane, CA), and used as received unless otherwise noted. All reactions were performed under a nitrogen atmosphere unless otherwise noted. Reactions were

monitored using thin-layer chromatography (TLC) using Silica Gel 60 F254 plates from EMD Chemicals (San Diego, CA), and visualized with a UV lamp at 254 nm or by staining with Hannesian's stain (90 ml Water, 2.5 g of $(NH_4)_6Mo_7O_{24}•4H_2O$, 1 g of $Ce(NH_4)_4(SO_4)_4•2H_2O$, 10 ml of conc. H_2SO_4). Additional experimental details are provided in Appendix B.

Compound purification and analyses. Flash chromatography was performed using Geduran Silica gel 40–63 μm particle size from EMD Chemicals (San Diego, CA). HPLC was performed using an Alltima C_{18} column (10 × 250 mm, 5 μm) from Alltech Associates (Deerfield, Il) with a linear gradient of acetonitrile and water for IAF-labeled control steroid probe synthesis. NMR spectra were recorded at 500 MHz and 125 MHz for ^1H and ^{13}C NMR, respectively, and referenced to residual $CHCl_3$ (7.24 and 77.0 ppm, for ^1H and ^{13}C, respectively). High-resolution mass spectra (HRMS) were obtained from the mass spectral facilities at Georgia Institute of Technology or the University of California, San Diego.

Rotifer strains. We used *Brachionus manjavacas*[177] as test animals, a species originally collected from the Azov Sea,[178] and formerly known as *B. plicatilis* Russian.[168] This species has been cultured continuously in the lab since 1983, with periodic collection and storage of resting eggs.

Rotifer culturing. Rotifers were obtained by hatching resting eggs in 15 ppt artificial seawater (ASW) made from Instant Ocean sea salts at 25°C under constant fluorescent illumination of 2000 lux. Rotifers were fed the green alga *Tetraselmis suecica* cultured in f/2 medium[179] at 25°C and ASW in 5 L bags under constant fluorescent illumination. Flask cultures were inoculated by transferring about 100 females into a dense *T. suecica* culture of 250 ml and gently aerating at 25°C. Males were obtained from the five-day old cultures in log phase growth.

Confocal fluorescence microscopy. *B. manjavacas* ovigerous females and males were transferred to 24-well plates in 1 ml 15 ppt ASW with or without *T. suecica*, and 1 µg of **2** or **3** was added to each well in DMSO (0.5 mg/ml solution). The rotifers were allowed to incubate with **2** or **3** at 25°C in the dark for 30 min. The rotifers were anesthetized with 0.5 ml seltzer water and then fixed with 50 µl 10% formalin. The rotifers were imaged immediately using a Zeiss LSM/NLO 510 confocal/multi-photon microscope at Georgia Institute of Technology, with magnifications of 10× (females) or 20× (males) with excitiation at 375±10 nm and emission at 458±10 nm and excitiation at 488±10 nm and emission at 518±10 nm for DAPI and FITC, respectively.

Isolation of dietary steroids from B. manjavacas extracts. *B. manjavacas* bodies were exhaustively extracted with MeOH and MeOH/DCM mixtures (1:1 and 1:2). The combined extracts were filtered, reduced *in vacuo*, and partitioned between MeOH/H_2O (9:1) and petroleum ether. The aqueous fraction was adjusted to MeOH/H_2O (3:2) and then partitioned against $CHCl_3$. The petroleum ether fraction was separated by normal-phase HPLC (Agilent Zorbax RX-SIL, 9.4 × 250 mm, 5 µm) using a linear gradient of hexanes/ethyl acetate to yield campesterol (**5**), campesta-5,7-dien-3-β-ol (**6**), and 5-α-campest-7-en-3-β-ol (**7**). Crude fractions used in the progesterone EIA were generated by saponification of the petroleum ether fraction using 0.3M KOH in 90% aqueous MeOH. After heating for 2 h at 90 ^oC, steroids were extracted using hexanes, combined, and concentrated *in vacuo*, and used without further purification.

LC-MS/MS rotifer steroid analysis. LC-tandem mass spectrometry analyses were carried out using normal-phase HPLC fractions generated from the petroleum ether fraction. A Shimadzu LC-10 AD VP binary pump system coupled to a Perkin Elmer Series 200 autoinjector was interfaced to a 4000 quadrupole linear-ion trap operating in multiple reaction monitoring (MRM) mode. An Ascentis C_{18} column (1.0 × 150 mm, 3 µm)

was held at 30 ºC. The effulent was directed to the ion source needle held at 5500V and a heated desolvation gas of 200 ºC. Two MRM channels were optimized with regard to declustering potential (DP), collision energy (CE), and collision exit potential (CXP). They were as follows: *m/z* 315.3 / 109.0, DP - 80, CE – 38V, CXP – 8V and *m/z* 315.3 / 97.1, DP – 80V, CE – 35V, CXP – 6V. Serial dilutions of known concentrations of progesterone were used to generate a calibration curve for determination of concentration of progesterone in the extracted sample.

Progesterone enzyme immunoassay (EIA). The progesterone EIA kit (Cat. No. 900-011) was purchased from Assay Designs (Ann Arbor, MI). The assay was run according to the provided protocol. Both fractions generated from saponification of the petroleum ether fraction (i.e. steroid-containing fraction and saponified fatty acid fraction) were tested in the assay, along with controls. A progesterone standard curve was generated as outlined in the protocol. The steroid-containing fraction (4.8 mg, 0.06% crude extract) was taken up in 400 ml of the provided assay buffer, and the fraction was serially diluted by half twice, to provide a total of 3 samples, each sample assayed in duplicate. The fatty acid-containing fraction (29 mg, 1.5% crude extract) was also treated in a similar manner, to provide a total of 3 samples, with each tested in duplicate. Progesterone was present only in the treatment wells containing the steroid-containing fraction.

***B. manjavacas* lysate.** Adult rotifer biomass (1 g wet weight) was placed in modified RIPA buffer (150 mM NaCl, 50 mM Tris-HCl, pH 7.4, 1% Triton X-100, 1 mM EDTA, 1 mM PMSF, 5 µg/ml aprotinin, 1 µg/ml pepstatin-A, 2 µg/ml lLeupeptin, 1 mM Na_3VO_4, 1 mM NaF). The cells were ruptured by sonication for 5 min at 4 °C and centrifuged for 5 min at 13,000 RPM at 4 °C. The soluble fraction was spin dialysed 3 volumes of RIPA buffer on an Ultracel YM-3 3 kDa filter and concentrated to 1.3 mg/ml by Bradford analysis.

Immunoprecipitation studies with probe 2. Samples of the resulting lysate (200 µl) were treated with 10 µl of a 0.1 mg/ml DMSO stock of probe **2**. The sample was incubated with rotary shaking for 4 h at 4 °C. The sample was then immunoprecipitated by the addition of Affigel 10 resin containing 3.5 mg/ml of the XRI-TF35 mAb (40 µl). The resulting mixture was agitated for 12 h at 4 °C with the resin. The resin was then washed with ice cold PBS (3 x 2 ml). The bound protein was eluted from the resin incubating with 35 µl of 1 mg/ml of dimethylamino-4-coumarin acetic acid in RIPA buffer for 1 h at rt. SDS-PAGE analysis was run on a 4-12% gradient gel (Novex) with MOPS running buffer and silver stained (Invitrogen). Samples of the identified bands were excised and submitted to Nano-LC/MS/MS analysis conducted by contract services from the Center for Functional Genomics (CFG) at the University of Albany, State University of New York or the University of California, San Diego.

Western blotting studies using probe 4. An aliquot of rotifer lysate (400 µl) was treated with 20 µl of a 1 mg/ml stock of **4** in DMSO for 4 h at 4 °C. The sample was then immunoprecipitated by the addition of 15 µl of a ~0.01 mg/ml stock of a mouse anti-progesterone IgG mAb (Ann Arbor, MI) containing 1 mg/ml of bovine serum albumin (BSA) for 2 h at 4 °C. This was then followed by addition of 50 µl of protein A fast flow resin from GE Healthcare (Piscataway, NJ). The resulting mixture was agitated for 12 h at 4 °C with the resin. The resin was then washed with ice cold PBS (2 x 1 ml). The bound protein was boiled in SDS-PAGE gel loading buffer S3401-1VL (Sigma-Aldrich). SDS-PAGE gel analysis was conducted on a Novex X-cell station using NuPage 4-12% Bis-Tris gels and MOPS SDS running buffer. Western blotting was conducted by transfer to Hybond-P PVDF membrane by GE Healthcare (Piscataway, NJ) followed by blocking for 2 h with a solution of 0.1% Tween-20 with 5% w/v nonfat dry milk 20 in tris-buffered saline (TBS, pH 7.6), staining with the primary antibody, a mouse anti-progesterone IgG

mAb from Assay Designs (Ann Arbor, MI), in 0.1% Tween-20 with 5% BSA in TBS, mouse anti-progesterone mAb and a Goat anti-mouse IgG HRP mAb conjugate from Promega (Madison, WI) in 0.1% Tween-20 with 5% BSA in TBS. The primary and secondary antibodies were applied at 1:100 and 1:2,000 dilution, respectively, from their manufactures preparation. The total protein content in each gel was determined by staining with ponceau S from Promega (Madison, WI).

RNAi knockdown methods. *B. manjavacas* resting eggs were decapsulated in order to render them more permeable to dsRNA.[180] Resting eggs were then hatched in 15 ppt ASW with transfection solution for the progesterone receptor treatment or elongation factor 1α control (for binding assay), and the hatchlings were isolated fresh 15 ppt ASW and exposed to freshly prepared transfection solution overnight. The transfection solution consisted of 2 µl Fugene HD lipofection transfection reagent (Roche Diagnostics), 43 µl sterile PBS, plus 5 µl sterile water containing 10–20 ng progesterone receptor or elongation factor dsRNA. dsRNA derived from *B. manjavacas* progesterone receptor and elongation factor gene was synthesized *in vitro*.[181] Intensity of fluorescence in confocal microscopy images was quantified using ImageJ and a two sample, one-tailed paired t-Test (n = 8) was calculated.

Gene expression analysis. After 24h exposure of rotifer hatchlings to transfection solution, individual rotifers were preserved in RNAlater (Qiagen) for up to 5 days at -80 °C prior to RNA extraction. RNA extractions were performed immediately prior to qPCR. Total RNA was isolated from individual rotifers using RNeasy Micro Kit (Qiagen) with the modification that rotifer cells were disrupted by vortexing with glass beads (425-600 µm). A 1:9 dilution of rotifer RNA was used as template for triplicate one-step reverse transcription and qPCR reactions using EXPRESS One-Step SYBR GreenER Kit (Invitrogen). qPCR primers for the target progesterone receptor gene (qPR1for 5'-

CGGTCCGTATTCCGTATTTG-3', qPR1rev 5'-TTCGGCTGACTCTTCTTCGT-3') were designed from *B. manjavacas* progesterone receptor membrane component 1-like protein nucleotide sequence (FJ829246). qPCR primers for the actin reference housekeeping gene (actinQBfor 5'-GCATCCACGAGACCACCTAT-3', actinQBrev 5'-TAGGATCGAACCACCAATCC-3') were designed from *B. plicatilis* actin mRNA nucleotide sequence (GenBank accession AB111352). Amplification and detection of progesterone receptor and actin genes were conducted using a Mastercycler Realplex 2 (Eppendorf). Expression levels of progesterone receptor were normalized to actin levels and relative expression of progesterone receptor gene in progesterone receptor-transfected rotifers to PBS control rotifers was determined using the $\Delta\Delta C_T$ method.[182]

Mixis and mating bioassays. Mixis[168] and mating[181] bioassays were performed as previously described. RNAi knockdown for treatments and controls for each bioassay were performed as described in the previous section.

CHAPTER 7

CONCLUSIONS

Natural products represent a valuable resource for biomedical research and drug discovery, necessitating continued activity in this vital area. Rare and understudied macroalgal species are excellent sources of novel and exciting secondary metabolites, including compounds of mixed biogenesis, such as the bromophycolides. As evident from the study of *Callophycus serratus* and *Neurymenia fraxinifolia*, tropical macroalgae represent a treasure trove of unique bioactive natural products, and these natural products (i.e., bromophycolides and neurymenolides) have pharmaceutical potential against relevant human diseases including drug-resistant malarial strains and bacterial infections.

Following elucidation of bromophycolide A's antimalarial mechanism of action as a heme crystallization inhibitor, new bromophycolide-inspired compounds can now be pursued through chemical synthesis and optimized for interaction with heme with the aid of molecular modeling. Heme represents an excellent drug target because heme crystallization is a physicochemical process rather than an enzymatic one that allows for facile evolution of resistance by the parasite. These studies identified a new class of natural products that target heme detoxification, suggesting an avenue to circumvent drug resistance. Not only is bromophycolide A potent against drug-sensitive *Plasmodium falciparum*, the natural product is even more effective against chloroquine-resistant *P. falciparum*.

Despite its exciting mechanism of action and promising potency, bromophycolide A is unlikely to become a commercial drug for a number of reasons. First, bromophycolide A is impractical and environmentally unsustainable to procure through large-scale collections and extraction of the macroalga *Callophycus serratus.* While the

structural complexity of bromophycolide A – 27 carbons, 5 stereocenters – makes this natural product a daunting but exciting challenge for organic synthesis, a short and concise total synthesis on a multi-gram scale is needed to make this compound feasible for further *in vitro* and *in vivo* studies. Furthermore, the antimalarial activity of bromophycolide A is ~660 nM, and while inhibition of this magnitude can result in good leads, more potent activity is often necessary for the continued development of new drugs. For instance, current antimalarial drugs inhibit parasite growth in the low nanomolar range (i.e., artemisinin IC_{50} value against the malaria parasite is 7 nM). Resistance of human cells and tissues is also important when developing new drug leads, such that the drug should be selective for the disease-causing organisms and not toxic to the human host. Bromophycolide A exhibited a 50-fold difference in activity between *P. falciparum* parasites and human Vero cells, whereas a 200-fold or greater difference in activity is ideal for potential drug candidates. Lastly, bioavailability of a drug candidate is crucial for advancing a drug lead into a new drug. The physical properties of bromophycolide A, such as its strong hydrophobicity and low solubility in aqueous environments, make this natural product less than ideal from a pharmacokinetics perspective. Therefore, synthesizing optimized derivatives inspired by bromophycolide A with increased potency, selectivity, and bioavailability is the next logical step to further progress this class of molecules as antimalarial drugs. For example, as demonstrated with callophycolide A (Chapter 3), bromines are not essential for antimalarial activity. Thus, a compound without bromines (lower molecular weight) and additional polar groups such as amines or amides (to slightly increase compound polarity) could represent a reasonable starting point for further development of bromophycolide-inspired derivatives.

Drug resistance is also of immense concern with antibacterial infections. The neurymenolides represent structurally unique, but relatively simple compounds with

promising antibacterial activity. These compounds inhibited both Gram-positive and Gram-negative bacteria, and thus could be utilized as broad spectrum antibiotics. Through collaboration with researchers at Rutgers University, initial studies suggested that neurymenolide A inhibits bacterial RNA polymerase (Professors Richard Ebright and Eddy Arnold, unpublished), an essential enzyme in both Gram-positive and Gram-negative bacteria. Furthermore, while bacteria RNA polymerase subunit sequences are highly conserved, eukaryotic RNA polymerase subunit sequences are not, making this enzyme an excellent target for bacterial inhibition while also permitting therapeutic selectivity. Future research further exploring this potential mechanism of action, coupled with synthesis of neurymenolide-inspired analogs could result in the development of a new scaffold for antibiotic drug discovery. For example, reports of syntheses of structurally related compounds are available in the literature and thus a similar carbon skeleton to that of neurymenolide A can be synthesized from inexpensive starting materials in only 3-5 steps, depending on the desired size of the macrocylic ring. Thus, several synthetic avenues exist to elaborate or simplify the core structure of the neurymenolides. The synthetic derivatives could then be assessed by collaborators at Rutgers University for their ability to effectively inhibit RNA polymerase. Overall, this project is worthwhile to pursue since a potential mechanism of action has been proposed, synthetic derivatives can be easily prepared, and an efficient synthetic plan could allow for variation of functional groups to explore structure-activity relationships for the therapeutic target.

As previously discussed, natural products are not only essential in drug discovery, but are also essential as molecular probes in the understanding of biochemical processes. Unlike almost all other animals currently in existence, the ancient marine micro-invertebrate *Brachionus manjavacas* benefits from both asexual and sexual reproduction, a strategy central to their evolutionary success. By exploring

chemical signaling in *B. manjavacas* using a fluorescent probe synthesized from progesterone, we were able to gain insights into their reproductive signaling. This work suggested that the well-studied mammalian hormone progesterone plays an essential role in *B. manjavacas* reproduction and that endocrine regulation of mammalian reproduction may be derived from primitive regulatory pathways.

Collectively, the continued study of marine natural products will enrich the drug discovery library, provide exciting challenges for organic synthesis, and can be used to explore pharmaceutically and evolutionarily important biological processes and chemical signaling.

APPENDIX A

NMR SPECTRAL DATA

1 and 2D NMR Spectral Data for Chapter 3

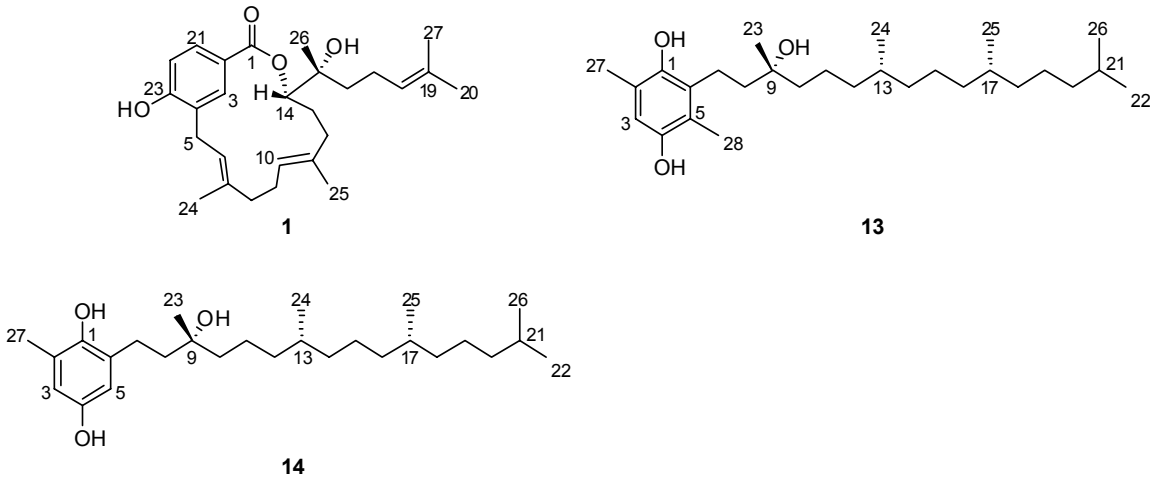

Figure A.1. Natural products isolated from Fijian red macroalgae; callophycolide A (**1**) from *Callophycus serratus*; β-tocopherylhydroquinone (**13**) and δ-tocopherylhydroquinone (**14**) from *Amphiroa crassa*.

Table A.1. ^{13}C and ^{1}H NMR spectroscopic data for **1** and **13-14** (500 MHz; in $CDCl_3$).

	1		**13**		**14**	
	δ_C	δ_H (J in Hz)	δ_C	δ_H (J in Hz)	δ_C	δ_H (J in Hz)
1	169.2	-	146.0	-	146.1	-
2	122.4	-	124.1	-	127.4	-
3	131.1	7.85 s	115.3	6.46 s	115.6	6.45 d (2.8)
4	127.7	-	145.6	-	147.6	-
5	26.0	3.17 dd (17, 7.0), 3.49 dd (17, 8.5)	119.1	-	112.5	6.37 d (2.8)
6	122.7	5.45 dd (7.6,	120.3	-	121.5	-
7	136.8	-	21.0	2.58 t (6.8)	22.5	2.67 m

Table A.1 continued

8	39.3	2.17 m, 2.27 m	31.4	1.75 dt (13, 7.0), 1.78 dt (13, 6.5)	31.3	1.72 dt (14, 6.8), 1.76 dt (14, 6.7)
9	23.8	2.15 m, 2.23 m	74.5	-	75.6	-
10	123.5	5.19 m	39.7	1.52 m	39.9	1.52 m
11	135.2	-	21.0	1.35 m, 1.41 m	21.0	1.35 m, 1.41 m
12	35.8	1.87 dd (12.3, 9.4), 2.11 m	37.4	1.24 m	37.4	1.24 m
13	29.2	1.61 m, 2.03 m	32.8	1.36 m	32.8	1.36 m
14	82.1	4.75 d (11)	37.4	1.04 m	37.4	1.04 m
15	74.8	-	24.4	1.19 m	24.4	1.19 m
16	40.0	1.48 m, 1.52 m	37.4	1.24 m	37.4	1.24 m
17	21.9	2.14 m	32.8	1.36 m	32.8	1.36 m
18	124.3	5.10 t (6.9)	37.4	1.04 m	37.4	1.04 m
19	131.8	-	24.8	1.28 m	24.8	1.28 m
20	25.7	1.66 s	39.4	1.13 m	39.4	1.13 m
21	129.6	7.73 d (8.3)	28.0	1.50 m	28.0	1.50 m
22	114.8	6.78 d (8.3)	22.7	0.86 d (6.7)	22.7	0.86 d (6.7)
23	158.0	-	23.8	1.20 s	24.1	1.22 s
24	14.5	1.60 s	19.6	0.85 d (6.4)	19.6	0.85 d (6.4)
25	15.7	1.59 s	19.6	0.85 d (6.4)	19.6	0.85 d (6.4)
26	22.0	1.16 s	22.7	0.86 d (6.7)	22.7	0.86 d (6.7)
27	17.7	1.60 s	15.8	2.08 s	16.1	2.10 s
28	NA	NA	10.9	2.06 s	NA	NA
OH	-	5.83 br s	-	-	-	-

br=broad; s=singlet; d=doublet; dd=doublet of doublets; t=triplet; m=multiplet

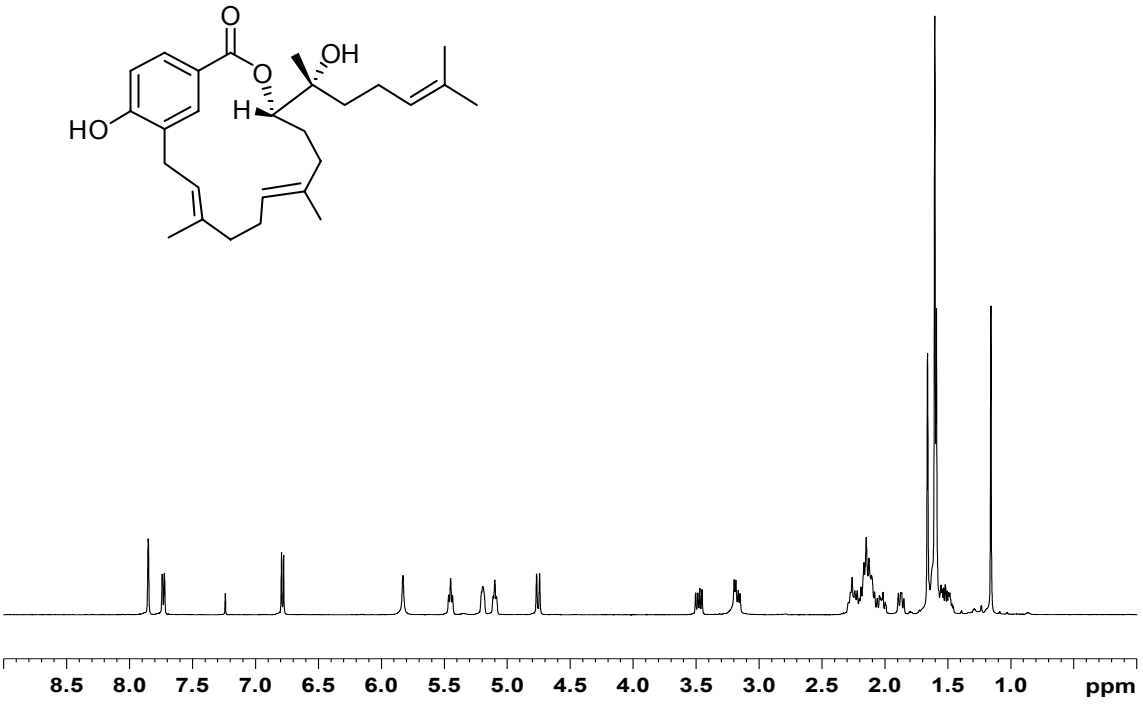

Figure A.2. ^{1}H NMR spectrum of callophycolide A (**1**) (500 MHz; $CDCl_3$).

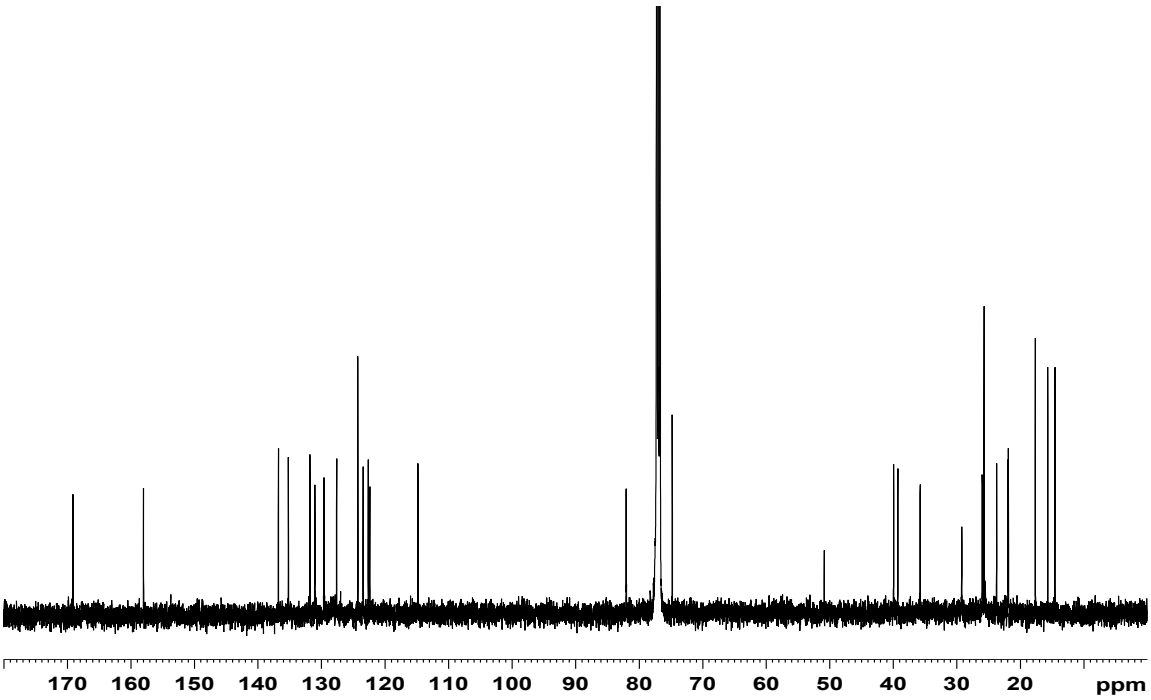

Figure A.3. ^{13}C NMR spectrum of callophycolide A (**1**) (125 MHz; $CDCl_3$).

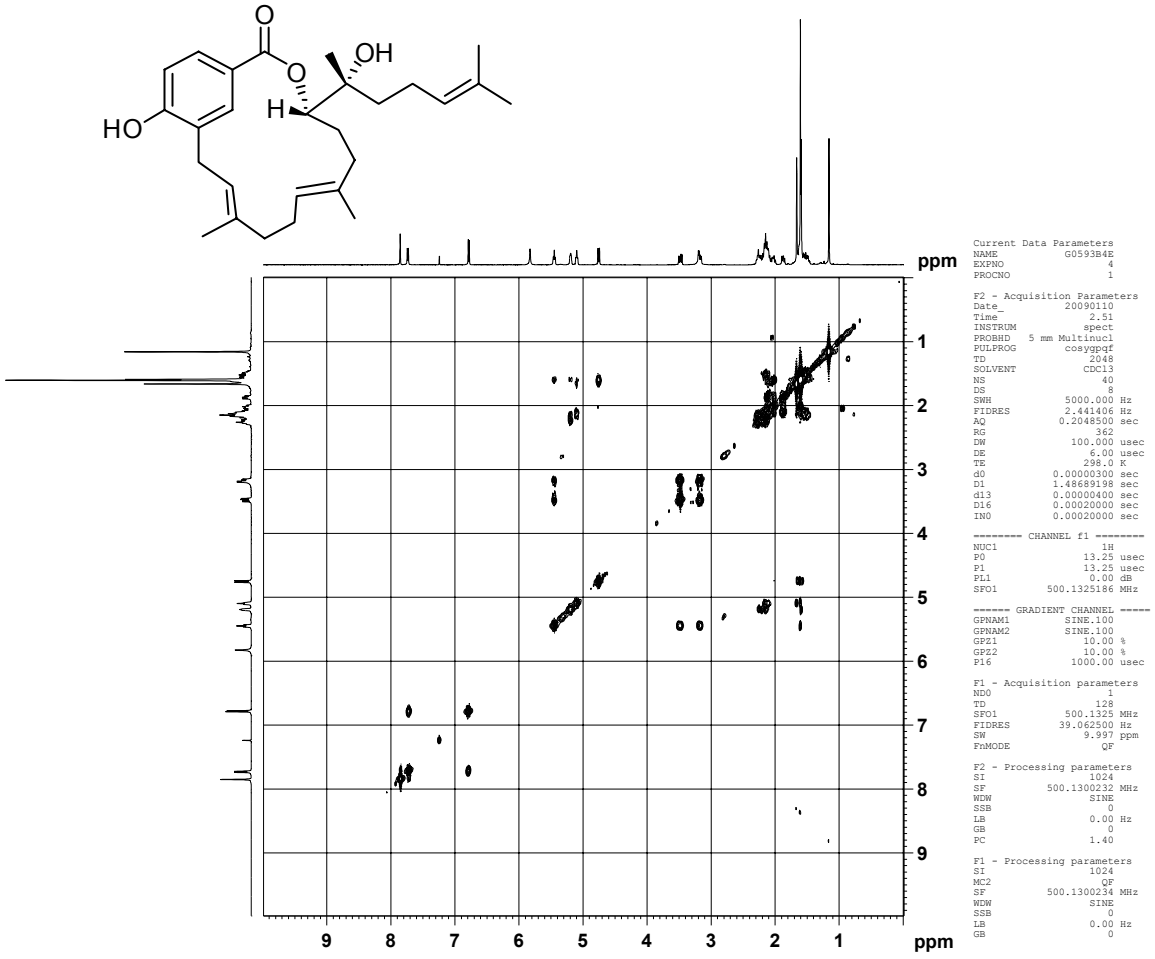

Figure A.4. ^{1}H-^{1}H COSY spectrum of callophycolide A (**1**) (500 MHz; $CDCl_3$).

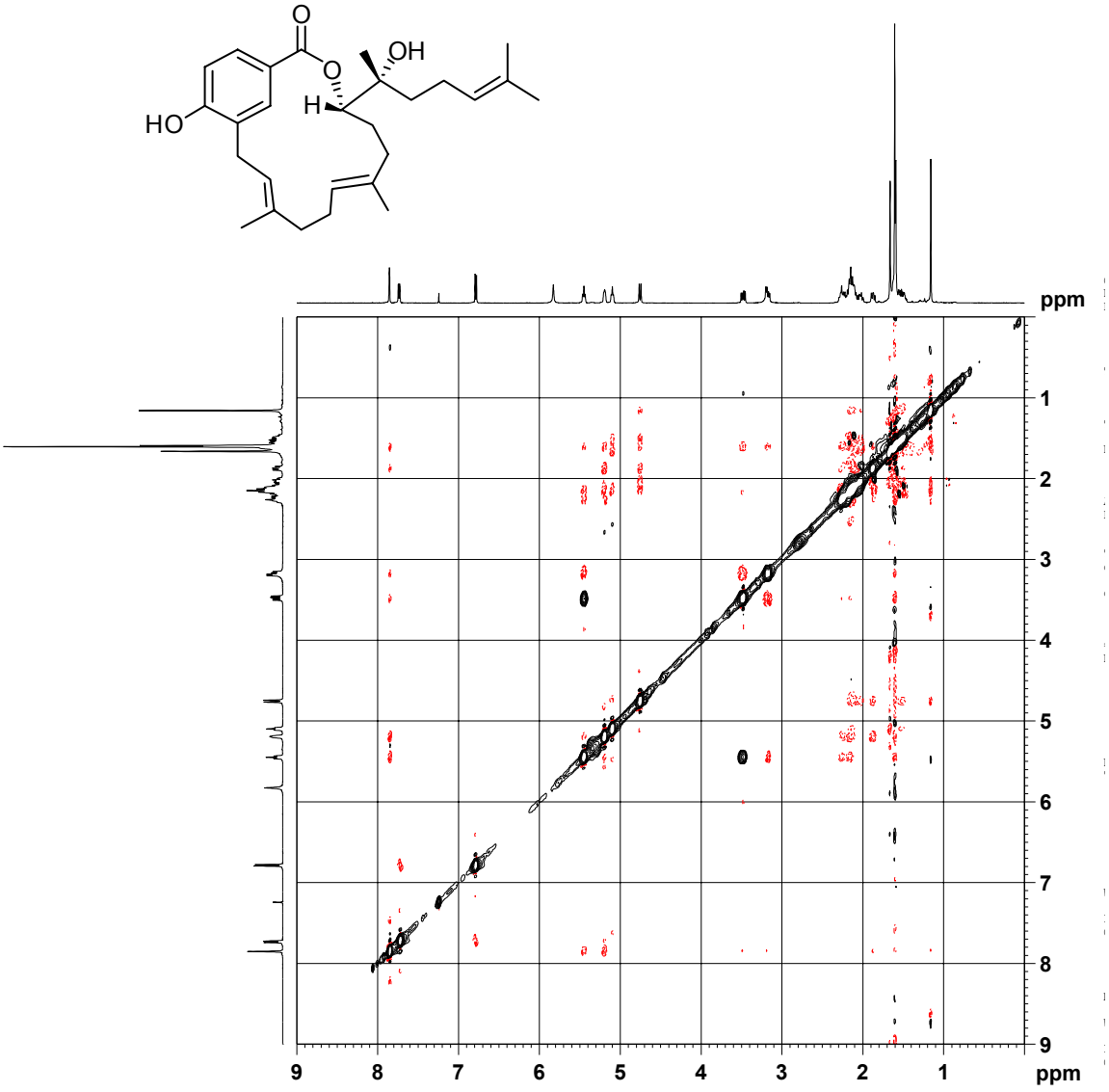

Figure A.5. ROESY spectrum of callophycolide A (**1**) (500 MHz; $CDCl_3$).

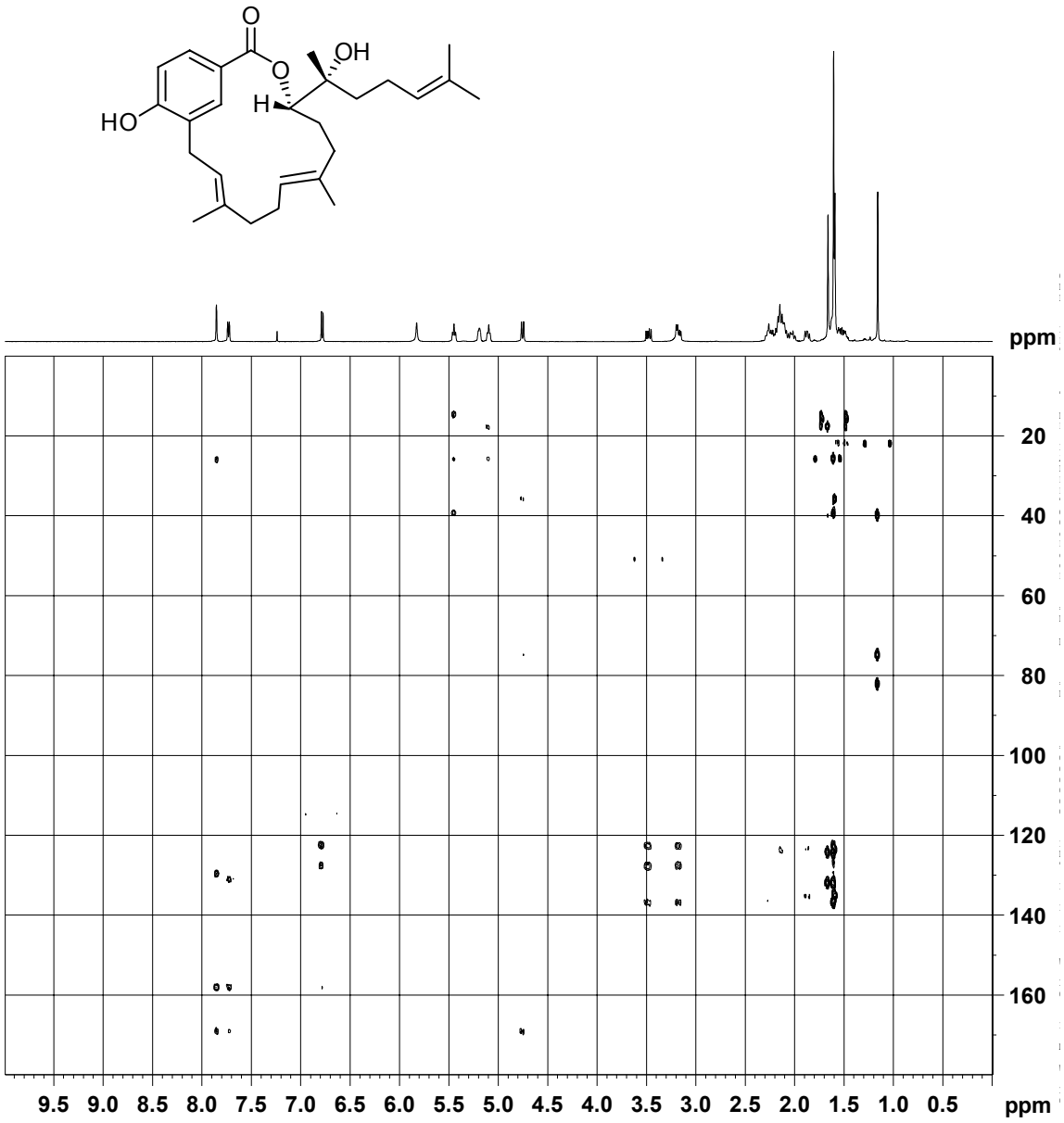

Figure A.6. HMBC spectrum of callophycolide A (**1**) (500 MHz; $CDCl_3$).

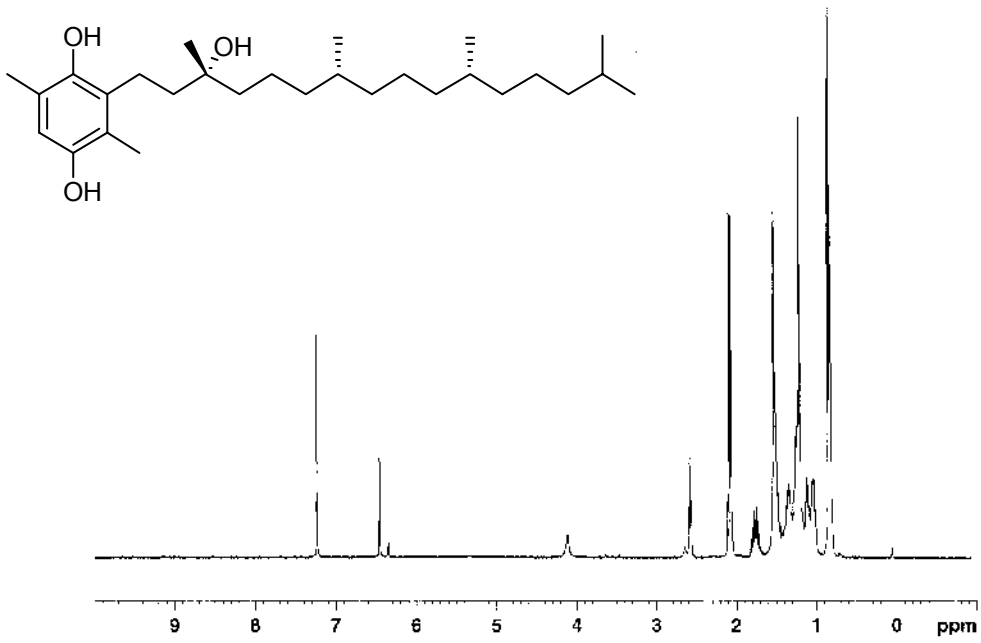

Figure A.7. ^{1}H NMR spectrum of β-tocopherylhydroquinone (**13**) (500 MHz; $CDCl_3$).

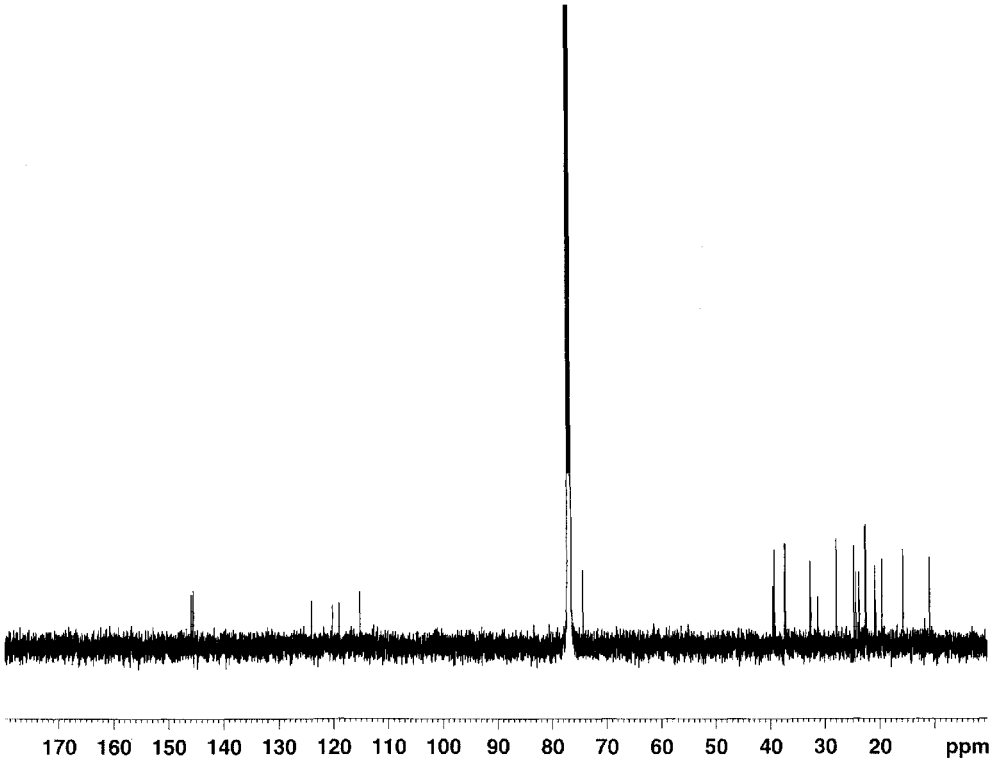

Figure A.8. ^{13}C NMR spectrum of β-tocopherylhydroquinone (**13**) (125 MHz; $CDCl_3$).

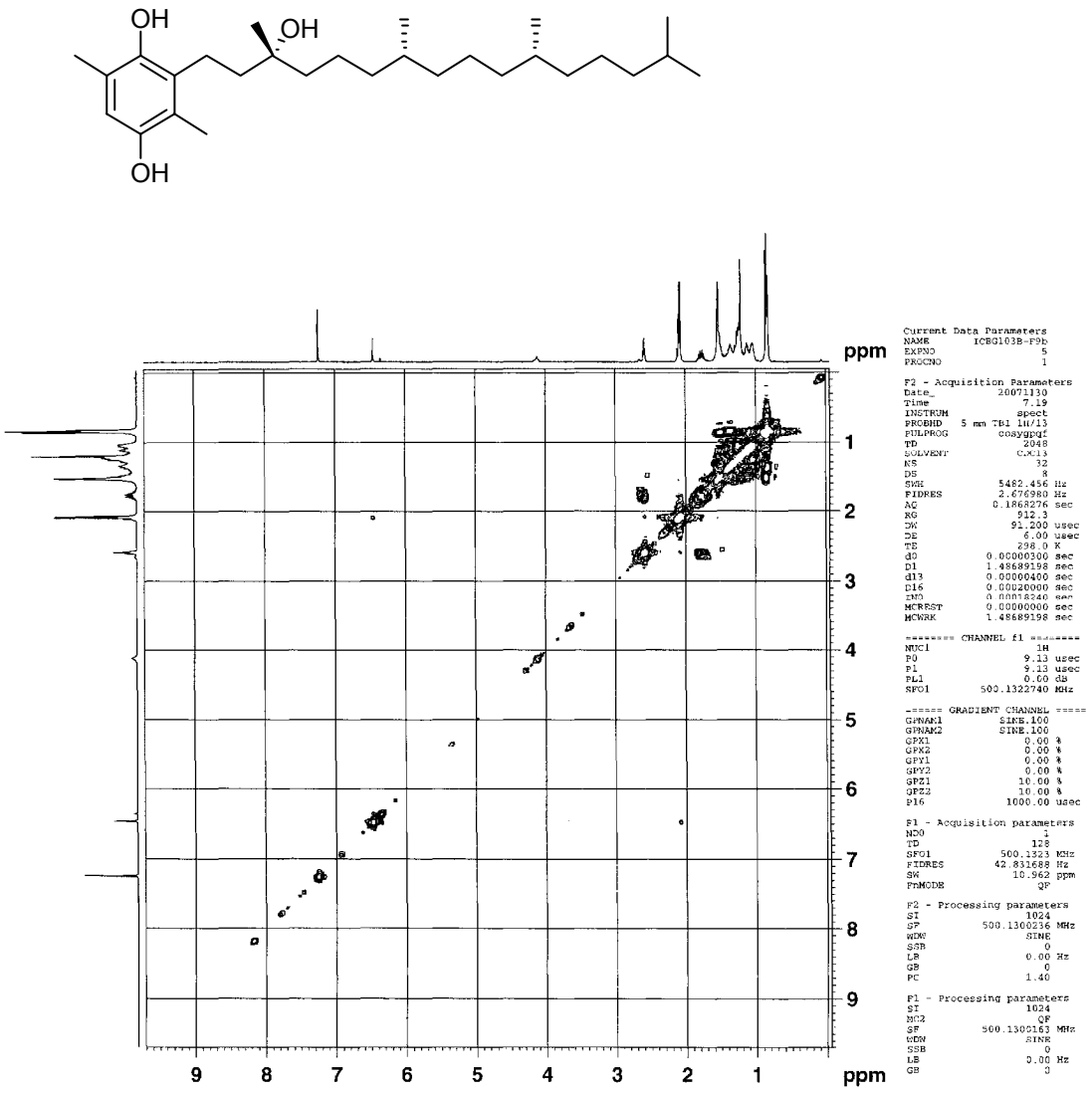

Figure A.9. ^{1}H-^{1}H COSY spectrum of β-tocopherylhydroquinone (**13**) (500 MHz; $CDCl_3$).

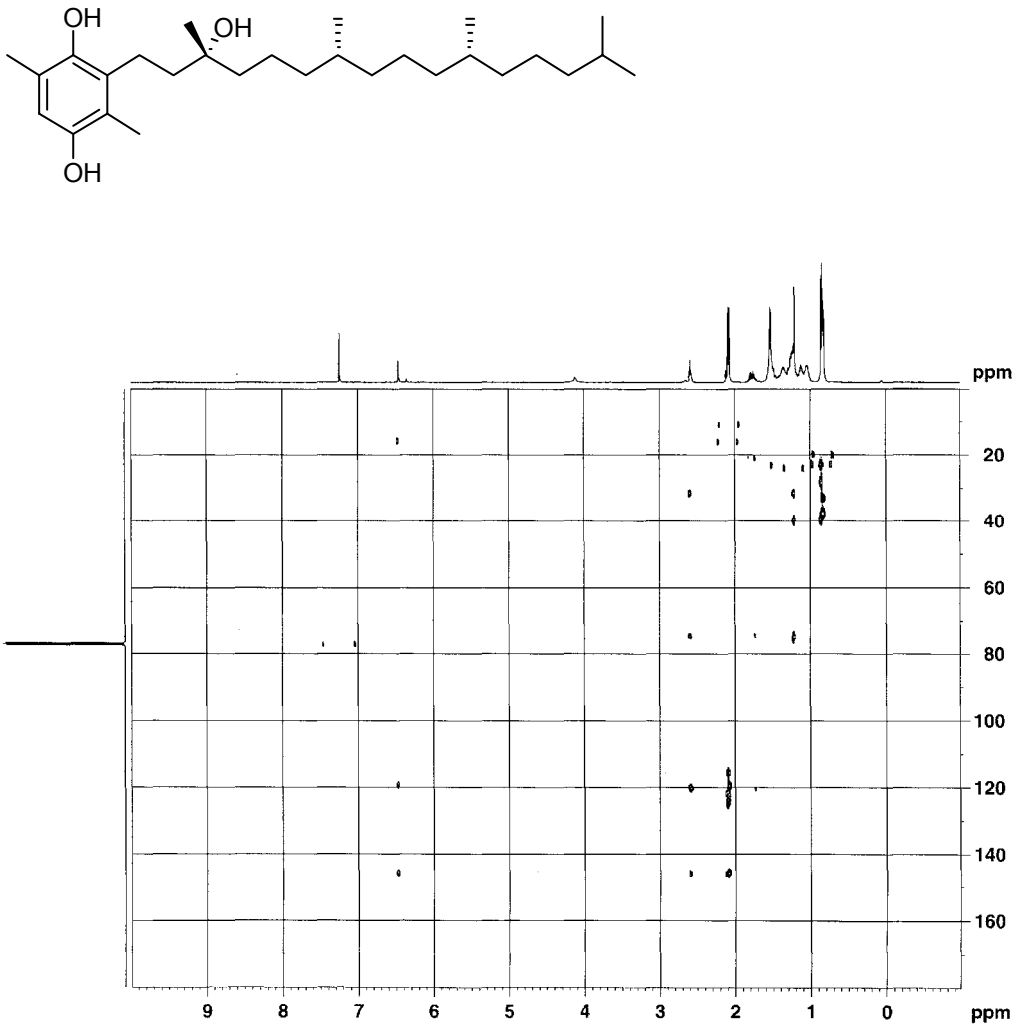

Figure A.10. HMBC spectrum of β-tocopherylhydroquinone (**13**) (500 MHz; $CDCl_3$).

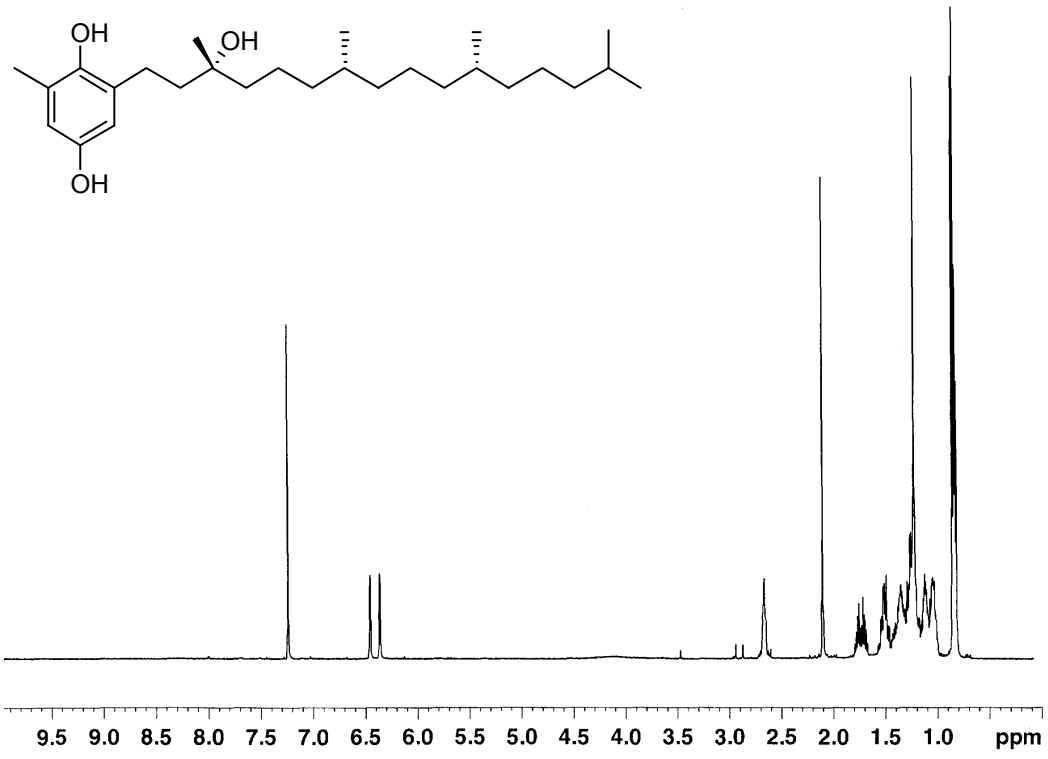

Figure A.11. ^{1}H NMR spectrum of δ-tocopherylhydroquinone (**14**) (500 MHz; $CDCl_3$).

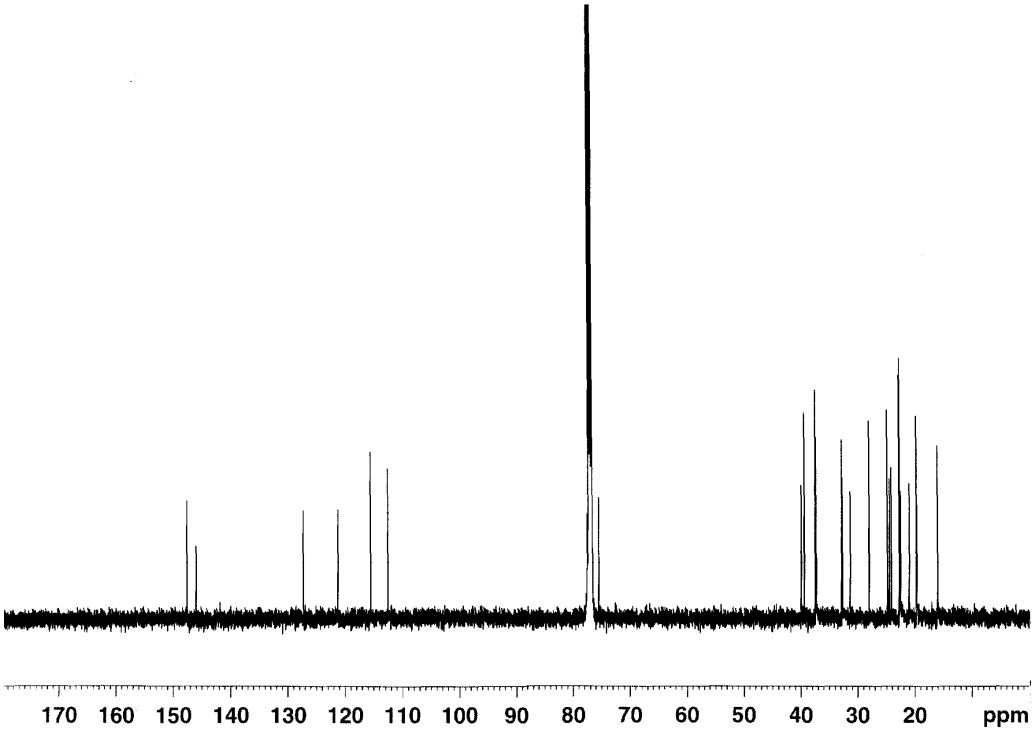

Figure A.12. ^{13}C NMR spectrum of δ-tocopherylhydroquinone (**14**) (125 MHz; $CDCl_3$).

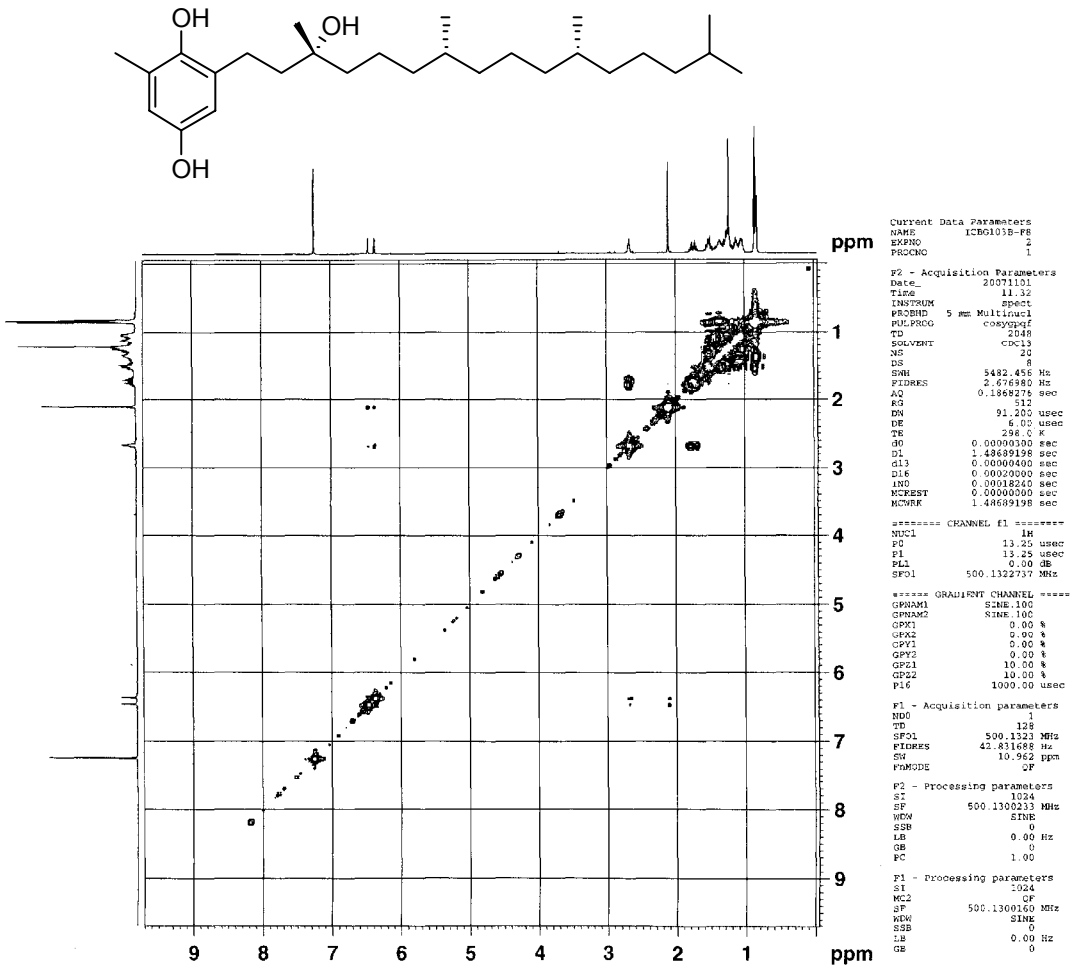

Figure A.13. ^{1}H-^{1}H COSY spectrum of δ-tocopherylhydroquinone (**14**) (500 MHz; $CDCl_3$).

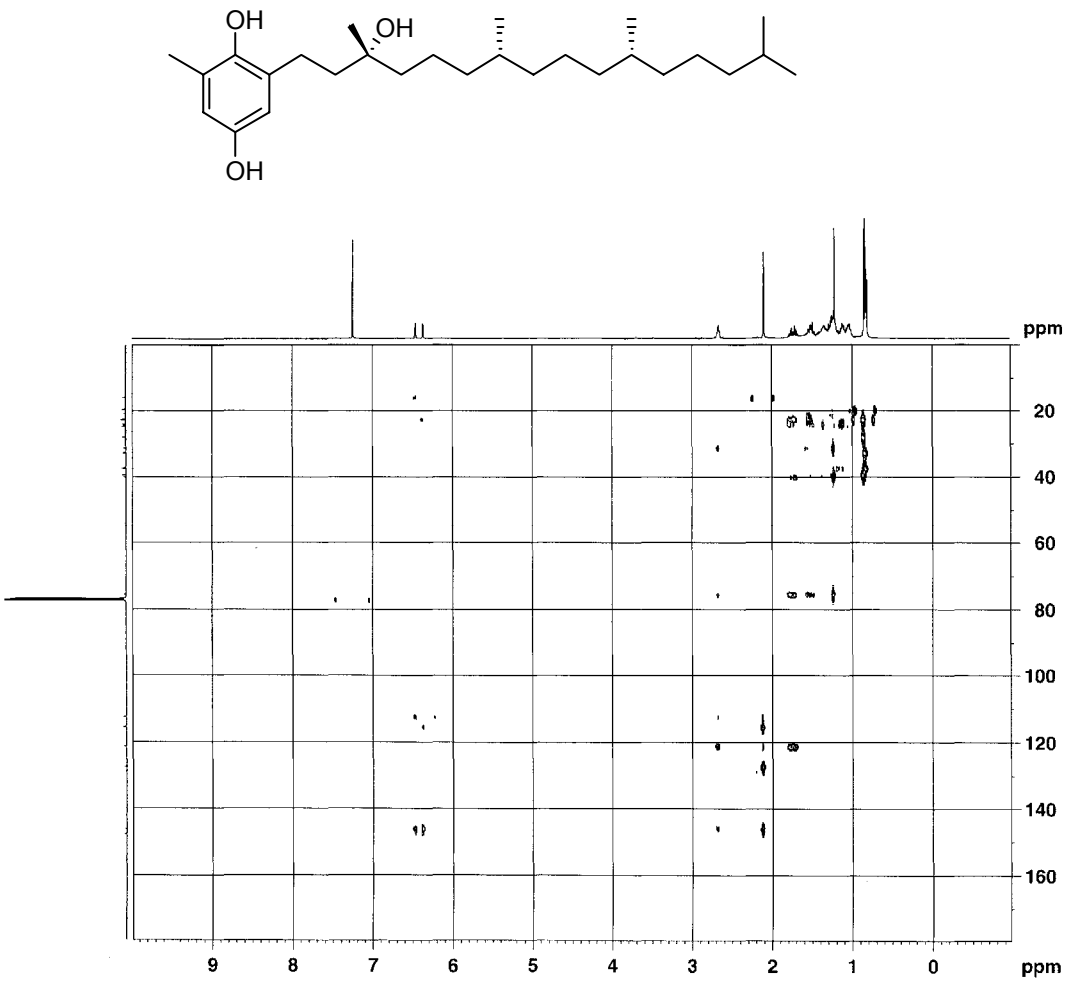

Figure A.14. HMBC spectrum of δ-tocopherylhydroquinone (**14**) (500 MHz; $CDCl_3$).

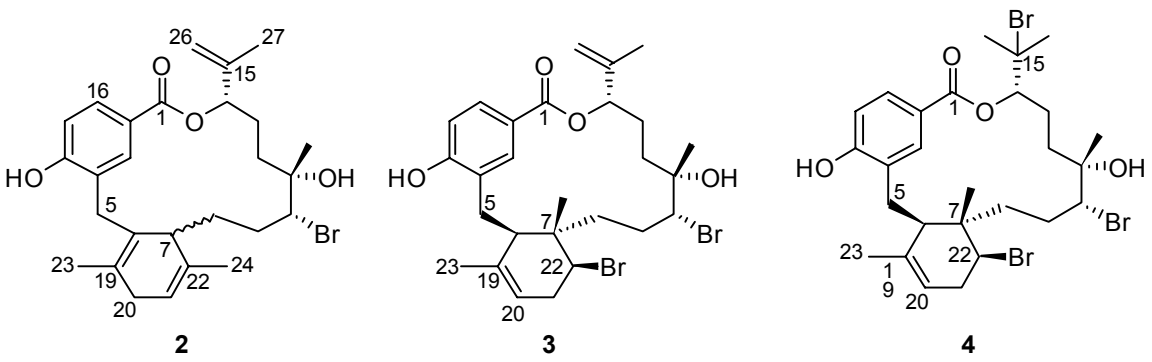

Figure A.15. Natural products isolated from the Fijian red macroalga *Callophycus serratus*; bromophycolides L (**2**), N (**3**), and O (**4**).

Table A.2. ^{13}C and ^{1}H NMR spectroscopic data for **2-4** (500 MHz; in $CDCl_3$).

	2		**3**		**4**	
	δ ^{13}C	δ ^{1}H ($J_{H,H}$)	δ ^{13}C	$\delta^{1}H$ ($J_{H,H}$)	δ ^{13}C	δ ^{1}H ($J_{H,H}$)
1	165.9	-	164.7	-	165.5	-
2	122.9	-	123.0	-	123.0	-
3	132.3	7.67 d (1.9)	131.4	7.82 s	129.5	7.89 s
4	124.6	-	129.5	-	128.4	-
5	29.7	3.22 d (15), 3.46 d (15)	27.3	2.60 d (15), 2.83 dd (15, 9.0)	25.8	2.82 m, 2.98 d (13)
6	132.6	-	47.8	2.67 m	43.7	2.84 m
7	49.0	3.41 m	41.3	-	40.9	-
8	27.1	1.53 m, 1.97 m	37.2	1.58 m, 2.18 m	36.6	1.23 m, 2.08 m
9	30.7	2.44 m, 2.50 m	26.0	2.20 m, 2.39 m	28.5	1.98 m, 2.00 m
10	67.8	3.97 dd (11, 3)	66.4	4.20 d (11)	70.0	3.79 d (11)
11	73.0	-	74.4	-	73.0	-

Table A.2 continued

12	31.6	1.67 m, 1.74 m	32.2	1.86 m 2.02 m	33.8	1.53 m, 1.98 m
13	25.8	1.73 m, 1.86 m	27.0	1.70 m 2.05 m	26.4	2.13 m, 2.47 m
14	74.9	5.52 brs	76.0	5.23 brs	79.2	5.00 dd (9.4, 3.4)
15	140.7	-	140.9	-	66.5	-
16	129.2	7.73 dd (8.4, 1.9)	129.3	7.75 d (7.9)	129.3	7.74 d (8.3)
17	115.6	6.78 d (8.3)	115.9	6.76 d (8.3)	115.7	6.81 d (8.3)
18	158.0	-	156.6	-	156.5	-
19	136.8	-	137.2	-	135.8	-
20	37.8	2.30 m, 2.42 m	120.3	5.19 m	119.4	5.33 br s
21	122.5	4.81 t (6.5)	34.4	2.53 m 2.59 m	34.0	2.65 m
22	138.8	-	59.8	4.28 dd (11, 5.3)	60.2	4.24 dd (6.8, 6.2)
23	14.0	1.89 s	20.9	1.50 s	22.0	1.65 s
24	18.2	1.38 s	17.1	1.06 s	18.8	0.89 s
25	27.5	1.30 s	28.0	1.40 s	29.3	1.32 s
26	111.5	4.98 s, 5.07 s	111.0	4.84 s 4.95 s	30.2	1.81 s
27	19.5	1.79 s	19.7	1.79 s	31.5	1.83 s
OH	-	5.31 s	-	5.33 brs	-	5.21 brs

br=broad; s=singlet; d=doublet; dd=doublet of doublets; t=triplet; m=multiplet

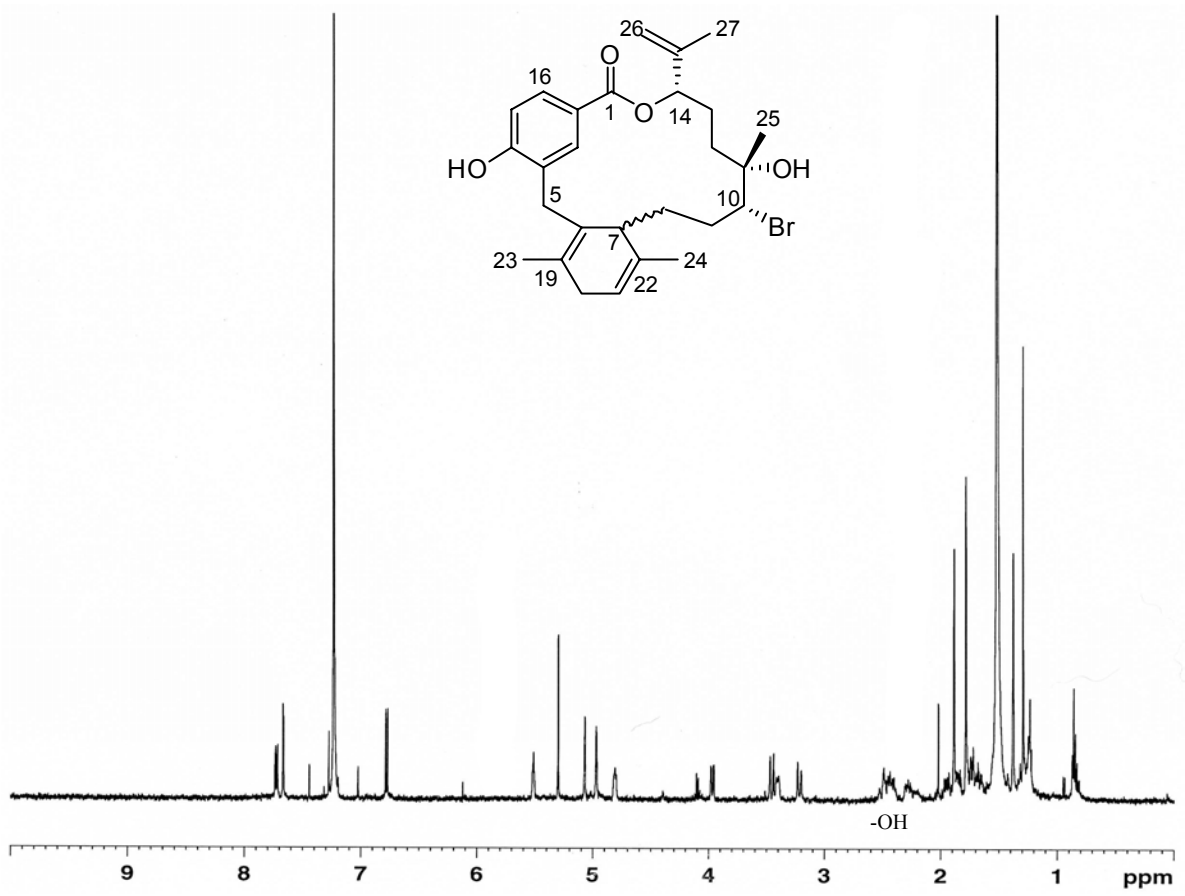

Figure A.16. ^{1}H NMR spectrum of bromophycolide L (**2**) (500 MHz; $CDCl_3$)

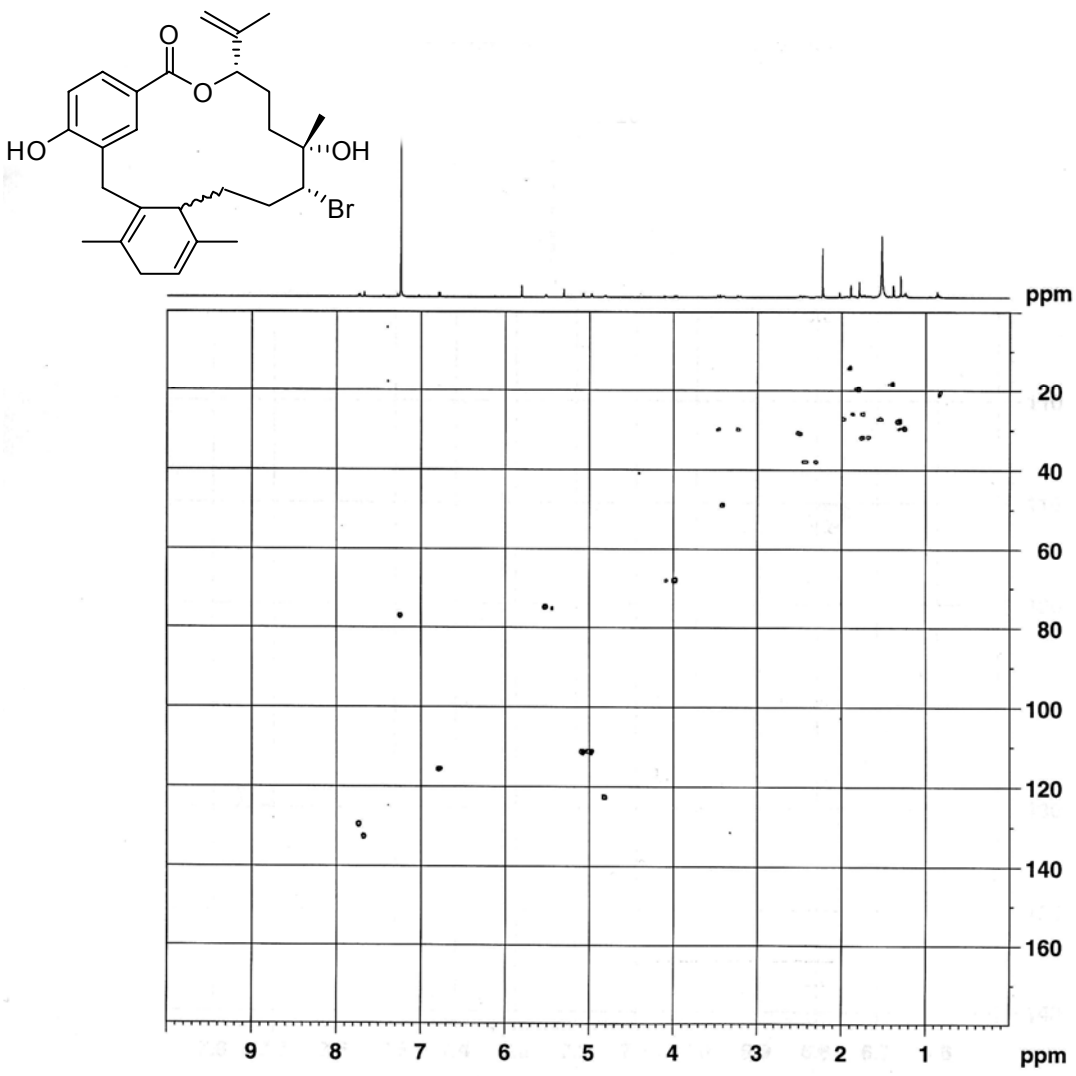

Figure A.17. HSQC spectrum of bromophycolide L (**2**) (500 MHz; $CDCl_3$)

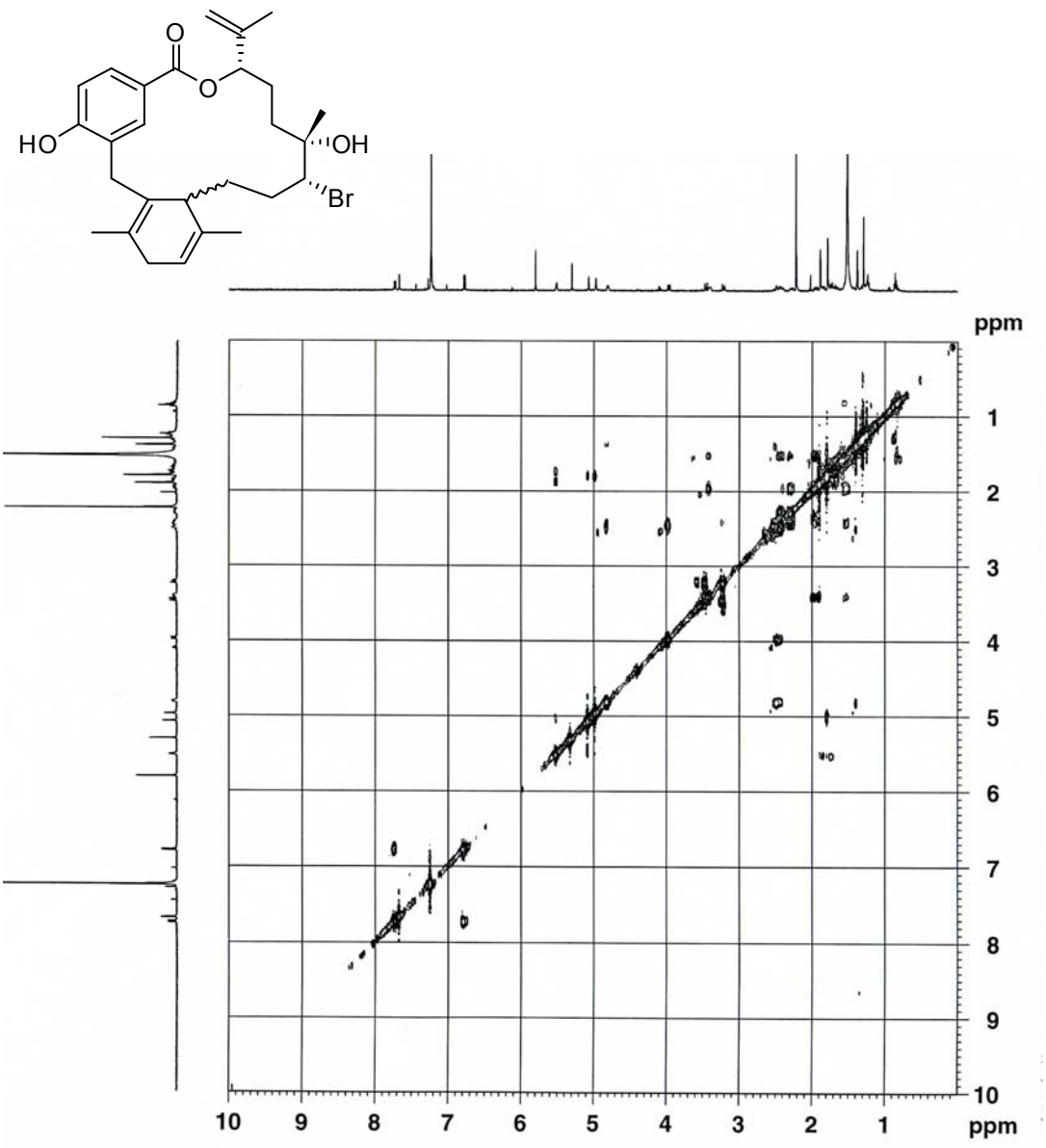

Figure A.18. ^{1}H-^{1}H COSY spectrum of bromophycolide L (**2**) (500 MHz; $CDCl_3$)

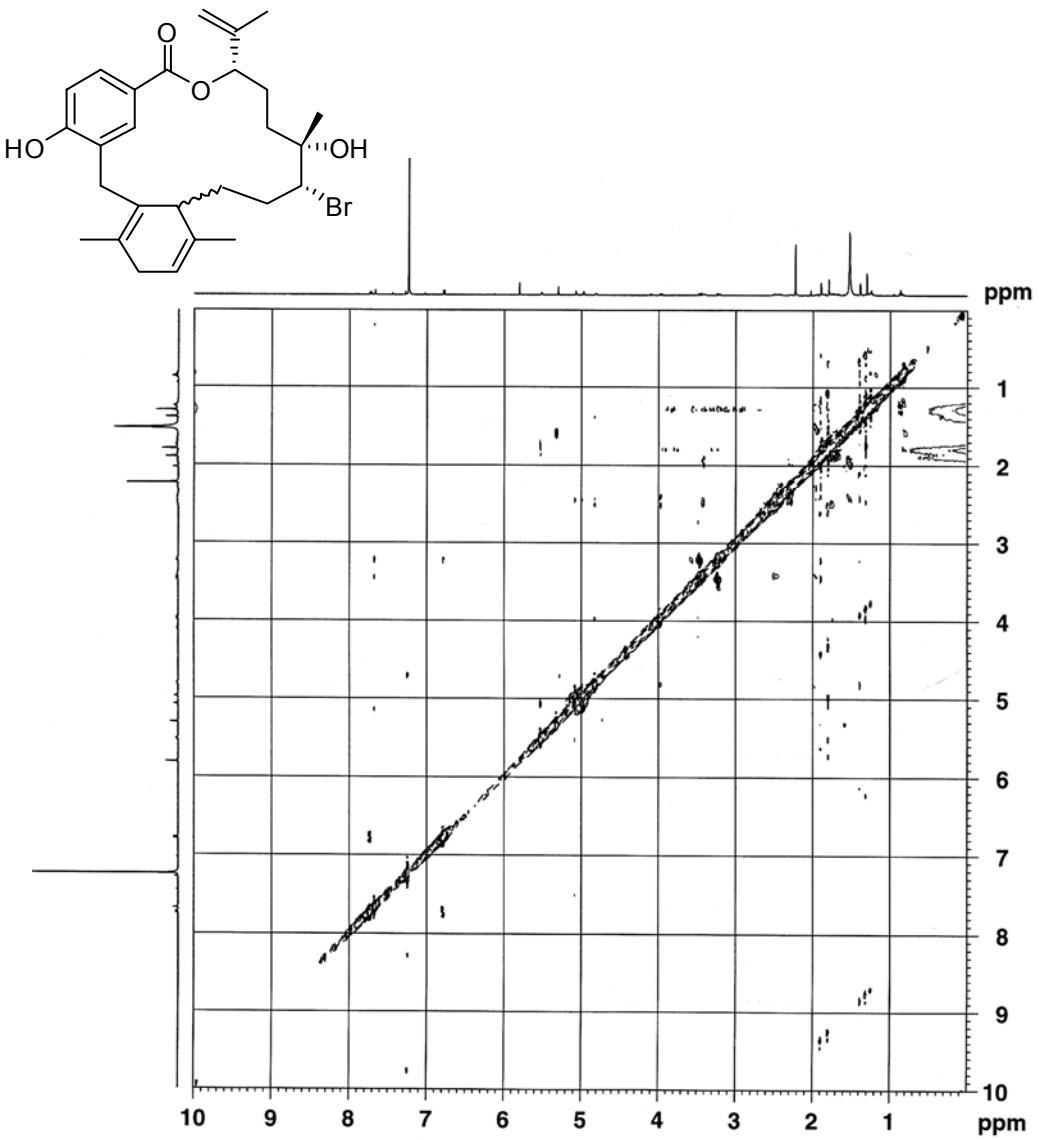

Figure A.19. ROESY spectrum of bromophycolide L (**2**) (500 MHz; $CDCl_3$)

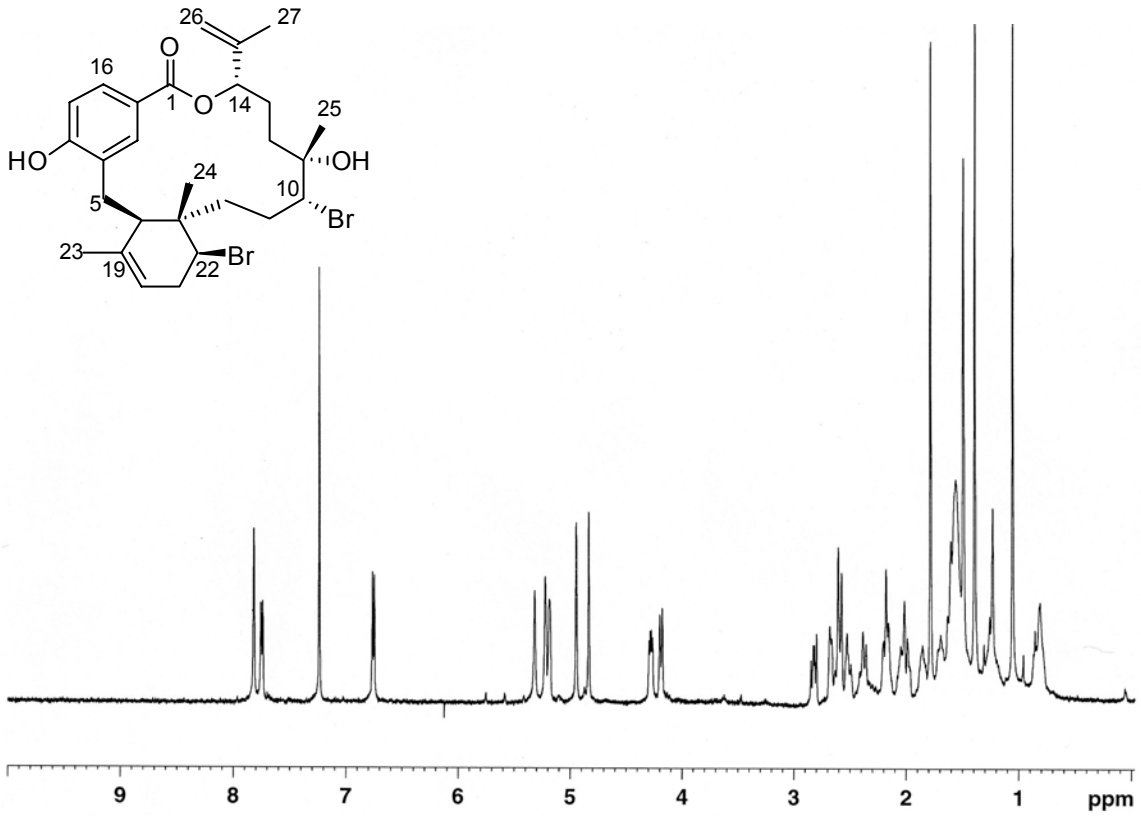

Figure A.20. ^{1}H NMR spectrum of bromophycolide N (**3**) (500 MHz; $CDCl_3$)

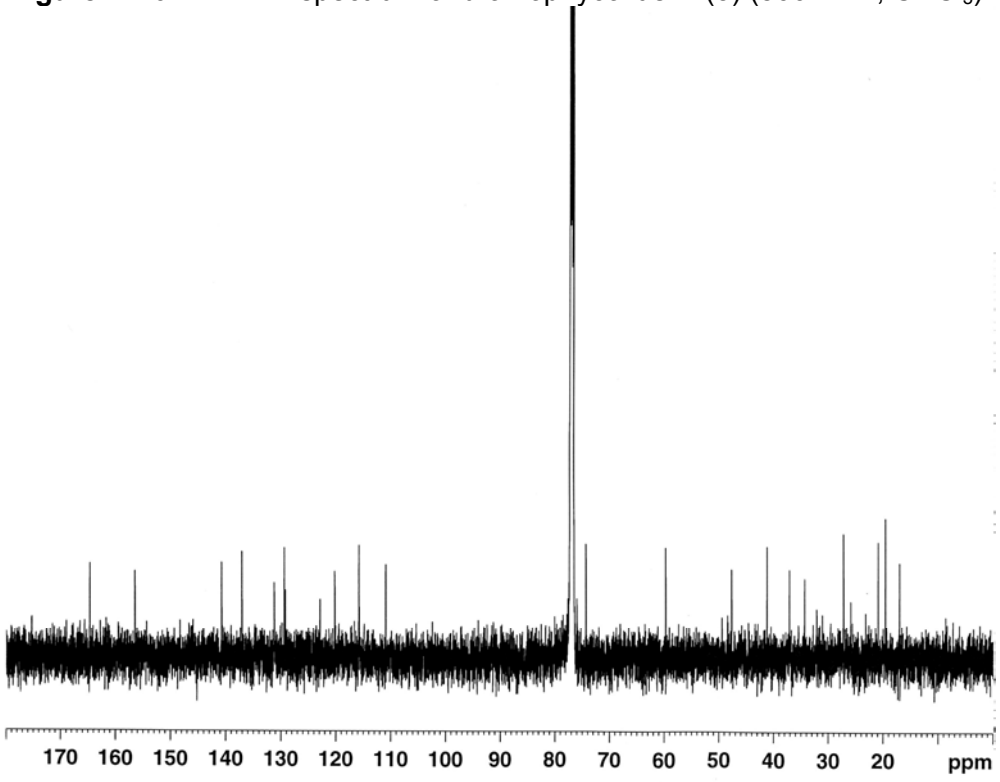

Figure A.21. ^{13}C NMR spectrum of bromophycolide N (**3**) (125 MHz; $CDCl_3$)

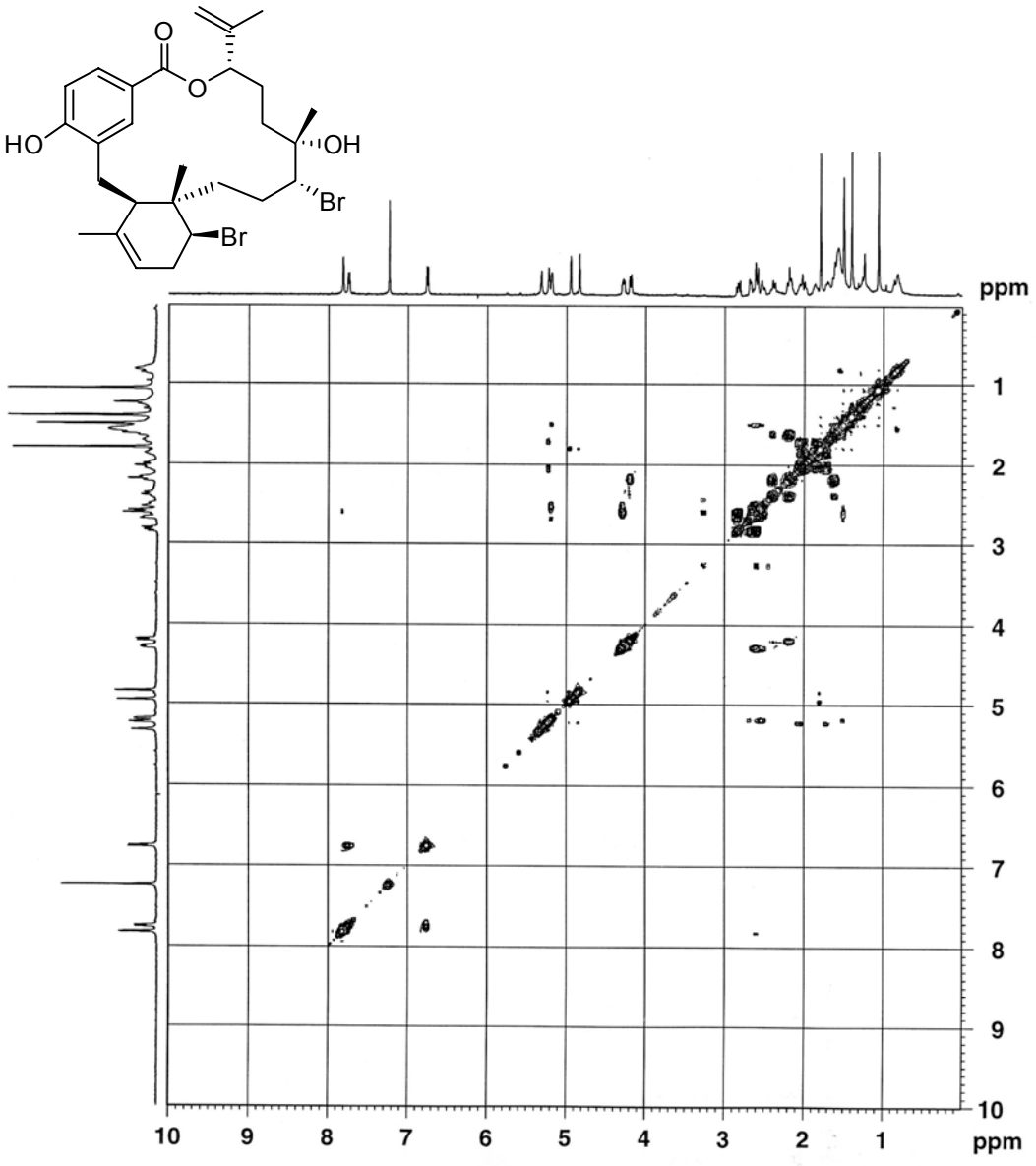

Figure A.22. ^{1}H-^{1}H COSY spectrum of bromophycolide N (**3**) (500 MHz; $CDCl_3$)

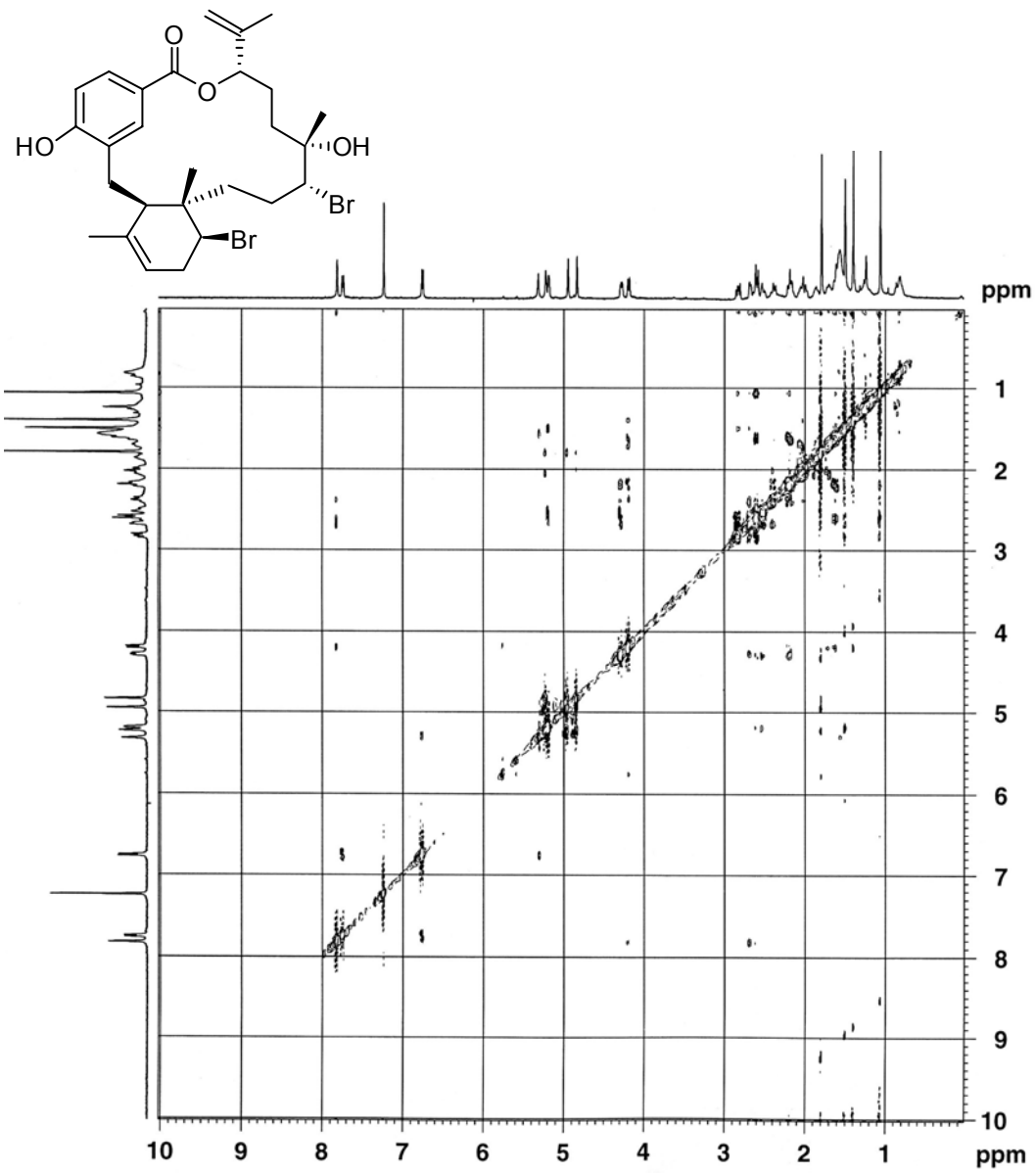

Figure A.23. ROESY spectrum of bromophycolide N (**3**) (500 MHz; $CDCl_3$)

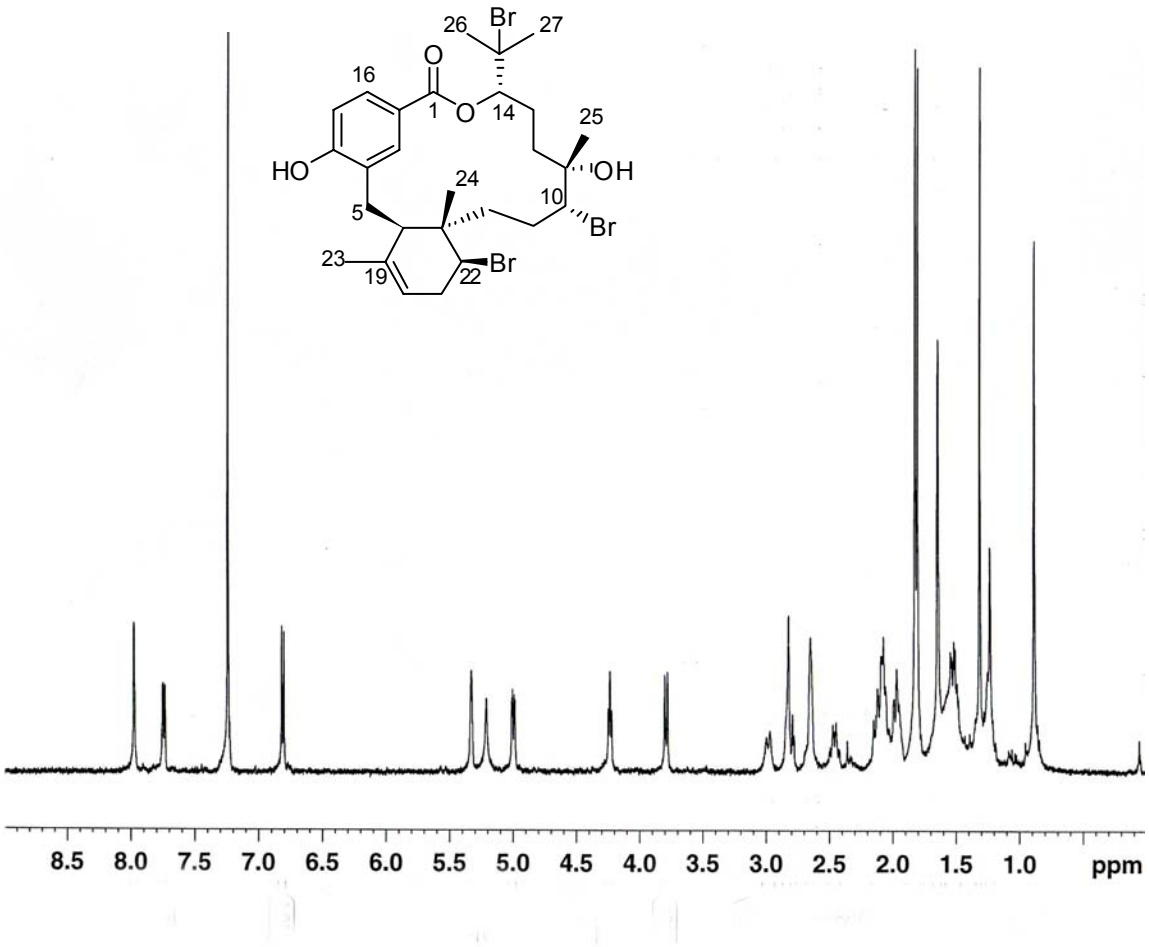

Figure A.24. ^{1}H NMR spectrum of bromophycolide O (**4**) (500 MHz; $CDCl_3$)

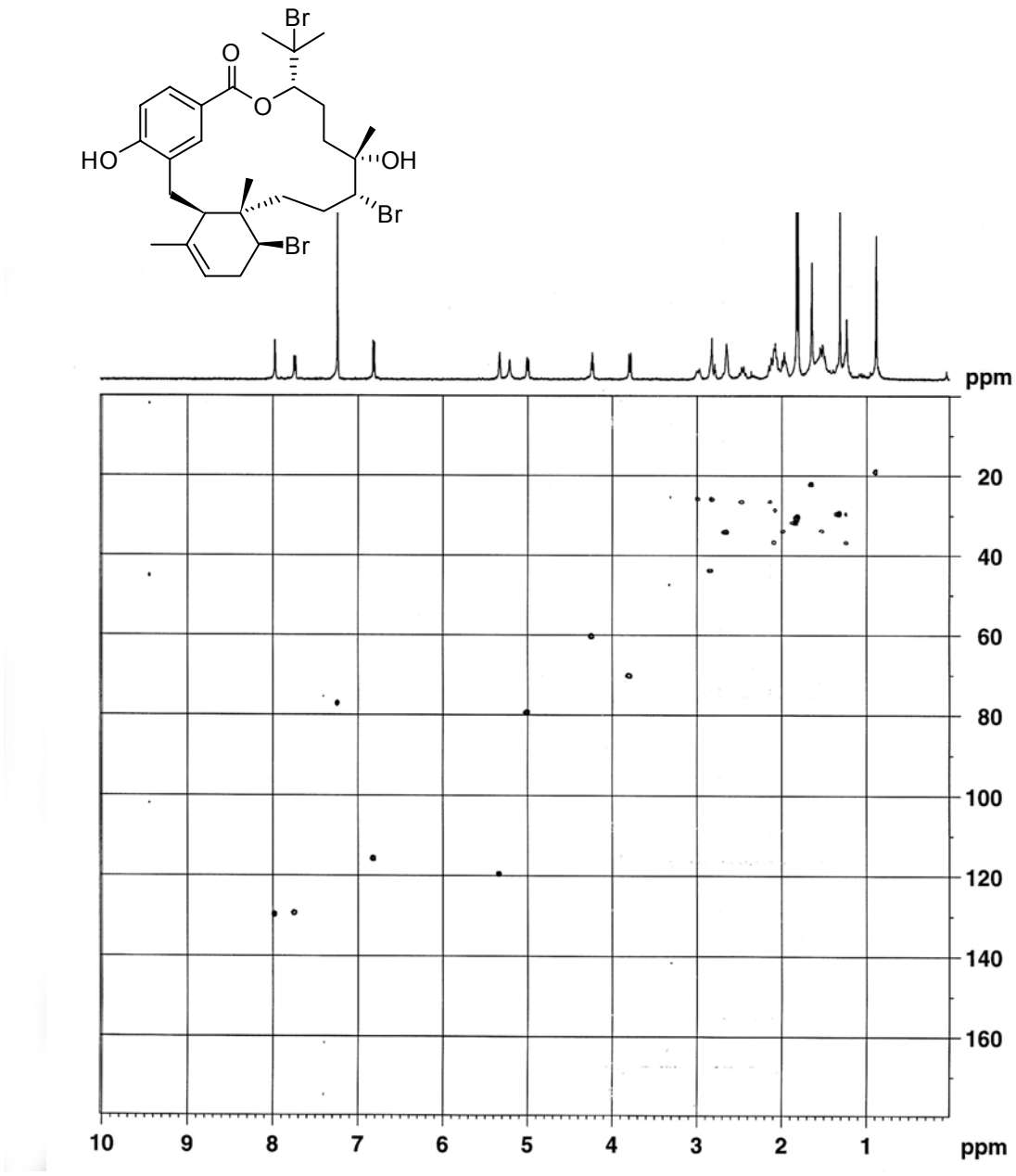

Figure A.25. HSQC spectrum of bromophycolide O (**4**) (500 MHz; $CDCl_3$)

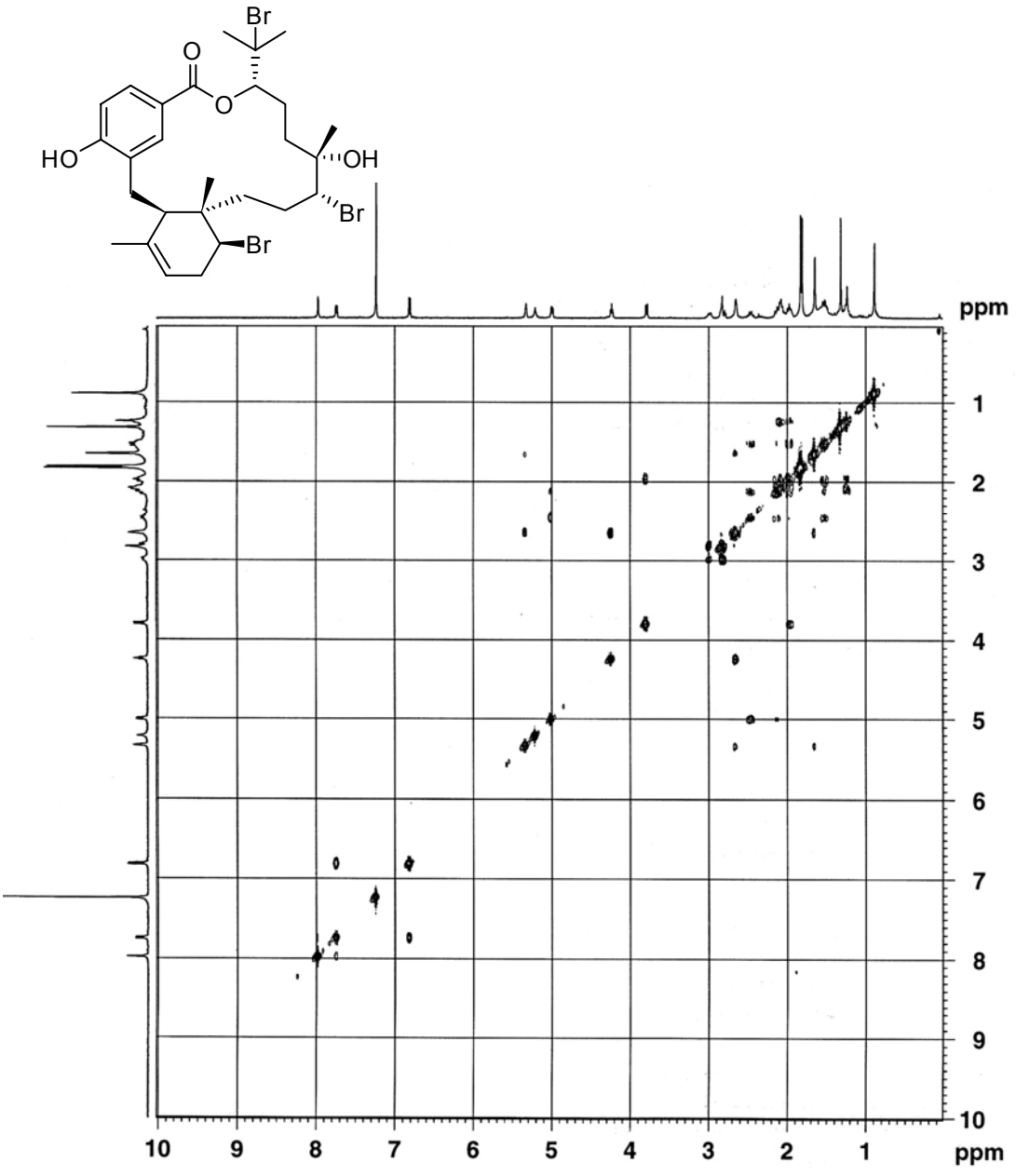

Figure A.26. ^{1}H-^{1}H COSY spectrum of bromophycolide O (**4**) (500 MHz; $CDCl_3$)

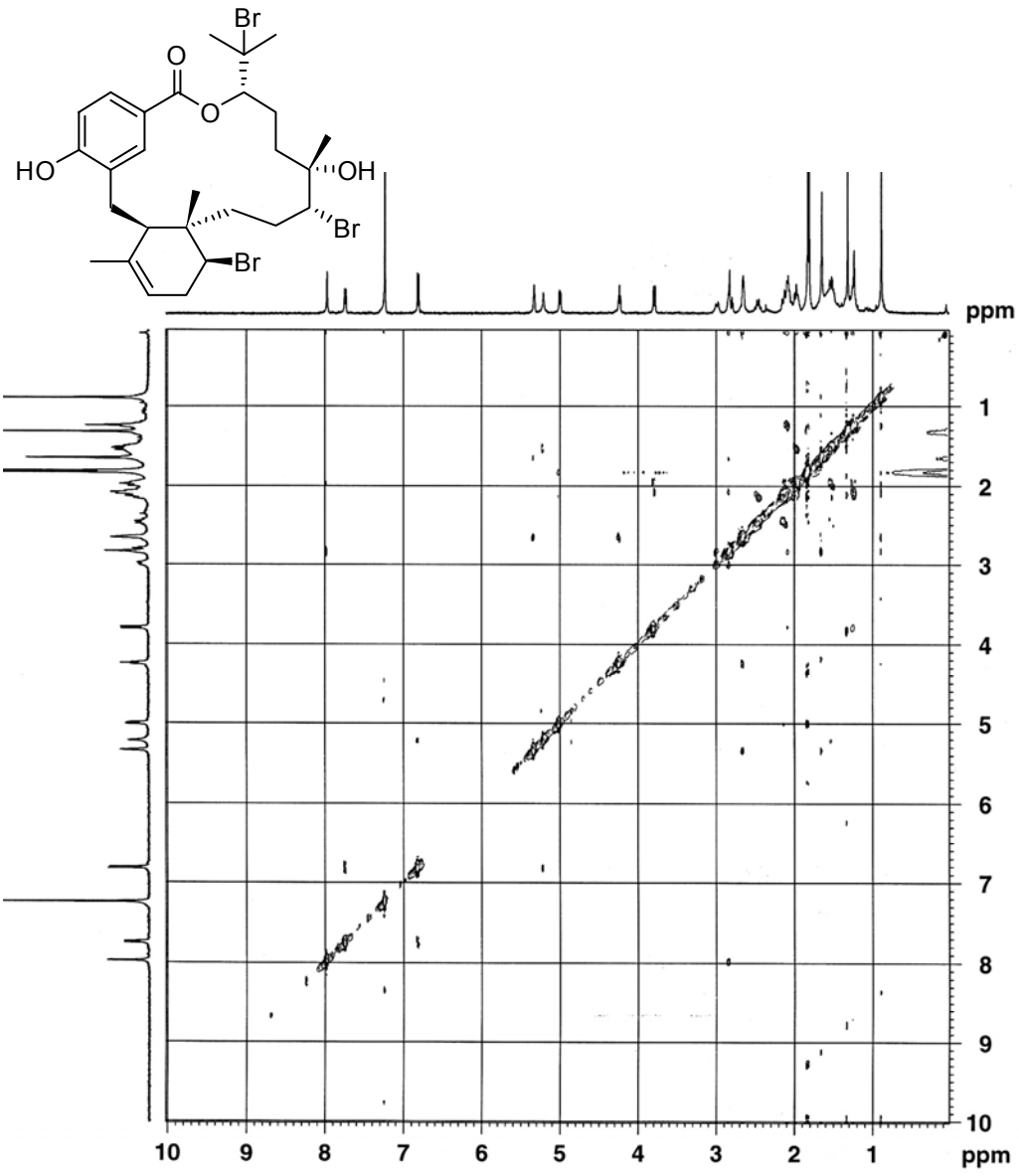

Figure A.27. ROESY spectrum of bromophycolide O (**4**) (500 MHz; $CDCl_3$)

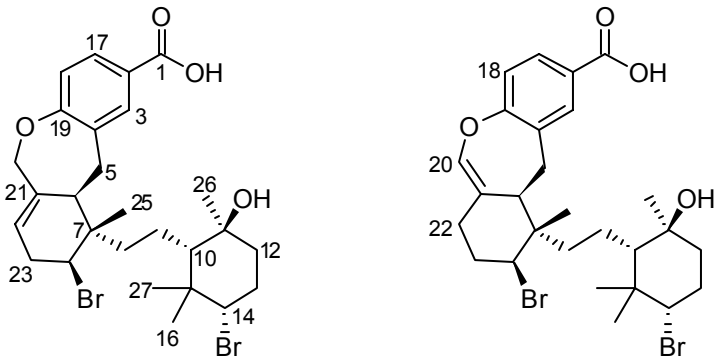

5 **6**

Figure A.28. Natural products isolated from the Fijian red macroalga *Callophycus serratus*; callophycolic acid C-D (**5-6**).

Table A.3. ^{13}C and ^{1}H NMR spectroscopic data for **5-6** (500 MHz; $(CD_3)_2CO$)

	5		**6**	
	δ ^{13}C	δ ^{1}H ($J_{H,H}$)	δ ^{13}C	δ ^{1}H ($J_{H,H}$)
1	167.2	-	167.1	-
2	124.2	-	127.4	-
3	135.6	7.91br s	133.0	8.08br s
4	129.1	-	134.5	-
5	33.3	3.02d (15.7), 3.14dd (15.1, 12.0)	30.5	3.20m, 3.28dd (13.3, 4.3)
6	42.8	2.98m	44.1	2.64dd (10.1, 3.7)
7	41.7	-	44.7	-
8	41.4	1.78dd (13.4, 5.2), 2.16dd (13.8, 4.4)	41.8	1.76m, 1.96m
9	20.8	1.41m, 1.46m	20.5	1.43m, 1.74m
10	57.6	1.29dd (3.9, 3.9)	58.0	1.35m
11	73.0	-	73.4	-

Table A.3 continued

12	44.4	1.60m, 1.69m	44.5	1.70m, 1.84m
13	32.7	2.00dd (12.9, 3.3), 2.08m	33.5	2.13m
14	68.9	4.10dd (12.2, 4.4)	68.9	4.15dd (11.0, 5.4)
15	41.6	-	41.9	-
16	30.8	1.16s	30.8	1.19s
17	129.9	7.73d (8.4)	130.0	7.83d (8.0)
18	119.5	6.84d (8.4)	120.2	7.00d (8.1)
19	163.2	-	164.2	-
20	74.6	4.44d (13.5), 4.97d (13.5)	140.9	6.61br s
21	138.9	-	122.6	-
22	123.6	5.63br s	33.2	2.08m
23	36.1	2.66m, 2.77m	35.2	2.07m, 2.18m
24	60.6	4.68dd (10.9, 6.0)	63.9	4.61dd (11.5, 4.0)
25	16.1	0.91s	17.9	0.92s
26	23.1	0.99s	23.5	1.32s
27	17.7	0.87s	18.0	0.98s

br=broad; s=singlet; d=doublet; dd=doublet of doublets; t=triplet; m=multiplet

Table A.4. ^{1}H-^{1}H COSY correlations for **5-6**. For diastereotopic protons with dissimilar chemical shifts, the proton whose chemical shift is listed first in Table A.3 is termed “a” and the other is “b”. “NA” (not applicable) indicates that no proton signal exists for that position.

^{1}H at position #:	**COSY correlations observed between protons listed on far left and those below:**	
	5	**6**
3	17	17
5a	5b, 6	5b, 6
5b	5a, 6	5a, 6
6	5a, 5b, 22	5a, 5b
7a	NA	NA
7b	NA	NA
8a	8b, 9a, 9b	8b, 9a, 9b
8b	8a, 9a, 9b	8a, 9a, 9b
9a	8a, 8b, 9b, 10	8a, 8b, 9b, 10
9b	8a, 8b, 9a, 10	8a, 8b, 9a, 10
10a	9a, 9b	9a, 9b
10b	NA	NA
11a	NA	NA
11b	NA	NA
12a	12b, 13a, 13b	12b, 13
12b	12a, 13a, 13b	12a, 13
13a	12a, 12b, 13b, 14	12a, 12b, 14
13b	12a, 12b, 13a, 14	NA
14a	13a, 13b	13
14b	NA	NA
15a	NA	NA
15b	NA	NA
16	-	-
17	3, 18	3, 18
18	17	17
20a	20b	-
20b	20a	NA
21a	NA	NA
21b	NA	NA
22a	6, 23a, 23b	23a, 23b
22b	NA	-
23a	22, 23b, 24	22, 23b, 24
23b	22, 23a, 24	22, 23a, 24
24	23a, 23b	23a, 23b
25	-	-
26a	-	-
26b	NA	NA
27	-	-

Table A.5. HMBC correlations for **5-6**. For diastereotopic protons with dissimilar chemical shifts, the proton whose chemical shift is listed first in Tables A.3 is termed “a” and the other is “b”. “NA” (not applicable) indicates that no proton signal exists for that position.

^{1}H at position #:	HMBC correlations observed between protons listed on far left and carbons at positions listed below:	
	5	**6**
3	1, 5, 17, 19	1, 5, 17, 19
5a	3, 4, 6, 19, 21	3, 4, 6, 19, 21
5b	4, 6, 21	3, 4, 6, 19, 21
6	4, 5, 7, 21	5, 7
7a	NA	NA
7b	NA	NA
8a	7, 9, 24	7, 9, 10
8b	7, 24	9, 10, 24
9a	8, 10, 11	8, 10
9b	8, 10, 11	8
10a	9, 11, 15, 16	9, 11, 15, 26
10b	NA	NA
11a	NA	NA
11b	NA	NA
12a	11, 13, 26	11
12b	11, 13, 26	10
13a	14	11, 12
13b	14	NA
14a	13, 16, 27	16, 27
14b	NA	NA
15a	NA	NA
15b	NA	NA
16	10, 14, 15, 27	10, 14, 15, 27
17	1, 3, 19	3, 19
18	2, 4, 19	2, 4, 19
20a	6, 19, 21, 22	6, 19, 21, 22
20b	19, 21, 22	NA
21a	NA	NA
21b	NA	NA
22a	-	6, 20, 21, 23
22b	NA	NA
23a	7, 21, 22, 24	7, 21, 22, 24
23b	7, 21, 22, 24	21
24	7, 23, 25	23
25	6, 7, 8, 24	6, 7, 8, 24
26a	10, 11, 12	10, 11, 12
26b	NA	NA
27	10, 14, 15, 16	10, 14, 15, 16

Table A.6. Observed NOEs from ROESY NMR experiments **5-6**. For diastereotopic protons with dissimilar chemical shifts, the proton whose chemical shift is listed first in Table A.3 is termed “a” and the other is “b”. Only NOEs important to determinations of stereochemistry are listed.

^{1}H at position #:	NOE observed between protons listed on far left and protons at positions listed below:	
	5	**6**
5a	25	25
5b	25	25
6	9b, 24	9b, 24
7a		
7b		
8a	10, 16, 25	10, 16, 25
8b	10, 25	10, 25
9a	16, 24, 27	16, 24, 27
9b	6, 26	6, 26
10	8a, 8b, 12a, 14, 16	8a, 8b, 12a, 14, 16
12a	10, 14	10, 14
12b	26	26
14a	10, 12a, 16	10, 12a, 16
14b		
16	8a, 9a, 10, 14	8a, 9a, 10, 14
18		
20a	22	22
20b		
22a	20	20
22b		
23		
24	6, 9a	6, 9a
25	5a, 5b, 8a, 8b, 12b	5a, 5b, 8a, 8b
26	9b, 12b, 27	9b, 12b, 27
27	9a, 26	9a, 26

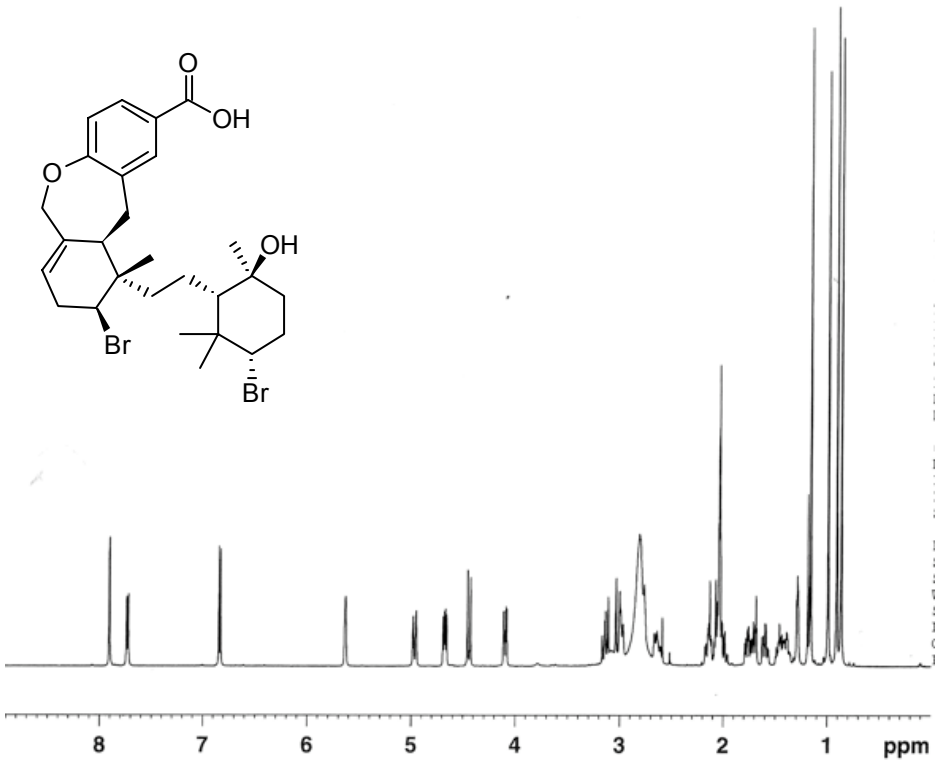

Figure A.29. ^{1}H NMR spectrum of callophycoic acid C (**5**) (500 MHz; $(CD_3)_2CO$)

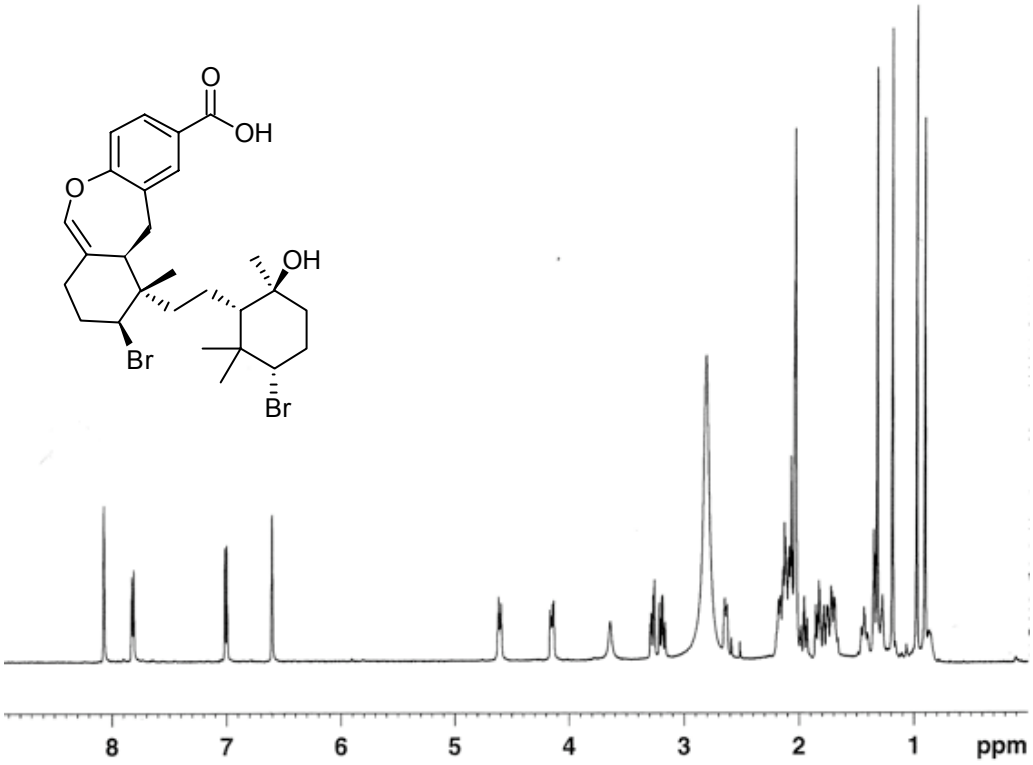

Figure A.30. ^{1}H NMR spectrum of callophycoic acid D (**6**) (500 MHz; $(CD_3)_2CO$)

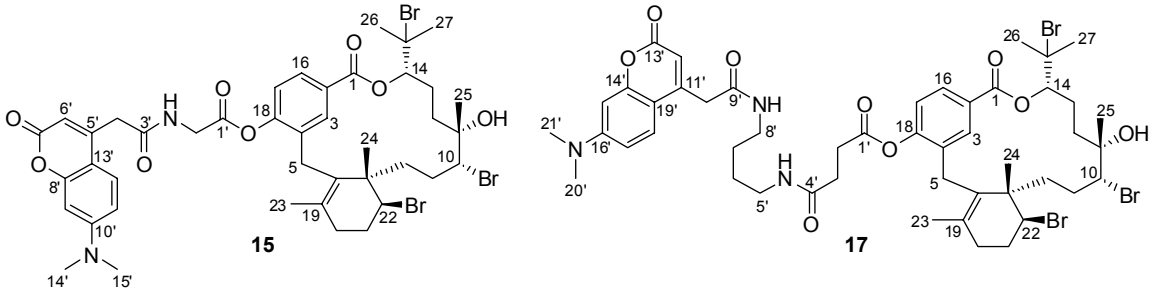

Figure A.31. Fluorescent IAF-labeled bromophycolide A probes.

Table A.7. NMR Spectral Data for Probes **15** and **17** (500 MHz, $CDCl_3$)[a]

position	15		17	
	δ_C	δ_H mult. (*J*, Hz)	δ_C	δ_H mult. (*J*, Hz)
1	165.0	-	164.9	-
2	127.1	-	127.0	-
3	131.0	8.08 s	131.0	8.06 s
4	131.8	-	131.9	-
5	29.1	3.16 d (18), 3.37 d (18)	29.1	3.20 m, 3.41 d (18)
6	129.4	-	129.4	-
7	43.4	-	43.4	-
8	37.4	1.25 m, 1.88 m	37.4	1.26 m, 1.86 m
9	28.7	1.73 m, 2.02 m	28.7	1.73 m, 2.02 m
10	73.1	3.47 m	73.3	3.47 m
11	72.2	-	72.2	-
12	34.2	1.05 m, 1.73 m	34.3	1.05 m, 1.71 m
13	28.3	2.05 m, 2.12 m	28.3	2.05 m, 2.12 m
14	80.9	4.66 d (10.9)	80.9	4.66 d (9.3)
15	67.0	-	66.9	-
16	129.2	7.92 dd (1.5,8.3)	129.2	7.91 d (8.3)
17	122.4	7.14 d (8.3)	122.4	7.16 d (8.3)
18	152.3	-	152.8	-
19	134.0	-	134.0	-
20	33.2	2.01 m, 2.27 m	33.3	2.01 m, 2.27 m
21	30.5	2.26 m	30.5	2.26 m
22	60.6	4.45 dd (5.7, 8.2)	60.6	4.46 m
23	21.0	1.35 s	21.0	1.35 s
24	26.1	1.24 s	26.1	1.27 s
25	33.6	1.29 s	33.6	1.29 s

Table A.7 continued

26	30.9	1.81 s	30.9	1.81 s
27	31.7	1.80 s	31.7	1.80 s
1’	166.5	-	170.6	-
2’	41.8	4.32 dd (5.8, 7.8)	30.2	2.62 m
3’	169.4	-	29.5	2.98 m
3’-NH	-	6.32 t (5.5)	NA	NA
4’	39.9	3.76 s	171.0	-
4’-NH	NA	NA	-	6.01 t (5.9)
5’	149.2	-	39.0	3.21 m
6’	110.3	6.13 s	26.3	1.45 m
7’	162.4	-	26.3	1.45 m
8’	156.0	-	39.0	3.21 m
9’	98.1	6.51 d (2.4)	168.5	-
9’-NH	NA	NA	-	6.15 t (5.6)
10’	154.3	-	40.5	3.60 s
11’	109.6	6.62 dd (2.4, 9.0)	149.2	-
12’	125.5	7.46 d (9.0)	110.3	6.03 s
13’	108.2	-	162.4	-
14’	40.0	3.04 s	156.0	-
15’	40.0	3.04 s	98.1	6.48 d (2.3)
16’	NA	NA	154.3	-
17’	NA	NA	109.3	6.61 dd (2.3, 8.9)
18’	NA	NA	125.5	7.45 d (8.9)
19’	NA	NA	108.2	-
20’	NA	NA	40.0	3.03 s
21’	NA	NA	40.0	3.03 s

[a]Carbon assignments were based on HSQC and HMBC data collected at 500 MHz

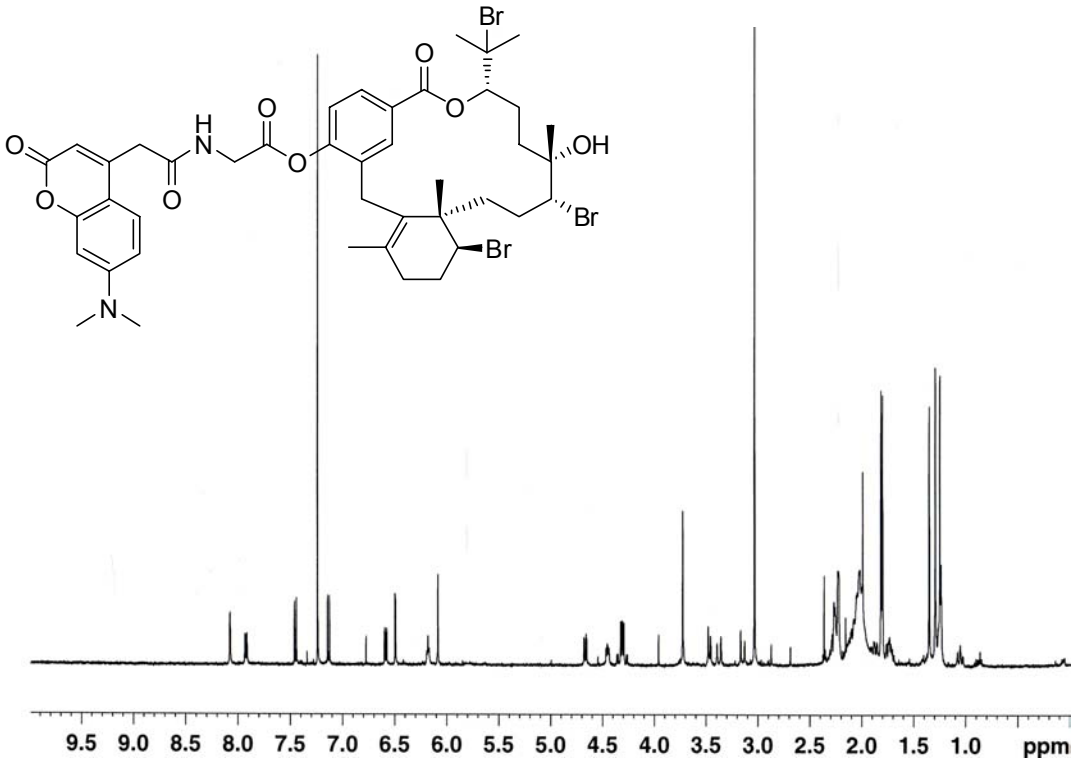

Figure A.32. ^{1}H NMR spectrum of bromophycolide 'short-linker' probe **15** (500 MHz; $CDCl_3$)

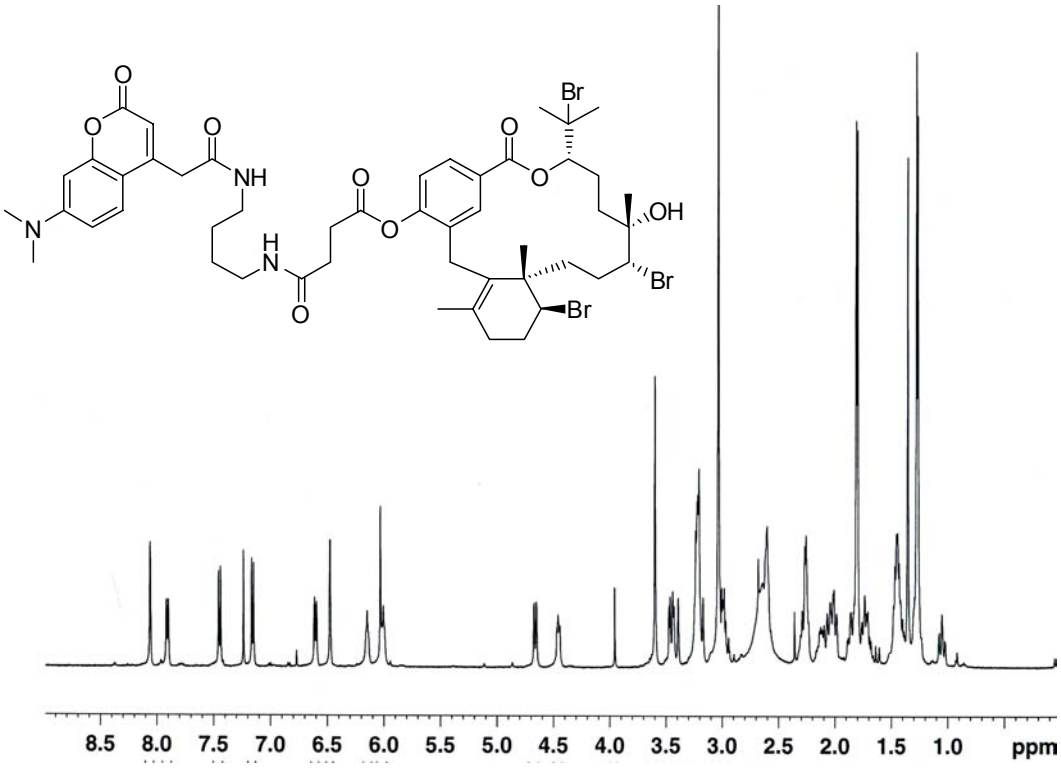

Figure A.33. ^{1}H NMR spectrum of bromophycolide 'long-linker' probe **17** (500 MHz; $CDCl_3$)

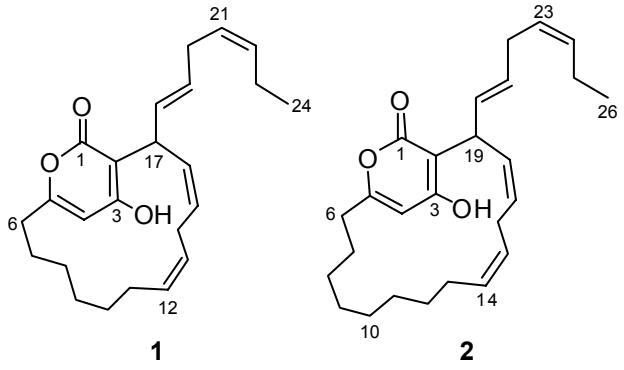

1 **2**

Figure A.34. Natural products isolated from the Fijian red macroalga *Neurymenia fraxinifolia*; neurymenolides A-B (**1-2**).

Table A.8. ^{1}H-^{1}H COSY correlations for **1-2**. For diastereotopic protons with dissimilar chemical shifts, the proton whose chemical shift is listed first in Table 5.1 is termed “a” and the other is “b”. “NA” (not applicable) indicates that no proton signal exists for that position.

^{1}H at position #:	**COSY correlations observed between protons listed on far left and those below:**	
	1	**2**
4	-	-
6a	6b, 7a, 7b	6b, 7a, 7b
6b	6a, 7a, 7b	6a, 7a, 7b
7a	6a, 6b, 7b, 8a	6a, 6b, 7b, 8a, 8b
7b	6a, 6b, 7a, 8b	6a, 6b, 7a, 8b
8a	7a	7a
8b	7b, 9a	7a, 7b, 9a
9a	8b, 9b	8b, 9b, 10a, 10b
9b	9a, 10a, 10b	9a
10a	9b	9a
10b	9b, 11a, 11b	9a
11a	10b	-
11b	10b, 12	-
12a	11b	13a, 13b
12b	NA	13a, 13b
13a	14a, 14b	12a, 12b, 13b, 14
13b	NA	12a, 12b, 13a, 14
14a	13, 14b, 15	13a, 13b

Table A.8 continued

14b	13, 14a, 15	NA
15	14a, 14b	16a, 16b
16a	17	15, 16b, 17
16b	NA	15, 16a, 17
17	16, 18	16a, 16b
18	17	19
19	20	18, 20
20	19, 21	19
21	20, 22	22
22	21, 23	21, 23
23	22, 24	22, 24
24	23	23, 25
25	NA	24, 26
26	NA	25

Table A.9. HMBC correlations for **1-2**. For diastereotopic protons with dissimilar chemical shifts, the proton whose chemical shift is listed first in Table 1 of the main article is termed “a” and the other is “b”. “NA” (not applicable) indicates that no proton signal exists for that position.

^{1}H at position #:	**HMBC correlations observed between protons listed on far left and those below:**	
	1	**2**
4	2, 5, 6	2, 5, 6
6a	4, 5, 7	-
6b	4, 5, 7	5
7	-	-
8	-	-
9a	8, 10	-
9b	8, 10	-
10a	9	9
10b	9	9
11a	10	-
11b	-	10
12a	14	-
12b	NA	13
13a	14	14
13b	NA	14
14a	-	13
14b	15	NA
15	14, 17	16
16a	17	-

Table A.9 continued

16b	NA	15
17	2, 18	-
18	17, 20	-
19	17, 20	-
20	19, 21	19,22
21	-	19, 22
22	-	21
23	22, 24	-
24	22, 23	-
25	NA	23, 24, 26
26	NA	24, 25
-OH	3, 4	2, 3, 4

Table A.10. Observed NOEs from ROESY NMR experiments **1-2**. For diastereotopic protons with dissimilar chemical shifts, the proton whose chemical shift is listed first in Table 5.1 is termed “a” and the other is “b”. Only NOEs important to determinations of stereochemistry are listed.

^{1}H at position #:	**NOEs observed between protons listed on far left and protons at positions listed below:**	
	1	**2**
4	9a	
9a	4	
11a	-	
11b	14a, 14b	
13a		16a
13b		16b
14a	11b, 17	
14b	11b, 17	
16a		13a, 19
16b		13b, 19
17	14a, 14b	
19		16a, 16b
20	23	
22		25
23	20	
25		22

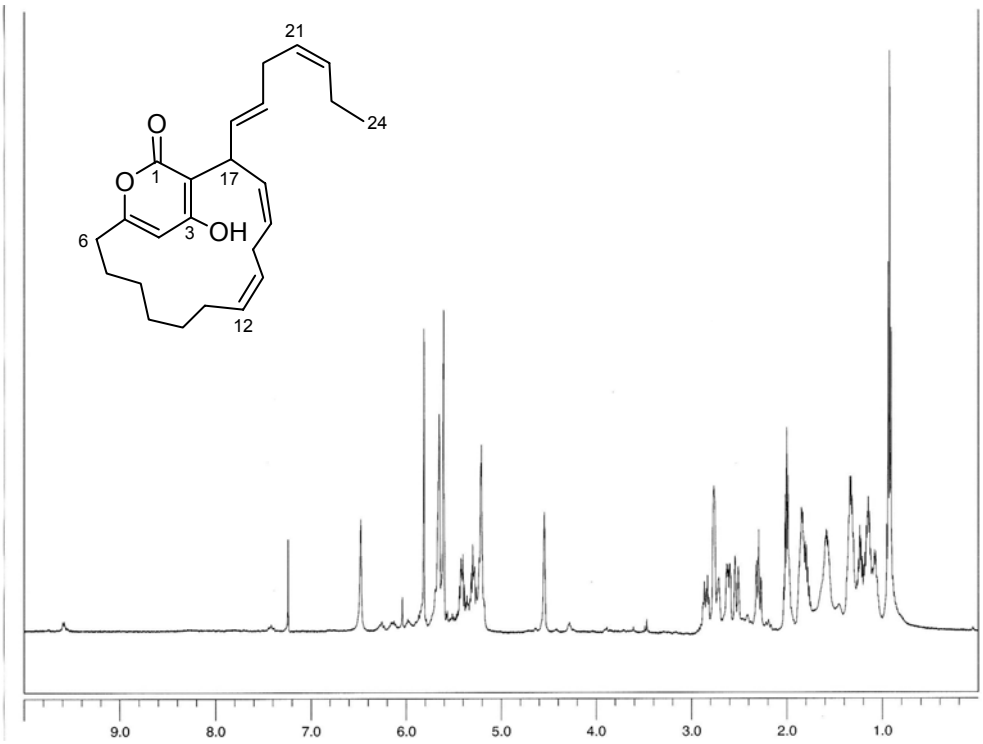

Figure A.35. ^{1}H NMR spectrum of neurymenolide A (**1**) (500 MHz; $CDCl_3$)

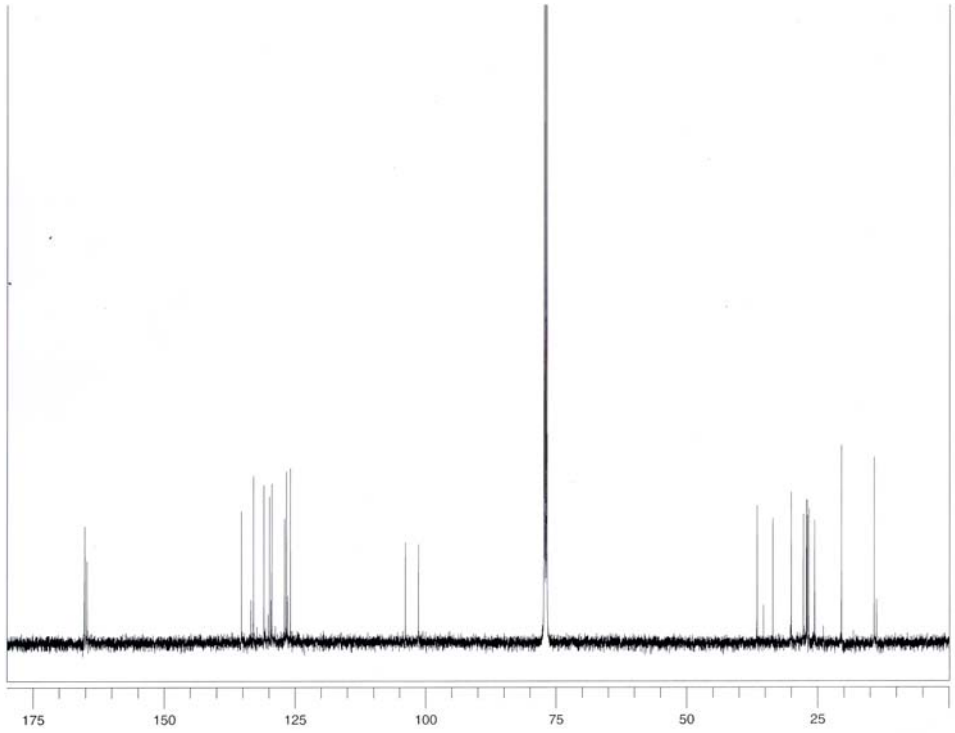

Figure A.36. ^{13}C NMR spectrum of neurymenolide A (**1**) (125 MHz; $CDCl_3$)

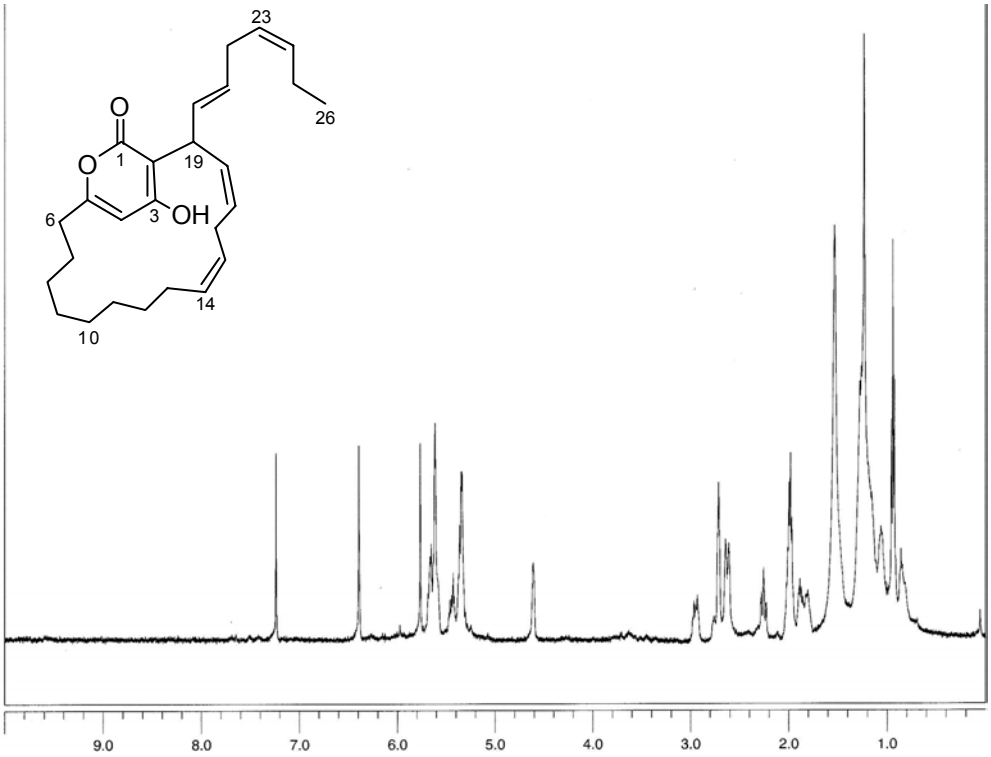

Figure A.37. ^{1}H NMR spectrum of neurymenolide B (**2**) (500 MHz; $CDCl_3$)

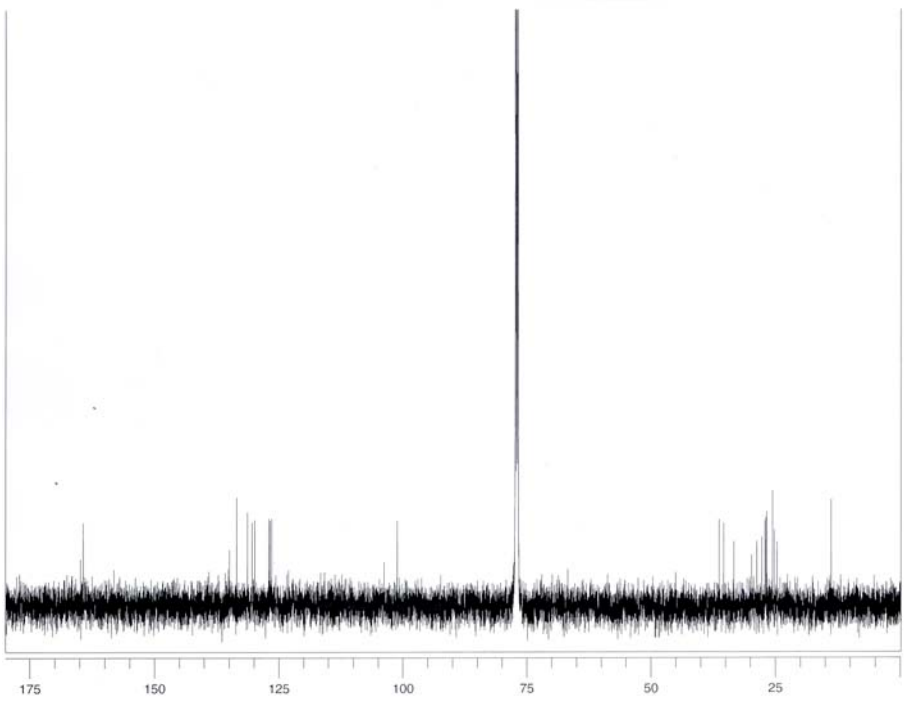

Figure A.38. ^{13}C NMR spectrum of neurymenolide B (**2**) (125 MHz; $CDCl_3$)

APPENDIX B

ADDITIONAL EXPERIMENTAL DATA

Experimental Data for Chapter 6

Supporting Figures

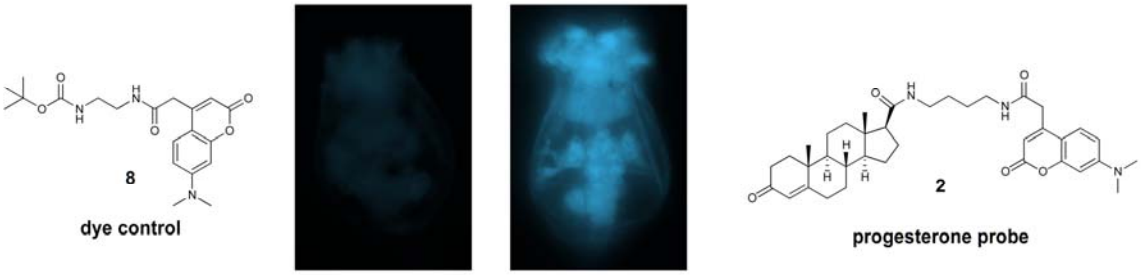

Figure B.1. *Brachionus manjavacas* hatchlings incubated with the IAF-labeled progesterone probe **2** (right) and a fluorescent control **8** (left) at 10 µg/ml. Uptake of **8** was not detected under the conditions used to image hatchlings incubated with **2**.

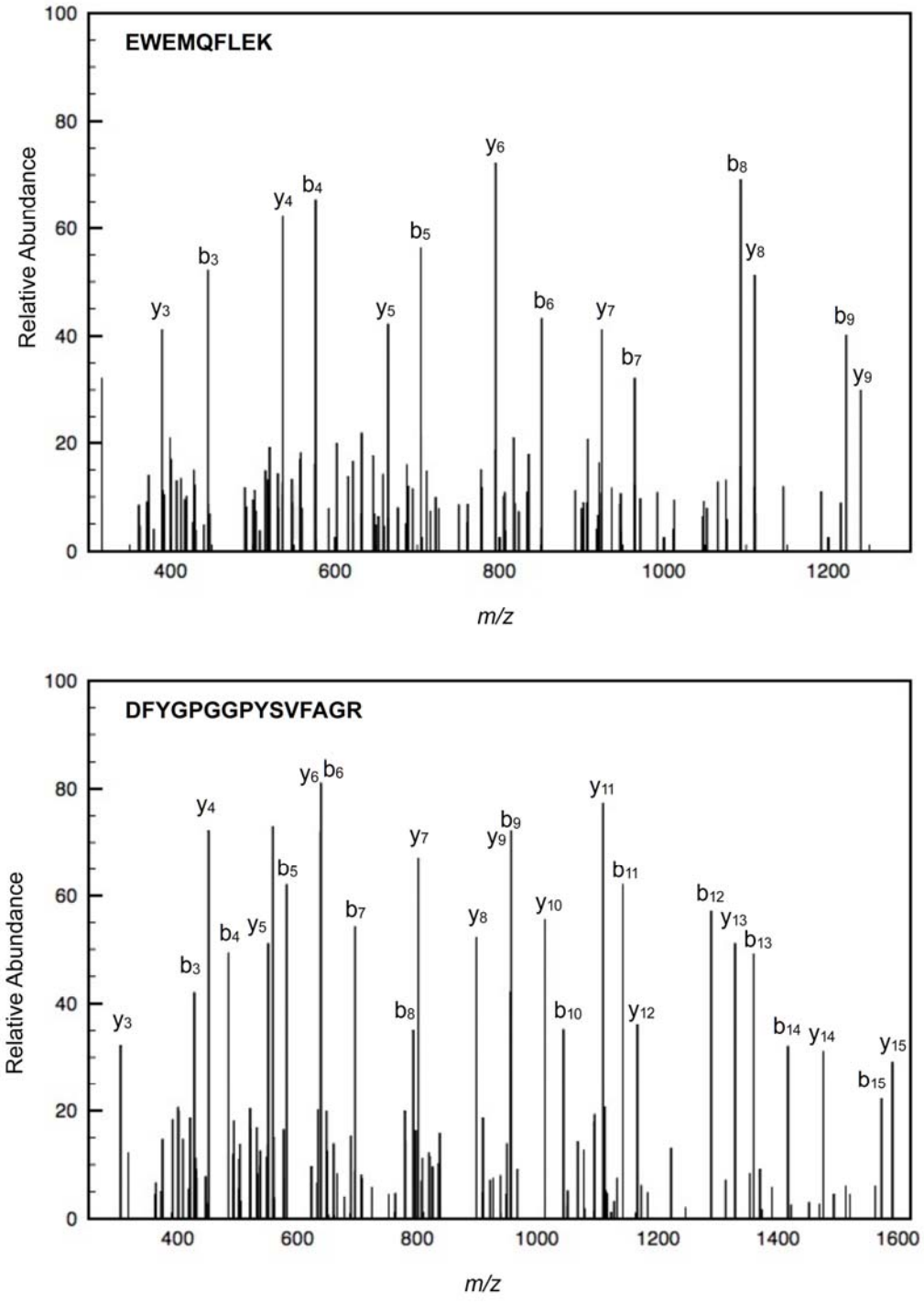

Figure B.2. MS/MS detection of peptides: (top) daughter ions of *m/z* 1239.57 corresponding to EWEMQFLEK and (bottom) daughter ions of *m/z* 1589.74 corresponding to DFYGPGGPYSVFAGR.

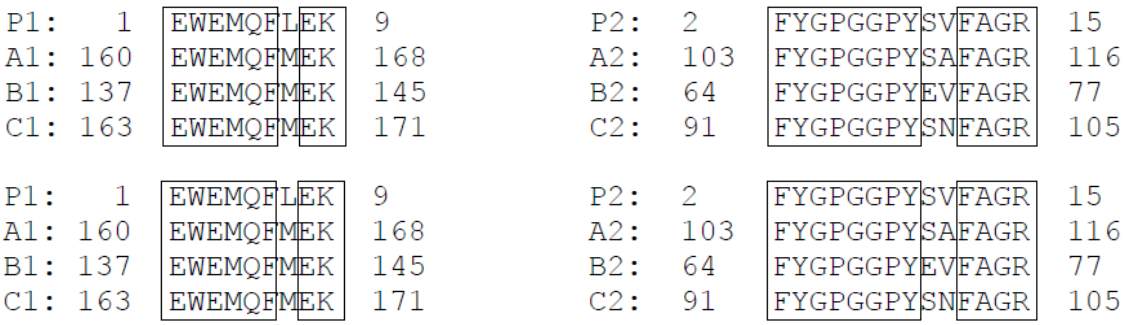

Figure B.3. Blast searches on the respective peptides EWEMQFLEK (P1) and DFYGPGGPYSVFAGR (P2). Peptide A1 is found in the progestin membrane receptor component 2 from *Oncorhynchus mykiss* (gb|ABD58973.1|, 88% identities); B1 is found in the progesterone receptor membrane component 1 from *Strongylocentrotus purpuratus* (ref|XP_783332.1|, 88% identities); and C1 is found in the progesterone receptor membrane component 2 from *Danio rerio* (gb|AAH53415.1|, 88% identities). Peptide A2 is found in the progestin membrane receptor component 1 from *Penaeus monodon* (gb|ACC62174.1|, 92% identities); B2 is found in the steroid binding protein 1 from *Thalassiosira pseudonana* (gb|EED96317.1|, 92% identities); and C2 is found in the hypothetical protein FG02758.1 from *Gibberella zeae* PH-1 (ref|XP_382934.1|, 86% identities).

ATGGCC**CGACGGTTCTTTGACGATGT**CATATCATCTCCGGTCAATATTTTTCTAGTA
GGTTTGATCTGCTACTTCTCGTACAAATTGATCAAAAAAGATAGCACCAAATCGCCG
GCGAGAAAAAACTCAAAATCAGAAAATGATTTGGCTAAAATGCCAAAACAAGATTTT
ACTTTGGAAGAGCTAAAGCAATATGACGGGATTAAATCCGATGGACGTATTTTAATT
GGGGTACTTGGCAAAGTTTTTGATGTTTCAAAAGCGAAAGATTTCTATGGACCGGG
CGGTCCGTATTCCGTATTTGCTGGTCGCGATGCATCCAGAGCGTTGGGCACTTTTT
CTGTGGACAAATCCCAATTTAAAGATGAATACGATGATCTAAGCGATCTGAAGAGTT
CTCAGATGGAAAGTATCAAAGAATGGGAGATGCAATTTTTGGAAAAATATCCACTTG
TTGGTAATTTGCTAAGGCCTGGTGAAGAGCCCACTGTTT**ACGAAGAAGAGTCAGC**
CGAAGTTAAAAAACAACTTTAA

Figure B.4. ORF within the rotifer progesterone gene (GenBank accession FJ829246) from the *Brachionus manjavacas* cDNA database. This is the reverse complement of the contig sequence. Bold and underlined bases indicate primer sequences; yellow indicates area amplified for the dsRNA used in RNAi knockdown experiments.

Supporting Western Blot Methods

Western blotting studies using reactive probe **4**

The method was first tested by screening for PR expression in a MCF-7 cell lysates. Whole MCF-7 cell lysate was prepared by homogenization in modified RIPA buffer (150 mM NaCl, 50 mM Tris-HCl, pH 7.4, 1% Triton X-100, 1 mM EDTA, 1 mM PMSF, 5 µg/ml aprotinin, 1 µg/ml pepstatin-A, 2 µg/ml lLeupeptin, 1 mM Na_3VO_4, 1 mM NaF). The debris was removed by centrifugation and the protein concentration was concentrated to 1 mg/mL using a 3 kDa cutoff filter. An aliquot of this lysate (500 µL) was treated with 20 µL of a 1 mg/mL stock of **4** in DMSO at 4 °C. A 50 µL sample was taken at 4 h and boiled for 5 min in SDS sample buffer (50 mM Tris-HCl pH 6.8, 12.5% glycerol, 1% SDS, 0.01% bromophenol blue containing 5% □-mercaptoethanol). SDS-PAGE gel analysis

was conducted on a Novex X-cell station using NuPage 4-12% Bis-Tris gels and MOPS SDS running buffer. Western blotting was conducted by transfer to Hybond-P PVDF membrane by GE Healthcare (Piscataway, NJ) followed by blocking for 2 h with a solution of 0.1% Tween-20 with 5% w/v nonfat dry milk 20 in tris-buffered saline (TBS, pH 7.6). One lane was stained with a mouse anti-progesterone receptor 00005241-M01 Anti-PGR (1-110) mAb (anti-PR) from Abnova (Ann Arbor, MI), in 0.1% Tween-20 with 5% BSA in TBS, and a Goat anti-mouse IgG HRP mAb conjugate from Promega (Madison, WI) in 0.1% Tween-20 with 5% BSA in TBS. A second lane was stained a mouse anti-progesterone IgG mAb (anti-P) from Assay Designs (Tapei City, Taiwan), in 0.1% Tween-20 with 5% BSA in TBS, and a Goat anti-mouse IgG HRP mAb conjugate from Promega (Madison, WI) in 0.1% Tween-20 with 5% BSA in TBS. For both experiments, the primary and secondary antibodies were applied at 1:100 and 1:2,000 dilution, respectively, from their manufactures preparation. The total protein content in each gel was determined by staining with ponceau S from Promega (Madison, WI).

Synthetic Procedures and Compound Characterization

tert-butyl-4-((8S,9S,10R,13S,14S,17S)-10,13-dimethyl-3-oxo-2,3,6,7,8,9,10,11,12,13,14,15,16,17-tetradecahydro-1H-cyclopenta-[α]phenanthrene-17-carboxamido)butylcarbamate (**10**). HATU (157 mg, 0.41 mmol) was added to a mixture of 3-keto-4-etiocholenic acid **9** (65 mg, 0.021 mmol), *N*-boc-1,4-butyldiamine (53.5 mg, 0.28 mmol), and EtN^iPr_2 (108 µL, 0.62 mmol) in anhydrous DMF (5 mL). The reaction was allowed to stir for 12 h at rt and then dried under vacuum. Any remaining HATU was precipitated with CH_2Cl_2 and removed via filtration. Compound **10** (94 mg) was obtained as a colorless oil, 89% yield. ^{1}H NMR ($CDCl_3$, 500 MHz) δ: 7.98 (bs, 1H); 6.99 (bs, 1H); 6.51 (s, 1H); 3.63 (m, 1H); 3.35 (m 3H); 2.90 (s, 6H); 2.66-2.41 (m, 2H); 2.36-2.22 (m, 1H); 2.27-2.16 (m, 3H); 2.11-2.01 (m, 2H); 2.00-1.88 (m, 1H); 1.87-1.73 (m, 1H); 1.67-

1.42 (m, 6H); 1.41-1.25 (m, 5H); 1.23 (s, 3H); 1.19-1.05 (m, 3H); 1.02 (s, 3H); 0.94-0.58 (m, 4H); 0.39 (s, 3H). ^{13}C NMR ($CDCl_3$, 100 MHz) δ: 197.5; 171.7; 170.3; 155.9; 123.5; 77.5; 56.4; 55.6; 54.1; 43.6; 39.9; 38.6; 38.5; 38.2; 37.9; 35.8; 35.6; 33.7; 32.5; 32.1; 27.9; 27.5; 27.2; 24.4; 23.5; 20.8; 16.8; 13.0. HR-ESI-MS (*m/z*): Calcd for $C_{31}H_{51}N_2O_4$ [M + H], 515.3771; Found 515.3784.

(*R*)-*N*-(4-(2-(7-(dimethylamino)-2-oxo-2H-chromen-4-yl)acetamido)butyl)-4-(3*R*,5*S*,7*R*,8*R*,9*S*,10*S*,12*S*,13*R*,14*S*,17*R*)-3,7,12-trihydroxy-10,13-dimethyl-hexadeca-hydro-1H-cyclopenta-[α]phenanthren-17-yl)pentanamide (**2**). Intermediate **10** (54 mg, 0.10 mmol) was dissolved in CH_2Cl_2 (1 mL). Trifluoroacetic acid (0.020 mL, 0.285 mmol) was added dropwise and the reaction was allowed to stir at room temperature for 1 h. The reaction was then diluted with CH_2Cl_2 (10 mL) and washed with 0.001 N NaOH (1 mL) and water. The organic layer was concentrated *in vacuo*, and crude amine was used without further purification. HATU (80 mg, 0.20 mmol) was added to a solution of the crude amine, 7-dimethylamino-4-coumarinacetic acid (31 mg, 0.13 mmol), and EtN^iPr_2 (55 µL, 0.31 mmol) in anhydrous DMF (1.5 mL). The reaction was allowed to stir for 16 h and then dried. Remaining HATU was precipitated with MeOH and removed via filtration. The crude product was subjected to flash chromatography (2:1 hexanes/EtOAc to 1:5 MeOH/EtOAc) with **2**, eluting with 1:10 MeOH/EtOAc, collected as a yellow wax (45 mg, 67% yield). ^{1}H NMR (acetone-d_6, 500 MHz) δ: 9.44 (s, 2H); 8.99 (d, 1H, *J* = 11.3Hz) ;8.94 (bm, 1H); 8.00 (bm, 1H); 7.91 (dd, 1H, *J* = 3.2, 11.2 Hz); 7.72 (d, 1H, *J* = 3.2 Hz); 7.01 (s, 1H); 6.50 (s, 1H); 4.35 (m, 2H); 4.21 (dt, 1H, *J* = 8.0, 8.0, 16.1 Hz); 4.06 (s, 2H); 3.70 (m, 2H); 3.59 (m, 1H); 3.51 (m, 2H); 3.39 (m, 1H); 3.34 (s, 2H); 2.90 (s, 6H); 2.61-2.42 (m, 3H); 2.33 (ddd, 1H, *J* = 3.0, 5.0, 18.1 Hz); 2.26-2.17 (m, 2H); 2.09-1.97 (m, 1H); 1.95-1.78 (m, 3H); 1.62-1.42 (m, 4H); 1.41-1.22 (m, 2H); 1.28 (s, 3H); 1.27

(s, 3H); 1.24 (d, 3H, *J* = 9.1 Hz); 1.17-1.04 (m, 4H); 1.01 (s, 3H); 0.90-0.63 (m, 4H); 0.35 (s, 3H). HR-ESI-MS (*m/z*): Calcd for $C_{37}H_{50}N_3O_5$ [M + H], 616.3672; Found 616.3618.

t-butyl-4-((*R*)-4-((3*R*,5*S*,7*R*,8*R*,9*S*,10*S*,12*S*,13*R*,14*S*,17*R*)-3,7,12-trihydroxy-10,13-dimethyl-hexadecahydro-1H-cyclopenta[α]phenanthren-17yl)pentanamido) butylcarbamate (**11**). HATU (175 mg, 0.46 mmol) was added to a solution of cholic acid (100 mg, 0.24 mmol), *N*-boc-1,4-butanediamine (95 mL, 0.49 mmol), and Et_3N (0.15 mL, 1.1 mmol) in anhydrous DMF (1.5 mL). The reaction was allowed to stir for 16 h, then diluted with deionized H_2O (20 mL) and extracted with EtOAc (20 mL). The organics were washed three times with deionized H_2O (15 mL), dried over $MgSO_4$, and concentrated *in vacuo.* Any remaining HATU was precipitated with CH_2Cl_2 and removed via filtration. Compound **11** (114 mg) was obtained as a clear oil, 80% yield. ^{1}H NMR ($CDCl_3$, 500 MHz) δ: 6.58 (br s, 1H); 4.92 (br s, 1H); 3.90 (s, 1H); 3.78 (s, 1H); 3.41 (s, 9H); 3.17 (br d, 2H, *J* = 5.4 Hz); 3.06 (br d, 2H, *J* = 4.6 Hz); 2.27 (br s, 2H); 2.15 (t, 2H, *J* = 13.2 Hz); 1.14 (m, 1H); 1.88-1.75 (m, 2H); 1.70 (t, 3H, *J* = 13.7 Hz); 1.65-1.49 (m, 2H); 1.47 (br s, 6H); 1.38 (s, 12H); 1.2 (m, 1H); 1.02 (m, 1H); 0.94 (d, 3H, *J* = 5.5 Hz); 0.83 (s, 3H); 0.62 (s, 3H). ^{13}C NMR ($CDCl_3$, 125 MHz) δ: 174.5; 156.3; 79.1; 73.1; 71.8; 68.4; 50.4; 46.3; 41.5; 41.3; 40.1; 39.5; 39.3; 39.0; 35.3; 35.2; 34.7; 34.6; 32.9; 31.7; 30.2; 28.3 (3C); 28.0; 27.5; 27.4; 26.6; 26.2; 23.2; 22.3; 17.4; 12.4. HR-ESI-MS (*m/z*): Calcd for $C_{33}H_{58}N_2O_6Na$ [M + Na], 601.4192; Found 601.4176.

(*R*)-*N*-(4-(2-(7-(dimethylamino)-2-oxo-2H-chromen-4-yl)acetamido)butyl)-4-((3*R*,5*S*,7*R*,8*R*,9*S*,10*S*,12*S*,13*R*,14*S*,17*R*)-3,7,12-trihydroxy-10,13-dimethyl-hexadecahydro-1H-cyclopenta-[α]-phenanthren-17-yl)pentanamide (**3**). Intermediate **11** (55 mg, 0.095 mmol) was dissolved in CH_2Cl_2 (1 mL). Trifluoroacetic acid (0.020 mL,

0.285 mmol) was added dropwise and the reaction was allowed to stir at room temperature for 1 h. The reaction was then diluted with CH_2Cl_2 (10 mL) and washed with deionized H_2O (10 mL). The organic layer was concentrated *in vacuo*, and crude amine was used without further purification. HATU (63 mg, 0.167 mmol) was added to a solution of the crude amine, 7-dimethylamino-4-coumarinacetic acid (21 mg, 0.084 mmol), and Et_3N (0.035 mL, 0.25 mmol) in anhydrous DMF (1.5 mL). The reaction was allowed to stir for 16 h, then diluted with deionized H_2O (25 mL) and extracted with EtOAc (25 mL). The organics were washed 3× with deionized H_2O (20 mL), dried over $MgSO_4$, and concentrated *in vacuo.* Remaining HATU was precipitated with MeOH and removed via filtration. The organics were subjected to reversed-phase HPLC, and **2**, eluting with 58% aqueous acetonitrile, was collected as a yellow powder (35 mg, 52% yield). ^{1}H NMR ($CDCl_3$, 500 MHz) d: 7.49 (d, 1H, *J* = 9.0 Hz); 7.00 (t, 1H, *J* = 5.2 Hz); 6.57 (dd, 1H, *J* = 9.0, 2.4 Hz); 6.45 (t, 1H, *J* = 5.2 Hz); 6.39 (d, 1H, *J* = 2.4 Hz); 6.05 (s, 1H); 3.92 (br m, 1H); 3.8 (br s, 1H); 3.61 (s, 2H); 3.46 (d, 1H, *J* = 5.5 Hz); 3.40 (br m, 1H); 3.25-3.10 (m, 4H); 3.00 (s, 6H); 2.65 (s, 1H); 2.18 (t, 2H, *J* = 11.7 Hz); 2.10-1.95 (m, 4H); 1.79 (m, 2H); 1.82-1.53 (m, 8H); 1.48 (br m, 9H); 1.36 (m, 2H); 1.21 (m, 1H); 1.07 (m, 1H); 0.96 (d, 3H, *J* = 5.8 Hz); 0.85 (s, 3H); 0.63 (s, 3H). ^{13}C NMR ($CDCl_3$, 125 MHz) d: 174.5; 168.5; 162.3; 155.9; 153.0; 150.7; 125.9; 109.9; 109.2; 108.6; 98.0; 73.0; 71.9; 68.4; 46.4; 46.2; 41.8; 41.5; 40.3; 40.1 (3C); 39.7; 39.6; 39.5; 38.9; 35.3; 34.7 (2C); 32.7; 31.7; 30.5; 28.2; 27.6; 27.0; 26.4; 26.3; 23.2; 22.5; 17.5; 12.5. HR-ESI-MS (*m/z*): Calcd for $C_{41}H_{62}N_3O_7$ [M + H], 708.4582; Found 708.4583.

(*R*)-*N*-(4-(2-(7-(dimethylamino)-2-oxo-2H-chromen-4-yl)acetamido)butyl)-4-((3*R*,5*S*,7*R*,8*R*,9*S*,10*S*,12*S*,13*R*,14*S*,17*R*)-3,7,12-trihydroxy-10,13-dimethylhexadecahydro-1H-cyclopenta-[a]phenanthren-17-yl)pentanamide (**4**). HATU (157 mg, 0.41 mmol) was added to a mixture of 3-keto-4-etiocholenic acid **9** (65 mg, 0.021 mmol), and EtN^iPr_2 (108 µL, 0.62 mmol) in anhydrous DMF (5 mL). The reaction was allowed to stir for 12 h at rt and then dried under vacuum. Compound **4** (84 mg) was obtained as a clear wax, 94% yield after flash chromatography (2:1 hexanes/EtOAc to 1:10 MeOH/EtOAc). ^{1}H-NMR ($CDCl_3$, 500 MHz) δ: 8.70 (d, 1H, *J* = 4.5 Hz); 8.40 (d, 1H J = 8.4 Hz); 7.48 (dd, 1H, *J* = 4.5, 8.4 Hz); 5.73 (s, 1H); 4.09 (dd, 1J, *J* = 7.1, 7.1 Hz); 2.89 (t, 1H, *J* = 9.3 Hz); 2.49-2.16 (m, 6H); 2.14-2.03 (m, 2H); 1.95-1.77 (m, 5H); 1.76-1.37 (m, 2H); 1.35-1.22 (m, 1H); 1.21 (s, 3H); 1.18-1.00 (m, 2H); 1.00 (s, 3H). ^{13}C-NMR ($CDCl_3$, 125 MHz) δ: 199.7; 170.8; 170.2; 151.8; 140.8; 135.2; 129.7; 124.3; 121; 60.6; 55.8; 53.8; 52.9; 45.6; 38.8; 38; 36.1; 36; 34.2; 32.9; 32.1; 24.8; 24.2; 21.3; 17.6; 14.4; 13.8. HR-ESI-MS (*m/z*): Calcd for $C_{25}H_{31}N_4O_3$ [M + H], 435.2318; Found 435.2389.

REFERENCES

1. Newman, D. J.; Cragg, G. M.; Snader, K. M., The influence of natural products upon drug discovery. *Nat. Prod. Rep.* **2000,** *17* (3), 215-234.

2. Konig, H. G. G. M., Terpenoids from marine organisms: unique structures and their pharmacological potential. *Phytochem. Rev.* **2006,** *5*, 115-141.

3. McClintock, J. B.; Baker, B. J., *Marine Chemical Ecology*. CRC Press: New York, 2001.

4. Coseri, S., Natural Products and their Analogues as Efficient Anticancer Drugs. *Mini-Rev. Med. Chem.* **2009,** *9* (5), 560-571.

5. (a) Haefner, B., Drugs from the deep: marine natural products as drug candidates. *Drug Discov. Today* **2003,** *8* (12), 536-544; (b) van Kesteren, C.; de Vooght, M. M. M.; Lopez-Lazaro, L.; Mathot, R. A. A.; Schellens, J. H. M.; Jimeno, J. M.; Beijnen, J. H., Yondelis (R) (trabectedin, ET-743): the development of an anticancer agent of marine origin. *Anti-Cancer Drugs* **2003,** *14* (7), 487-502; (c) Jimeno, J.; Lopez-Martin, J. A.; Ruiz-Casado, A.; Izquierdo, M. A.; Scheuer, P. J.; Rinehart, K., Progress in the clinical development of new marine-derived anticancer compounds. *Anti-Cancer Drugs* **2004,** *15* (4), 321-329.

6. Newman, D. J.; Cragg, G. M., Marine natural products and related compounds in clinical and advanced preclinical trials. *J. Nat. Prod.* **2004,** *67* (8), 1216-1238.

7. (a) Pettit, G. R.; Kamano, Y.; Herald, C. L.; Tuinman, A. A.; Boettner, F. E.; Kizu, H.; Schmidt, J. M.; Baczynskyj, L.; Tomer, K. B.; Bontems, R. J., The isolation and structure of a remarkable marine animal antineoplastic constituent: dolastatin 10. *J. Am. Chem. Soc.* **1987,** *109* (22), 6883-6885; (b) Bai, R.; Petit, G. R.; Hamel, E., Dolastatin 10, a powerful cytostatic peptide derived from a marine animal: Inhibition of tubulin

polymerization mediated through the vinca alkaloid binding domain. *Biochem. Pharmacol.* **1990,** *39* (12), 1941-1949.

8. (a) Gunasekera, S. P.; Gunasekera, M.; Longley, R. E.; Schulte, G. K., Discodermolide: a new bioactive polyhydroxylated lactone from the marine sponge Discodermia dissoluta. *J. Org. Chem.* **1990,** *55* (16), 4912-4915; (b) terHaar, E.; Kowalski, R. J.; Hamel, E.; Lin, C. M.; Longley, R. E.; Gunasekera, S. P.; Rosenkranz, H. S.; Day, B. W., Discodermolide, a cytotoxic marine agent that stabilizes microtubules more potently than taxol. *Biochemistry* **1996,** *35* (1), 243-250.

9. (a) Hamann, M. T.; Scheuer, P. J., Kahalalide F: a bioactive depsipeptide from the sacoglossan mollusk Elysia rufescens and the green alga Bryopsis sp. *J. Am. Chem. Soc.* **1993,** *115* (13), 5825-5826; (b) GarciaRocha, M.; Bonay, P.; Avila, J., The antitumoral compound Kahalalide F acts on cell lysosomes. *Cancer Lett.* **1996,** *99* (1), 43-50.

10. Pettit, G. R.; Herald, C. L.; Doubek, D. L.; Herald, D. L.; Arnold, E.; Clardy, J., Isolation and structure of bryostatin 1. *J. Am. Chem. Soc.* **1982,** *104* (24), 6846-6848.

11. Newman, D. J.; Cragg, G. M., Natural products as sources of new drugs over the last 25 years. *J. Nat. Prod.* **2007,** *70* (3), 461-477.

12. Fischbach, M. A.; Walsh, C. T., Antibiotics for emerging pathogens. *Science* **2009,** *325*, 1089-1093.

13. Rahman, H.; Austin, B.; Mitchell, W. J.; Morris, P. C.; Jamieson, D. J.; Adams, D. R.; Spragg, A. M.; Schweizer, M., Novel Anti-Infective Compounds from Marine Bacteria. *Marine Drugs* **2010,** *8* (3), 498-518.

14. (a) Lane, A. L.; Kubanek, J., Secondary metabolite defenses against pathogens and biofoulers. In *Algal Chemical Ecology*, Amsler, C. D., Ed. Springer-Verlag Berlin Heidelberg: 2008; pp 229-243; (b) Stout, E. P.; Hasemeyer, A. P.; Lane, A. L.; Davenport, T. M.; Engel, S.; Hay, M. E.; Fairchild, C. R.; Prudhomme, J.; Le Roch, K.;

Aalbersberg, W.; Kubanek, J., Antibacterial Neurymenolides from the Fijian Red Alga Neurymenia fraxinifolia. *Org. Lett.* **2009,** *11* (1), 225-228.

15. Yousaf, M.; Hammond, N. L.; Peng, J. N.; Wahyuono, S.; McIntosh, K. A.; Charman, W. N.; Mayer, A. M. S.; Hamann, M. T., New manzamine alkaloids from an indo-pacific sponge. Pharmacokinetics, oral availability, and the significant activity of several manzamines against HIV-I, AIDS opportunistic infections, and inflammatory diseases. *J. Med. Chem.* **2004,** *47* (14), 3512-3517.

16. Snow, R. W.; Guerra, C. A.; Noor, A. M.; Myint, H. Y.; Hay, S. I., The global distribution of clinical episodes of Plasmodium falciparum malaria. *Nature* **2005,** *434* (7030), 214-217.

17. Kaur, K.; Jain, M.; Kaur, T.; Jain, R., Antimalarials from nature. *Bioorg. Med. Chem.* **2009,** *17* (9), 3229-3256.

18. (a) Lane, A. L.; Stout, E. P.; Hay, M. E.; Prusak, A. C.; Hardcastle, K.; Fairchild, C. R.; Franzblau, S. G.; Le Roch, K.; Prudhomme, J.; Aalbersberg, W.; Kubanek, J., Callophycoic acids and callophycols from the Fijian red alga Callophycus serratus. *J. Org. Chem.* **2007,** *72* (19), 7343-7351; (b) Lane, A. L.; Stout, E. P.; Lin, A. S.; Prudhomme, J.; Le Roch, K.; Fairchild, C. R.; Franzblau, S. G.; Hay, M. E.; Aalbersberg, W.; Kubanek, J., Antimalarial Bromophycolides J-Q from the Fijian Red Alga Callophycus serratus. *J. Org. Chem.* **2009,** *74* (7), 2736-2742; (c) Stout, E. P.; Prudhomme, J.; Le Roch, K.; Fairchild, C. R.; Franzblau, S. G.; Aalbersberg, W.; Hay, M. E.; Kubanek, J., Unusual Antimalarial Meroditerpenes from Tropical Red Macroalgae. *Bioorg. Med. Chem. Lett.* **2010**.

19. (a) Hamel, E., Antimitotic natural products and their interactions with tubulin. *Med. Res. Rev.* **1996,** *16* (2), 207-231; (b) Kingston, D. G. I., Tubulin-Interactive Natural Products as Anticancer Agents. *J. Nat. Prod.* **2009,** *72* (3), 507-515.

20. Parsons, A. B.; Lopez, A.; Givoni, I. E.; Williams, D. E.; Gray, C. A.; Porter, J.; Chua, G.; Sopko, R.; Brost, R. L.; Ho, C. H.; Wang, J. Y.; Ketela, T.; Brenner, C.; Brill, J. A.; Fernandez, G. E.; Lorenz, T. C.; Payne, G. S.; Ishihara, S.; Ohya, Y.; Andrews, B.; Hughes, T. R.; Frey, B. J.; Graham, T. R.; Andersen, R. J.; Boone, C., Exploring the mode-of-action of bioactive compounds by chemical-genetic profiling in yeast. *Cell* **2006,** *126* (3), 611-625.

21. Bottcher, T.; Pitscheider, M.; Sieber, S. A., Natural Products and Their Biological Targets: Proteomic and Metabolomic Labeling Strategies. *Angewandte Chemie-International Edition* **2010,** *49* (15), 2680-2698.

22. Carlson, E. E., Natural Products as Chemical Probes. *ACS Chem. Biol.* **2010,** *5* (7), 639-653.

23. Alexander, M. D.; Burkart, M. D.; Leonard, M. S.; Portonovo, P.; Liang, B.; Ding, X. B.; Joullie, M. M.; Gulledge, B. M.; Aggen, J. B.; Chamberlin, A. R.; Sandler, J.; Fenical, W.; Cui, J.; Gharpure, S. J.; Polosukhin, A.; Zhang, H. R.; Evans, P. A.; Richardson, A. D.; Harper, M. K.; Ireland, C. M.; Vong, B. G.; Brady, T. P.; Theodorakis, E. A.; La Clair, J. J., A central strategy for converting natural products into fluorescent probes. *ChemBioChem* **2006,** *7* (3), 409-416.

24. Hughes, C. C.; Yang, Y. L.; Liu, W. T.; Dorrestein, P. C.; La Clair, J. J.; Fenical, W., Marinopyrrole A Target Elucidation by Acyl Dye Transfer. *J. Am. Chem. Soc.* **2009,** *131* (34), 12094-12096.

25. Taunton, J.; Collins, J. L.; Schreiber, S. L., Synthesis of natural and modified trapoxins, useful reagents for exploring histone deacetylase function. *J. Am. Chem. Soc.* **1996,** *118* (43), 10412-10422.

26. Taunton, J.; Hassig, C. A.; Schreiber, S. L., A mammalian histone deacetylase related to the yeast transcriptional regulator Rpd3p. *Science* **1996,** *272* (5260), 408-411.

27. Stout, E. P.; La Clair, J. J.; Snell, T. W.; Shearer, T. L.; Kubanek, J., Conservation of progesterone hormone function in invertebrate reproduction. *Proc. Natl. Acad. Sci. U. S. A.* **2010,** *107* (26), 11859-11864.

28. Kobayashi, J.; Ishibashi, M., Marine Natural Products and Marine Chemical Ecology. In *Comprehensive Natural Products Chemistry*, 1st ed.; Barton, D.; Nakanishi, K.; Meth-Cohn, O.; Mori, K., Eds. Elsevier: Amsterdam, 1999; Vol. 8, pp 415-637.

29. Blunt, J. W.; Copp, B. R.; Munro, M. H. G.; Northcote, P. T.; Prinsep, M. R., Marine natural products. *Nat. Prod. Rep.* **2010,** *27* (2), 165-237.

30. Mayer, A. M. S.; Gustafson, K. R., Marine pharmacology in 2005-2006: Antitumour and cytotoxic compounds. *Eur. J. Cancer* **2008,** *44* (16), 2357-2387.

31. Bourguet-Kondracki, M.; Kornprobst, J. M., Marine pharmacology: Potentialities in the treatment of infectious diseases, osteoporosis and Alzheimer's disease. In *Marine Biotechnology II*, 2005; Vol. 97, pp 105-131.

32. Bhadury, P.; Wright, P. C., Exploitation of marine algae: biogenic compounds for potential antifouling applications. *Planta* **2004,** *219* (4), 561-578.

33. Torssell, K. B. G., *Natural Product Chemistry: A Mechanistic, Biosynthetic, and Ecological Approach*. 2nd ed.; Swedish Pharmaceutical Society: Stockholm, 1997.

34. (a) Hay, M. E.; Fenical, W., Marine plant-herbivore interactions - the ecology of chemical defense. *Annu. Rev. Ecol. Syst.* **1988,** *19*, 111-145; (b) Paul, V. J., *Ecological Roles of Marine Natural Products*. Comstock Publishing Associates: Ithaca, NY, 1992.

35. Dewick, P. M., *Medicinal Natural Products: A Biosynthetic Approach*. 2nd ed.; John Wiley & Sons, Ltd.: West Sussex, England, 2001.

36. Chinou, I., Labdanes of natural origin-biological activities (1981-2004). *Curr. Med. Chem.* **2005,** *12* (11), 1295-1317.

37. Iliopoulou, D.; Mihopoulos, N.; Roussis, V.; Vagias, C., New brominated labdane diterpenes from the red alga Laurencia obtusa. *J. Nat. Prod.* **2003,** *66* (9), 1225-1228.

38. Briand, A.; Kornprobst, J. M.; AlEasa, H. S.; Rizk, A. F. M.; Toupet, L., (-)-paniculatol, a new ent-labdane bromoditerpene from Laurencia paniculata. *Tetrahedron Lett.* **1997,** *38* (19), 3399-3400.

39. Suzuki, M.; Nakano, S.; Takahashi, Y.; Abe, T.; Masuda, T. A. M.; Takahashi, H.; Kobayashi, K., Brominated labdane-type diterpenoids from an Okinawan Laurencia sp. *J. Nat. Prod.* **2002,** *65* (6), 801-804.

40. Estrada, D. M.; Ravelo, J. L.; Ruizperez, C.; Martin, J. D.; Solans, X., Dactylomelol, a new class of diterpene from the sea hare Aplysia dactylomela. *Tetrahedron Lett.* **1989,** *30* (45), 6219-6220.

41. Findlay, J. A.; Li, G. Q., Novel terpenoids from the Sea Hare Aplysia punctata. *Can. J. Chem.* **2002,** *80* (12), 1697-1707.

42. Etahiri, S.; Bultel-Ponce, V.; Caux, C.; Guyot, M., New bromoditerpenes from the red alga Sphaerococcus coronopifolius. *J. Nat. Prod.* **2001,** *64* (8), 1024-1027.

43. Fernandez, J. J.; Souto, M. L.; Gil, L. V.; Norte, M., Isolation of naturally occurring dactylomelane metabolites as Laurencia constituents. *Tetrahedron* **2005,** *61* (37), 8910-8915.

44. (a) Kubanek, J.; Prusak, A. C.; Snell, T. W.; Giese, R. A.; Hardcastle, K. I.; Fairchild, C. R.; Aalbersberg, W.; Raventos-Suarez, C.; Hay, M. E., Antineoplastic diterpene-benzoate macrolides from the Fijian red alga Callophycus serratus. *Org. Lett.* **2005,** *7* (23), 5261-5264; (b) Kubanek, J.; Prusak, A. C.; Snell, T. W.; Giese, R. A.; Fairchild, C. R.; Aalbersberg, W.; Hay, M. E., Bromophycolides C-I from the Fijian red alga Callophycus serratus. *J. Nat. Prod.* **2006,** *69* (5), 731-735; (c) Lin, A. S.; Stout, E. P.; Prudhomme, J.; Le Roch, K.; Fairchild, C. R.; Franzblau, S. G.; Aalbersberg, W.; Hay, M. E.; Kubanek, J., Bioactive Bromophycolides R-U from the Fijian Red Alga Callophycus serratus. *J. Nat. Prod.* **2010,** *73* (2), 275-278.

45. Lane, A. L.; Nyadong, L.; Galhena, A. S.; Shearer, T. L.; Stout, E. P.; Parry, R. M.; Kwasnik, M.; Wang, M. D.; Hay, M. E.; Fernandez, F. M.; Kubanek, J., Desorption electrospray ionization mass spectrometry reveals surface-mediated antifungal chemical defense of a tropical seaweed. *Proc. Natl. Acad. Sci. U. S. A.* **2009,** *106* (18), 7314-7319.

46. Navarro, G.; Fernandez, J. J.; Norte, M., Novel meroditerpenes from the brown alga Cystoseira sp. *J. Nat. Prod.* **2004,** *67* (3), 495-499.

47. Hay, M. E., Marine chemical ecology: What's known and what's next? *J. Exp. Mar. Biol. Ecol.* **1996,** *200* (1-2), 103-134.

48. (a) Lubchenco, J.; Gaines, S. D., A unified approach to marine plant-herbivore interactions .1. populations and communities. *Annu. Rev. Ecol. Syst.* **1981,** *12*, 405-437; (b) Duffy, J. E.; Hay, M. E., Seaweed adaptations to herbivory - chemical, structural, and morphological defenses are often adjusted to spatial or temporal patterns of attack. *Bioscience* **1990,** *40* (5), 368-375.

49. Bolser, R. C.; Hay, M. E., Are tropical plants better defended? Palatability and defenses of temperate vs tropical seaweeds. *Ecology* **1996,** *77* (8), 2269-2286.

50. (a) Littler, M. M.; Littler, D. S.; Taylor, P. R., Animal plant defense associations - effects on the distribution and abundance of tropical reef macrophytes. *J. Exp. Mar. Biol. Ecol.* **1987,** *105* (2-3), 107-121; (b) Hay, M. E.; Fenical, W.; Gustafson, K., Chemical defense against diverse coral-reef herbivores. *Ecology* **1987,** *68* (6), 1581-1591.

51. Hardt, I. H.; Fenical, W.; Cronin, G.; Hay, M. E., Acutilols, potent herbivore feeding deterrents from the tropical brown alga, Dictyota acutiloba. *Phytochemistry* **1996,** *43* (1), 71-73.

52. Cronin, G.; Paul, V. J.; Hay, M. E.; Fenical, W., Are tropical herbivores more resistant than temperate herbivores to seaweed chemical defenses? Diterpenoid

metabolites from Dictyota acutiloba as feeding deterrents for tropical versus temperate fishes and urchins. *J. Chem. Ecol.* **1997,** *23* (2), 289-302.

53. Cruz-Rivera, E.; Hay, M. E., Prey nutritional quality interacts with chemical defenses to affect consumer feeding and fitness. *Ecol. Monogr.* **2003,** *73* (3), 483-506.

54. Hillis-Colinvaux, L., *Ecology and taxonomy of Halimeda: primary producer of coral reefs*. Academic Press: London, 1980; Vol. 17.

55. Paul, V. J.; Fenical, W., Novel bioactive diterpenoid metabolites from tropical marine algae of the genus Halimeda (Chlorophyta). *Tetrahedron* **1984,** *40* (16), 3053-3062.

56. Paul, V. J.; Vanalstyne, K. L., Chemical defense and chemical variation in some tropical pacific species of Halimeda (Halimedaceae, Chlorophyta). *Coral Reefs* **1988,** *6* (3-4), 263-269.

57. Paul, V. J.; Vanalstyne, K. L., Activation of chemical defenses in the tropical green algae Halimeda spp. *J. Exp. Mar. Biol. Ecol.* **1992,** *160* (2), 191-203.

58. Cetrulo, G. L.; Hay, M. E., Activated chemical defenses in tropical versus temperate seaweeds. *Marine Ecology-Progress Series* **2000,** *207*, 243-253.

59. Jung, V.; Pohnert, G., Rapid wound-activated transformation of the green algal defensive metabolite caulerpenyne. *Tetrahedron* **2001,** *57* (33), 7169-7172.

60. Jonassohn, M.; Davidsson, R.; Kahnberg, P.; Sterner, O., The reactivity of drimane unsaturated dialdehydes towards nucleophiles. *Tetrahedron* **1997,** *53* (1), 237-244.

61. (a) Jahn, A.; Griebe, T.; Nielsen, P. H., Composition of Pseudomonas putida biofilms: Accumulation of protein in the biofilm matrix. *Biofouling* **1999,** *14* (1), 49-57; (b) Bhosale, S. H.; Nagle, V. L.; Jagtap, T. G., Antifouling potential of some marine organisms from India against species of Bacillus and Pseudomonas. *Mar. Biotechnol.* **2002,** *4* (2), 111-118.

62. Konig, G. M.; Wright, A. D., Laurencia rigida: Chemical investigations of its antifouling dichloromethane extract. *J. Nat. Prod.* **1997,** *60* (10), 967-970.

63. de Nys, R.; Leya, T.; Maximillien , R.; Afsar, A.; Nair, P. S. R.; Steinberg, P., The need for standardised broad scale bioassay testing: A case study using the red alga Laurencia rigida *Biofouling* **1996,** *10* (1-3), 213-224.

64. Smyrniotopoulos, V.; Abatis, D.; Tziveleka, L. A.; Tsitsimpikou, C.; Roussis, V.; Loukis, A.; Vagias, C., Acetylene sesquiterpenoid esters from the green alga Caulerpa prolifera. *J. Nat. Prod.* **2003,** *66* (1), 21-24.

65. Engel, S.; Jensen, P. R.; Fenical, W., Chemical ecology of marine microbial defense. *J. Chem. Ecol.* **2002,** *28* (10), 1971-1985.

66. Puglisi, M. P.; Tan, L. T.; Jensen, P. R.; Fenical, W., Capisterones A and B from the tropical green alga Penicillus capitatus: unexpected anti-fungal defenses targeting the marine pathogen Lindra thallasiae. *Tetrahedron* **2004,** *60* (33), 7035-7039.

67. Fuller, R. W.; Cardellina, J. H.; Kato, Y.; Brinen, L. S.; Clardy, J.; Snader, K. M.; Boyd, M. R., A pentahalogenated monoterpene from the red alga Portieria hornemannii produces a novel cytotoxicity profile against a diverse panel of human tumor-cell lines. *J. Med. Chem.* **1992,** *35* (16), 3007-3011.

68. (a) Schlama, T.; Baati, R.; Gouverneur, V.; Valleix, A.; Falck, J. R.; Mioskowski, C., Total synthesis of (+/-)-halomon by a Johnson-Claisen rearrangement. *Angewandte Chemie-International Edition* **1998,** *37* (15), 2085-2087; (b) Sotokawa, T.; Noda, T.; Pi, S.; Hirama, M., A three-step synthesis of halomon. *Angewandte Chemie-International Edition* **2000,** *39* (19), 3430-+.

69. Jha, R. K.; Zi-rong, X., Biomedical compounds from marine organisms. *Marine Drugs* **2004,** *2*, 123-146.

70. Blunt, J. W.; Hartshorn, M. P.; McLennan, T. J.; Munro, M. H. G.; Robinson, W. T.; Yorke, S. C., Thyrsiferol: a squalene-derived metabolite of. *Tetrahedron Lett.* **1978,** *19* (1), 69-72.

71. Gonzalez, A. G.; Arteaga, J. M.; Fernandez, J. J.; Martin, J. D.; Norte, M.; Ruano, J. Z., Terpenoids of the red alga laurencia pinnatifida. *Tetrahedron* **1984,** *40* (14), 2751-2755.

72. Suzuki, T.; Suzuki, M.; Furusaki, A.; Matsumoto, T.; Kato, A.; Imanaka, Y.; Kurosawa, E., Teurilene and thyrsiferyl 23-acetate, meso and remarkably cytotoxic compounds from the marine red alga laurencia obtusa (hudson) lamouroux. *Tetrahedron Lett.* **1985,** *26* (10), 1329-1332.

73. Matsuzawa, S.-i.; Suzuki, T.; Suzuki, M.; Matsuda, A.; Kawamura, T.; Mizuno, Y.; Kikuchi, K., Thyrsiferyl 23-acetate is a novel specific inhibitor of protein phosphatase PP2A. *FEBS Lett.* **1994,** *356* (2-3), 272-274.

74. (a) Fernández, J.; Souto, M. L.; Norte, M., Evaluation of the cytotoxic activity of polyethers isolated from Laurencia. *Bioorg. Med. Chem.* **1998,** *6* (12), 2237-2243; (b) Souto, M. L.; Manríquez, C. P.; Norte, M.; Leira, F.; Fernández, J. J., The inhibitory effects of squalene-derived triterpenes on protein phosphatase PP2A. *Bioorg. Med. Chem. Lett.* **2003,** *13* (7), 1261-1264.

75. Albizati, K. F.; Martin, V. A.; Agharahimi, M. R.; Stolze, D. A., Synthesis of Marine Natural Products 1: Terpenoids. In *Bioorganic Marine Chemistry*, Scheuer, P. J., Ed. Springer-Verlag: Berlin, 1992; Vol. 5, p 254.

76. Rodríguez, A. D.; González, E.; Ramírez, C., The structural chemistry, reactivity, and total synthesis of dolabellane diterpenes. *Tetrahedron* **1998,** *54* (39), 11683-11729.

77. Durán, R.; Zubía, E.; Ortega, M. J.; Salvá, J., New diterpenoids from the alga Dictyota dichotoma. *Tetrahedron* **1997,** *53* (25), 8675-8688.

78. Tringali, C.; Piattelli, M.; Nicolosi, G., Structure and conformation of new diterpenes based on the dolabellane skeleton from a Dictyota species. *Tetrahedron* **1984,** *40* (4), 799-803.

79. Piattelli, M.; Tringali, C.; Neri, P.; Rocco, C., Stereochemistry and Conformation of Dolabellane Diterpenes: An Nmr and Molecular Mechanics Study. *J. Nat. Prod.* **1995,** *58* (5), 697-704.

80. Suzuki, M.; Takahashi, Y.; Matsuo, Y.; Guiry, M. D.; Masuda, M., Scanlonenyne, a novel halogenated C15 acetogenin from the red alga Laurencia obtusa in Irish waters. *Tetrahedron* **1997,** *53* (12), 4271-4278.

81. (a) Suzuki, M.; Sasage, Y.; Ikura, M.; Hikichi, K.; Kurosawa, E., Structure revision of okamurallene and structure elucidation of further C15 non-terpenoid bromoallenes from Laurencia intricata. *Phytochemistry* **1989,** *28* (8), 2145-2148; (b) Suzuki, M.; Kawamoto, T.; Vairappan, C. S.; Ishii, T.; Abe, T.; Masuda, M., Halogenated metabolites from Japanese Laurencia spp. *Phytochemistry* **2005,** *66* (23), 2787-2793.

82. Ji, N.-Y.; Li, X.-M.; Li, K.; Wang, B.-G., Laurendecumallenes A–B and Laurendecumenynes A–B, Halogenated Nonterpenoid C15-Acetogenins from the Marine Red Alga Laurencia decumbens. *J. Nat. Prod.* **2007,** *70* (9), 1499-1502.

83. Kubanek, J.; Jensen, P. R.; Keifer, P. A.; Sullards, M. C.; Collins, D. O.; Fenical, W., Seaweed resistance to microbial attack: A targeted chemical defense against marine fungi. *Proc. Natl. Acad. Sci. U. S. A.* **2003,** *100* (12), 6916-6921.

84. Carmeli, S.; Moore, R. E.; Patterson, G. M. L., Tolytoxin and New Scytophycins from Three Species of Scytonema. *J. Nat. Prod.* **1990,** *53* (6), 1533-1542.

85. Nagai, H.; Yasumoto, T.; Hokama, Y., Manauealides,1 Some of the Causative Agents of a Red Alga Gracilaria coronopifolia Poisoning in Hawaii. *J. Nat. Prod.* **1997,** *60* (9), 925-928.

86. Moore, R. E.; Blackman, A. J.; Cheuk, C. E.; Mynderse, J. S.; Matsumoto, G. K.; Clardy, J.; Woodard, R. W.; Craig, J. C., Absolute stereochemistries of the aplysiatoxins and oscillatoxin A. *J. Org. Chem.* **1984,** *49* (13), 2484-2489.

87. (a) Kato, Y.; Scheuer, P. J., Aplysiatoxin and debromoaplysiatoxin, constituents of the marine mollusk Stylocheilus longicauda. *J. Am. Chem. Soc.* **1974,** *96* (7), 2245-2246; (b) Mynderse, J. S.; Moore, R. E.; Kashiwagi, M.; Norton, T. R., Anti-leukemia activity in Oscillatoriaceae - isolation of debromoaplysiatoxin from Lyngbya. *Science* **1977,** *196* (4289), 538-540.

88. McPhail, K. L.; France, D.; Cornell-Kennon, S.; Gerwick, W. H., Peyssonenynes A and B, Novel Enediyne Oxylipins with DNA Methyl Transferase Inhibitory Activity from the Red Marine Alga Peyssonnelia caulifera. *J. Nat. Prod.* **2004,** *67* (6), 1010-1013.

89. Paul, V. J.; Fenical, W., Toxic acetylene-containing lipids from the red marine alga lamouroux. *Tetrahedron Lett.* **1980,** *21* (35), 3327-3330.

90. (a) Kazlauskas, R.; Murphy, P. T.; Quinn, R. J.; Wells, R. J., A new class of halogenated lactones from the red alga (bonnemaisoniaceae). *Tetrahedron Lett.* **1977,** *18* (1), 37-40; (b) de Nys, R.; Wright, A. D.; König, G. M.; Sticher, O., New halogenated furanones from the marine alga delisea pulchra (cf. fimbriata). *Tetrahedron* **1993,** *49* (48), 11213-11220.

91. (a) Maximilien, R.; de Nys, R.; Holmstrom, C.; Gram, L.; Givskov, M.; Crass, K.; Kjelleberg, S.; Steinberg, P. D., Chemical mediation of bacterial surface colonisation by secondary metabolites from the red alga Delisea pulchra. *Aquat. Microb. Ecol.* **1998,** *15* (3), 233-246; (b) Steinberg, P. D.; de Nys, R., Chemical mediation of colonization of seaweed surfaces. *J. Phycol.* **2002,** *38* (4), 621-629.

92. Dworjanyn, S. A.; de Nys, R.; Steinberg, P. D., Chemically mediated antifouling in the red alga Delisea pulchra. *Marine Ecology-Progress Series* **2006,** *318*, 153-163.

93. Wright, J. T.; de Nys, R.; Poore, A. G. B.; Steinberg, P. D., Chemical defense in a marine alga: Heritability and the potential for selection by herbivores. *Ecology* **2004,** *85* (11), 2946-2959.

94. Kurata, K.; Taniguchii, K.; Takashima, K.; Hayashi, I.; Suzuki, M., Feeding-deterrent bromophenols from Odonthalia corymbifera. *Phytochemistry* **1997,** *45* (3), 485-487.

95. Xu, N.; Fan, X.; Yan, X.; Li, X.; Niu, R.; Tseng, C. K., Antibacterial bromophenols from the marine red alga Rhodomela confervoides. *Phytochemistry* **2003,** *62* (8), 1221-1224.

96. Li, K.; Li, X.-M.; Ji, N.-Y.; Wang, B.-G., Bromophenols from the Marine Red Alga Polysiphonia urceolata with DPPH Radical Scavenging Activity. *J. Nat. Prod.* **2007,** *71* (1), 28-30.

97. Hamann, M. T.; Otto, C. S.; Scheuer, P. J.; Dunbar, D. C., Kahalalides: Bioactive peptide from a marine mollusk Elysia rufescens and its algal diet Bryopsis sp. *J. Org. Chem.* **1996,** *61* (19), 6594-6600.

98. Goetz, G.; Yoshida, W. Y.; Scheuer, P. J., The absolute stereochemistry of Kahalalide F. *Tetrahedron* **1999,** *55* (25), 7739-7746.

99. Hill, R. T.; Hamann, M. T.; Enticknap, J.; Rao, K. V. Kahalalide-Producing Bacteria and Methods of Identifying Kahalalide-Producing Bacteria and Preparing Kahalalides. 2005.

100. (a) Goetz, G.; Nakao, Y.; Scheuer, P. J., Two Acyclic Kahalalides from the Sacoglossan Mollusk Elysia rufescens1. *J. Nat. Prod.* **1997,** *60* (6), 562-567; (b) Kan, Y.; Fujita, T.; Sakamoto, B.; Hokama, Y.; Nagai, H., Kahalalide K: A New Cyclic Depsipeptide from the Hawaiian Green Alga Bryopsis Species. *J. Nat. Prod.* **1999,** *62* (8), 1169-1172; (c) Bonnard, I.; Manzanares, I.; Rinehart, K. L., Stereochemistry of Kahalalide F. *J. Nat. Prod.* **2003,** *66* (11), 1466-1470; (d) Horgen, F. D.; delos Santos, D.

B.; Goetz, G.; Sakamoto, B.; Kan, Y.; Nagai, H.; Scheuer, P. J., A New Depsipeptide from the Sacoglossan Mollusk Elysia ornata and the Green Alga Bryopsis Species1. *J. Nat. Prod.* **1999,** *63* (1), 152-154; (e) Dmitrenok, A.; Iwashita, T.; Nakajima, T.; Sakamoto, B.; Namikoshi, M.; Nagai, H., New cyclic depsipeptides from the green alga Bryopsis species; application of a carboxypeptidase hydrolysis reaction to the structure determination. *Tetrahedron* **2006,** *62* (6), 1301-1308.

101. Hay, M. E.; Paul, V. J.; Lewis, S. M.; Gustafson, K.; Tucker, J.; Trindell, R. N., Can tropical seaweeds reduce herbivory by growing at night - diel patterns of growth, nitrogen-content, herbivory, and chemical versus morphological defenses. *Oecologia* **1988,** *75* (2), 233-245.

102. Öztunç, A.; Imre, S.; Lotter, H.; Wagner, H., Ent-13-epiconcinndiol from the red alga Chondria tenuissima and its absolute configuration. *Phytochemistry* **1989,** *28* (12), 3403-3404.

103. Palermo, J. A.; Flower, P. B.; Seldes, A. M., Chondriamides A and B, new indolic metabolites from the red alga Chondria sp. *Tetrahedron Lett.* **1992,** *33* (22), 3097-3100.

104. Gupta, L.; Talwar, A.; Chauhan, P. M. S., Bis and tris indole alkaloids from marine organisms: New leads for drug discovery. *Curr. Med. Chem.* **2007,** *14* (16), 1789-1803.

105. Davyt, D.; Entz, W.; Fernandez, R.; Mariezcurrena, R.; Mombrú, A. W.; Saldaña, J.; Domínguez, L.; Coll, J.; Manta, E., A New Indole Derivative from the Red Alga Chondria atropurpurea. Isolation, Structure Determination, and Anthelmintic Activity1. *J. Nat. Prod.* **1998,** *61* (12), 1560-1563.

106. Kuramochi, K.; Osada, Y.; Kitahara, T., Synthetic study on indolic enamides. *Tetrahedron* **2003,** *59* (47), 9447-9454.

107. N'Diaye, I.; Guella, G.; Chiasera, G.; Mancini, I.; Pietra, F., Almazole A and almazole B, unusual marine alkaloids of an unidentified red seaweed of the family delesseriaceae from the coasts of Senegal. *Tetrahedron Lett.* **1994,** *35* (27), 4827-4830.

108. Guella, G.; N'Diaye, I.; Fofana, M.; Mancini, I., Isolation, synthesis and photochemical properties of almazolone, a new indole alkaloid from a red alga of Senegal. *Tetrahedron* **2006,** *62* (6), 1165-1170.

109. Gross, H.; Goeger, D. E.; Hills, P.; Mooberry, S. L.; Ballantine, D. L.; Murray, T. F.; Valeriote, F. A.; Gerwick, W. H., Lophocladines, Bioactive Alkaloids from the Red Alga Lophocladia sp. *J. Nat. Prod.* **2006,** *69* (4), 640-644.

110. Janot, M. M.; Guilhem, J.; Contz, O.; Wenera, G.; Cionga, E., *Ann. Pharm. Fr.* **1979,** *37*, 413-420.

111. Sun, Y.; Xu, Y.; Liu, K.; Hua, H.; Zhu, H.; Pei, Y., Gracilarioside and Gracilamides from the Red Alga Gracilaria asiatica. *J. Nat. Prod.* **2006,** *69* (10), 1488-1491.

112. (a) Yotsu-Yamashita, M.; Haddock, R. L.; Yasumoto, T., Polycavernoside A: a novel glycosidic macrolide from the red alga Polycavernosa tsudai (Gracilaria edulis). *J. Am. Chem. Soc.* **1993,** *115* (3), 1147-1148; (b) Yotsu-Yamashita, M.; Seki, T.; Paul, V. J.; Naoki, H.; Yasumoto, T., Four new analogs of polycavernoside A. *Tetrahedron Lett.* **1995,** *36* (31), 5563-5566; (c) Yotsu-Yamashita, M.; Abe, K.; Seki, T.; Fujiwara, K.; Yasumoto, T., Polycavernoside C and C2, the new analogs of the human lethal toxin polycavernoside A, from the red alga, Gracilaria edulis. *Tetrahedron Lett.* **2007,** *48* (13), 2255-2259.

113. Higa, T.; Kuniyoshi, M., Toxins associated with medicinal and edible seaweeds. *Journal of Toxicology-Toxin Reviews* **2000,** *19* (2), 119-137.

114. Fujiwara, K.; Murai, A.; Yotsu-Yamashita, M.; Yasumoto, T., Total Synthesis and Absolute Configuration of Polycavernoside A. *J. Am. Chem. Soc.* **1998,** *120* (41), 10770-10771.

115. Williams, D. E.; Sturgeon, C. M.; Roberge, M.; Andersen, R. J., Nigricanosides A and B, Antimitotic Glycolipids Isolated from the Green Alga Avrainvillea nigricans Collected in Dominica. *J. Am. Chem. Soc.* **2007,** *129* (18), 5822-5823.

116. Ohtani, I.; Kusumi, T.; Kashman, Y.; Kakisawa, H., High-field FT NMR application of Mosher's method. The absolute configurations of marine terpenoids. *J. Am. Chem. Soc.* **1991,** *113* (11), 4092-4096.

117. (a) Frelek, J.; Klimek, A.; Ruskowska, P., Dinuclear transition metal complexes as auxiliary chromophores in chiroptical studies on bioactive compounds. *Curr. Org. Chem.* **2003,** *7* (11), 1081-1104; (b) Gorecki, M.; Jablonska, E.; Kruszewska, A.; Suszczynska, A.; Urbanczyk-Lipkowska, Z.; Gerards, M.; Morzycki, J. W.; Szczepek, W. J.; Frelek, J., Practical method for the absolute configuration assignment of tert/tert 1,2-diols using their complexes with Mo-2(OAc)(4). *J. Org. Chem.* **2007,** *72* (8), 2906-2916.

118. Tai-Sun, S.; Godber, J. S., Isolation of four tocopherols and four tocotrienols from a variety of natural sources by semi-preparative high-performance liquid chromatography. *J. Chromatogr. A* **1994,** *678* (1), 49-58.

119. Amico, V.; Oriente, G.; Piattelli, M.; Ruberto, G.; Tringali, C., A quinone-hydroquinone couple from the Brown alga Cystoseira stricta. *Phytochemistry* **1982,** *21* (2), 421-424.

120. Reddy, P.; Urban, S., Meroditerpenoids from the southern Australian marine brown alga Sargassum fallax. *Phytochemistry* **2009,** *70* (2), 250-255.

121. Munne-Bosch, S.; Alegre, L., The function of tocopherols and tocotrienols in plants. *Crit. Rev. Plant Sci.* **2002,** *21* (1), 31-57.

122. Niki, E., Tocopherylquinone and tocopherylhydroquinone. *Redox Rep.* **2007,** *12* (5), 204-210.

123. Littler, D. S. L. a. M. M., *South Pacific Reef Plants*. Offshore Graphics, Inc.: Washington, D.C., 2003.

124. Saladino, R.; Neri, V.; Farina, A.; Crestini, C.; Nencioni, L.; Palamara, A. T., A novel and efficient synthesis of tocopheryl quinones by homogeneous and heterogeneous methyltrioxorhenium/hydrogen peroxide catalytic systems. *Adv. Synth. Catal.* **2008,** *350* (2), 321-331.

125. Smilkstein, M.; Sriwilaijaroen, N.; Kelly, J. X.; Wilairat, P.; Riscoe, M., Simple and inexpensive fluorescence-based technique for high-throughput antimalarial drug screening. *Antimicrob. Agents Chemother.* **2004,** *48* (5), 1803-1806.

126. Bennett, T. N.; Paguio, M.; Gligorijevic, B.; Seudieu, C.; Kosar, A. D.; Davidson, E.; Roepe, P. D., Novel, rapid, and inexpensive cell-based quantification of antimalarial drug efficacy. *Antimicrob. Agents Chemother.* **2004,** *48* (5), 1807-1810.

127. Trager, W.; Jensen, J. B., HUMAN MALARIA PARASITES IN CONTINUOUS CULTURE. *Science* **1976,** *193* (4254), 673-675.

128. Lee, F. Y. F.; Borzilleri, R.; Fairchild, C. R.; Kim, S. H.; Long, B. H.; Reventos-Suarez, C.; Vite, G. D.; Rose, W. C.; Kramer, R. A., BMS-247550: A novel epothilone analog with a mode of action similar to paclitaxel but possessing superior antitumor efficacy. *Clin. Cancer Res.* **2001,** *7* (5), 1429-1437.

129. Collins, L. A.; Franzblau, S. G., Microplate Alamar blue assay versus BACTEC 460 system for high-throughput screening of compounds against Mycobacterium tuberculosis and Mycobacterium avium. *Antimicrob. Agents Chemother.* **1997,** *41* (5), 1004-1009.

130. Hyde, J. E., Drug-resistant malaria. *Trends Parasitol.* **2005,** *21* (11), 494-498.

131. (a) Klayman, D. L.; Lin, A. J.; Acton, N.; Scovill, J. P.; Hoch, J. M.; Milhous, W. K.; Theoharides, A. D., Isolation of artemisinin (qinghaosu) from Artemisia annua grouping in the United States. *J. Nat. Prod.* **1984,** *47* (4), 715-717; (b) Klayman, D. L., Qinghaosu (artemisinin) - an antimalarial drug from China. *Science* **1985,** *228* (4703), 1049-1055.

132. (a) Noedl, H.; Se, Y.; Schaecher, K.; Smith, B. L.; Socheat, D.; Fukuda, M. M.; Consortium, A. R. C. S., Evidence of Artemisinin-Resistant Malaria in Western Cambodia. *N. Engl. J. Med.* **2008,** *359* (24), 2619-2620; (b) Dondorp, A. M.; Nosten, F.; Yi, P.; Das, D.; Phyo, A. P.; Tarning, J.; Lwin, K. M.; Ariey, F.; Hanpithakpong, W.; Lee, S. J.; Ringwald, P.; Silamut, K.; Imwong, M.; Chotivanich, K.; Lim, P.; Herdman, T.; An, S. S.; Yeung, S.; Singhasivanon, P.; Day, N. P. J.; Lindegardh, N.; Socheat, D.; White, N. J., Artemisinin Resistance in Plasmodium falciparum Malaria. *N. Engl. J. Med.* **2009,** *361* (5), 455-467.

133. Goldberg, D. E.; Slater, A. F. G.; Cerami, A.; Henderson, G. B., Hemoglobin degradation in the malaria parasite Plasmodium falciparum - an ordered process in a unique organelle. *Proc. Natl. Acad. Sci. U. S. A.* **1990,** *87* (8), 2931-2935.

134. Rosenthal, P. J.; Meshnick, S. R., Hemoglobin catabolism and iron utilization by malaria parasites. *Mol. Biochem. Parasitol.* **1996,** *83* (2), 131-139.

135. Chou, A. C.; Chevli, R.; Fitch, C. D., Ferriprotoporphyrin-IX fulfulls the criteria for identification as the chloroquine receptor of malaria parasites. *Biochemistry* **1980,** *19* (8), 1543-1549.

136. Fidock, D. A.; Nomura, T.; Talley, A. K.; Cooper, R. A.; Dzekunov, S. M.; Ferdig, M. T.; Ursos, L. M. B.; Sidhu, A. B. S.; Naude, B.; Deitsch, K. W.; Su, X. Z.; Wootton, J. C.; Roepe, P. D.; Wellems, T. E., Mutations in the P-falciparum digestive vacuole transmembrane protein PfCRT and evidence for their role in chloroquine resistance. *Mol. Cell* **2000,** *6* (4), 861-871.

137. (a) Robert, A.; Meunier, B., Is alkylation the main mechanism of action of the antimalarial drug artemisinin? *Chem. Soc. Rev.* **1998,** *27* (4), 273-279; (b) Hong, Y. L.; Yang, Y. Z.; Meshnick, S. R., The interaction of artemisinin with malarial hemozoin *Mol. Biochem. Parasitol.* **1994,** *63* (1), 121-128.

138. Eckstein-Ludwig, U.; Webb, R. J.; van Goethem, I. D. A.; East, J. M.; Lee, A. G.; Kimura, M.; O'Neill, P. M.; Bray, P. G.; Ward, S. A.; Krishna, S., Artemisinins target the SERCA of Plasmodium falciparum. *Nature* **2003,** *424* (6951), 957-961.

139. Li, W.; Mo, W. K.; Shen, D.; Sun, L. B.; Wang, J.; Lu, S.; Gitschier, J. M.; Zhou, B., Yeast model uncovers dual roles of mitochondria in the action of arternisinin. *PLoS Genet.* **2005,** *1* (3), 329-334.

140. Cervantes, S.; Stout, E. P.; Prudhomme, J.; Engel, S.; Bruton, M.; Cervantes, M.; Carter, D.; Tae-Chang, Y.; Hay, M. E.; Aalbersberg, W.; Kubanek, J.; Le Roch, K., High content live cell imaging evaluation for the discovery of new antimalarial natural products. *Submitted to Antimicrobial Agents and Chemotherapy* **2010**.

141. Pisciotta, J. M.; Coppens, I.; Tripathi, A. K.; Scholl, P. F.; Shuman, J.; Bajad, S.; Shulaev, V.; Sullivan, D. J., The role of neutral lipid nanospheres in Plasmodium falciparum haem crystallization. *Biochem. J.* **2007,** *402*, 197-204.

142. Egan, T. J.; Mavuso, W. W.; Ross, D. C.; Marques, H. M., Thermodynamic factors controlling the interaction of quinoline antimalarial drugs with ferriprotoporphyrin IX. *J. Inorg. Biochem.* **1997,** *68* (2), 137-145.

143. (a) Vyas, N.; Avery, B. A.; Avery, M. A.; Wyandt, C. M., Carrier-mediated partitioning of artemisinin into Plasmodium falciparum-infected erythrocytes. *Antimicrob. Agents Chemother.* **2002,** *46* (1), 105-109; (b) Stocks, P. A.; Bray, P. G.; Barton, V. E.; Al-Helal, M.; Jones, M.; Araujo, N. C.; Gibbons, P.; Ward, S. A.; Hughes, R. H.; Biagini, G. A.; Davies, J.; Amewu, R.; Mercer, A. E.; Ellis, G.; O'Neill, P. M., Evidence for a common non-heme chelatable-iron-dependent activation mechanism for semisynthetic and synthetic endoperoxide antimalarial drugs. *Angewandte Chemie-International Edition* **2007,** *46* (33), 6278-6283.

144. Ncokazi, K. K.; Egan, T. J., A colorimetric high-throughput beta-hematin inhibition screening assay for use in the search for antimalarial compounds. *Anal. Biochem.* **2005,** *338* (2), 306-319.

145. Rush, M. A.; Baniecki, M. L.; Mazitschek, R.; Cortese, J. F.; Wiegand, R.; Clardy, J.; Wirth, D. F., Colorimetric High-Throughput Screen for Detection of Heme Crystallization Inhibitors. *Antimicrob. Agents Chemother.* **2009,** *53* (6), 2564-2568.

146. Hughes, C. C.; MacMillan, J. B.; Gaudencio, S. P.; Fenical, W.; La Clair, J. J., Ammosamides A and B Target Myosin. *Angewandte Chemie-International Edition* **2009,** *48* (4), 728-732.

147. Dorn, A.; Stoffel, R.; Matile, H.; Bubendorf, A.; Ridley, R. G., Malarial haemozoin beta-hematin supports heme polymerization in the absence of protein. *Nature* **1995,** *374* (6519), 269-271.

148. Srivastava, I. K.; Morrisey, J. M.; Darrouzet, E.; Daldal, F.; Vaidya, A. B., Resistance mutations reveal the atovaquone-binding domain of cytochrome b in malaria parasites. *Mol. Microbiol.* **1999,** *33* (4), 704-711.

149. Hawley, S. R.; Bray, P. G.; Mungthin, M.; Atkinson, J. D.; O'Neill, P. M.; Ward, S. A., Relationship between antimalarial drug activity, accumulation, and inhibition of heme polymerization in Plasmodium falciparum in vitro. *Antimicrob. Agents Chemother.* **1998,** *42* (3), 682-686.

150. Janouskovec, J.; Horak, A.; Obornik, M.; Lukes, J.; Keeling, P. J., A common red algal origin of the apicomplexan, dinoflagellate, and heterokont plastids. *Proc. Natl. Acad. Sci. U. S. A.* **2010,** *107* (24), 10949-10954.

151. Gerritz, S. W.; Sefler, A. M., 2,5-dimethylfuran (DMFu): An internal standard for the "traceless" quantitation of unknown samples via H-1 NMR. *J. Comb. Chem.* **2000,** *2* (1), 39-41.

152. Egan, T. J.; Ncokazi, K. K., Effects of solvent composition and ionic strength on the interaction of quinoline antimalarials with ferriprotoporphyrin IX. *J. Inorg. Biochem.* **2004,** *98* (1), 144-152.

153. McGlacken, G. P.; Fairlamb, I. J. S., 2-Pyrone natural products and mimetics: isolation, characterisation and biological activity. *Nat. Prod. Rep.* **2005,** *22* (3), 369-385.

154. (a) Kazlauskas, R.; Murphy, P. T.; Wells, R. J.; Blackman, A. J., Macrocyclic enol-ethers containing an acetylenic group from the red alga Phacelocarpus labillardieri *Aust. J. Chem.* **1982,** *35* (1), 113-120; (b) Shin, J.; Paul, V. J.; Fenical, W., New macrocyclic alpha-pyrones and gamma-pyrones from the marine red alga Phacelocarpus labillardieri. *Tetrahedron Lett.* **1986,** *27* (43), 5189-5192.

155. Berson, J. A.; Jones, W. M.; Ocallaghan, L. F., Spectra as a guide to structure in the hydroxypyrone and hydroxypyridone series. *J. Am. Chem. Soc.* **1956,** *78* (3), 622-623.

156. Sato, M.; Uehara, F.; Sato, K.; Yamaguchi, M.; Kabuto, C., Convenient-synthesis of chiral cyclophanes that can coordinate to metals. *J. Am. Chem. Soc.* **1999,** *121* (36), 8270-8276.

157. (a) Metz, J. G.; Roessler, P.; Facciotti, D.; Levering, C.; Dittrich, F.; Lassner, M.; Valentine, R.; Lardizabal, K.; Domergue, F.; Yamada, A.; Yazawa, K.; Knauf, V.; Browse, J., Production of polyunsaturated fatty acids by polyketide synthases in both prokaryotes and eukaryotes. *Science* **2001,** *293* (5528), 290-293; (b) Kaulmann, U.; Hertweck, C., Biosynthesis of polyunsaturated fatty acids by polyketide synthases. *Angewandte Chemie-International Edition* **2002,** *41* (11), 1866-1869.

158. Mizuta, T.; Kubokawa, K., Presence of sex steroids and cytochrome P450 genes in amphioxus. *Endocrinology* **2007,** *148* (8), 3554-3565.

159. Thornton, J. W.; Need, E.; Crews, D., Resurrecting the ancestral steroid receptor: Ancient origin of estrogen signaling. *Science* **2003,** *301* (5640), 1714-1717.

160. Thornton, J. W., Evolution of vertebrate steroid receptors from an ancestral estrogen receptor by ligand exploitation and serial genome expansions. *Proc. Natl. Acad. Sci. U. S. A.* **2001,** *98* (10), 5671-5676.

161. Di Cosmo, A.; Di Cristo, C.; Paolucci, M., A estradiol-17 beta receptor in the reproductive system of the female of Octopus vulgaris: Characterization and immunolocalization. *Mol. Reprod. Dev.* **2002,** *61* (3), 367-375.

162. Keay, J.; Thornton, J. W., Hormone-Activated Estrogen Receptors in Annelid Invertebrates: Implications for Evolution and Endocrine Disruption. *Endocrinology* **2009,** *150* (4), 1731-1738.

163. Mimoto, A.; Fujii, M.; Usami, M.; Shimamura, M.; Hirabayashi, N.; Kaneko, T.; Sasagawa, N.; Ishiura, S., Identification of an estrogenic hormone receptor in Caenorhabditis elegans. *Biochem. Biophys. Res. Commun.* **2007,** *364* (4), 883-888.

164. Thomas, P., Characteristics of membrane progestin receptor alpha (mPR alpha) and progesterone membrane receptor component 1 (PGMRC1) and their roles in mediating rapid progestin actions. *Front. Neuroendocrinol.* **2008,** *29* (2), 292-312.

165. Halanych, K. M., The new view of animal phylogeny. *Annu. Rev. Ecol. Evol. Syst.* **2004,** *35*, 229-256.

166. Kohler, H. R.; Kloas, W.; Schirling, M.; Lutz, I.; Reye, A. L.; Langen, J. S.; Triebskorn, R.; Nagel, R.; Schonfelder, G., Sex steroid receptor evolution and signalling in aquatic invertebrates. *Ecotoxicology* **2007,** *16* (1), 131-143.

167. Snell, T. W.; Kubanek, J., Quorum Sensing in Rotifers. In *Chemical Communications Among Microbes*, Winans, S. C.; Bassler, B. L., Eds. American Society of Microbiology: Washington, D.C., 2008; pp 453-463.

168. Snell, T. W.; Kubanek, J.; Carter, W.; Payne, A. B.; Kim, J.; Hicks, M. K.; Stelzer, C. P., A protein signal triggers sexual reproduction in Brachionus plicatilis (Rotifera). *Marine Biology* **2006,** *149* (4), 763-773.

169. Patterson, G. W.; Tsitsatzardis, E.; Wikfors, G. H.; Gladu, P. K.; Chitwood, D. J.; Harrison, D., Sterols of Tetraselmis (Prasinophyceae). *Comparative Biochemistry and Physiology B-Biochemistry & Molecular Biology* **1993,** *105* (2), 253-256.

170. Williams, S. P.; Sigler, P. B., Atomic structure of progesterone complexed with its receptor. *Nature* **1998,** *393* (6683), 392-396.

171. Center, N. C. Progesterone Historical Reference Ranges.

172. Ollevier, F.; Declerck, D.; Diederik, H.; Deloof, A., Identification of nonecdysteriod steroids in hemolymph of both male and female Astacus leptodactylus (Crustacea) by gas-chromatography mass-spectrometry. *Gen. Comp. Endocrinol.* **1986,** *61* (2), 214-228.

173. Gronemeyer, H.; Govindan, M. V., Affinity labeling of steroid-hormone receptors. *Mol. Cell. Endocrinol.* **1986,** *46* (1), 1-19.

174. Zhu, Y.; Hanna, R. N.; Schaaf, M. J. M.; Spaink, H. P.; Thomas, P., Candidates for membrane progestin receptors-Past approaches and future challenges. *Comparative Biochemistry and Physiology C-Toxicology & Pharmacology* **2008,** *148* (4), 381-389.

175. (a) Hughes, A. L.; Powell, D. W.; Bard, M.; Eckstein, J.; Barbuch, R.; Link, A. J.; Espenshade, P. J., Dap1/PGRMC1 binds and regulates cytochrome P450 enzymes. *Cell Metab.* **2007,** *5* (2), 143-149; (b) Losel, R. M.; Besong, D.; Peluso, J. J.; Wehling, M., Progesterone receptor membrane component 1 - Many tasks for a versatile protein. *Steroids* **2008,** *73* (9-10), 929-934.

176. (a) Lavery, D. N.; McEwan, I. J., Structure and function of steroid receptor AF1 transactivation domains: induction of active conformations. *Biochem. J.* **2005,** *391*, 449-464; (b) Gronemeyer, H., Transcription activation by estrogen and progesterone receptors. *Annu. Rev. Genet.* **1991,** *25*, 89-123.

177. Fontaneto, D.; Giordani, I.; Melone, G.; Serra, M., Disentangling the morphological stasis in two rotifer species of the Brachionus plicatilis species complex. *Hydrobiologia* **2007,** *583*, 297-307.

178. Rico-Martinez, R.; Snell, T. W., Comparative binding of antibody to a mate recognition pheromone on female Brachionus plicatilis and Brachionus rotundiformis (Rotifera). *Hydrobiologia* **1997,** *358*, 71-76.

179. (a) Guillard, R. R.; Ryther, J. H., Studies of marine planktonic diatoms .1. Cyclotella nana Hustedt, and Detonula confervacea (cleve) Gran. *Can. J. Microbiol.* **1962,** *8* (2), 229-239; (b) Berg, C. J., Jr., *Culture of Marine Invertebrates*. Hutchinson Ross: Stroudsburg, PA, 1983.

180. Snell, T. W.; Shearer, T. L.; Smith, H. A., Exposure to dsRNA elicits RNA interference in Brachionus manjavacas (Rotifera). *Mar. Biotechnol.* **2010,** *12*.

181. Snell, T. W.; Shearer, T. L.; Smith, H. A.; Kubanek, J.; Gribble, K. E.; Welch, D. B. M., Genetic determinants of mate recognition in Brachionus manjavacas (Rotifera). *BMC Biol.* **2009,** *7*, 60-72.

182. Livak, K. J.; Schmittgen, T. D., Analysis of relative gene expression data using real-time quantitative PCR and the 2(T)(-Delta Delta C) method. *Methods* **2001,** *25* (4), 402-408.